Rheological behaviour of polymer melts and its relationship with underlying structure and topology

CARL DAVID REYNOLDS

Rheological behaviour of polymer melts and its relationship with underlying structure and topology

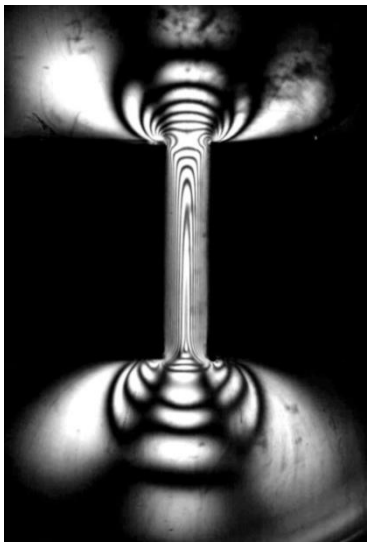

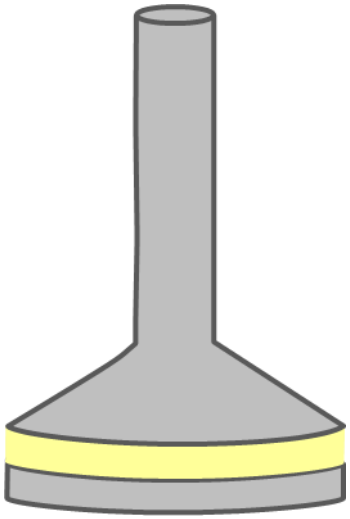

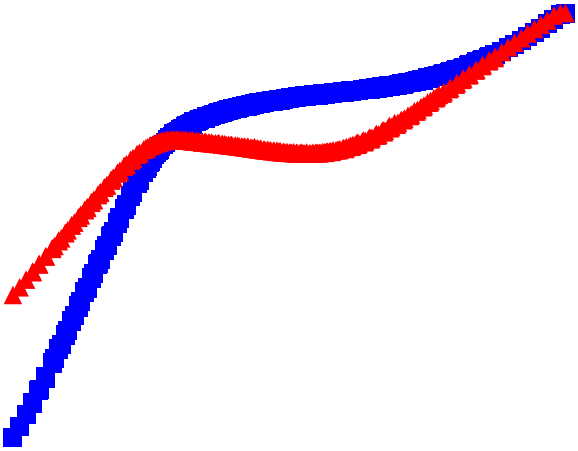

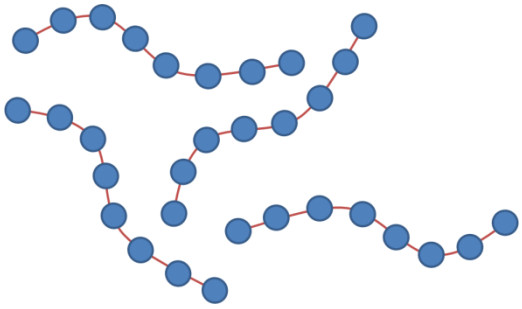

Carl David Reynolds

2018

Department of Chemistry, Durham University

Thesis submitted in fulfilment for the degree of Doctor of Philosophy

Durham University

Abstract

This thesis contains a detailed study of the relationship between the rheological properties of polymers and their underlying structure. Starting from model polymer systems, rheological complexity has been built up to enable predictions for industrially complex mixtures relevant to tyre processing and manufacture. Polymers which are representative of the tyre industry have been used (e.g. polyisoprene, polybutadiene, polystyrene).

Small amplitude oscillatory shear (SAOS) tests have been reported for a range of polymers of different molecular weight and architecture. Combining this with molecular modelling, in particular using branch-on-branch theory, is shown to allow predictions of polymer topology. Extensional rheometry is also reported using a variety of techniques (Sentmanat extensional rheometry, capillary breakup extensional rheometry, falling weight rheometry) and is shown to be sensitive to multiple branch points in the sample.

Complex flow has been examined using the multi-pass rheometer apparatus and the study of stress decays using a well-defined contraction-expansion geometry is reported, including a novel method of extracting of relaxation times. Cross-slot geometries are used to obtain steady state extensional measurements, not attainable using other techniques.

Large and medium amplitude oscillatory shear (LAOS and MAOS) have been explored with regards to elucidating polymer structure. Well-controlled amplitude sweeps are reported and analysed by Fourier transform and are shown to be sensitive to polymer structure. Frequency sweeps are also performed in the MAOS region, reporting phases and magnitudes, and results related to molecular models. By study of a range of linear polymers, stars and blends, the results are shown to relate to Rouse behaviour of the polymers.

The results detailed show that rheology is a multi-faceted technique that has great potential for identifying polymer structure. It is a key technique that should form part of the suite of analysis techniques available to the synthetic chemist in order to best characterise polymers produced.

Table of contents

Table of abbreviations

CaBER	Capillary breakup extensional rheometer
CCR	Convective constraint release
CLF	Contour length fluctuations
ETC	Environmental test chamber
FiSER	Filament stretching extensional rheometer
FT	Fourier transform
FFT	Fast Fourier transform
GLaMM	Graham, Likhtman, Milner and McLeish (theory)
GPC	Gel permeation chromatography
HDPE	High density polyethylene
LAOS	Large amplitude oscillatory shear
LCST	Lower critical solution temperature
LDPE	Low density polyethylene
LLDPE	Linear low density polyethylene
MAOS	Medium amplitude oscillatory shear
MPR	Multi-pass rheometer
NMR	Nuclear magnetic resonance
PBD	Polybutadiene
PDI	Polydispersity index
PE	Polyethylene
PI	Polyisoprene
PMMA	Polymethyl methacrylate
PS	Polystyrene
PVME	Polyvinyl methyl ether
SAOS	Small amplitude oscillatory shear
SBR	Styrene butadiene rubber
SER	Sentmanat extensional rheometer
SOC	Stress optic coefficient
THF	Tetrahydrofuran
TTS	Time-temperature superposition
UCST	Upper critical solution temperature
WLF	Williams-Landel-Ferry

Table of symbols

$tr\boldsymbol{\sigma}$	Amount of chain stretch
θ	Angle of rotation of the principle stress
ω	Angular frequency
β	Barus/pressure coefficient
k	Boltzmann constant
G_B	Bulk modulus
a	Capillary radius
L	Capillary/slit length
δ	CCR suppression factor (rolie-poly theory)
A_p, B_p	Coefficients used to fit pressure drop decays
A_σ, B_σ	Coefficients used to fit stress decays
η^*	Complex viscosity
C_v	Constraint release parameter in Likhtman-McLeish theory
D_e	Deborah number of a relaxation pathway
ρ	Density
ρ_0	Density of material at 0 °C
d	Depth of slit geometry
κ	Dimensionless factor for dependence of viscosity on molecular weight for branched polymers
G_e	Entanglement molecular weight
τ_e	Entanglement time
$\boldsymbol{I}$	Equilibrium value of stress tensor
$\dot{\varepsilon}$	Extension rate
ζ	Factor representing CCR (rolie-poly theory)
D	Filament diameter
C_1, C_2, C_3	Fit parameters in WLF time-temperature superposition, C_1 and C_2 define the horizontal shift and C_3 the vertical
χ	Flory-Huggins interaction parameter
Q_f	Flow rate
ΔG_m	Free energy of mixing per unit volume
T_g	Glass transition temperature
a_T	Horizontal shift factor (in TTS)
D_0	Initial filament diameter
l_0	Initial length of sample
Δp_0	Initial pressure drop used in stress decay fits
σ_0	Initial stress used in stress decay fits
I_n	Intensity of nth harmonic
l_s	Length of sample
G''	Loss modulus (viscous modulus)
Q	MAOS parameter
M_w	Mass average molecular weight
γ_0	Maximum strain amplitude (in oscillatory rheology)

M_e	Molecular weight between entanglements
M_0	Monomer mass
M_n	Number average molecular weight
Z	Number of entanglements
F	Number of fringes
N_e	Number of monomers in one entanglement length (BOB Theory)
N_i	Number of monomers per chain for polymer *i*
y_0	Offset used in stress/pressure drop decay fits
A, B, C	Parameters quantifying the dependence of the Flory-Huggins interaction parameter on temperature
l	Path length
ϕ_n	Phase of nth harmonic
v_{piston}	Piston speed
G_p	Plateau modulus
p	Pressure
β_E	Pressure dependence of early relaxation time
β_L	Pressure dependence of late relaxation time
Δp	Pressure drop
Q_0	Q parameter at zero strain
n	Rabinowitsch correction factor
$\dot{\delta}$	Rate of deformation
T_0	Reference temperature (in TTS)
v_0	Reference volume in Flory-Huggins Theory
$\frac{d_n}{d_c}$	Refractive Index Increment (GPC)
$G(t)$	Relaxation Modulus (at time t)
τ_i	Relaxation time of pathway *i*
τ_D	Reptation relaxation time
τ_R	Rouse relaxation time
a_r	Reservoir radius (MPR)
v_3	Shear Chebyshev coefficient
d	Slit depth
w	Slit width
G'	Storage modulus (elastic modulus)
γ	Strain
e_3	Strain Chebyshev coefficient
$\dot{\gamma}$	Strain rate
σ	Stress
$\boldsymbol{\sigma}$	Stress tensor
T	Temperature
$G3'$	Third harmonic ‘elastic’ modulus
$G3''$	Third harmonic ‘viscous’ modulus
t	Time
τ_{flow}	Time for flow to stop after deformation in the MPR
$R(t)$	Tube relaxation function (Likhtman-McLeish theory)

$\mu(t)$	Tube segment occupation function (Likhtman-McLeish theory)
b	Unit separation (reptation model)
$\boldsymbol{\kappa}$	Velocity gradient tensor
b_T	Vertical shift factor (in TTS)
η	Viscosity
v	Volume
ϕ	Volume fraction
v_i	Volume of single monomer unit for polymer *i*
σ_w	Wall shear stress
λ_{light}	Wavelength of light
W_i	Weissenberg number for relaxation pathway *i*
E	Young's modulus
η_0	Zero shear viscosity

Statement of copyright

Published work

Reynolds, C., Thompson, R.L., McLeish, T., “Pressure and shear rate dependence of the viscosity and stress relaxation of polymer melts”, Journal of Rheology 2018 62:2, 631-642

Reynolds, C. Hoyle, D., Thompson, R.L., “Frequency Sweeps of Polybutadienes and Polyisoprenes under Medium Amplitude Oscillatory Shear” (Under preparation)

International Congress of Rheology – Kyoto, Japan, August 2016 (Conference Presentation), “Large Amplitude Oscillatory Shear Rheology of Monodisperse Polybutadiene and Polyisoprene Rubbers”

Acknowledgements

Firstly, I would like to acknowledge Michelin, who sponsored this project and made this work possible. In particular, I would like to thank Michel Valtier and Gaëtan Maurel, for their help and direction throughout the project.

I would, of course, like to acknowledge my supervisor, Dr. Richard Thompson, for the support throughout my PhD. I have immensely appreciated that you are always approachable and friendly and have pushed me to succeed. I have really enjoyed my PhD and that was largely due to having such a great supervisor.

I would also like to acknowledge all the members of Thompson group, past and present, for their help and advice as well as the fun and supportive atmosphere. In particular I would like to acknowledge Dr. Stephen Boothroyd, who as well as being a great friend, has given me invaluable advice and guidance on virtually a daily basis, without which I would not have been able to complete this work.

I would like to thank my housemates at the Rowans: Mel, Eddy, Jasmine and Chris. We had some excellent times in the house and it was great to have such a fun place to live. Also thanks to the friends I made at Ustinov college, in particular Ruth and Libby, my flatmates in Alder, for making my first year so great. I would also like to acknowledge all of the other friends that I have had during my PhD, including but not limited to: Kristian, Tom and Lara. I really appreciate having such good friends.

I would like to acknowledge Matthew Oti and his supervisor Prof. Lian Hutchings, for synthesis of the polymers that made all the interesting rheology possible, and for the help and advice. I also would like to acknowledge Prof. Tom McLeish for advice and discussions which helped greatly throughout the project. For performing modelling on my experimental data, I would like to acknowledge Dr. David Hoyle, as well as for many discussions that improved my understanding of rheology.

Thanks to both the mechanical and electrical workshop in the chemistry department, for accommodating my odd requests and producing and maintaining a lot of the equipment that made my work possible. Thanks also must go to the support staff in the department who keep everything running, supply vital tea and are always around with a smile.

Finally, I would like to acknowledge my family; my Mom and Dad and sister, Jilly, who have always been there to support me.

1 Introduction

Polymeric materials, as well as being found in the many plastics we use daily, are the main component in rubber materials such as tyres. Polymers are made up of long chains of repeat units, but can have a variety of structures, e.g. linear chains, stars, H shaped. The underlying structure of a polymeric material has a significant impact on its rheological properties and this in turn affects the processability of the material. The objective of this work is to study the relationship between polymer structure and rheological properties and examine the extent to which detailed rheology can be used to analyse the structure of the polymer and make predictions about the behaviour of the polymer in complex flows and mixtures.

In this thesis, models have been fit to rheological data to extract structural information as well as the use of several novel rheological techniques. The introduction contains a review of the literature related to polymer rheology and a discussion of the different techniques available that can be used to characterise it. Experimental methods for measuring shear and extensional rheology, which will be used in this thesis, are discussed and their use reviewed. Modelling strategies are discussed for linear and branched polymers and the models introduced that will be applied to experimental results. Polymer blends and rheological methods for studying phase transitions are discussed, comparing rheology to alternative methods. The topics of large and medium amplitude oscillatory shear are then introduced, which is used in this thesis. Finally techniques for evaluating the pressure dependence of rheology are discussed as well as existing results, which will later be compared to new data.

1.1 What is rheology?

Rheology is the study of the deformation and flow of matter. It deals with the relationship between force applied to a material (or stress – the force per unit area) and its deformation. At one end of the spectrum are elastic solids. These materials obey Hooke's law, the stress (σ) in the material is proportional to the deformation applied, or the strain (γ), with the constant of proportionality being the Young's modulus, (E):

$$\sigma = E\gamma \tag{1.1}$$

At the other end are liquid materials that obey the law described by Newton and reformulated by Stokes. This states that stress is proportional to the rate of

deformation, or strain rate ($\dot{\gamma}$). The constant of proportionality here is the viscosity of the liquid, η (i.e. the Newtonian fluid in Figure 1.1).

$$\sigma = \eta\dot{\gamma} \tag{1.2}$$

The mechanical behaviour of many materials conforms to Hooke's or Newton's law with viscoelastic behaviour providing only small deviations (e.g. creeping of glass, which otherwise demonstrates mostly solid behaviour). However, there also lies a broad spectrum of materials, in between these extremes, which are known as viscoelastic, and have properties of both solids and liquids. One example is clay, most would describe it as a solid, but it can be moulded to fill the space of its container, in the same way as a liquid. [1-2]

For polymer systems, viscoelasticity governs the majority of their behaviour and hence knowledge of their rheology becomes important. In industrial processing, polymer melt rheology is an important factor to be considered because a material may endure many external forces at different rates and its response to these can be very different i.e. a mixture which is relatively liquid to pour, could become much more viscous and solid-like if passed through tubes at high pressure (dilatant or shear thickening materials become more viscous at high shear rates, as shown in Figure 1.1). Understanding rheology-structure relationships allows the design of materials that give the required end properties and are easy to process.[3-4] For example in oil fracking, where high pressure fluids are used to fracture shale and release oil, a fluid with a range of rheology is required. The fluid, at the high pressures used, must be viscous enough to supress turbulence and to carry a suspended proppant (a type of sand used to keep the fractures open), however not so viscous that it cannot be pumped through the system. Often additives are used at different stages to modify the rheology, although some systems are designed to respond to environmental changes (e.g. temperature, pressure, pH).[5]

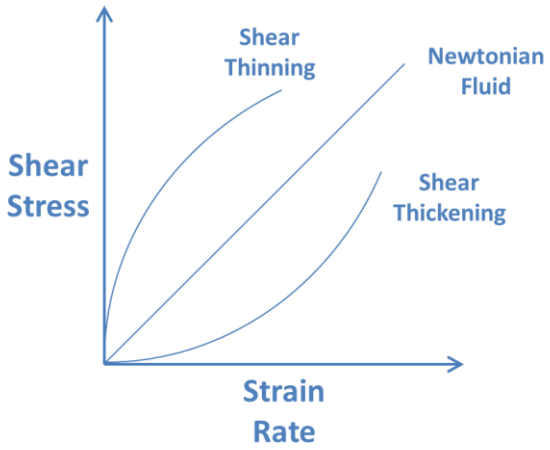

Figure 1.1: Example behaviour of shear stress with strain rate for Newtonian, shear thickening and shear thinning materials, the dynamic or shear viscosity is given by the gradient of the graph

As well as varying between materials, rheological behaviour can vary in

different types of flow. Flows can be defined as shear or extension (or a mixture of the two). Shear flow is produced when forces are applied in such a way to create a velocity gradient perpendicular to the direction of the force applied. This is shown in Figure 1.2, where opposite forces are applied to the top and bottom of a square of material. This would create a vertical velocity gradient, i.e. the material in the middle is moving slowest and the material closest to the top/bottom is moving fastest. However the direction of movement is horizontal, perpendicular to this velocity gradient. If the material is visualised as multiple layers, moving at different speeds, this means the layers will slide over one another. This is a shear flow and the stress measured from this deformation is a shear stress.

Alternatively, if the two forces are applied to the entire side of the square, so it now experiences an equal and opposite force on each side, this time the velocity gradient is parallel to the direction of movement. Here, an extensional stress will be produced, stretching the material.

Shear rheology is usually measured with a rotational or capillary rheometer. Since it is possible to maintain the overall shape of the sample in shear, the geometries can be well defined and hence techniques for measurement under shear are well developed. As this is not possible in extension, methods to measure extensional

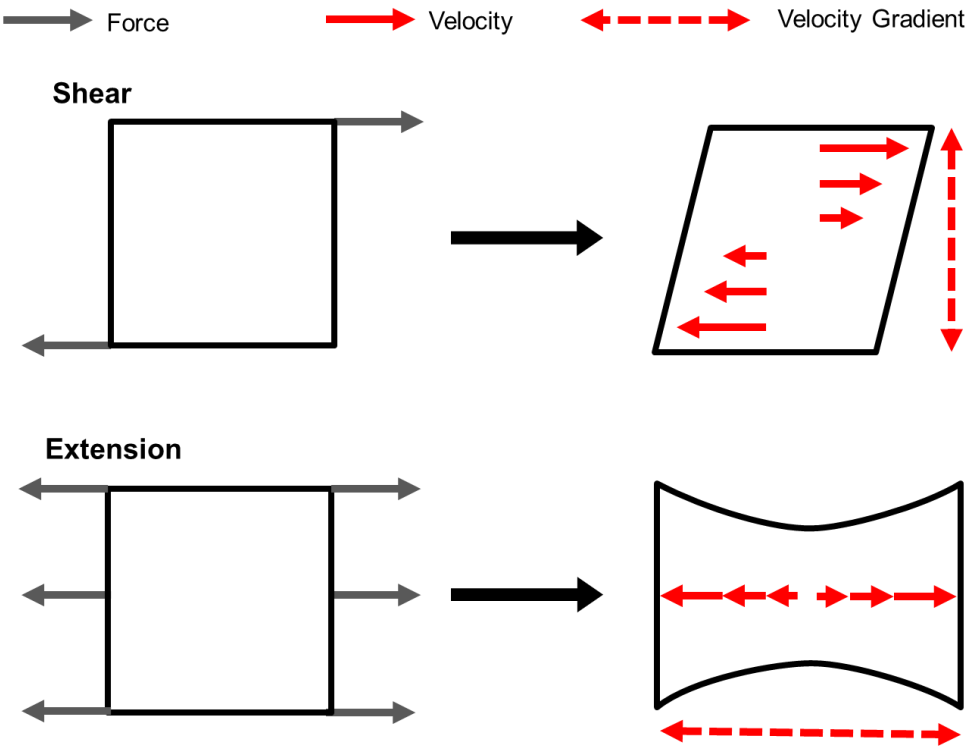

Figure 1.2: Sketch showing how applied forces can generate shear and extensional flow

flow are more difficult and generally less advanced, but there are several commercially available methods such as the capillary breakup extensional rheometer (CaBER), Sentmanat extensional rheometer (SER), multi-pass rheometer (MPR) or a capillary rheometer with a combination of dies.

1.2 Measuring rheology: types of rheometer

1.2.1 Rotational rheometers

Rotational rheometers can be used to obtain the viscoelastic response of a material under shear. They usually operate by sandwiching the sample between a fixed and a rotating element. This can be two parallel plates (pioneered by Weissenberg[6]), a cone and plate, a cup and bob or a variety of other geometries. Examples are shown in Figure 1.3, in different variations either component may be rotated in each of these systems.

Cup and bob geometries (or concentric cylinders) are generally used for low viscosity fluid samples (where the bob can be easily immersed in the sample). In this case the bob can be fully rotated until a steady state is reached, and the viscosity of the sample measured using Equation 1.2, where the stress can be extracted from the force measured via a transducer in the bob, and the shear rate is proportional to the rotation speed. Note that in a shear flow, the strain rate is equivalent to the shear rate applied to the sample hence the same symbol is used. For a large enough diameter of bob and a small gap between the bob and cup, the

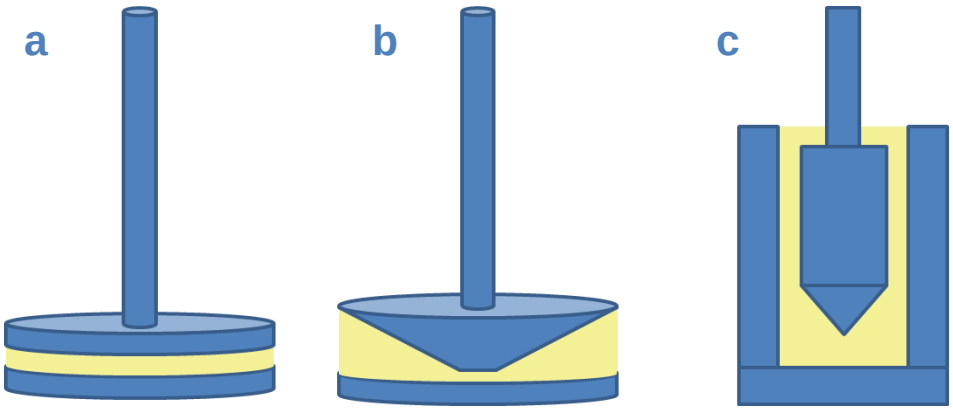

Figure 1.3: illustration of geometries that can be used with a rotational rheometer, a) parallel plates, b) cone and plate, c) cup and bob or concentric cylinder geometry. The upper element is shown attached to a spindle for rotation; however in each case the lower plate or cup could instead be rotated; a Couette cell is a cup and bob in which the cup moves. The cone angle is exaggerated (angles are usually 1° or 2°) and is shown truncated which prevents wear and friction occurring where the tip would touch the lower plate

shear rate is near constant at all points and roughly equivalent to the shear between two plates (because over a small area with a large diameter bob, the curvature can be neglected).

For the measurement of linear rheology of rubbery polymers, parallel plates and cone and plate geometries are the most relevant, as the samples are too viscous to immerse a bob into, and so are instead sandwiched between two plates.

The main advantage of a cone and plate geometry is that it keeps the shear conditions homogenous across the entire gap and therefore, theoretically gives more accurate results than parallel plates, where the shear rate is proportional to the distance from the centre of the plate. A correction can be applied which makes the difference between the two geometries negligible for most tests in the linear viscoelastic range (i.e. where Hooke and Newton's laws are obeyed), however when viscoelastic behaviour is non-linear, the standard correction can cause errors. Despite this source of error, parallel plates are still used widely as with cones there is a limit on the maximum particle size in the sample being measured. If particles are too large there is not enough free space between them during motion and too many will be in contact with the surface causing friction. Both of these effects change the flow and cause erroneous results. Therefore cones cannot be used on gels and solids. They also require a long time to equilibrate when setting the gap with highly viscous samples, such as polymer melts. In addition, cones are usually only suitable for use at a constant temperature, because thermal expansion has a large effect and the gap cannot be adjusted to compensate for this. In order to obtain the homogenous shear rate, cones must be positioned with the tip of the lower plate touching the lower plate, and so a fixed gap must be used (although practically cones are usually slightly truncated to prevent actual contact causing friction and wear). The gap between parallel plates can be compensated slightly to correct for changes in temperature, which enables temperature ramps and sweeps to be performed. This can be done by initial calibration of the change in gap with temperature or some rheometers can measure the gap directly. Hence, parallel plates are usually preferred for polymer melts.

In either case, for most rubbery polymers, the plates cannot be fully rotated to obtain the steady shear viscosity (as with a Couette cell) because the force on the samples would become too great, and cause them to leave the gap or fracture. Hence a small amplitude oscillating motion is most commonly used. The plate moves back and forward, applying a sinusoidal strain (which here corresponds to the amplitude

of the oscillation or the angle the plate is moved to). Either the shear stress or strain can be controlled and the other quantity measured. In a strain controlled experiment, where a periodic sinusoidal strain is applied, the stress can be shown to be:

$$\sigma = \gamma_0(G' \sin \omega t + G'' \cos \omega t) \tag{1.3}$$

where γ_0 is the maximum amplitude of the strain, ω is the angular frequency at which the strain is varied, t is the experiment time and G' and G'' are the storage or elastic modulus and the loss or viscous modulus respectively.

To get a measure of the viscosity of the sample, the complex viscosity, η^* can be calculated from the complex modulus, G^* as shown:

$$\eta^* = \frac{G^*}{\omega} = \frac{\sqrt{G'^2 + G''^2}}{\omega} \tag{1.4}$$

The Cox-Merz rule states that this complex viscosity obtained from oscillatory shear is approximately equal to the steady shear viscosity, when the frequency of oscillation is equal to the shear rate applied in steady shear:

$$\eta^*(\omega) = \eta(\dot{\gamma}) \tag{1.5}$$

This is an empirical relationship that has been shown to be true for most polymer melts, however there are exceptions, including biopolymers and foods.[7] There is no physical reason for this relationship to be true, as the two types of flow are distinctly different. However constitutive models[8] have been derived for polymer melts which satisfy the Cox-Merz rule, and it is generally accepted to be valid for polymer melts.

However, the extracted moduli can give more information about the behaviour than the viscosity alone. The storage modulus, G', (measured in Pa) represents the energy stored by the sample after the deformation caused by the shear. This energy is used, on removing the load, to regain (fully or partially) the sample's original conformation. Hence, this modulus represents the elastic behaviour of the sample.

The loss modulus, G'', (also measured in Pa) is a measure of the energy lost in changing the sample's structure when shear is applied. This energy is dissipated as heat (to the sample and surroundings) due to the friction of components in the material moving against each other. Therefore this energy is lost and is not used to regain the original shape, so the deformation caused by this part of the shear energy is irreversible. G'' thus represents the viscous behaviour of the material.[3]

A sketch of a viscoelastic spectrum for a rubbery polymer is shown in Figure 1.4. It shows how G' and G'' vary with angular frequency, which describes the behaviour of the material when force is applied on different time scales. For the example shown, G'' is larger than G' at low frequencies, hence over long times the material will have viscous behaviour, so this polymer might flow gradually under its own weight. At high frequencies G' exceeds G'', hence under a short impact the material will behave like an elastic solid. So this polymer might bounce if thrown at the ground. The shape of this graph follows the behaviour of a Maxwell fluid, (an in series combination of a spring for the elastic component and a dashpot, for the viscous component). This gives the following equations for the frequency dependence of the two moduli,

$$G'(\omega) = G_p \frac{\omega^2 \tau_i^2}{1 + \omega^2 \tau_i^2} \tag{1.6}$$

$$G''(\omega) = G_p \frac{\omega \tau_i}{1 + \omega^2 \tau_i^2} \tag{1.7}$$

where G_p is the plateau modulus of the material (Pa) and τ_i is its relaxation time (s). Hence, on a log-log plot, at low frequencies (as $1 + \omega^2 \tau_i^2$ tends to 1), the slope of G' is 2 and G'' is 1 and at higher frequencies (as $1 + \omega^2 \tau_i^2$ tends to $\omega^2 \tau_i^2$), G' tends to the plateau modus G_p and G'' has a slope of -1.

The behaviour at different frequencies is very important for applications, for example in tyre manufacture. Rubber produced for tyres needs to produce high friction when brakes are applied rapidly, to have a short braking distance and improve wet braking

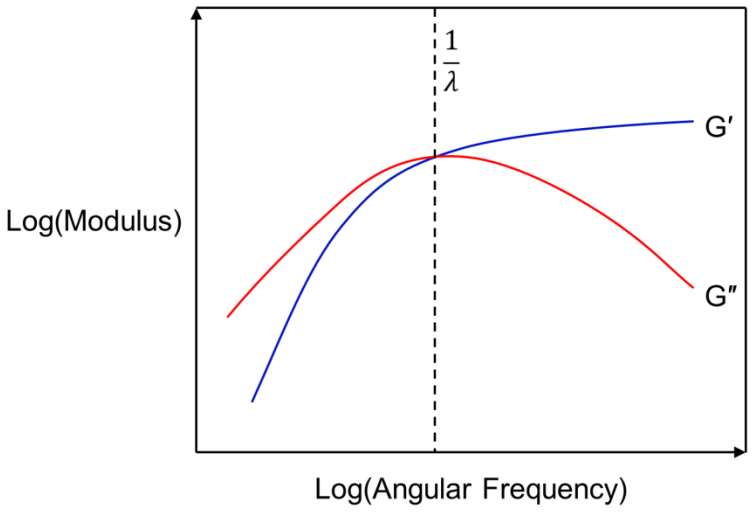

Figure 1.4: Sketch of a viscoelastic spectrum of a monodisperse linear polymer

performance, yet produce minimal friction (and so energy dissipation) during normal driving, to reduce rolling resistance and hence the amount of fuel used. A softer, more viscous material will dissipate the force faster and give faster breaking, but a harder more elastic material will reduce the friction experienced under normal conditions. However these two processes occur under different conditions, a rapid brake applies a force at a much higher shear rate than a normal rotation of the tyre. Hence the behaviour at different frequencies can be used to tune this behaviour, the higher frequency behaviour will correspond to the wet braking performance (where a higher viscous modulus is required to give faster breaking) and in the low frequency region gives information about rolling resistance (where a higher elastic modulus would be required to give less friction). Hence these frequency sweeps are very useful in tuning materials properties.[9]

When measuring linear rheology, the results are very dependent on the temperature of measurement; changing temperature often shifts the frequency range of the response. To quantity the temperature dependence, and to get a larger region of the rheological spectrum, time-temperature superposition is often used. This involves measuring the frequency dependence at multiple temperatures and shifting all the spectra to produce one overlaid spectrum at a single chosen temperature. This is often done using the Williams-Landel-Ferry model.[2] This shifts the frequency data at different temperatures to a reference temperature by multiplying by a factor $a_{T,}$, where:

$$\log(a_T) = -\frac{C_1(T - T_0)}{T + C_2} \tag{1.8}$$

and T is the experimental temperature, T_0 is the reference temperature, and C_1 and C_2 are parameters fit to the data.

Different software can be used to perform this shift. One of these is REPTATE[10], which contains a database of materials parameters for different polymers (averaged over various literature values). Hence for materials in the database, shift factors obtained can be compared to the known values, as significant differences could indicate that experimental inconsistencies (e.g. produced by incorrect gap compensation) have been incorporated into the results.

1.2.2 Capillary rheometers

Capillary rheometers are used for single shot steady flows. They differ from rotational rheometers in that the entire sample is enclosed from all sides whereas in

a rotational rheometer only the top and bottom of the sample touch the plates and the sides are left exposed.[11] The sample is forced from a larger reservoir through a capillary of known cross section. The pressure gradient is measured (by a pressure transducer) alongside the volume flow rate (known from the area and speed of the piston driving the sample). This can be used as a guide in industrial processing to the pressures that will be experienced when the material is forced through pipes at a given rate.

If pressure transducers are placed before and after the capillary, the pressure drop can be calculated and the viscosity can then be calculated using the Hagen-Poiseuille equation[12],

$$\Delta p = \frac{8\eta L Q}{\pi a^4} \tag{1.9}$$

where Δp is the pressure drop, a and L are the radius and length of the capillary respectively, Q is the volume flow rate and η is the dynamic viscosity.

However, most capillary rheometers simply extrude from the capillary into the open air. This means only the pressure before the capillary can be measured, and the viscosity calculated from this is dependent on the capillary used. To obtain a standard value of the viscosity which can be compared to those from other capillaries and different rheometers, measurements can be conducted with two capillaries of the same diameter but different lengths. The Bagley correction[13] can then be applied to correct for entrance and exit effects and give a viscosity based on the wall shear in the capillary. Many capillary rheometers have twin bores, so that these measurements can be done simultaneously and the correction applied. Some make use of a short or orifice die, which has as little length as possible (dies are common that are equivalent to a capillary of length 0.25 mm). This means that entry effects dominate, and they can be subtracted from the results obtained from a longer capillary to give only wall shear effects.[14-15]

Using orifice dies can also give a measure of the extensional viscosity by using a model such as the Cogswell model.[16] It makes the assumptions that the flow is purely extensional, that the flow takes the shape that minimises the pressure drop and that the flow is zero at the boundary between the moving flow and the vortices created at the entrance (Figure 1.5). This model has been improved upon by Binding[17] but still strictly represents a resistance to entry flow rather than a true extensional viscosity. The main limitation is that the analysis relies on analysis of the

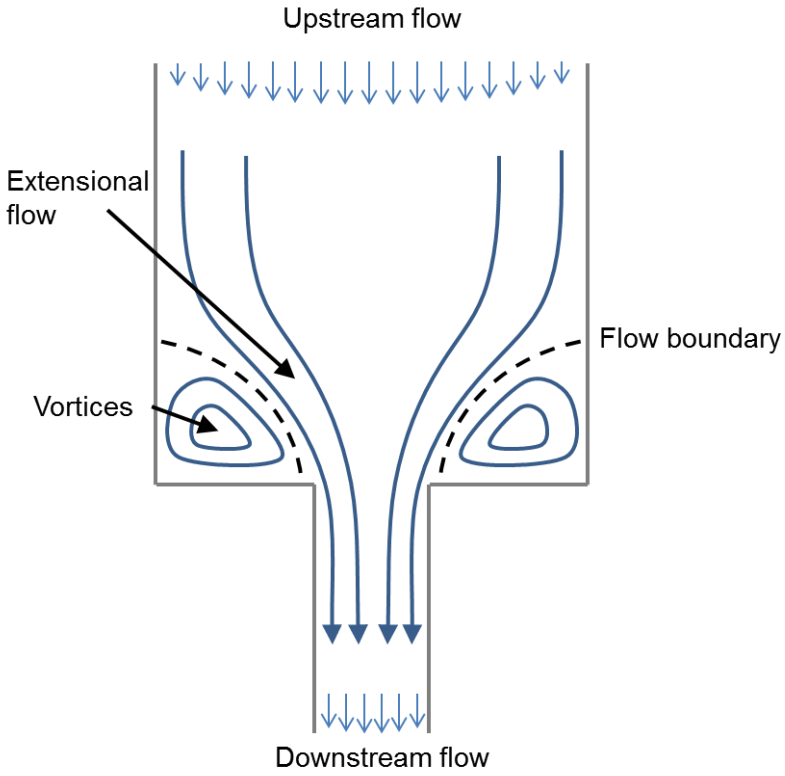

Figure 1.5: Sketch of flow through a contraction, showing flow boundary between the vortices generated at the entrance and the 'wine glass' extensional flow

viscous forces and so when elasticity contributes significantly to the stress it is invalid. However, for polymers melts at medium flow rates the viscous dissipation will dominate and hence it is a valid approximation and is still most commonly used to calculate the extensional viscosity in capillary rheometer software.[18-19]

Traditionally, capillary rheometers were used to measure linear rheology of low viscosity materials at high shear rates (where they would be forced out of the sides of a rotational rheometer).[20] They can also measure steady shear viscosities of more elastic materials that would also escape the gap under steady shear in a rotational rheometer (however complex viscosities can instead be measured for these materials using an oscillatory test). The flow in a capillary rheometer can also be more representative of the conditions found in industrial processing where materials are often passed through enclosed pipes.

One disadvantage of capillary rheometers is that wall slip can occur when the shear stress at the walls becomes too high, which gives anomalous results to those found with rotational rheometry.[21] As the system is enclosed, they also can be very difficult to clean to change samples, and they also lack the ability to perform oscillatory measurements which can give more information about the sample.

1.2.3 Sentmanat extensional rheometer

Although capillary rheometry can be used to get approximate extensional viscosities, it relies on analytical methods that make various assumptions and hence entry flow is not the preferred method of quantifying extensional behaviour. There are generally two ways to experimentally generate pure, well controlled extensional flow. These are stretching the sample or generating flow around a stagnation point. Controlled stretching can be performed with a tensile extensional or filament stretching rheometer, or with a Sentmanat extensional attachment for a rotational rheometer.[22] Flow around a stagnation point can be generated with multi-roll mills or using a cross-slot attachment to the multi-pass rheometer (see Section 1.2.5), amongst other methods.

The Sentmanat extensional rheometer (SER) is attached to a rotational rheometer as shown in Figure 1.6. Rotation of the rheometer spindle causes rotation of the two drums in opposite directions. A sample of fixed dimensions is clipped to each drum with the clips shown. When the drums rotate a uniaxial extension is generated in the sample and the extensional stress is measured via the torque transducer in the rheometer.[23]

Figure 1.6: Sentmanat extensional rheometer attachment

This is a relatively simple way to measure extensional rheology, requiring a small amount of sample, (around 0.1 g) which can then be re-pressed and reused to conduct multiple experiments.

However, it has some drawbacks, the sample needs to be suitably solid at room temperature to mount on the drums (although an oven can then be closed around the sample to change the temperature and measurements can be undertaken as long as the sample is viscous enough to stay on the drums and not sag significantly). There can also be errors introduced by defects in samples which can cause early tearing, samples slipping out of the clips, or tearing at the clips if fixed too tight. For these reasons measurements have to be repeated multiple times to

ensure consistency.

Strain in extension is commonly measured using the Hencky or logarithmic strain which can be calculated as:

$$\gamma = \ln\left(\frac{l}{l_0}\right) \tag{1.10}$$

where l is the final length and l_0 is the initial length of the sample.

The SER has a measuring range of up to 4.0 Hencky strain, as beyond this the drums have completed a full rotation and the sample begins to overlap. This limit can be exceeded by newer versions which mount the sample diagonally between the drums. However, many samples will undergo necking and tearing before this point, which can limit the range of extension rates that can be studied.

1.2.4 Capillary breakup extensional rheometer

The CaBER (capillary breakup extension rheometer) was developed to study the extensional viscoelastic properties of fluids. It works by sandwiching a sample between two plates, which are then rapidly moved apart to apply a step strain. The diameter of the resulting filament is then observed using a camera and laser micrometer, and followed over time as it thins and eventually breaks, as illustrated in Figure 1.7. The relaxation of this capillary can be fit to different models in order to extract extensional viscosities of the fluid and information about how it behaves under extension. Capillary thinning is very relevant to fibre spinning and inkjet printing applications, amongst others, so this is a useful technique for industry. One of the key parameters generated is the critical time to breakup, which is simple to obtain and of interest industrially. An apparent extensional viscosity can also be calculated; which is useful for comparing materials behaviour under breakup. However, as the strain and strain rate are constantly changing during necking, it is more difficult to extract true rheological parameters, but this can be achieved by fitting a model to the observed diameters and images of the filament. Distinguishable modes of breakup are observed for Bingham plastics, power law fluids, Newtonian fluids, weakly elastic fluids and elastic fluids. These classes of material can be identified using the images and the diameters then fit to the respective constitutive equation to extract rheological parameters.[24]

Experimentally, the limitations of this technique are that the sample must adhere sufficiently to both plates, meaning it works well for dilute polymer solutions but it is less suitable for polymer melts, which are often rubbery and relax over much longer

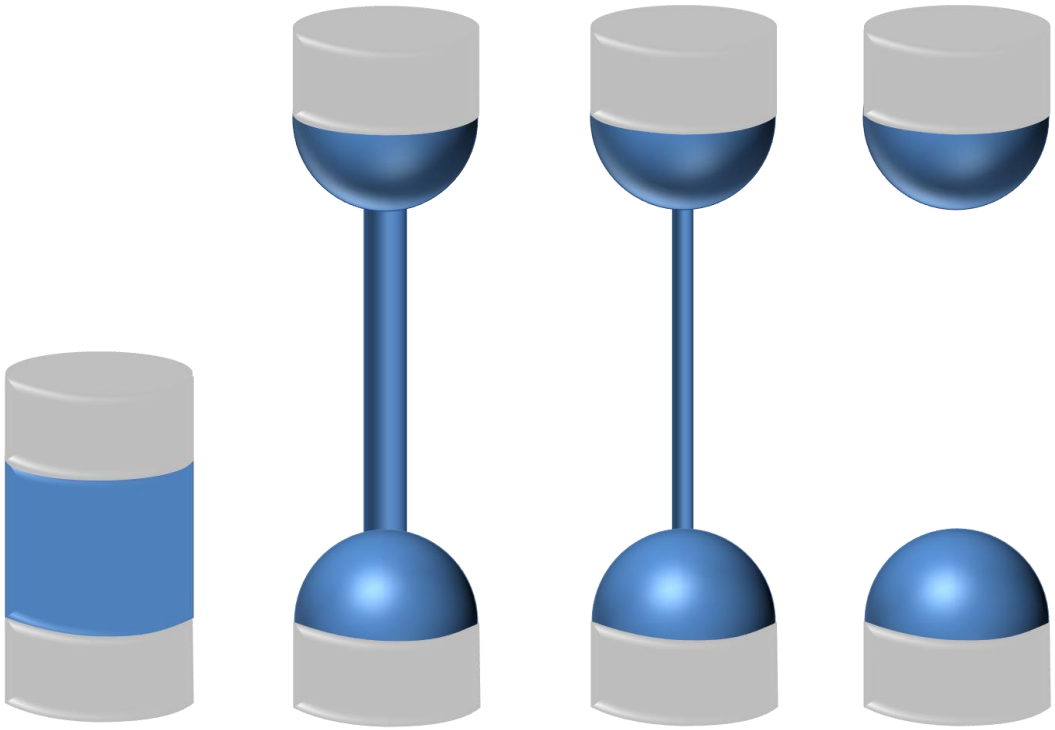

Figure 1.7: Illustration of a CaBER experiment, showing the first step before movement of the plates, thinning of the capillary, and breakup

timescales (so in some cases the timescale of the experiment can become limiting). There is no force transducer in the plates, meaning that the stress cannot be directly measured, which is why fitting to constitutive models must be relied upon. Since the laser micrometer is in a fixed position, the diameter also cannot be measured during an extension, only the post extension thinning, however this can be obtained through image processing.

Several other rheometers have been produced based on a similar principle to the CaBER. The filament stretching extensional rheometer (FiSER) adds force control and a moveable laser micrometer to provide stress measurements during extension, which allows direct determination of the extensional viscosity.[25] Another rheometer, the Cambridge Trimaster has also been developed to produce much higher strain rates (up to 1000 s^{-1}), as there are some materials that show different behaviour under very high extension rates, outside the range of the CaBER.[26]

1.2.5 The multi-pass rheometer

The principle of the multi-pass rheometer in its current form was first described by Mackley[11] in 1995. Similar to a capillary rheometer, the principle of operation is based around pushing the material through a test section, which can be a capillary or a variety of other geometries, to induce shear, extensional or complex flow.

As shown in Figure 1.8, the MPR uses two pistons arranged vertically above and below the central test section. The sample to be tested is introduced into the top and bottom reservoirs, the pistons can then be moved to force it into the test section, which can include one of a variety of geometries, (capillaries, slots, cross-slots etc.). The pistons are moved together, one towards and one away from the test section, keeping the spacing constant, in order to create flow through the geometry.

Pressure sensors in the reservoir walls allow time-dependent pressure readings which can be used to extract rheological parameters. If the pistons are driven at a constant velocity until equilibrium, steady shear data can be obtained.

In this mode, the pressure difference across the capillary is measured and the strain rate is then given by:

$$\dot{\gamma} = \frac{4Q}{\pi a^3} \tag{1.11}$$

where a is the radius of the capillary and Q is the fixed flow rate, equal to $v_p \pi a_r$ where v_p is the piston velocity and a_r is the radius of the upper/lower reservoir. This equation must include a correction for shear thinning fluids, such as the Rabinowich correction, which adjusts the shear rate by a factor of $(n+2)/3$, where n is defined as the gradient of a plot of log (shear rate) vs log(shear stress).[11, 27-28]

For a narrow slit instead of a cylindrical capillary the equation becomes:

$$\dot{\gamma} = \frac{6Q}{w^2 d} \tag{1.12}$$

where w is the slit width and d the slit depth.

In addition to measuring the pressure drop, the sample can be observed using optical windows. By using circularly polarised light, stress birefringence can be observed, where dark and light fringes are seen due to the stress in the sample, allowing the stress to be mapped onto different areas of the flow.

The system is enclosed, which has several advantages. Repeat measurements can be made on the same sample by simply reversing the piston direction. Oscillations can also be performed in order to generate data comparable with a rotational rheometer.[11] This also allows a pressure to be applied, allowing pressure dependent rheology to be studied, as well as adding the potential for linking to a polymerisation

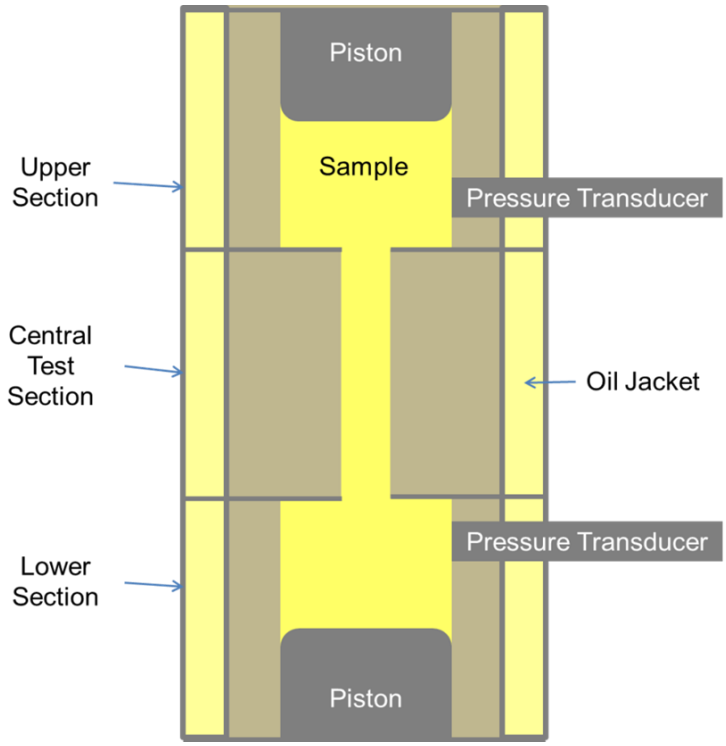

Figure 1.8: Illustration of the multi-pass rheometer equipped with a capillary or slot geometry

reactor, to measure the viscoelastic properties of samples and allow quality control.[29]

Hence, the MPR allows the extraction of both oscillatory shear data (usually found using a rotational rheometer) and steady shear flow curves (usually found using capillary devices) and obtains both as a function of pressure. This is useful in industrial polymer processing when high pressures are often required as the effect of these pressures can be measured.[27]

There are however several disadvantages of the MPR. Large samples are required, on the order of 10 g, this is similar to the quantity required by a benchtop capillary rheometer, whereas rotational rheology can be performed on samples of less than a gram. The apparatus is also very difficult to clean and hence it is time consuming to change samples.

Mackley[27] measured polyethylene melts in an MPR and compared the results to those measured using a parallel plate rotational rheometer and a capillary rheometer. They found the MPR produced similar, although not identical results to a rotational rheometer for oscillatory shear. The MPR produced slightly lower values of G' and G'' for a given frequency, the reason for which was unclear but was suggested to have been due to incorrect temperature calibration. The MPR data

were consistent over multiple passes and was generally within 20 % of that from the rotational rheometer. It produced steady shear data in good agreement with the capillary rheometer however using the steady state mode of the rotational rheometer produced higher values to both at low shears. At low strains, both rotational rheometry and the MPR showed time independence but at higher strains, the moduli decrease over time for the rotational rheometer, caused by the polymer being forced out of the gap out of the open sides. The MPR avoids this problem as the sample is enclosed and gives time independent data at high strains (up to 27 % were demonstrated).

Rangathan and Mackley[30] also performed time dependent capillary flow measurements on high density polyethylene (HDPE) using the MPR, demonstrating its use in this way and producing results that suggested compressibility rather than viscoelastic effects determine the time dependence of capillary flow pressure measurements, supporting previous work.[31] They also adapted a model developed by Molenaar and Koopmans[32] for capillary flow to the boundary conditions of the MPR and found good agreement with the experimental data.

MPR apparatus has been used to study flow-induced crystallisation behaviour; Scelsi and Mackley[33] looked at high density polyethylene and an isotactic polypropylene using birefringence to identify crystallised regions as the materials pass through the narrow capillary. Here optical windows were used to pass circularly polarised light through the sample which allows birefringence to be imaged which is proportional to the stress in the sample. It has also been used to determine the cloud point and viscosity of polyethylene solutions. This was achieved by using the apparatus to measure viscosity (from shear stress) at a set temperature and fixed shear rate. The cloud point was then calculated from the discontinuity in the viscosity-pressure curve, by fixing temperature and altering the pressure.[34] In industrial applications this apparatus has also been used to demonstrate 'work softening' behaviour in cocoa butter and chocolate.[35]

The MPR is versatile in terms of the geometry used. The single capillary or slit can be replaced with cross-slots and narrow slits incorporating reservoirs. Lee *et al.*[36] used the MPR with a double cavity die (rather than the sample just passing through one slit, there is a central reservoir so the sample flows into one slit, out into the reservoir and back into a second slit). They also used an optic cell, shining polarised light onto the sample and collecting birefringence patterns with a camera in order to visualise the flow. They showed the ability of this technique in determining the flow

patterns of polymer melts, useful in polymer processing (and hence also showed application in testing numerical simulations of viscoelastic flow).

Using a cross-slot test section (as shown in Figure 1.9), the MPR can be used to study extensional flow. Previously the four roll mill (suggested by Taylor[37]) had been used to create stagnation point flow and observe extension in polymer solutions.[38] This method is limited to low viscosity solutions and problems are caused by flow instabilities. Cross-slot apparatus addresses some of these problems by using two opposing orthogonal flow channels with a central stagnation point.

The cross-slot geometry can produce well controlled extensional flow with well-defined boundary conditions. Optical windows are used to observe the fringes at the stagnation point and the cross-slot geometry is equipped with a reservoir at each side, as shown in Figure 1.9. The pistons are both moved inwards, forcing sample in through the top and bottom arms and out through the side arms into the reservoirs. Slave pistons were also added to the reservoir to force the sample back through and allow the experiment to be repeated multiple times with the same sample.[39-40]

Cross-slot flow has many similarities to flow encountered in industrial processing.

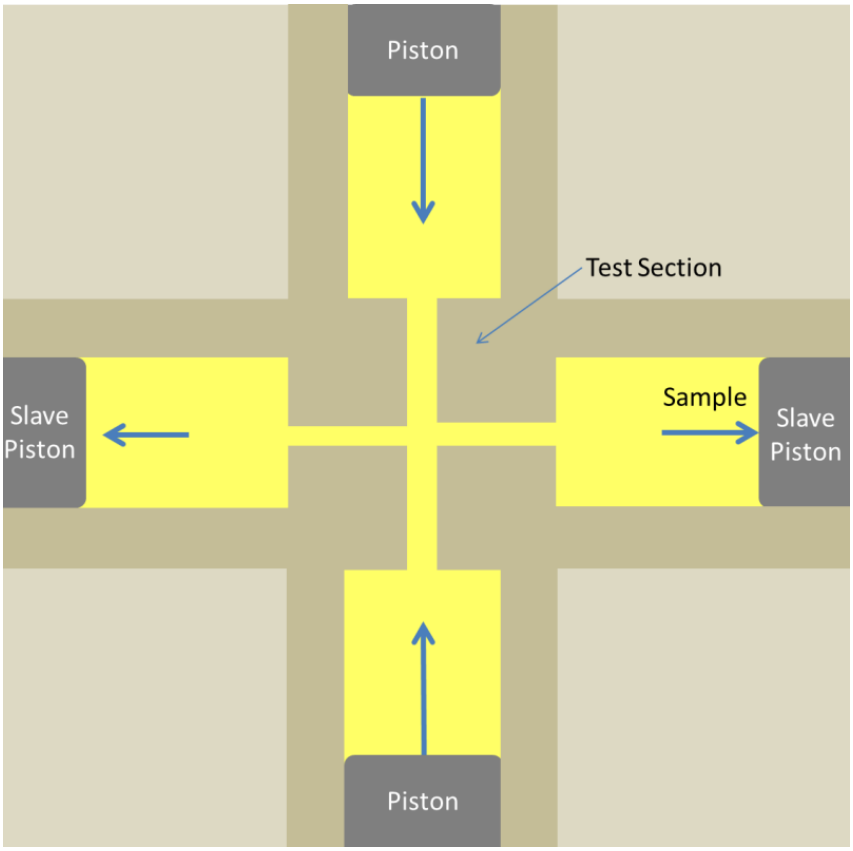

Figure 1.9: Illustration of cross-slot flow in the MPR. The top and bottom pistons are driven inward forcing polymer out via the reservoirs at the sides.

Being forced into a small narrow capillary generates areas of shear and extensional flow. A cross-slot test section has been used to rank the processability of polymers, showing that a commercial polydisperse polystyrene (PS) required lower pressures to process than a monodisperse polystyrene of similar weight average molecular weight. This demonstrates the importance of low molecular weight components in processability.[41]

The MPR is a versatile technique that has many direct uses in both industrial applications and in research into the behaviour of polymer flows. As of yet its use is still relatively novel and there are relatively few (around 20) of the instruments worldwide (many of which are not in operation), perhaps because of the time consuming nature of the sample preparation and the wide spread rheological techniques already established.

1.3 Modelling polymer rheology

The rheology of polymers is complex, depending on structural characteristics of the polymer, environmental conditions, nature of applied forces etc. Hence modelling polymer rheology is a complex task, but the field is very large and well advanced. Models for the rheology of monodisperse linear polymers are very well established. Synthetic techniques have allowed the production of polymers with very low polydispersity indexes $\left(\frac{M_w}{M_n} \leq 1.1\right)$ which have allowed developments in the study of their rheology and the ability to better test and develop theoretical models. This in turn has led to more advanced models for materials that are polydisperse in molecular weight and structure, as well as polymer blends.

Here constitutive models for predicting the linear rheology of linear and branched polymers will be discussed, however there are a massive range of other theories and simulation approaches available for prediction of more complex polymers (e.g. asymmetric branched polymers, block copolymers), rheology of blends and for predicting non-linear rheology (e.g. extensional rheology such as the results of multi-pass rheometer experiments[42]).

1.3.1 Linear polymers

One of the simplest models for polymer motion is the use of beads and sticks such as in the freely jointed chain model. This models a polymer chain as a series of beads joined by sticks, where the sticks have a fixed length and the beads a fixed size but the bond angles between them are free to change. The beads represent one or more monomer units, in this way the model is a coarse-grained version of an

atomistic version where each atom would be a bead and each bond a stick.[43] An expansion of this replaces the rigid sticks with springs, in order to model the viscoelasticity by combining the elastic springs with the viscous drag on the beads.

The Rouse model is the simplest version of the bead-spring model.[44] It models a polymer chain as a string of beads each a distance *b* apart, where each bead is a chain segment. The beads move according to random walk statistics and chain dynamics can be incorporated by giving each bead a local friction coefficient and a corresponding thermal energy.[45] This is analogous to the Maxwell model discussed in Section 1.2.1, the difference being that the Rouse model has a molecular basis for the assignment of springs and dashpots; the beads behave as viscous dashpots, and the string segments behave as springs. This leads to a dependence of the relaxation time on the chain length (or molecular weight) squared.

For long polymers, entanglements between polymer chains begin to become important, i.e. the chains no longer behave independently and their movement is restricted by neighbouring chains. The effect of this is the restriction of movement perpendicular to the chain length. Doi and Edwards[46-49] first proposed the tube model which incorporates this effect and is the basis for many modern models of linear polymer rheology. It considers all chains surrounding the selected polymer chain as one effective field, which acts as a tube around it, preventing any motion perpendicular to its chain length. It can therefore only relax via movement along its chain length, known as reptation, the simultaneous motion of all monomers in one direction. Reptation was incorporated into the model by de Gennes.[50] This is analogous to replacing the chain with a flexible rod of fixed length and only one degree of freedom. The chain ends are not affected by these topological constraints from other chains so, via reptation, can occupy new tube segments selected from an isotropic distribution and hence undergo relaxation (see Figure 1.10).

Using the reptation approach, the reptation relaxation time is dependent on the cube of the chain length (or molecular weight). However, experimentally, the relaxation

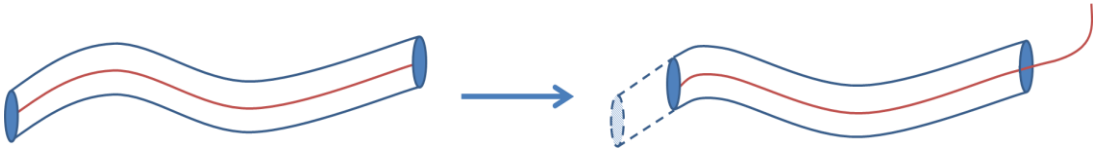

Figure 1.10: Illustration of a polymer chain (red) trapped inside a tube as in the tube model, the subsequent image shows the polymer having undergone reptation, relaxing the one chain end (which is now free to move outside the tube) and "forgetting" the section of tube at the opposite end which it no longer occupies, so there would be no penalty for reptation back in the opposite direction (it would never reoccupy the tube)

time is found to have a dependence on chain length to the power of 3.4, and further improvements to the model are required to obtain this result. The main two advances in this model have been the incorporation of constraint release and contour length fluctuations, both of which were discussed by Doi and Edwards but not included in their model.

Constraint release is essentially allowing movement of the tube in tube theory. Because the tube is made up of other chains, it is not fixed. De Gennes[51] suggested that tube motion would be similar to Rouse-like motion, and it is frequently modelled in this way. Allowing the surrounding polymers to move will mean that occasionally, part of the tube will be removed, and the polymer of interest will have an additional path to relax. Incorporation of this effect gives a dependence of relaxation time on molecular weight that matches experiment.

Contour length fluctuations are a process of relaxation most important for small chains. The pure reptation picture assumes the length of the chain is constant, but in reality the polymer can contract and expand. In the model this is essentially the process of the beads in the chain moving closer together or further apart (see Figure 1.11). The chain can therefore contract within the tube, and stretch out again, "forgetting" the original orientation of the ends, relaxing the stress in aligning the chain ends.[52]

Milner-McLeish theory adds contour length fluctuations to the Doi Edwards model.[53] Likhtman and McLeish[52] further developed this model by adding the effect of both constraint release and contour length fluctuations. The derived equation for the relaxation modulus (G(t)) is:

$$G(t) = G_e\left(\frac{4}{5}\,\mu(t)R(t) + \frac{1}{5Z}\sum_{p=1}^{Z-1}\exp\left(-\frac{p^2 t}{\tau_R}\right) + \frac{1}{Z}\sum_{p=Z}^{N}\exp\left(-\frac{2p^2 t}{\tau_R}\right)\right) \qquad (1.13)$$

where t is time, G_e is the entanglement modulus, Z is the number of entanglements and τ_R the Rouse time. $\mu(t)$ is the tube-segment occupation function, representing

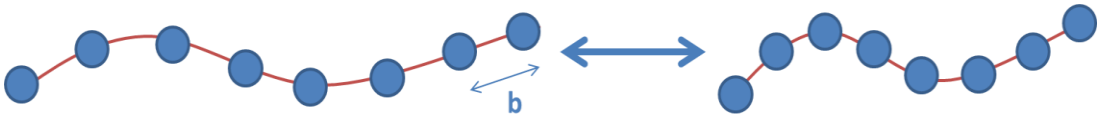

Figure 1.11: Simple reptation models the polymer as a string of beads separated by distance b as illustrated, however contour length fluctuations incorporate the contraction and stretching of the polymer chain as shown, which can also act as a mode of relaxation, especially important for short chains

escape from the tube by reptation including the effect of contour length fluctuations, $R(t)$ is the relaxation function of the tube, i.e. representing the effect of constraint release. The second term represents longitudinal relaxation and the third fast Rouse relaxation. They found this produced a model that worked well for polystyrene, but less so for polybutadiene. The reason for this is not clear but could be attributed to the variation in microstructure of polybutadiene which could act as an effective polydispersity, or the difference in packing length (the molecular diameter of the repeat unit in the chain)[54] between polybutadiene and polystyrene. The theory does not account for this difference which could change the effect of contour length fluctuations.

Further improvements are made in the Graham, Likhtman, Milner and McLeish (GLaMM) Theory, which is based on the same improvements to Doi-Edwards theory but extends the model into non-linear regions (i.e. extensional measurements, steady shear) by treating the constraint release on a local scale.[55]

Although GlaMM theory provides a rigorous approach to non-linear rheology, it is computationally complex, and so difficult to apply to complex flow simulations. Hence, it has been approximated for a single mode as the Rouse linear entangled polymers or rolie-poly model [56] For one mode this has the equation:

$$\frac{d\boldsymbol{\sigma}}{dt} = \boldsymbol{\kappa}.\boldsymbol{\sigma} + \boldsymbol{\sigma} + \boldsymbol{\kappa}^T - \frac{1}{\tau_d}(\boldsymbol{\sigma} - \boldsymbol{I}) - \frac{2\left(1 - \sqrt{\frac{3}{tr\boldsymbol{\sigma}}}\right)}{\tau_R}\left(\boldsymbol{\sigma} + \zeta\left(\frac{tr\boldsymbol{\sigma}}{3}\right)^{\delta}(\boldsymbol{\sigma} - \boldsymbol{I})\right) \qquad (1.14)$$

where $\boldsymbol{\sigma}$ is the polymer stress tensor, (in units of the entanglement modulus), t is time, $\boldsymbol{\kappa}$ is the velocity gradient tensor, ζ is a factor determining the convective constraint release, δ determines the suppression of CCR by chain stretch, $tr\boldsymbol{\sigma}$ is the amount of chain stretch and $\boldsymbol{I}$ is the equilibrium value of the stress tensor. τ_R and τ_d are the Rouse and reptation times respectively.

Since the model is simplified to one mode with a single relaxation time, several modes must be used to capture experimental data, and must be fit to the data (oscillatory shear and extension if chain stretching is relevant). Despite requiring experimental data, approximating the rheology to a series of modes makes the model computationally much simpler, and so it can be applied to complex geometries (cross-slots, extruders etc.) and be used to map the stress and flow, which is not possible with other models. Multiple modes must be combined to capture the relevant behaviour in the experimental data. A program, FlowSolve has

been developed that can use this equation to predict the flow through complex geometries.[57]

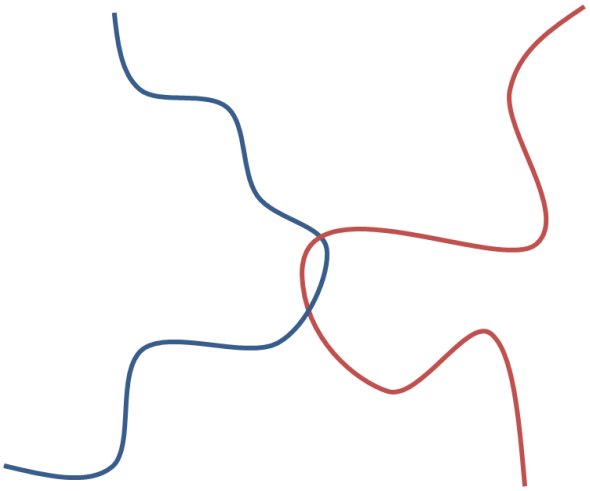

Figure 1.12: Illustration of a stress point in the double reptation model. When either polymer can reptate past the entanglement, the stress is fully relaxed

An alternative method for treating constraint release to that used by Milner, Likhtman and McLeish (modelling the tube motion as moving with Rouse like behaviour) is double reptation.[58] It assumes there is a random distribution of 'stress points' along the polymer, where it is entangled with another chain (see Figure 1.12). These are considered fully relaxed when the shorter of the two chains involved can move its free end past the entanglement.[59] For linear polymers this allows prediction of the rheology of polydisperse polymers as well as the inversion of a measured linear viscoelastic spectrum to obtain the molecular weight distribution.[60]

1.3.2 Branched polymers

A similar tube approach can be taken towards branched polymer modelling. However, polymers with a branch point cannot relax via reptation, as there is no single path along which they can move. One method by which they can relax is arm retraction (see Figure 1.13). The chain ends move further into the tube and then out again, again essentially "forgetting" the section of the tube it retracted along, however this process is entropically unfavourable. The other basic process by which they can relax is branch point diffusion, (see Figure 1.14), however movement of the branch point is highly entropically unfavourable and hence slow, especially for polymers with more than 3 arms.[61-62]

Pearson and Helfand[63] had previously calculated the dependence of zero shear viscosity on molecular weight using the tube model for branched polymers as,

$$\eta_0 \approx \frac{M_a^{\frac{1}{2}}}{M_e} \exp\left(\kappa \frac{M_a}{M_e}\right) \qquad (1.15)$$

where M_a is the molecular weight of the arms, M_e is the molecular weight between entanglements, and κ is a dimensionless number which the tube model predicts as 15/8. Experiments confirmed this exponential form but find κ as 0.6. This difference

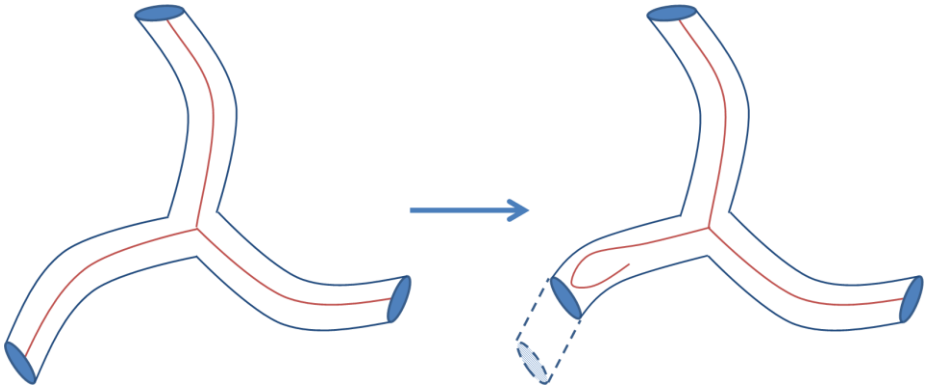

Figure 1.13: Illustration of arm retraction in a 3 armed star polymer in the tube model

implies that for a given viscosity, there are actually fewer entanglements (i.e. higher M_e) than the tube model predicts, hence there is another method of relaxation present.

Ball and McLeish[64] developed the dynamic dilution model for star polymers. This accounted for the difference between experiment and tube model predictions for star polymers. To account for this, another process was introduced, similar to constraint release in linear polymers; the neighbouring chains (i.e. the tube) were allowed to diffuse and move providing an alternate relaxation pathway. The dynamic dilution model also allows the relaxed chains to act as a solvent for the remainder, stress then falls with the square of the unrelaxed chain length. For very long arms, this approaches a step function between the Rouse time and the time scale for complete relaxation of an arm. This approach is more relevant to branched polymers than linear, where the difference in relaxation times between segments is too small for it to apply. This dynamic dilution approach explains the experimental discrepancies in viscosity, recoverable compliance and relaxation modulus of star polymers.[65-66] It assumes that the branch point is fixed, and arm lengths are equal, and needs modification if these assumptions are not true. Adams *et al.*[65] applied the dynamic dilution model to a range of star polybutadienes and showed good fits. There was only deviation at high frequencies, which was attributed to the onset of the glass transition (T_g). These frequencies were recorded at temperatures of -75 to -65 °C which are approaching the T_g and in this region G'' was seen to increase faster than predicted.

Larson and McLeish[67] developed this model including arm retraction and dynamic dilution, to include linear, star and comb polymers by considering them all as special cases of a 'Pom-Pom' polymer, i.e. a polymer with a backbone and a branch point at each end. Hence for a linear polymer, the arm length would be zero leaving only the

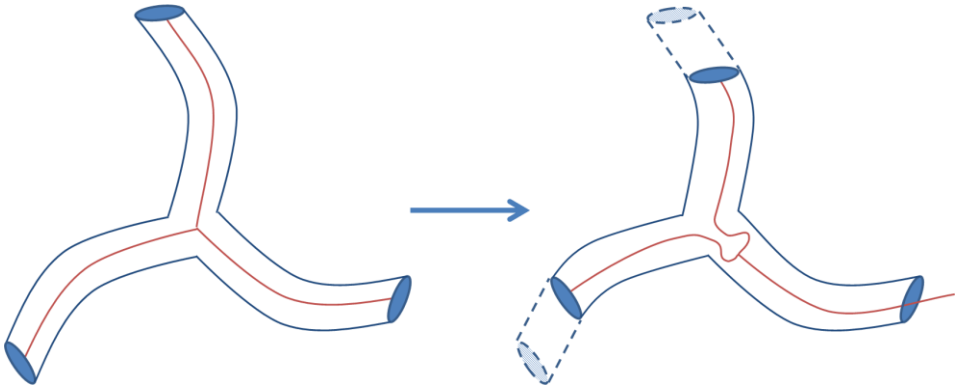

Figure 1.14: Illustration of entropically unfavourable branch point diffusion in a 3 armed star polymer in the tube model

backbone, whereas for a star the backbone length would be zero leaving the arms around a single branch point. This simplification means that fitting to linear rheology and extension is required to determine a series of relaxation times of different modes in a similar way to rolie-poly theory.[45] However this also allows the Pom-Pom model to be used in complex geometries with the Flowsolve program. This model was extended to include chain retraction at the chain ends[68] and was applied to lightly branched polyethylenes by negating additional branch points on the arms.[69]

Das *et al.*[70] have developed a model that can deal with highly branched material. Their 'branch-on-branch' (BOB) theory works for a greater range of polymers, including those with hierarchal branch points, but is made a little more computationally complex, so is less suited to use in complex geometries. However it gives very good predictions for linear, star and branched polymers and their blends, and hence has the potential for distinguishing polymer architecture from rheological data, although it's effectiveness in determining structure has not yet been evaluated. The main limitation of this model is that it uses a single set of materials parameters for the predictions, and so cannot be applied to blends of polymers with different chemistry.

1.3.3 Dimensionless numbers – Weissenberg and Deborah

Using these models, characteristic relaxation times can be extracted for relaxation via a given pathway. For example, for linear polymers important parameters are the reptation relaxation time, τ_D (the time taken to reptate out of the 'tube' of entanglements as discussed) and the Rouse relaxation time, τ_R (the time taken to relax via Rouse motion when individual chains are distorted).

When comparing these results to experiment, useful quantities are the dimensionless Deborah and Weissenberg numbers, which are defined as:

$$D_e = \tau_i \dot{\delta} \tag{1.16}$$

$$W_i = \tau_i \dot{\delta} \gamma \tag{1.17}$$

where τ_i is the relaxation time of the pathway (e.g. Rouse motion or reptation), γ is the strain applied and $\dot{\delta}$ is the rate of deformation (e.g. for shear rheology this is the shear rate, or for extensional tests it is the extension rate). The Weissenberg number takes into account the strain of the measurement as well as the strain rate, which can be important in some situations, but for steady shear/extension measurements the measures can be assumed to be equivalent. The values of these numbers allow the rates of relaxation and deformation to be compared. When below 1, the material is relaxing faster than it is being deformed and when exceeding 1, the rate of deformation is faster than relaxation, and so stress builds up in the material.[71]

1.4 Polymer blends: miscibility and phase boundaries

Polymer blends are important in a wide range of applications; many materials used commercially are blends of two or more types of polymer. Also as many commercial polymers are polydisperse, they are miscible blends of different molecular weight chains and this distribution greatly affects their properties.

Polymer blends generally fall into three categories; miscible blends that are thermodynamically stable and form a blend with a single glass transition temperature, immiscible blends that are thermodynamically unstable and will eventually separate, and compatible blends, which are immiscible but stabilised by additional components or interactions between functional groups.

The miscibility of polymers is highly dependent on temperature, and blends have a lower critical solution temperature (LCST), meaning they phase separate on heating or upper critical solution temperature, (UCST) meaning they compatibilise on heating. Occasionally both LCST and UCST behaviour is seen for 1 blend, as shown in Figure 1.15. There are two curves for each, the spinodal and binodal curves. The spinodal curve encloses the region which is thermodynamically unstable, so inside this region the two polymers will spontaneously phase separate. However the binodal curve, or the coexistence curve represents the region in which more than one phase exists. Hence in between these two curves the mixture will be

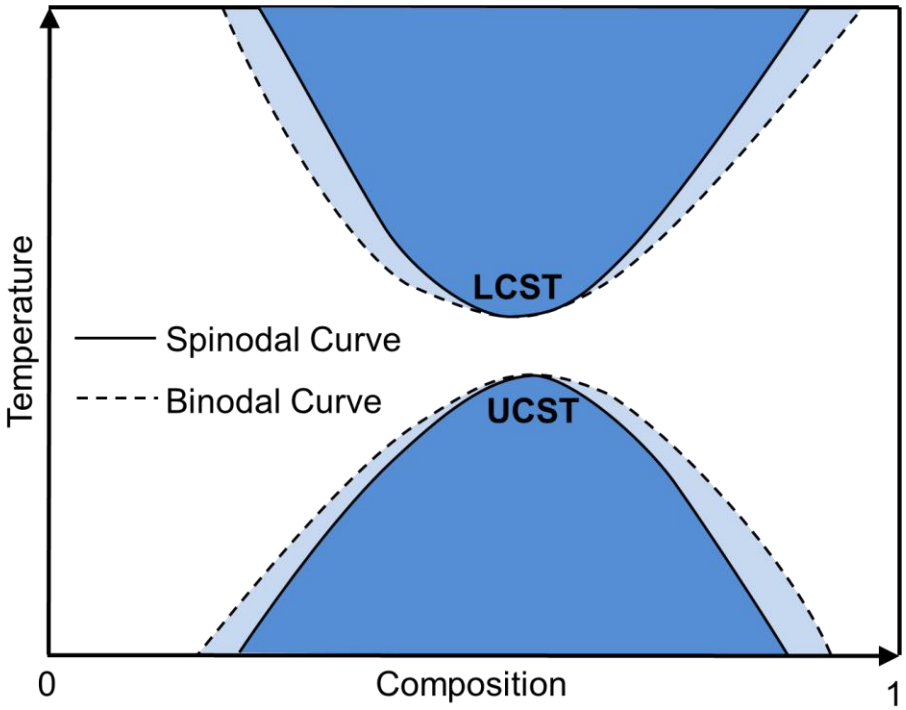

Figure 1.15: Illustration of lower and upper critical solution point blends, where the dark blue regions are unstable to spinodal decomposition and the light blue are binodal (multiple phases coexist)

metastable and can exist as a single phase because there is an energy barrier to phase separation.

Modelling the rheology of polymer blends is still a difficult task. As discussed, many theories are available for homopolymers and their blends, but a model for heteropolymer blends remains elusive, because of the unclear effect of the polymer mixture on tube dimensions and relaxation times. Some attempts have been made to model miscible linear polymer blends using constitutive models, such as poly(vinylethylene) and polyisoprene blends[72], which do agree with experiment. However this model makes several assumptions about the system (e.g. that the tube is the same for each component) and hence only works for some systems and the underlying dynamics is not well enough understood to incorporate the effects of immiscibility and polymer structure.

However this does not mean that rheology of polymer blends cannot give us any insight into the polymer properties; in particular it can be used to locate the transition between miscibility and immiscibility and study the phase boundary.

1.4.1 Flory-Huggins theory

Flory-Huggins theory can be used to describe the miscibility of a polymer blend. It is an expression for the free energy of mixing in polymer systems, where the

thermodynamics of mixing are dependent on the Flory-Huggins interaction parameter, χ determined from experiment.

The expression for the free energy density of mixing two polymers, a and b, is,

$$\frac{\Delta G_m}{kT} = \frac{\phi ln\phi}{v_a N_a} + \frac{(1-\phi)\ln(1-\phi)}{v_b N_b} + \frac{\chi\phi(1-\phi)}{v_0} \quad (1.18)$$

where N_i and v_i are the number of monomers in a chain and the volume of a single monomer for polymer i respectively. ϕ is the volume fraction of component a, ΔG_m is the free energy of mixing per unit volume, k is the Boltzmann constant, T the absolute temperature and v_0 is an arbitrary reference volume.[73]

From this the spinodal curve can be calculated, the curve enclosing the region where the homogenous mixture is thermodynamically unstable, as well as the binodal curve, the locus of points at which the mixture is at thermal equilibrium. The spinodal curve is simple to calculate whereas the binodal curve requires numerical methods.[74]

χ values are temperature dependent so are usually fit to a quadratic function, where,

$$\chi(T) = A + \frac{B}{T} + \frac{C}{T^2} \quad (1.19)$$

using χ at a range of temperatures, A , B and C can be found through fitting.[75-77] These parameters have been recorded for a range of polymer pairs and so can be used to predict the phase behaviour of many systems. In some cases, χ is linearly dependant on $\frac{1}{T}$ so C is negligible and this has been found for many hydrocarbon polymer pairs.[78]

1.4.2 Rheology near the phase boundary

Miscibility affects the rheology of a blend, as rheology is not only changed before and after phase separation, but also when close to the phase boundary. Knowledge and control of this is important at the range of temperatures used in polymer processing. For example in order to recycle plastics, they are usually melted and reformed and if this takes a polymer blend through a phase boundary it can significantly change the properties of the final product.

Changes in rheology can be used to distinguish the phase boundary of systems and construct phase diagrams; this is particularly useful in systems such as polyisoprene and polybutadiene where the refractive indexes of each polymer are so similar the

phase separation cannot be seen by turbidity measurements (although light scattering can usually be used).

Kapnistos *et al.*[79] used turbidity measurements to determine the phase diagram of polystyrene (PS) and polyvinyl methyl ether (PVME) and then studied the rheology near the boundary. The constructed phase diagram showed that the system phase separated on heating and a large difference in rheology was noted when the phase boundary was approached. They used a temperature ramp (i.e. oscillating at a set frequency as the sample is heated) at a slow heating rate (0.1 or 0.5 °C/min) and low frequency (0.1 - 0.5 rad/s). Here, there are three relevant contributions to the elastic modulus. Firstly, the bulk contribution resulting from chain dynamics and entanglements, secondly, concentration fluctuations caused by thermal noise, and finally interfacial contributions that arise when there are phase separated domains. In the miscible region, increasing temperature caused a decrease in G', i.e. the elastic modulus decreased because of increased mobility of the polymer chains. In this region the bulk contributions dominate. However, as the phase boundary was approached, the trend in G' was seen to reverse. As temperature increases, the amplitude of concentration fluctuations also increases. Near to the phase boundary, as domains of the 'hard' component (here PS) are formed, the interfaces also begin to have an effect. The interfaces and concentration fluctuations dominate over the mobility effects, causing an increase in G'. As the boundary is passed, and no additional interfaces are created, the bulk mobility again begins to take over and the viscosity again begins to decrease with temperature. This effect was most pronounced for G' but variation in G'' was also noted at the same temperatures. [79-81]

Kapnistos also observed good agreement between phase separation temperatures obtained from turbidity and the temperature of the point of inflection in the G' curve, suggesting rheology alone can be used to obtain a phase diagram. In a later paper, he discussed how rheological measurements could be used to determine the spinodal temperature, by extrapolation of a $\left(\frac{G''^2}{G'T}\right)^{2/3}$ vs $\frac{1}{T}$ graph and the binodal temperature could be determined more accurately using a G' vs T graph.[80]

This effect was also observed for mixtures of PI/PBD by Zhang *et al*.[82] and by Zou *et al.*[83], who also discussed the use of temperature ramps to determine the spinodal and binodal temperatures, using the minimum in G' as the binodal temperature. They noted that small shifts in the binodal point can be caused by different heating rates and that extrapolation of the spinodal point to low frequencies is required to

avoid the shift caused by critical fluctuations. Both PI/PBD and PS/PVME are lower critical solution temperature blends; they are miscible at low temperatures and phase separate on heating.

Liu *et al.*[84] studied the dependence of G' on measurement time for polyisoprene-polybutadiene blends and found that it was flat in the one phase region but was complicated by effects of the interfacial tension near to and after the phase boundary and so this is also a potential method for identifying the transition using rheology.

1.5 Large amplitude oscillatory shear rheology

Using large strains in shear rheology is a natural progression from conventional tests. The most common methods for measuring shear rheology utilise small amplitude oscillatory shear (SAOS). However, the majority of industrial processes (e.g. mixing, extrusion) that are commonly modelled using results from these tests, involve much higher strains that are well outside the linear viscoelastic region.

When a strain is applied that takes the sample outside the linear viscoelastic region, the response is no longer simple. At these strains, higher harmonics must be added to the linear oscillatory response (Equation 1.4) i.e. the resulting wave is a combination of waves at multiples of the applied frequency. It can be shown[85-86] that the shear stress will only contain contributions from odd harmonics. This results from the assumption that the sign of the stress changes with the sign of the strain, i.e. in oscillatory shear, the magnitude of the stress will be independent of the shear direction, but reversing the direction of the strain will reverse the direction of the stress. Hence only odd terms can contribute, which are dependent on the sign of the input strain, unlike even powers, where the sign cancels out. This assumption can be broken however by inhomogeneous flow in the geometry, (i.e. wall slip, instabilities, secondary flows), which can lead to the presence of even harmonics.

LAOS as a technique has been around as a concept for some time, with investigations into nonlinear behaviour being undertaken in the 1960s and 70s. One of the most well-known non-linear phenomena is the Payne effect, where the modulus of a filled rubber is seen to be dependent on the strain amplitude. However, progress into defining a standard method for using LAOS has been slow and although there is a large amount of research into the area, it is fragmented by the approaches taken. The reasons for this lie with both the experiment and the interpretation of the data. Experimentally, LAOS is very difficult, an excellent data

transfer rate is required to maximise the signal/noise ratio and observe the higher harmonics. Therefore shear rheometers are most commonly used, as modern models can provide such transfer rates (up to 1000 Hz). However their open sides mean that LAOS measurements frequently cause issues such as edge fracture, wall slip, and samples escaping the gap. Although all these phenomena are interesting and are the focus of many alternative studies[21, 87-89], they are undesirable because they are hard to separate from the non-linear behaviour of a polymer in the LAOS region. These problems can also lead to difficulties in reproducibility and lead to results that are very dependent on the sample loading and history. The use of a closed cavity geometry has been demonstrated which reduces these effects, through adapting a rubber process analyser but it requires a specialist setup, and the flow in the device deviates somewhat from simple shear.[90]

LAOS is also complicated because there is not a simple interpretation of the results. There are various methods for analysing LAOS data and with each there are complications with interpreting the results. The simplest way of interpreting LAOS experiments, without requiring any specialist software or equipment, is using the elastic and viscous moduli, G' and G'' respectively'. In amplitude sweeps, Hyun[86] has defined four types of response in terms of the behaviour of G' and G''. It can be classified as strain thinning, where both G' and G'' decrease with strain (as in Figure 1.16) or strain thickening, where both increase with strain. The further two types of behaviour are a weak strain overshoot, where G'' increases to an initial maximum before decreasing with higher strain, and a strong strain overshoot, where both G' and G'' show this maximum.

Strain thinning in shear is usually observed in polymer melts and solutions, and can be attributed to alignment of the polymer chains with the flow, decreasing entanglements in the sample. Strain thickening is less common and arises from complex interactions such as gelation induced by the shear. Strain overshoots are caused by competing effects, e.g. in a filled polymer, where filler-polymer interactions can be broken by the strain because the polymer behaviour dominates. Other types of behaviour have also been noted (such as minima and local minima in G' and G''), the origins of which are more complex.[91-93] Although this method is the simplest way of interpreting LAOS behaviour, it neglects the effect of all harmonics other than the first. The first harmonic is always dominant (for example, the third harmonic is shown to reach a maximum of 13 % of the magnitude of the first[91]) and so this is a useful way to observe LAOS behaviour without introducing the difficult

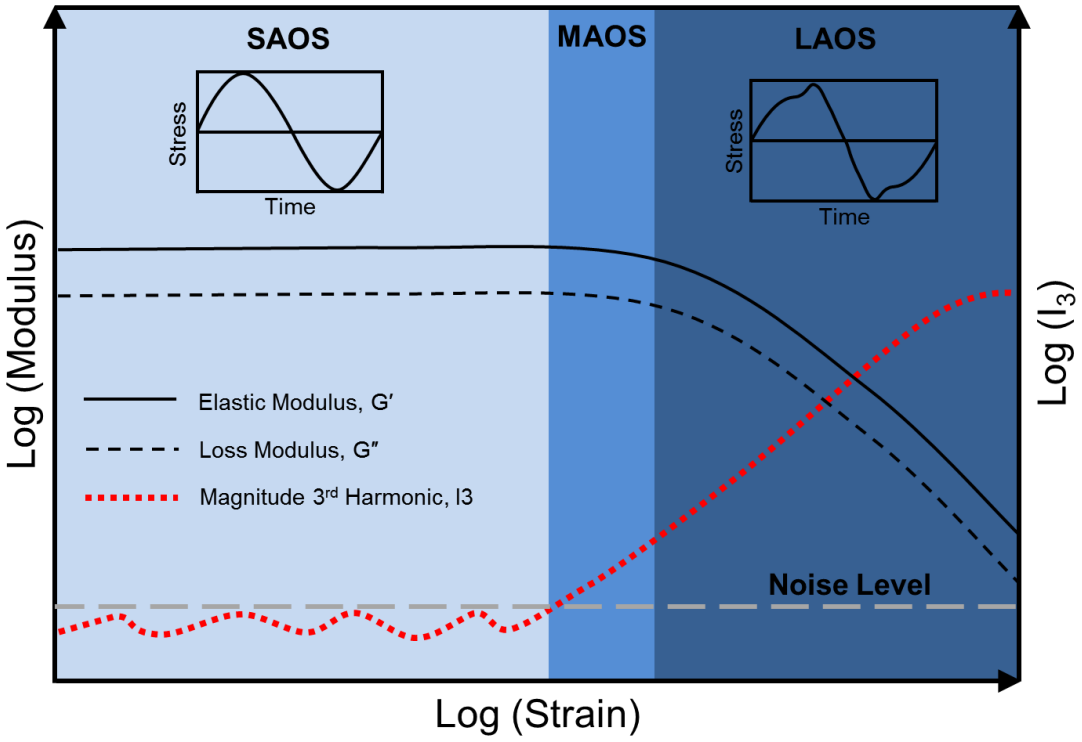

Figure 1.16: Illustration of an amplitude sweep for a strain thinning fluid, showing the transition from SAOS to LAOS behaviour, and the corresponding drop off of the linear moduli and increase in the third harmonic. Inset are example stress signals in the SAOS and LAOS regimes.

interpretation of higher harmonics. However the higher harmonics must be examined to obtain more detailed information about the behaviour.

Fourier transform (FT) analysis has recently become one of the most favoured methods for analysing LAOS data.[94] Decomposing the output stress into its component frequencies allows the odd harmonics to be easily identified and their magnitudes and phases extracted. The third harmonic is commonly reported to be highly dependent on the structure of the underlying polymer.[95-97] Most recent work concentrates on the magnitude of this harmonic, I_3 (often normalised by the magnitude of the first giving I_3/I_1), although it can also be separated using the phase into $G3'$ and $G3''$. Notably, the gradient of I_3/I_1 is observed to be 2 in the MAOS regime (arising from a dependence of I_3 on strain cubed and of I_1 on strain), however this gradient is seen to decrease when the polymer has a branched structure.[95-97] However, these scaling relationships are almost exclusively observed at low Deborah number and there has not been a definitive study on the effect of D_e on the scaling. For example, Niedhofer[98] observed the scaling of I_3/I_1 with strain to be less than 2 for linear polystyrenes, conducting experiments at low Deborah numbers (0.03 and 0.12), but even between these two small Deborah numbers, differences in gradient were observed. In later work, the behaviour of both I_3 and the

phase were shown to vary dramatically with Deborah number for linear polystyrene solutions.[99]

The I_3/I_1 vs strain data gathered by Höfl et al.[100] showed a power law gradient of around 1.7 for a linear 55k polyisoprene and 1.8 for linear 80k polyisoprene. The 55k PI could be seen to have a crossover point at 11.45 Hz at 283 K, however the measurement was performed at 1.6 Hz at 268K, which using a WLF shift gave a Deborah number of 0.82. The crossover point for the 80k PI is 8.24 Hz at 298 K which gives a Deborah number of 0.30 at 1.6 Hz and 293K. In theory, Giacomin[101] predicts to see third to first harmonic power laws of 2 (and fifth to first harmonic ratios giving a power law of 4) for polyisoprene up to D_e = 10, however experimental results are only obtained for D_e ~ 0.1.

Results at higher frequencies have also been reported, for example Poulos et al.[102] examined star like micelles of PEP-PEO block copolymers. They found that when $G'' > G'$ (i.e. D_e < 1), the slopes of I_3/I_1 were < 2 and were highly dependent on the frequency used. However when $G' > G''$ (i.e. D_e > 1) the slope was much steeper and the results were much less dependent on frequency.

It is clear that these low Deborah number tests give signatures of branched topologies in polymer melts, but Deborah number has to be carefully controlled to ensure consistency. Comparisons of the behaviour at higher Deborah number have not previously been performed, and may provide more information. However, these comparisons are all reasonably qualitative, because other than the magnitude of I_3 giving a measure of the non-linearity of the signal, no clear physical interpretation has been made of the third harmonic, as is done with G' and G''.

The stress response itself can also be examined.[103] Lissajous curves can be plotted (stress vs strain) for each point, with these giving an ellipse in the linear regime, and beginning to vary from this shape as non-linearities appear. This has the downside that it can be difficult to quantify this analysis and it is time consuming to graphically analyse every point. Cho[103] extended this type of analysis to a 3D surface, plotting stress against strain and strain rate normalised by frequency. This leads to plots that are a plane in the linear regime, but are no longer flat when the behaviour is non-linear. They also proposed a decomposition of the stress into elastic and viscous stresses which in many ways is analogous to a Fourier transform but offers more physical interpretation. However the polynomials used are not unique and so the coefficients depend on arbitrary choices in the fitting.

Another way of adding physical interpretation to LAOS measurements is using Chebyshev coefficients. Ewoldt *et al*.[104] report the decomposition of the stress using Chebyshev polynomials, which although giving results similar to Fourier analysis (and indeed the parameters extracted can be calculated from those resulting from FT rheology) offers some physical interpretation. Here e_3 and v_3 parameters are extracted where e_3 represents the strain response and v_3 represents the shear response (thickening or thinning depending on whether their sign is positive or negative respectively). e_3 and v_3 can be related to $G3'$ and $G3''$ as follows;

$$e_3 = -G3' \tag{1.20}$$

$$v_3 = \frac{G3''}{\omega} \tag{1.21}$$

Because the FT and Chebyshev coefficients are related in this way, the physical interpretation can be applied to standard FT results. $G3'$ will have an opposite sign to e_3, and $G3''$ the same sign as v_3 which leads to;

$$G3' \begin{cases} +ve : strain\ softening \\ -ve : strain\ hardening \end{cases} \tag{1.22}$$

$$G3'' \begin{cases} +ve : shear\ thickening \\ -ve : shear\ thinning \end{cases} \tag{1.23}$$

As well as the method of interpretation, the type of experiment also varies between studies. Typically in order to quantify LAOS behaviour, an amplitude sweep is performed at a single frequency. This has the advantage that the full range of behaviour can be observed from the linear to non-linear regimes. However a single frequency must be selected and, as in the linear regime, the behaviour of sample can vary dramatically with frequency. This also means it can be difficult to compare different samples to each other. For polymer systems, the Deborah number can be used to normalise measurements on samples with different relaxation times. This has the advantage that if we measure different systems at the same D_e, for simple systems (e.g. linear monodisperse polymers where reptation Deborah number can be calculated), the linear behaviour is identical and hence any differences in behaviour in the LAOS region can be compared. However, this also brings complications as there are many systems where relaxation times are not well defined (e.g. polydisperse polymers, complex architectures) and so it is more difficult to assign a Deborah number. Hence it would be advantageous to be able to observe this behaviour over a range of frequencies. One way of observing the

higher harmonics is by measuring rheology in the so called 'Medium Amplitude Oscillatory Shear' (MAOS) regime. This is defined as the region where G' and G'' appear linear but there is a measureable third harmonic. This allows us to study the third harmonic in a region where the behaviour of the first harmonic is consistent and repeatable. Performing measurements in this region of course gives limited insight into the behaviour at higher strains, but being able to observe the higher harmonics when the polymer is behaving linearly provides additional information that may give insight into the underlying polymer structure.

Hyun[105] has defined a parameter, Q, which corresponds to the intensity of the third harmonic divided by the first and then normalised by strain squared. Q should be strain independent if the scaling of the first and third harmonic behaves as expected in the MAOS region, which is seen for a range of linear and branched polymers. They have also defined a parameter Q_0, which is the value at the initial plateau observed in Q at low strains, calculated by extrapolating Q back to 0. The Q_0 from multiple experiments at different frequency can then be combined in order to produce a MAOS frequency sweep. 'Bounces' have been observed in these frequency sweeps that have been attributed to the level of branching in the polymer, as they were observed for stars and randomly branched materials but not linear polymers. It has also been shown that TTS can be applied to Q_0 results in the same way as for the linear parameters.[106-108]

There has even been Fourier analysis performed on capillary rheometry measurements. Filipe *et al*[109] used a specially designed slit with pressure transducers at three points along its length to measure the pressure inside the slit die, on a range of polyethylenes with different amounts of branching. When instabilities were present, these pressures fluctuated, and could be analysed by Fourier transform. This would give a single peak at 1 Hz when there were no instabilities and the pressure was flat with time, however when instabilities were present, different peaks were present depending on the type of instability (e.g. sharkskin, stick-slip, melt fracture), found at the inverse of the timescale of the instability. Materials displaying stick-slip behaviour showed peaks at less than 1 Hz, while those displaying sharkskin behaviour displayed frequencies of 2-6 Hz. They also correlated the amount of long chain branching, with the non-linearity in large amplitude oscillatory shear (measured in a rotation rheometer and closed cavity rheometer) and the instabilities in capillary flow. Higher long chain branching, lead to more non-linearity in LAOS, i.e. an earlier slip in rotational rheometry and a higher plateau of non-linearity (I_3/I_1) in the closed cavity rheometer (where slip was

suppressed), which in turn gave the most non-linear behaviour (stick-slip) in the capillary rheometer.

Cyriac *et al.*[110] expanded on this by using the same technique on a range of high density polyethylenes, to study the onset of 'sharkskinning' behaviour in extrusion (i.e. the extrudate becoming rough and uneven). However they concluded that slippage in a rotational rheometer could only be partially correlated with sharkskinning in extrusion due to the complexity of and differences between the two processes. It is possible that using a closed cavity rheometer to get the plateau of non-linearity would give a better indication of sharkskinning behaviour.

1.6 Pressure dependent rheology

The temperature dependence of rheology is well studied and TTS (such as in Equation 1.9) is routinely used throughout polymer rheology. However the pressure dependence of rheological properties is frequently ignored, despite being well known (e.g. there are numerous observations of the reduction in free volume and resulting increase in modulus with pressure [2, 111]). Part of this can be explained by the challenging nature of quantifying pressure dependence with standard instruments. Since rheological behaviour is usually studied on open systems (e.g. shear rheometers or capillary rheometers that extrude into open air), it is not possible to apply pressure to the material. Carrying forward these results into to simulations of industrial processes at high pressures (e.g. extrusion, injection moulding), ignoring pressure dependence could easily result in the selection of sub-optimal processing conditions. Since the pressure dependence of viscosity was first noted [112], numerous studies have explored the nature of this dependence in relation to features such as the glass transition temperature,[113] and free volume [114].

The relationship between pressure and viscosity can be quantified using the Barus or pressure coefficient, which at a given temperature, is defined by the Barus equation:

$$\beta_T = \frac{d\, ln(\eta)}{d\, p} \tag{1.24}$$

where η is the steady state viscosity, p the applied pressure, and β_T is the Barus or pressure coefficient at the experimental temperature.

Pressure coefficients have been documented for a range of materials under various environmental conditions, (e.g. polyethylene (PE) [115], polymethyl methacrylate (PMMA) [115], PS [115-118]). The most common method to measure the dependence is

using a modified capillary rheometer, with a back-flow regulator to maintain the pressure at the outlet.[119] However some studies also make use of slit rheometers, for example Volpe *et al.* [117] performed narrow slit experiments using an adapted injection moulding apparatus Kadijk and van der Brule[120] used a slit with pressure transducers mounted along the slit wall in order to remove the effects at the slit entrance and exit.

Pressure dependence of viscosity has generally been found to be greatest for materials that are close to their glass transitions, where it may be expected that a small change in free volume has a large influence on polymer chain dynamics.[113] The results are also highly dependent on the chemistry of the polymer, Sedlacek *et al.*[115] observed that polyethylenes, having a highly regular structure, show less response to pressure than more disordered polymers. For example, adding branching increases the dependence on pressure and β is measured as 10.36 GPa^{-1} for HDPE at 170-210 °C but a great value of 18.33 GPa^{-1} is found for branched LDPE at 150-190 °C. Polymers with bulky side groups showed even greater pressure dependencies (e.g. 43.45 GPa^{-1} for PS at 162-242 °C and 43.57 GPa^{-1} for PMMA at 230-250 °C). Hence it appears that free volume is the most significant contributor to the pressure dependence, rather than factors such as proximity to a melting transition. A similar trend is well established for the temperature dependence of relaxation time, whereby increasing temperature increases free volume.[115, 121-122]

Despite its wide use, there remains substantial debate on the universality of the β parameter. The pressure coefficient has separately been reported to be both dependent and independent on temperature, pressure, shear rate, and whether shear or extensional viscosity is examined. Other coefficients have been proposed that encompass these dependencies (e.g. on shear rate[119]), but pose extra challenges to verify experimentally.

As well as the change in viscosity, some simulations[123-124] and dielectric experiments[125] have shown a corresponding increase of the relaxation times of polymers with increasing pressure, and shown that the pressure dependence cannot be ignored. This is an important consideration for high pressure processes such as injection moulding, because residual stress in polymers can lead to significant problems of ageing and mechanical weakness in products.

A potential method of analysing the pressure dependence of rheology is using the MPR. The applicability of a multi-pass rheometer for studying rheology under

pressure has previously been established.[27, 30] The effects of pressure on steady shear and oscillatory viscosities have been examined previously, however early experiments did not have the capability to observe the sample optically and analyse the relaxation of stress.

1.7 Scope of project

This project aims to further understanding of the relationship between the rheological properties of polymers and their underlying structure. Starting from model systems rheological complexity has been built up to enable predictions for industrially complex mixtures relevant to tyre processing and manufacture. The ultimate goal is to add rheological techniques to the suite of characterisation methods used by synthetic polymer chemists in order to extract further information about the structure of reaction products.

Polymers which are representative of the tyre industry have been used (e.g. polyisoprene, the main component of natural rubber, polybutadiene, the most commonly utilised synthetic rubber and polystyrene, a component in styrene-butadiene rubber (SBR)). Initially studies were performed on linear monodisperse polymers, before examining branched structures, creating blends and polydisperse mixtures.

Small amplitude oscillatory shear tests have been performed on a range of architectures. Models such as those discussed have been applied and compared to rheological data. *Via* this method, their predicative capacity could be examined, both in predicting the rheology of a well-defined polymer, and in reverse, extracting parameters such as polymer relaxation times, molecular weights and structure from experimental data. These comparisons are detailed in Chapter 2.

As well as SAOS rheology, extensional rheometry will be used to explain behaviour in the processing steps (e.g. extrusion). The multi-pass rheometer and large amplitude oscillatory shear experiments will be used to produce conditions analogous to processing and to gain additional information about the underlying structure of the polymers.

Extensional rheology adds further potential for distinguishing polymer structures, because of the sensitivity of the extensional behaviour to multiple branch points in the sample. Extension will be characterised by various methods, using the Sentmanat extensional rheometer, the capillary breakup extensional rheometer (which has not been previously used for polymer melts) for lower viscosity materials

and *via* novel falling weight rheometry. The advantages and limitations of these methods will be discussed as well as the predicative capacity of extensional behaviour in general, which constitutes Chapter 3.

Chapter 4 examines complex flow situations, consisting of combinations of shear and extension, which are achievable using the multi-pass rheometer apparatus. Using contraction-expansion geometries, which are dominated by shear and the shear rates are well defined, novel stress decay measurements can be performed, and the relaxation times of materials extracted in a single measurement. This technique is demonstrated for linear polydisperse material and is used as a new way to measure the effect of shear rate and pressure on the relaxation times of polymer melts. Extensional behaviour, measured using cross-slot apparatus will also be discussed. Here the flow is again complex, but produces a stagnation point at the centre where pure extensional flow is generated, this allows extensional measurements for systems that may not be possible by other means.

As discussed, using higher strains in shear rheometry, in LAOS and MAOS tests also has the potential for elucidating polymer structure. Amplitude sweeps that take the polymer from SAOS to LAOS behaviour are performed for a range of polymers under various conditions, in order to produce a consistent method which allows results to be compared and the effect of structure separated from that of test conditions, loading and sample history. Measurements are performed at high Deborah number which has not been reported previously. Frequency sweeps are also performed in the MAOS region for a range of linear polymers, stars and blends, which gives information about the Rouse behaviour of the polymers. These measurements are the first to report both phase and magnitude information for rubbery polymers in the MAOS regime, and provide a catalogue of materials for refining understanding of behaviour in this regime. These results are discussed in Chapter 5.

The results detailed here show that rheology is a multi-faceted technique that has great potential for identifying polymer structure, when the correct technique and analysis are applied relevant to the information required. The details of the information that can be extracted from different techniques are summarised in Figure 1.17. Rheology is a key technique that should form part of the suite of analysis techniques available to the synthetic chemist in order to best characterise polymers produced.

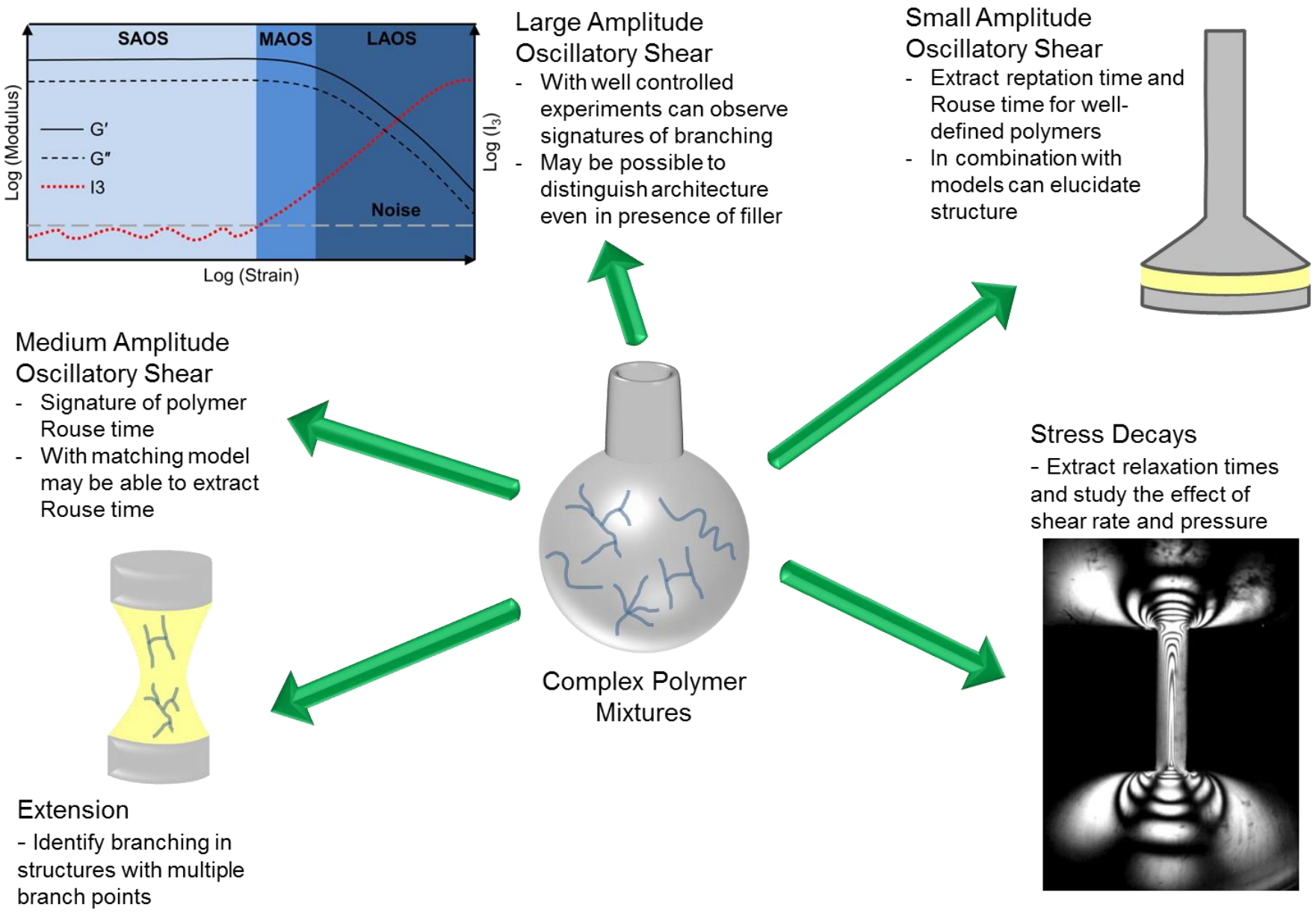

Figure 1.17: Scheme of different rheological techniques that can be applied to polymer melts and the information that can be extracted

2 Rheological characterisation by small amplitude oscillatory shear

Small amplitude oscillatory shear (SAOS) rheology is one of the most common methods of measuring the rheological properties of a material, especially polymer melts. The most common experimental method used is a frequency sweep, which as discussed in the introduction, gives the behaviour of a material with increasing deformation rate, and can be used to extract relaxation times for a polymer. In combination with molecular models, structural information can also be extracted. The aim of this chapter is to explore the capability of SAOS to extract molecular structure from rheology, and identify its limits. This will be achieved by studying the response in SAOS of well-defined systems and applying molecular models to the results, before attempting to solve the reverse problem

In this chapter, a range of linear and branched polybutadienes and polyisoprenes are characterised by SAOS frequency sweeps, and different rheological models are used to model and interpret the results. Branch-on-branch (BOB) theory, a key theory for branched polymers, is then applied to a range of star linear blends, which has been previously reported[126], but here the reverse problem is also tested to attempt to calculate the fraction of different components by fitting the rheology. Also characterised are randomly branched polymers and a fractionation is performed in order to get some insight into their structure. As well as homopolymers blends, a PI-PBD blend is examined and rheology used to detect the phase separation point of the blend. Finally, a brief study of the Cox-Merz rule is made on a linear polystyrene, to validate the application of the complex viscosities extracted from oscillations to problems involving steady shear.

2.1 REPTATE software

To avoid repetition throughout the chapter, the procedure for processing frequency sweeps in oscillatory shear will be given here. As discussed in the introduction (Section 1.2.1), in order to obtain a larger frequency range in the results, a common procedure in SAOS is the use of time-temperature superposition (TTS). Here, a Williams-Landel-Ferry (WLF) shift is used, which uses two parameters C_1 and C_2 to calculate a horizontal shift factor a_T and a further parameter C_3 to calculate b_T , the vertical shift factor according to the following equations:

$$\log(a_T) = -\frac{C_1(T - T_0)}{T + C_2} \quad (2.1)$$

$$b_T = \frac{(\rho_0 - TC_3.10^{-3})(T + 273.15)}{(\rho_0 - T_0C_3.10^{-3})(T_0 + 273.15)} \quad (2.\ 2)$$

where T is the experimental temperature, T_0 is the reference temperature the data is shifted to and ρ_0 is the density of the polymer at 0 °C.

This work makes use of the REPTATE[10] software package to perform these shifts. This has the advantage over many commercial rheometer software packages, of using a single set of parameters for all temperatures, rather than shifting each dataset to give the best overlap with the spectrum at the reference temperature.

The data from the rheometer was used an input, with a .OSC text file for each temperature in the form: Frequency (rad/s), G' (Pa), G'' (Pa), Temperature (°C). These files were loaded into the TTS module of REPTATE software as shown in Figure 2.1, and a WLF equation was selected and applied to the data, with the selected parameters, which can also be fit to give best overlap. This module can then output the shifted spectrum as a .TTS file, which has the same columns at the input file.

REPTATE software was also used for performing the majority of the fits of models to the data (with the exception of branch-on-branch theory, for which MATLAB code was written (see Appendix 2) as minimisation of this theory is not currently available in REPTATE. The rheological spectrum could be directly transferred to the linear viscoelasticity module after performing the TTS or a .TTS file imported. In this module a variety of models can be compared against and fit to the data. The model results with the chosen parameters can then be output in a .TTS file with the same columns as the input file

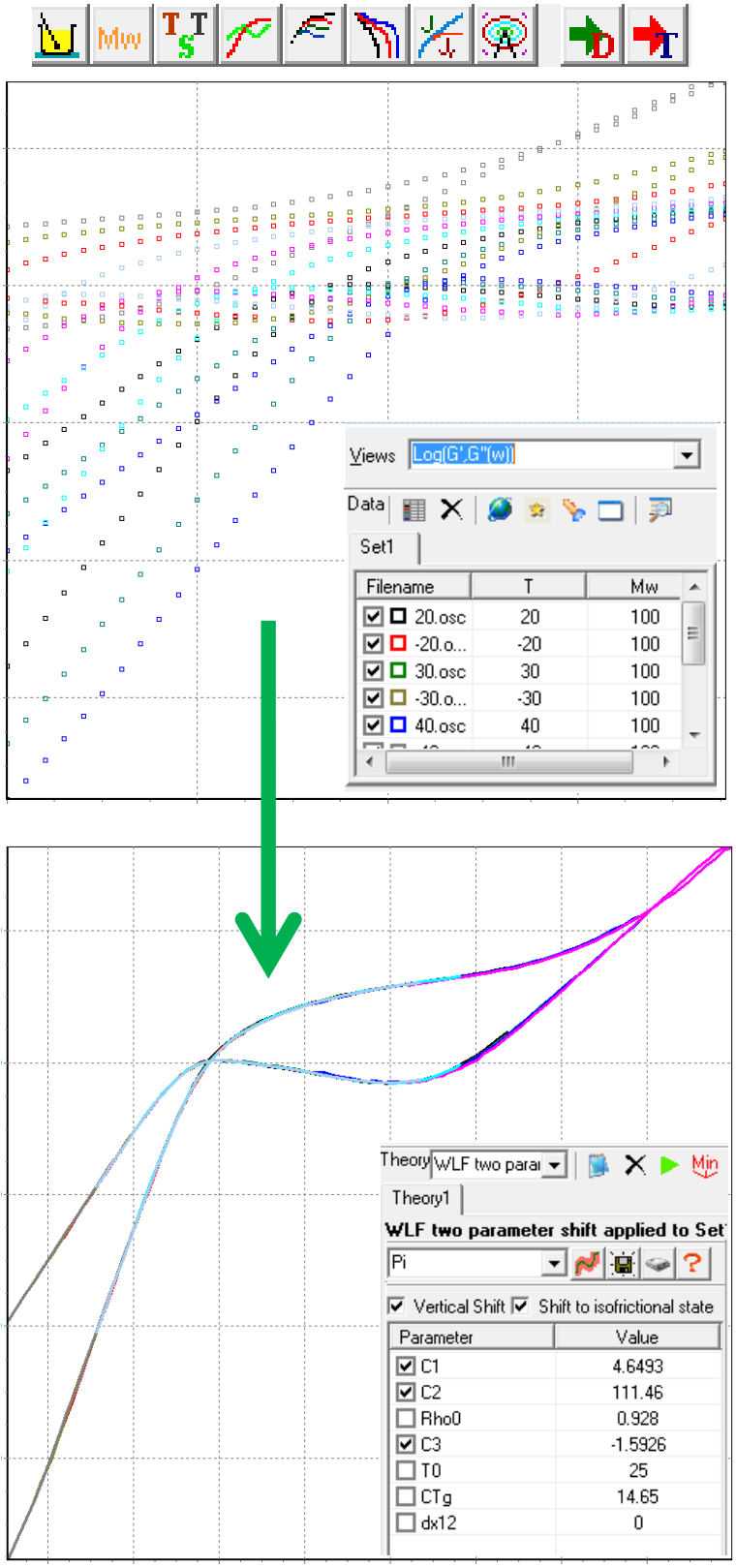

Select TTS Module

Load data files (.osc) for each temperature

Perform WLF shift with given parameters C_1, C_2 and C_3 that can be minimised to give the best overlap

Figure 2.1: Simplified procedure for time-temperature superposition, showing REPTATE software components. Data shown is for PI100K between -40 °C and 40 °C.

2.2 Linear polyisoprenes

A series of monodisperse linear polyisoprenes with different molecular weight were analysed using small amplitude oscillatory shear. In this way, the effect of molecular weight of the chains on the rheology can be quantified and the results compared to an advanced tube model for linear polymers, the linear theory of Likhtman and McLeish,[52] and materials parameters extracted from the model.

2.2.1 Materials

A series of linear polyisoprenes were synthesised by Matthew Oti at Durham University by standard high vacuum living anionic polymerisation methods.[127-128] Molecular weights, polydispersity indexes (PDI) and the percentages of 1,4 microstructure are listed in Table 2.1, as determined by gel permeation chromatography using a Viscotek TDA 302 with triple detection (right angle light scattering (690 nm), viscosity and refractive index) with twin PLgel 5 µm mixed C columns (300 x 75 mm). Tetrahydrofuran (THF) was used as the solvent at 35 °C and a flow rate of 1 ml/min. A single narrow distribution polystyrene standard (Polymer Laboratories) was used for calibration, and a dn/dc value of 0.130 mL/g was used for polyisoprene, as measured in house.

The microstructure was calculated by Matthew Oti[127] from ^{1}H nuclear magnetic resonance (NMR) using a Bruker DRX-400 MHz spectrometer on solutions dissolved in $CDCl_3$.[129-130] The structures of possible microstructures of polyisoprene are show in Figure 2.2.

2.2.2 Experimental

Materials were characterised using a either a TA Instruments AR-2000 or DHR2 rheometer. A 25 mm or 8 mm parallel plate geometry was used. Samples were

Table 2.1: Materials properties of linear polyisoprenes studied

Label	M_n (g/mol)	M_w (g/mol)	PDI	% 1,4
PI20K	21500	21500	1.02	89
PI100K	98000	100000	1.03	89
PI150K	142000	145000	1.02	87
PI300K	274000	301000	1.1	85
PI390K	375000	387000	1.03	91
PI420K	373000	420000	1.13	91
PI500K	482000	496000	1.03	88
PI1380K	1316000	1378000	1.05	87

pressed into 1 mm thickness discs of the required diameter (8mm or 25 mm) using a mould in a hydraulic press. They were pressed under a pressure of 4 tonnes for 10 minutes at room temperature. The samples which were too low viscosity to be pressed could be directly loaded into the rheometer.

Measuring gap was determined by incrementally decreasing the gap and performing a single oscillatory shear measurement until constant values were obtained irrespective of the gap. This procedure accounted for any differences in thickness of the samples. If this resulted in sample escaping the edges of the geometry, this was trimmed and the gap lowered a further 5 % to ensure there was no underfilling.

The environmental test chamber (ETC), an oven that closes around the geometry, was used to maintain temperature, and was supplied with nitrogen to prevent thermal degradation of the samples. This was done for all samples except PI20K, where a Peltier plate was used to reach low temperatures. An alternative method of reaching low temperatures is supplying the ETC with liquid nitrogen as well as nitrogen gas, using an automatic valve to switch between the two. This was done for PI100K, and gave a wider range of accessible temperatures. Frequency sweeps were performed at each temperature at 1 % strain amplitude between frequencies of 0.1 and 600 rad/s, recording 10 points per decade. The chosen strain is well within the linear region for all the materials studied, giving SAOS results. The effect of strain amplitude is discussed further in Chapter 5.

In order to quantify the temperature dependence and produce a single, larger rheological spectrum, the Reptate software[10] was used to apply a Williams-Landel-Ferry two parameter shift time-temperature superposition.[2] The parameters were fit

Table 2.2: Fitting parameters for linear polyisoprenes, used in the WLF shift (C_1, C_2, C_3) and linear theory fits (τ_e, G_e, M_e)

Label	C_1	C_2	C_3	τ_e (s)	G_e (Pa)	M_e (kg/mol)
PI20K	5.44	130	0.74	5.39E-06	788000	3.81
PI100K	4.65	111	-1.59	1.32E-05	595000	4.82
PI150K	5.24	129	-2.21	2.28E-05	356000	5.09
PI300K	4.94	119	0.25	7.12E-05	560000	7.62
PI390K	5.13	131	-0.58	4.53E-05	545000	6.72
PI420K	5.32	223	-5.96	6.66E-05	447000	7.95
PI500K	4.76	117	0.11	3.84E-05	536000	6.39
PI1380K	3.76	67.7	0.68	1.79E-05	352000	6.26

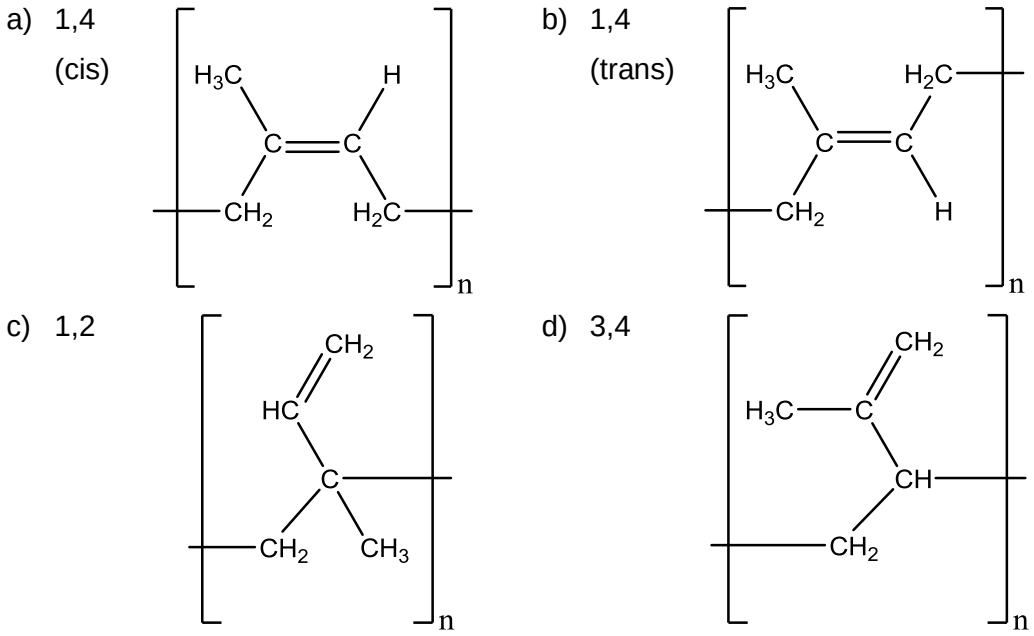

Figure 2.2: Different microstructures of polyisoprene

to give best overlap of the data and the values used for each material are given in Table 2.2. It was chosen to fit each dataset separately rather than use a single set of parameters because the samples vary in polydispersity and microstructure, which can cause variations in the fitting parameters between them. Although this does mean that differences in sample loading can be absorbed into the parameters (particularly C_3, which is seen to have the most variance), this makes little difference to the resulting spectrum and still gives valid rheological spectra.[131]

The resulting spectrum was then fit with Likhtman-McLeish full linear theory.[52] As discussed in the introduction, this is a tube model, incorporating constraint release and contour length fluctuations. The parameters for this model are the entanglement molar mass M_e, entanglement time τ_e and entanglement modulus G_e (which is equal to the plateau modulus multiple by 5/4)[131], as well as a constraint release parameter C_v. This is kept fixed at a value of 0.1, which is seen to give the most consistent results with start-up shear experiments.[52] The other parameters were fit to the data and are given in Table 2.2.

For PI1380K, a stress decay measurement was also performed, by applying a 5 % step strain at 25 °C (maintained by the ETC) using a 8 mm parallel plate geometry. This was transformed using the iRheo[132] software package into order to produce the frequency dependent spectrum.

2.2.3 Results

2.2.3.1 SAOS response at different molecular weight

Results of the rheological experiments are shown in Figure 2.3. All the spectra have a similar shape, beginning with the linear terminal region at low frequencies. In this region G'' exceeds G' and the polymer behaves more like a viscous liquid. Hence for the lower molecular weights, which are less viscous and less elastic, more of this region is seen, in particular for PI20K, where this region dominates the frequencies observed. At a defined frequency for each molecular weight, there is then a crossover point at the reptation time of the polymer, after which the polymers response becomes more rubbery. This is seen to occur at lower frequencies for increasing molecular weight, as the polymer chains become longer and the materials become more viscous and rubbery. After this point the rubbery plateau region is seen, where G' remains constant and G'' begins to decrease. The value of G' in this region (the plateau modulus) is relatively consistent between samples, which can be seen from the values of G_e in the fit curves, which vary from 3.5 to 5.95 x10^6 Pa, excluding the lowest molecular weight, for which the fit value is larger, but the plateau modulus is not well defined due to the small rubbery region. As expected, G'' decreases the most (and hence the behaviour becomes most solid like) for the highest molecular weight samples. The overall shapes of the spectra are similar to the idealised Maxwell model discussed in Section 1.3.1. Finally, for PI20K and PI100K, the chain stretching region can also be observed, where at high frequency, both G' and G'' increase rapidly, indicating the material response is becoming more solid like and brittle. Although this region should be accessible at similar temperatures for all the materials, liquid nitrogen cooling was only used for the lowest two molecular weights and so the chain stretching region is only visible in the spectra of these two. The spectra generally show good agreement with linear theory, which predicts the shapes and magnitudes of the curves well.

2.2.3.2 Comparison to stress relaxation

For the highest molecular weight, no data in the terminal region was obtained from frequency sweeps, as the high temperatures and long times required began to oxidise the sample. The results shown used a 2 hour experiment (from 0.001 rad/s - 600 rad/s) at 60 °C to reach the lowest frequencies and minimal difference was noted between the TTS shift of the 60 °C results compared with the lower temperatures. However using 2 hour experiments at higher temperatures (even just 70 °C) produced a noticeable difference in the results at the highest temperature when TTS was applied. Using a standard frequency range (0.01 - 600 rad/s) meant

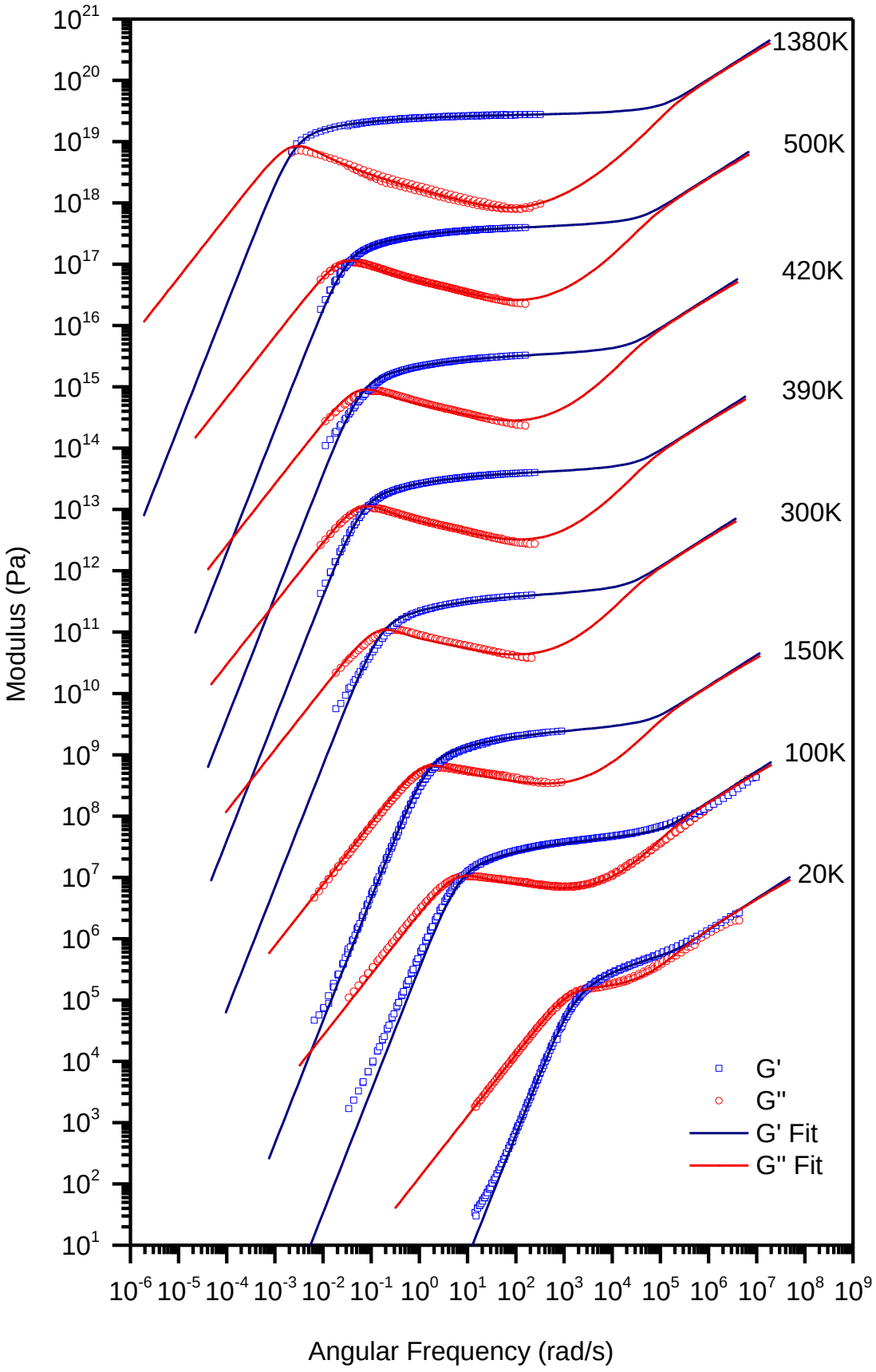

Figure 2.3: Variation of elastic modulus (G') and viscous modulus (G'') with frequency for linear polyisoprenes of different molecular weight, shifted to a temperature of 25 °C using WLF theory, and fit with full linear theory, both with parameters given in Table 2.1. Each spectrum is offset by a factor of 100.

experiments took 30 minutes and higher temperatures could be reached without degradation. However a temperature of at least of 150 °C were required to reach the crossover point using this range, by which point there was noticeable difference in the TTS shift of the higher and lower temperatures. It is likely due to compensation for some oxidisation (although noted to be minimal) that the TTS parameters for this material are far from the rest. Although the linear fit gives parameters in line with the other samples, so the resulting spectrum is valid. The results from an alternative method of collecting frequency dependant data are shown in Figure 2.4. Here, a time dependent stress decay is Fourier transformed into a frequency dependent spectra. Although this required long times, high temperatures are not required, and so oxidisation is prevented and lower frequencies can be accessed, as shown.

2.2.4 Discussion

2.2.4.1 SAOS response at different molecular weight

The shapes of the spectra are similar to those previously reported in literature.[131, 133] Linear theory fits the data well, and using the fits rheological parameters can be extracted (entanglement molar mass M_e, entanglement time τ_e and entanglement modulus G_e, as shown in Table 2.2). The number of entanglements, Z is then given by M_w/M_e.[52] The entanglement modulus broadly agrees with literature, where values have been reported for G_e of 5.95 x10^6 Pa[131] and between 4-6.25x10^6 Pa[133] (using the relation $G_e = \frac{5}{4}G_p$) for a range of PIs of different molecular weight.

The entanglement molecular mass of polyisoprene was reported by Auhl *et al.*[131] as 4.82 kg/mol. Our values range from 3.81-7.95 kg/mol, although the upper values are the slightly polydisperse samples, PI300K and PI420K and the polydispersity could contribute to this difference (the polydispersity in the work of Auhl *et al*.[131] was ~1.03 for similar molecular weight samples). The variation between samples could be due to differences in microstructure. Auhl *et al.* used polyisoprenes all having near 95 % 1,4 microstructure, whereas our samples have lower 1,4 ratios. Also, as the amount of cis and trans microstructure is unknown, as it was not clear from the NMR spectra, this could have been significantly different and had an effect on the materials parameters.

2.2.4.2 Comparison to stress relaxation

The i-Rheo results allowed access to much lower frequencies, but the results shown are shifted upwards in the moduli. This could be due to oxidisation that occurred in the oscillatory experiments, reducing the plateau modulus, as in order to obtain the

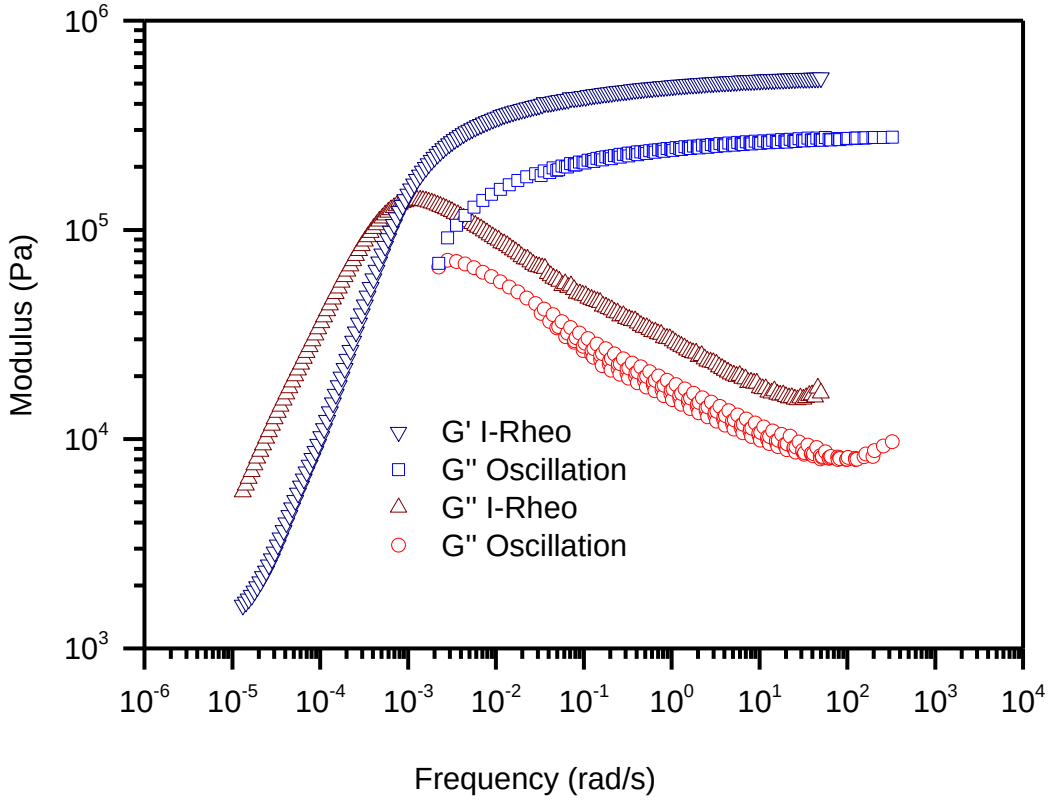

Figure 2.4: Comparison of i-Rheo transformed step strain decay transformed results to those obtained from the oscillatory experiments.

crossover, the sample was kept at 60 °C for two hours. Even with a flow of nitrogen over the sample, this could be enough to cause oxidisation. There is a clear advantage of using the step strain decay results here, as the results can be obtained at room temperature. However, there is also a difference in the shape of the spectrum. The terminal region shows gradients of G' and G'' that are very similar, and G' and G'' are much closer than is seen for the other polyisoprenes. G' is expected to have a gradient double that of G'', and for this reason, linear theory does not provide a good fit to the data. The reason for this is unclear, as data for the terminal region is not available for the oscillation, it is not clear whether this is a difference for this material or an effect of the method. The results of the transform are very dependent on the short time results in the decay and the number of points trimmed from the start, although oversampling reduced this dependence. It is possible that the slight overshoot at these short times that is observed when the rheometer applies a step strain could cause this difference.

2.2.5 Conclusion

Linear polyisoprenes with a large range of molecular weights have been studied by small amplitude oscillatory shear rheology. The resulting rheological spectra were in line with similar materials analysed in literature, and the behaviour was captured well using Likhtman-McLeish linear theory.

For the highest molecular weight, frequency sweeps in SAOS were compared to the results of a transformed stress decay experiment, however a shift between the two was noted, the reason for which was not clear but could have been due to oxidation present in the SAOS experiment.

2.3 Polybutadienes with complex architecture

Although linear polymers are relevant to many industrial applications, branched material is common in many synthetic processes and is often desired to control the properties of the resulting mixture. It is therefore important to understand the properties of these branched materials and understand the effect branching has on rheological properties.

Moving on from the linear polymers examined in Section 2.2, more complex architectures were analysed by frequency sweeps under SAOS. Polybutadienes were used, a common synthetic rubber with a range of different characteristics. Starting from linear monodisperse polymers similar to the polyisoprenes analysed, complexity was increased to those with higher polydispersity, and then different architectures, i.e. star polymers and randomly branched material. In this way the influence of these properties on rheology was observed. Branch-on-branch (BOB) theory, a tube model for branched polymers, was then applied to extract materials parameters, since it is the most widely applicable model available that can predict the rheology of branched polymers without fitting to experimental data.

2.3.1 Materials

A series of linear, star and randomly branched polybutadienes were synthesised by Matthew Oti at Durham University by living anionic polymerisation.[127] PBD310K was purchased from Sigma-Aldrich (Product code 181382 ALDRICH). PBD120K was purchased from Polymer Source (Product code P10589-Bd).

Molecular weights and polydispersity indexes (PDI) are listed in Table 2.3, as

Table 2.3: Polybutadienes studied, with materials properties and fitting parameters used in the WLF shift (C_1, C_2, C_3) and BOB theory fits (τ_e, Z)

Label	M_n (g/mol)	M_w (g/mol)	PDI	C_1	C_2 (K)	C_3	τ_e (s)	Z
PBD40K	32800	38400	1.17	9.81	495	7.97	8.90E-07	47.26
PBD50K	49700	51400	1.03	6.27	366	5.12	2.62E-06	53.11
PBD120K	118000	121000	1.03	4.03	180	1.45	2.20E-07	29.13
PBD160K	111000	165000	1.49	4.73	199	1.30	2.24E-07	34.15
PBD310K	161000	310000	1.93	3.59	132	1.17	4.64E-07	31.38
3ARM	159000	168000	1.05	14.61	500	2.51	8.77E-07	36.05
4ARM1	132000	145000	1.10	4.90	169	0.51	1.67E-06	47.22
4ARM2	126000	131000	1.04	5.02	176	1.57	2.32E-06	49.74
8ARM	204000	210000	1.03	4.97	192	0.41	2.15E-07	31.38
RB150K	15100	62800	4.14	5.55	206	0.26	N/A	N/A
RB480K	56400	478000	8.46	4.49	166	0.60	N/A	N/A

determined by GPC as described in Section 2.2.1, using a $\frac{d_n}{d_c}$ value of 0.124 mL/g for polybutadiene, as measured in house. The polymers all showed a single peak with broadness as described by their polydispersity, except for PBD160K, which had a significant high molecular weight shoulder, which is included in the PDI values and is shown in Figure 2.5.

2.3.2 Experimental

As with the polyisoprene samples, materials were characterised using a TA Instruments AR-2000 or DHR2 rheometer. A 25 mm or 8 mm parallel plate geometry was used. Samples were pressed into 1 mm thickness discs of the required diameter (8 mm / 25 mm) using a mould in a hydraulic press. They were pressed under a pressure of 4 tonnes for 10 minutes at room temperature. The samples which were too low viscosity to be pressed could be directly loaded into the rheometer.

Measuring gap was determined by the procedure described in 2.2.2. The ETC, supplied with nitrogen gas was used to maintain temperature. When temperatures below room temperature were required, a Peltier plate was used. Frequency sweeps were performed at each temperature at 1 % strain between frequencies of 0.1 and 600 rad/s recording 10 points per decade. A WLF TTS was applied to give one spectrum for each material at 25 °C. The parameters were fit to give best overlap of the data and the values used for each material are given in Table 2.3.

The materials were fit with branch-on-branch (BOB) theory, which is an expansion of tube theory for branched polymers incorporating Rouse motion, reptation, constraint

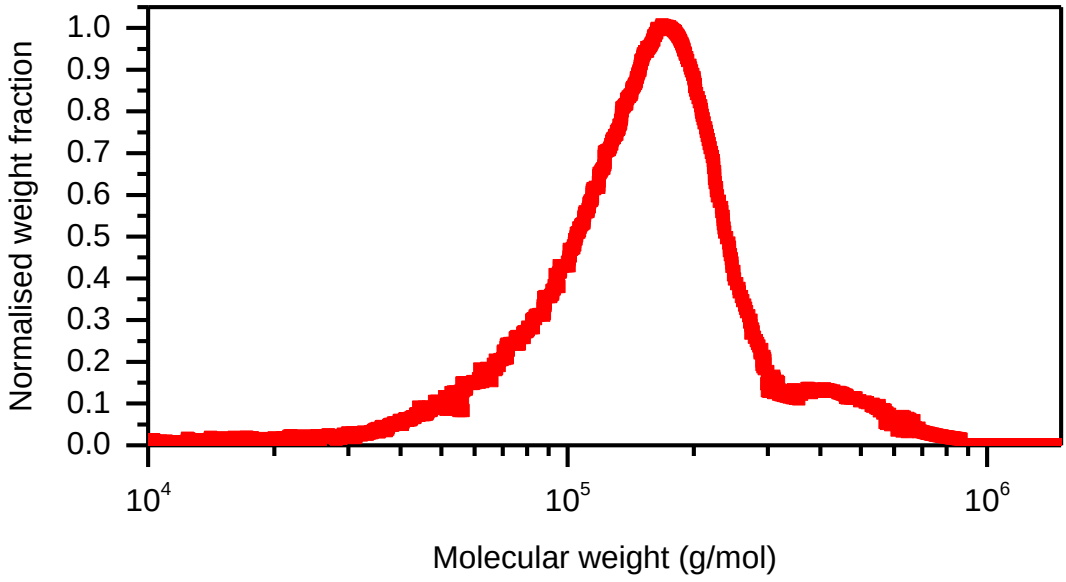

Figure 2.5: Gel permeation chromatogram of PBD160K, showing the high molecular weight shoulder.

release, arm retraction, side arm collapse and compound arm retraction (for branch-on-branch structures).[126] The parameters required for this are the monomer mass (M_0), number of monomers in one entanglement length (N_e), density (ρ) and entanglement time (τ_e). It also requires as input the type of polymer and polymer dimensions e.g. for a star polymer, the number of arms, molecular weight of each arm and polydispersity. N_e and τ_e were fit to the data using simple MATLAB code in addition to the BOB executable.[134] This was a simple algorithm written to run the BOB executable for the given molecule with various values of N_e and τ_e and select the best overlap with the data. Other parameters were kept to constant values from the REPTATE Materials database[10].

For the comparisons of the randomly branched material to the linear case, the GPCs was discretised into 10 points per decade of molecular weight using REPTATE, and fed into polydisperse double reptation theory.[135] The parameters for this model are the monomer mass (M_0), the entanglement molar mass (M_e), entanglement time (τ_e) and plateau modulus (G_p), as well as a constraint release parameter (α), which was set to 1. The other parameters were kept at standard values for polybutadiene according to the REPTATE materials database.[10]

2.3.3 Results

2.3.3.1 SAOS response of linear and star PBD

Results are shown in Figure 2.6, similar regions can be identified as in the linear polyisoprene spectra. As the linear materials have relatively low molecular weights, the majority are dominated by the linear, viscous region before the crossover point. As with the polyisoprenes, the crossover point of the linear polymers can be seen to move to lower frequencies with increasing molecular weight.

PBD160K is slightly more polydisperse than the lower molecular weights, due to the presence of the high molecular weight shoulder as shown in Figure 2.5. This can be seen in the terminal region, as G' and G'' are closer together, and do not show their characteristic gradients of 2 and 1 respectively. This effect becomes obvious when moving to PBD310K, which has a higher polydispersity, and shows a large crossover region where G' and G'' show similar values.

The star polymers have significantly longer relaxation times than would be expected for a linear polymer of similar molecular weight. All four show similar rheological behaviour, but are shifted in frequency according to their arm molecular weight, in a similar way to the change in behaviour of the linear polymers.

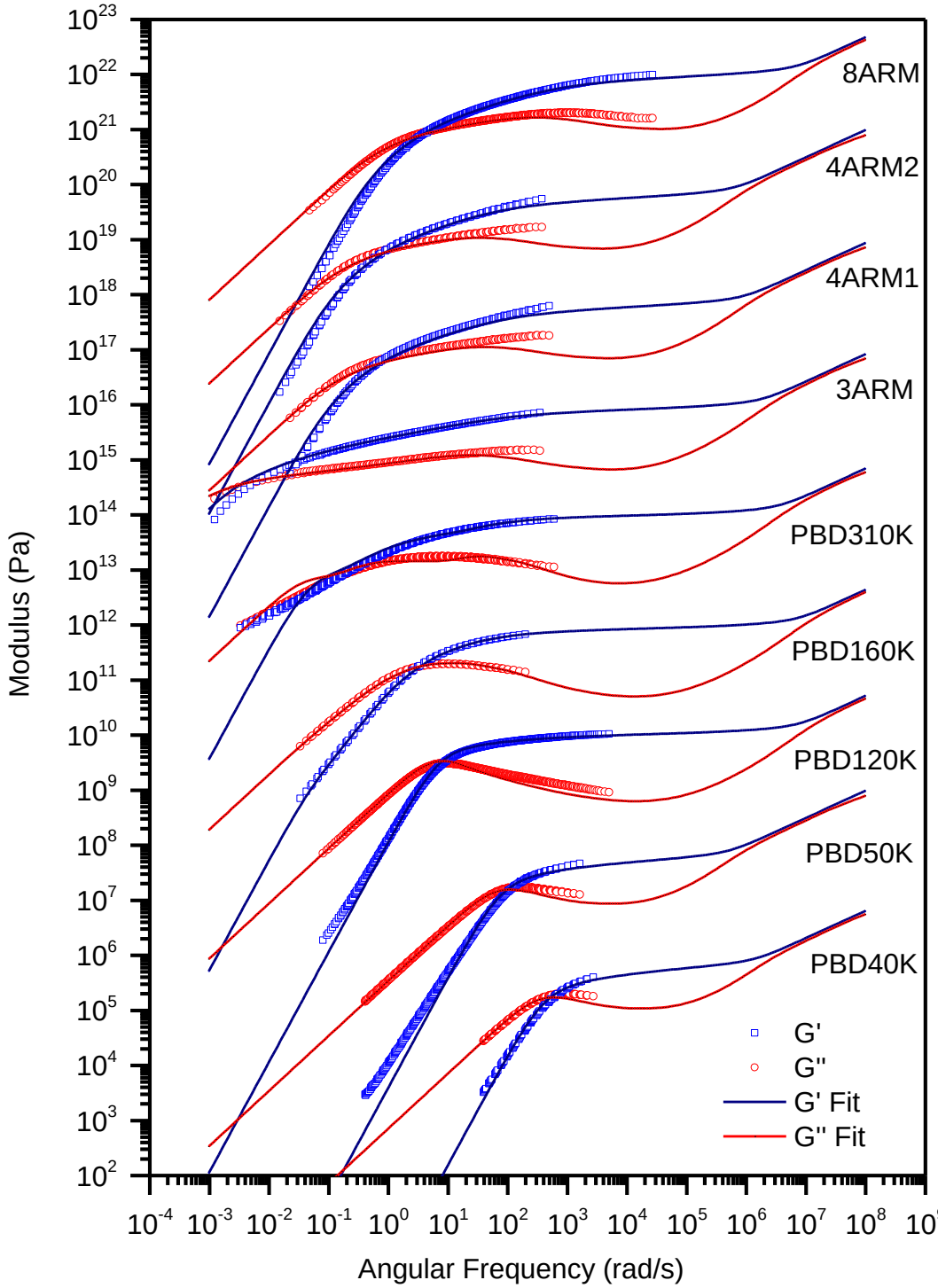

Figure 2.6: Frequency sweeps of polybutadienes, showing elastic modulus (G') and viscous modulus (G''). The moduli are shifted to a temperature of 25 °C using WLF theory and fit with BOB theory (parameters are given in Table 2.3). Each spectrum is offset by a factor of 100 from the last.

2.3.3.2 SAOS response of randomly branched PBD

The randomly branched polymers (Figure 2.7) both show an effect of a high polydispersity, similar to the polydisperse linear polymers. However the effect is much clearer for RB480K which has the large crossover region characteristic of a polydisperse material. There is a significant difference in the data to the predictions

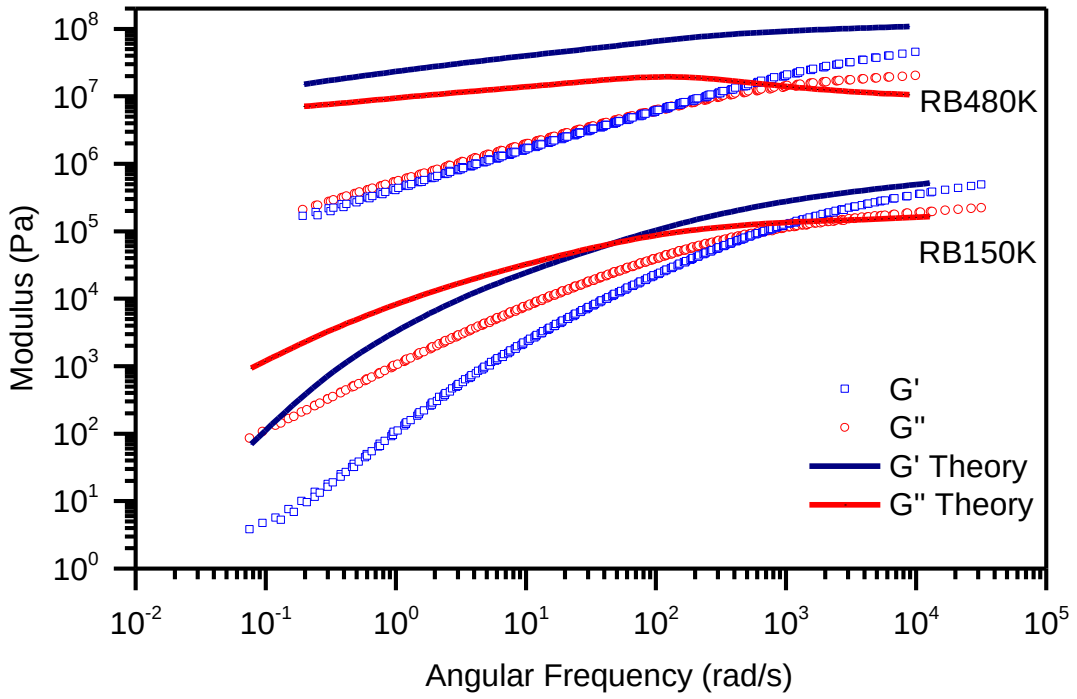

Figure 2.7: Frequency sweeps of randomly branched polybutadienes, showing elastic modulus (G') and viscous modulus (G''). The moduli are shifted to a temperature of 25 °C using WLF theory, and compared with simulation using polydisperse double reptation theory with the GPC data as input, to show the response if all components were linear. RB480K is offset by a factor of 100.

for a linear polymer of the same polydispersity, particularly for RB480K, which would be predicted to have a significantly longer relaxation time (and lower crossover frequency) if its chains were linear.

2.3.4 Discussion

2.3.4.1 SAOS response of linear and star PBD

The higher plateau modulus and lower crossover frequencies seen for linear polybutadiene compared with linear polyisoprenes of similar molecular weight are caused by the greater number density of entanglements in polybutadiene. The linear polybutadienes are fit with BOB theory and give relatively good fits. For PBD160K the material was bidisperse (showed two peaks in the GPC rather than one) and in general the effect of polydispersity on linear rheology is not trivial to incorporate. A distribution (e.g. Gaussian or normal) can be used to represent the range of molecular weights, but this fails in the case of bimodal or multimodal dispersities, where a more rigorous approach is required. Hence the polydispersity in PBD160K was accounted for by discretising the molecular weight distribution (from the GPC) and using 8 monodisperse components to represent the range of molecular weights present. This approach captured the rheology well, but could have been improved

by using more components or introducing polydispersity (through a distribution) to each component, although this would have made the BOB simulation significantly more computationally complex. For PBD310K, a commercially purchased sample, the distribution is much broader, and so it was modelled as a single component with a normal distribution of molecular weights and polydispersity from the GPC. This produced a good fit of the rubbery region, however did not capture the large crossover region created by the polydispersity. A broader distribution would possibly be required to capture this region.

The 3 arm star polymer (~51K per arm) is, at the temperatures/frequencies accessible, dominated by the solid like region. This is expected, as it is much more viscous than both the single linear arm and the linear PBD of the same molecular weight, due to the inhibition of reptation and reliance on arm retraction and branch point diffusion for relaxation, as described in Section 1.3.2. The BOB theory fits the shape of the spectrum well. The 4 arm polymers (each a different fraction of the same reaction mixture, both ~38K per arm) and the 8 arm polymer (~27K per arm) are less dominated by rubbery behaviour, which is due to the lower molecular weight of their arms. The number of arms on a star polymer is not expected to have a significant influence on their rheology since the arm retraction will happen at the same rate for every arm.[63, 136] It may have a small effect on branch point diffusion; however since this is a much slower process it has little effect on the resulting rheology, and this is seen in our data (Figure 2.6), with the arm length being the only significant factor.

2.3.4.2 SAOS response of randomly branched PBD

For the randomly branched material it was not possible to fit BOB theory as the underlying structure is unknown. They are shown with a prediction based on their GPC from polydisperse double reptation theory.[135] This is a theory for linear polymers and so shows a predication if all the molecules involved were linear. For RB150K, this prediction is only slightly shifted from the data, which suggests that the linear sections are dominating the rheology. This would be the case if the molecules had a long linear back bone and only short sections originating from branch points. The inclusion of some branching would mean the backbones were shorter than expected from the distribution of molecular weights, which would cause the shift of the data towards higher frequency than the model.

RB480K is more difficult to compare to the model, which predicts a much longer relaxation time than is seen for the data. It is clear that the structure is far from linear and is highly polydisperse (as seen from the large crossover region).

RB480K results from an identical reaction to RB150K, using monomer, a crosslinking agent (divinyl benzene) and potassium-tert-butoxide to enhance chain transfer, increase branching and prevent gelation. The conditions for each were the same, although slightly more crosslinking agent was used for RB480K.[137] The GPC of RB480K showed a similar peak to RB150K but with a large high molecular weight shoulder, indicating the additional cross linking agent had caused the formation of additional high molecular weight components, with highly networked structure. The presence of multiple components explains the increased polydispersity in rheology observed and the greater deviation than the linear prediction.

2.3.5 Conclusion

A range of polybutadienes with linear, star and randomly branched architecture have been analysed by SAOS rheology. The results were fit with BOB theory which matched the experimental data well across the linear and star polymers, although when significant polydispersity was introduced (using a commercial linear sample), the terminal region was not well represented. The randomly branched samples were not fit with a model due to the ambiguity and high polydispersity in their structure, but their rheology gave valuable information about their structure when related to reaction conditions.

2.4 Characterisation of star-linear blends using BOB theory

Branch-on-branch theory has been shown to be very useful in predicting the rheology of branched polybutadienes in Section 2.3. To further test this, a series of star linear blends were produced in order to test the capability of BOB to predict rheology of more complex mixtures. The reverse problem was then studied to quantify the characterisation capacity of BOB, i.e. can the quantity of star material in a blend be extracted from its rheology.

2.4.1 Materials

Materials used were 3ARM and PBD160K, which were blended in a range of defined compositions from 0.5 to 0.9 weight fraction of the star polymer. The blends were made up by dissolving both polymers in a minimal amount of toluene, combining the mixtures and precipitating out the polymer using methanol. After precipitation the sample was dried overnight in a vacuum oven at room temperature to remove any remaining solvent.

2.4.2 Experimental

The blends were characterised using a TA Instruments AR-2000 rheometer using an 8 mm parallel plate geometry. Samples were pressed into 1 mm thickness discs of the 8 mm diameter using a mould in a hydraulic press. They were pressed under a pressure of 4 tonnes for 10 minutes at room temperature.

Measuring gap was determined by the procedure described in 2.2.2. The ETC, supplied with nitrogen gas was used to maintain temperature. Frequency sweeps were performed at each temperature at 1 % strain between frequencies of 0.1 and 600 rad/s recording 10 points per decade. A WLF TTS was applied to give one spectrum for each material at 25 °C. The parameters were fit to give best overlap of the data and the values used for each material are given in Table 2.4.

2.4.2.1 Analysis strategy

BOB theory was used to model the results. Firstly, since only one set of materials

Table 2.4: WLF time-temperature superposition parameters for star-linear blends

Label	C_1	C_2 (K)	C_3
0.9STAR	4.22	136	0.637
0.8STAR	3.75	145	0.808
0.7STAR	5.15	172	-0.172
0.6STAR	4.52	150	-1.24
0.5STAR	4.93	196	0.690

parameters can be used as input for BOB, the best parameters for fitting both the 3ARM and PBD160K simultaneously were extracted using MATLAB code (see Appendix 2) and the BOB executable to produce predictions using various parameters and compare the output to the experimental data for the pure components, identifying the best fit. Predictions of the linear rheology for each of the blends were then generated using the best fit parameters for the pure components.

The reverse problem was then solved using similar MATLAB code. Again using the best fit parameters for the pure components, BOB predictions for different fractions of each component were generated and compared to the experimental data (code is identical to that in Appendix 2, except the input files were generated with different fractions of each polymer rather than N_e and τ_e). The best fit to the experimental data was identified as the predicted fraction of star in the blend.

2.4.3 Results:

2.4.3.1 Predicting SAOS response of blends

The optimum parameters for fitting both sets of experimental data were found to be, Monomers per entanglement length, N_e = 32.55 and entanglement time, τ_e = 1.81 x 10^7 s. These values are consistent with those obtained from the BOB fits in Section 2.3 although the entanglement time is slightly shorter than any of those obtained previously, and interestingly is shorter than those obtained for both of the pure components individually.

The predictions are shown in Figure 2.8, and show good overlap with the experimental data at all fractions, although is seen to deviate more at lower fractions of star.

2.4.3.2 Predicting component fraction in a blend

The fractions which give the best fit to experiment are shown in Table 2.5. The code succeeds in extracting back the pure components with little error, but for the blends the error varies. The fractions with a greater proportion of star appear to have better predictions than those with more linear component.

2.4.4 Discussion

2.4.4.1 Predicting SAOS response of blends

The experimental rheology of the blends matches BOB theory well, especially the bends with higher proportion of star, despite the crossover frequency of the pure star being under predicted. This suggests that the discrepancy in the pure star could

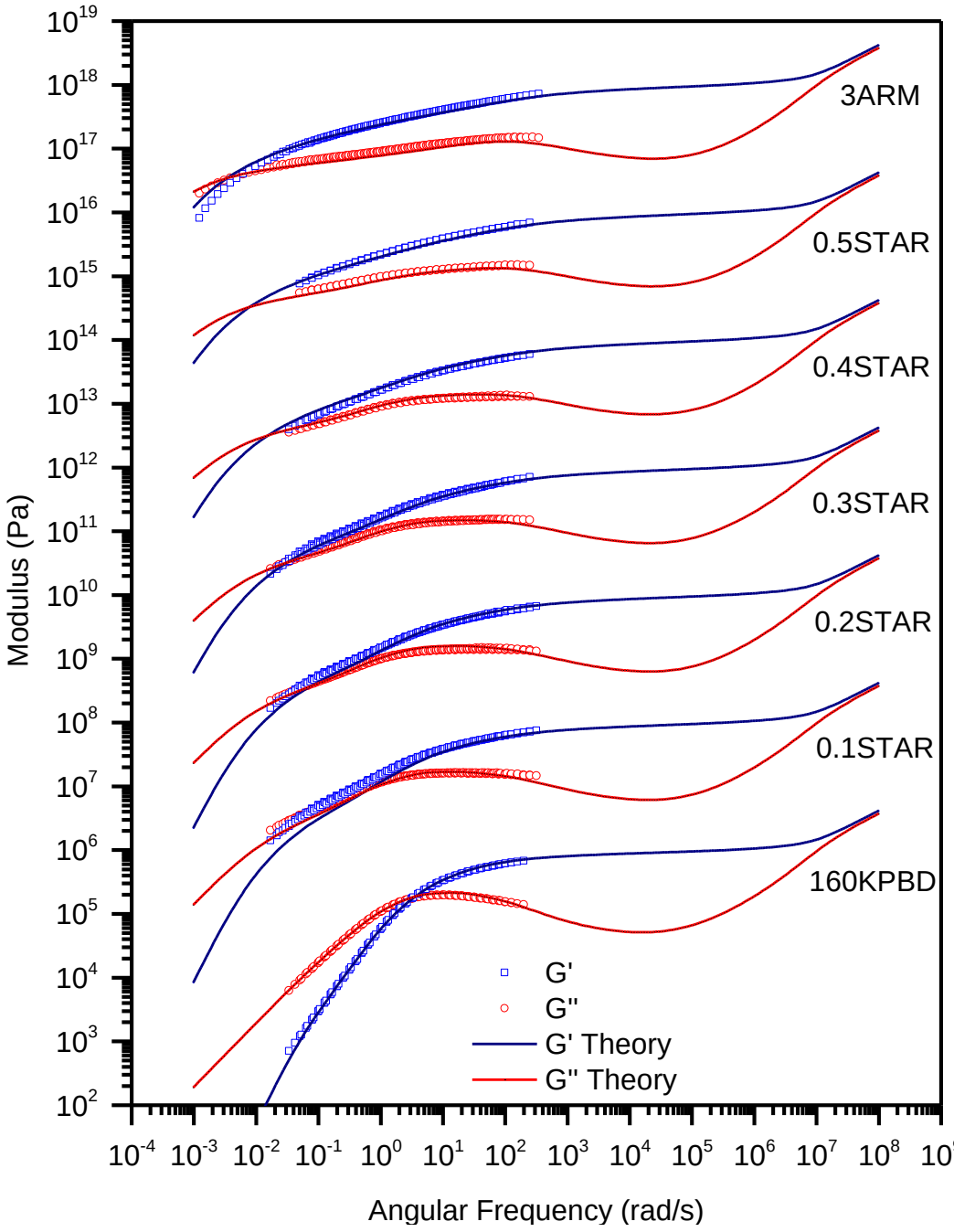

Figure 2.8: Frequency sweeps of a series of blends of star and linear PBD shown with fits using BOB theory. Each spectrum is offset by a factor of 100 from the last.

be down to the experimental results. Similar to the high molecular weight linear polyisoprene in Section 2.2, a low frequency (long time) test was required to reach the crossover frequency (2 hours at 60 °C). Although the overlap from the TTS was good, there was a slight shift noted for the results of this test to those at the other temperatures. There is a possibility that this is due to some oxidation of the sample, or this could point to a failure of the rheometer at these low frequencies. Further tests would be required to identify if this discrepancy is characteristic of the material or the measurement.

Table 2.5: Fraction of star polymer in prepared blends with the fractions extracted from fitting to BOB predictions, and the difference between the two

Fraction Star	Fraction from BOB Prediction	Error
1	0.99	0.01
0.9	0.91	0.01
0.8	0.75	0.05
0.7	0.75	0.05
0.6	0.68	0.08
0.5	0.64	0.14
0	0.00	0.00

There is clearly a greater discrepancy between the theory and experiment as the proportion of linear is increased. This is likely due to the complex nature of the linear polymer, having a significant high molecular weight shoulder (Figure 2.5), and the failure of the procedure used to capture this complexity (a combination of 8 fractions of monodisperse linear polymer based on the discretised GPC). A greater number of discretised points may improve the predictions, or the use of multiple polydisperse fractions, but this value was chosen to avoid the calculations becoming too complex.

2.4.4.2 Predicting component fraction in a blend

As could be expected from the rheology predictions, when BOB was used to predict the fraction of the components in the blend by choosing the best fit to the experimental data, the fractions were most accurate for high proportions of star. The pure linear and star were predicted very well but this is not surprising as the materials parameters were fit to these two data sets. It is likely that if more monodisperse polymers were used to represent the PBD160K, or if a combination of polydisperse polymers was used, different materials parameters would be extracted that would give a better match to the fractions (and match better to those of the pure components). However it is also possible that one set of materials parameters is not sufficient to model these two polymers, due to subtle differences in microstructure.

However, the values extracted are very promising; the three highest fractions of star are predicted within 5 %. It is clear that BOB is a powerful tool for extracting structure of polymers from their rheology, and would provide even more accurate fits to blends of monodisperse polymers, or even more randomly distributed polydisperse materials.

2.4.5 Conclusion

A series of blends of linear and star polybutadiene were prepared and used to test the capabilities of branch-on-branch theory which captured the rheology very well. The reverse problem was tested, and seen to be effective in predicting the fraction of each polymer from the rheology, however was less effective at higher quantities of the linear polymer (giving an error as large as 14 %). This is believed to be due to the polydispersity of this polymer not being fully captured by the procedure used to discretise the range of molecular weights. However, it can be concluded that BOB in linear rheology can be used to extract fractions of components in a mixture provided the nature of the components is known and they are well defined in terms of molecular weight and microstructure.

2.5 Fractionation of randomly branched polybutadiene

In order to better quantify the components in the randomly branched polymers studied, a fractionation was performed, which would separate the polymer into different molecular weights, and may separate some of the components by structure.

2.5.1 Materials

5 g of RB150K was dissolved in toluene, with a small amount of butylated hydroxytoluene (BHT) antioxidant. The solution was added to a separating funnel, and kept at 22 °C by placing it in a water bath. Methanol was added until the solution was cloudy, and the temperature increased to 28 °C and the solution left to clear. The temperature control was turned off and the solution left to cool and separate overnight. The fraction was taken off and the procedure repeated to extract further fractions. The extracted fractions were precipitated out by the addition of further methanol and the solvent poured off. Samples were then dried in a vacuum oven overnight to remove remaining solvent.

The molecular weights and polydispersity indexes (PDI) of the fractions are listed in Table 2.6, as determined by Gel Permeation Chromotography using a Viscotek TDA 302 with triple detection (right angle light scattering (690 nm), viscosity and refractive index) with twin PLgel 5 µm mixed C columns (300 x 75 mm). Tetrahydrofuran (THF) was used as the solvent at 35 °C and a flow rate of 1 ml/min. A single narrow distribution polystyrene standard (Polymer Laboratories) was used for calibration, and a $\frac{dn}{dc}$ value of 0.124 mL/g was used for Polybutadiene, as measured in house.

2.5.2 Experimental

The fractions were characterised using a TA Instruments AR-2000 rheometer using an 8 mm parallel plate geometry. A Peltier plate was used to control the temperature. Samples were low viscosity and could be directly loaded into the rheometer.

Measuring gap was determined by the procedure described in 2.2.2. The ETC, supplied with nitrogen gas was used to maintain temperature. Frequency sweeps were performed at each temperature at 1 % strain between frequencies of 0.1 and 600 rad/s recording 10 points per decade. A WLF TTS was applied to give one spectrum for each material at 25 °C. The parameters were fit to give best overlap of the data and the values used for each material are given in Table 2.7.

Table 2.6: GPC results for fractionated RB150K

Label	M_w (g/mol)	M_n (g/mol)	PDI
RB150K	58400	15800	3.69
RB150K F1	212000	78200	2.71
RB150K F2	120000	53600	2.24
RB150K F3	67000	39900	1.68
RB150K F4	39500	26200	1.51

2.5.3 Results: SAOS of fractionated randomly branched PBD

Six fractions were removed but only the first four contained enough sample for rheological analysis. After this point there was little precipitation in the remaining mixture when methanol was added, and based on the small quantities obtained from previous fractions, the fractionation was ended.

The extracted molecular weights from GPC of the fractions are shown in Table 2.6. All fractions showed decreased polydispersity index, although were still significantly polydisperse. The early fractions, which contained the larger molecular weight molecules which precipitate first, had larger polydispersities than the later fractions with lower molecular weight. The fractions showed similar rheological behaviour with a shift to lower frequency with increasing molecular weight as shown in Figure 2.9.

2.5.4 Discussion: SAOS of fractionated randomly branched PBD

The fractionation was successful in reducing the polydispersity of the randomly branched material, the fractions obtained had lower polydispersities and the rheology was seen to shift accordingly. It was clear some low molecular weight material had been lost, as all the fractions had lower frequency crossovers than the original polymer. This material was likely contained in the fractions that precipitated later that did not contain enough material to be analysed rheologically. The later fractions, with lower molecular weights had the lowest polydispersities, and this can be seen in the terminal and crossover regions of the rheology. F1 has a broad

Table 2.7: WLF time-temperature superposition parameters for fractions 1 to 4 of RB150K

Label	C_1	C_2 (K)	C_3
F1	7.44	341	0.69
F2	6.83	310	0.69
F3	7.30	351	0.69
F4	6.38	301	0.69

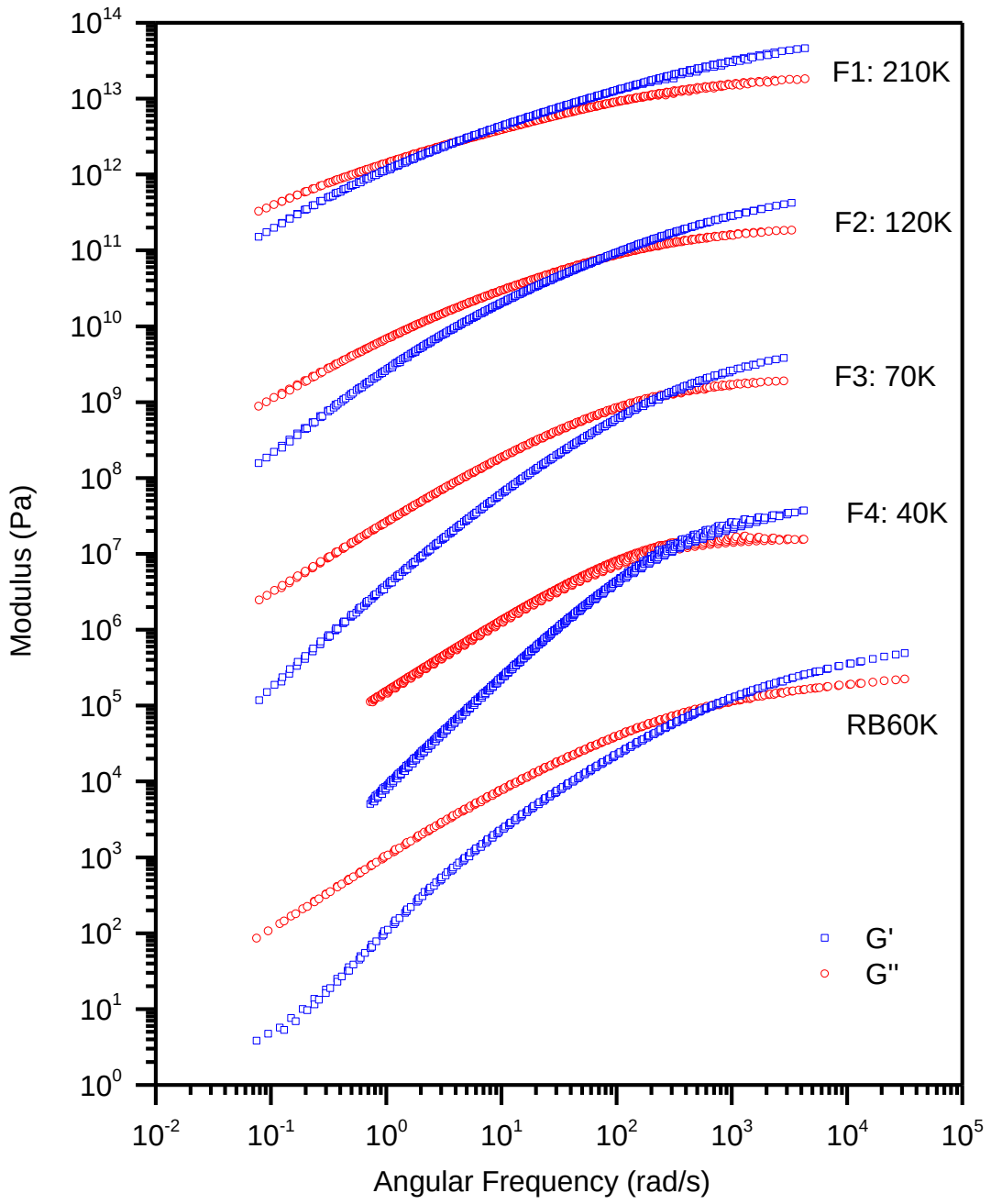

Figure 2.9: Frequency sweeps of a series of fractions of RB150K. Each spectrum is offset by a factor of 100 from the last.

crossover indicative of a large polydispersity, and moving to later fractions, the G' and G'' in the terminal region can be seen to become more distinct and closer to their characteristic gradients of 2 and 1 respectively. This trend would be expected from a random reaction, as with higher molecular weight, there are more possible structures that could be formed, and more potential for these structures to be distinctly different rheologically, i.e. there will be a mix of polymers with some long chain sections and those with short sections between branch points.

The fractionation did not reveal any separation by structure, as, other than the shift by molecular weight, the rheological behaviour was very similar in each fraction. If during the reaction there was preference for a certain type of product several fractions with different structures could have been obtained, and the fractionation would have given more monodisperse fractions at different molecular weights, with potentially significant different crossover points and shapes of the rheological spectrum. However the similarity confirms the original material was truly random in structure and hence the fractions extracted, although less polydisperse in molecular weight, are similarly random in structure.

2.5.5 Conclusion

Fractionation of a randomly branched material was performed in order to identify whether there was significant preference for certain products in their synthesis. The results showed that although polydispersity was reduced in the fractions, each fraction was still significantly polydisperse and behaved similarly rheologically, with a small shift due to the difference in molecular weight. This suggests that the material is highly random in structure and not a mixture of several preferred products, and so the reaction produces a truly randomly branched material. Fractionation can help identify components in a polydisperse complex mixture, although in such a complex mixture it is not sufficient to produce the well-defined individual components required for analysis by BOB theory.

2.6 Identifying phase separation in polymer blends using linear rheology

Another area where rheology can be useful in polymeric materials is studying phase transitions. Although conventional models (e.g. BOB) cannot predict the linear rheology of mixtures of polymers with different chemistry, rheology can be still useful for such blends. One example of this is that a signature of the phase transition can be observed in the rheology of phase separating blends. To demonstrate this, a blend of polyisoprene and polybutadiene was prepared that phase separates at a temperature accessible in the rheometer, and the rheology during the transition was examined.

2.6.1 Materials

0.05 g of each of PBD40K and PI150K were dissolved separately in approximately 2 ml toluene each. The solutions were combined, and methanol added causing the polymers to precipitate, until no additional precipitate formed. The solvent was removed and the polymer allowed to dry under vacuum at room temperature overnight. This system was chosen because similar systems had been seen to phase separate at temperatures above room temperature (e.g. 50 % 55K PBD with 50 % 34K PI phase separated at 59 °C[83]).

2.6.2 Experimental

The blend was characterised using a TA Instruments AR-2000 rheometer. An 8 mm parallel plate geometry was used and tests were performed in the environmental test chamber to maintain temperature and performed under nitrogen to prevent thermal degradation of samples. Measuring gap was determined by incrementally decreasing the sample gap and performing oscillatory shear measurements to obtain constant values. If this resulted in sample escaping the edges of the geometry, this was trimmed and the gap lowered a further 5 % to ensure there was no underfilling.

Temperature ramps were attempted at different heating rates (1 °C/min and 5 °C/min) and angular frequencies in the terminal region (0.25 rad/s and 0.5 rad/s). These were used to extract the phase separation temperatures of the blend and observe whether it is dependent on the experimental conditions. Frequency sweeps were then performed at temperatures above and below this temperature to identify any difference in rheology. Frequency sweeps were performed at 1 % strain between frequencies of 0.1 and 600 rad/s recording 10 points per decade.

REPTATE software[10] was used to apply a Williams-Landel-Ferry two parameter shift time-temperature superposition.[2] A difference in the shifts between temperatures before and after the phase transition was noted, and so the temperatures were separated and fit separately. The parameters were fit to give best overlap of the data and the values used are given in Figure 2.10

2.6.3 Results: SAOS across the phase boundary

The time-temperature superposition produces two slightly different rheological spectra before and after the phase transition, as shown in Figure 2.10, however the difference is small. Observing the elastic modulus at a single frequency during a temperature sweep, the change is more significant, as shown in Figure 2.11. There is a clear change in the behaviour of G' before and after the transition, when the blend is homogenous, the decrease in G' is steep with increasing temperature, however this becomes a plateau or gentle decrease after the transition.

The results are dependent on the measurement conditions; while changing the ramp rate does not appear to have a significant effect on the results, the frequency chosen does change the rheology at the phase transition. Of course it shifts the value of G', as demonstrated by the frequency sweeps, but also there is a dip in G'

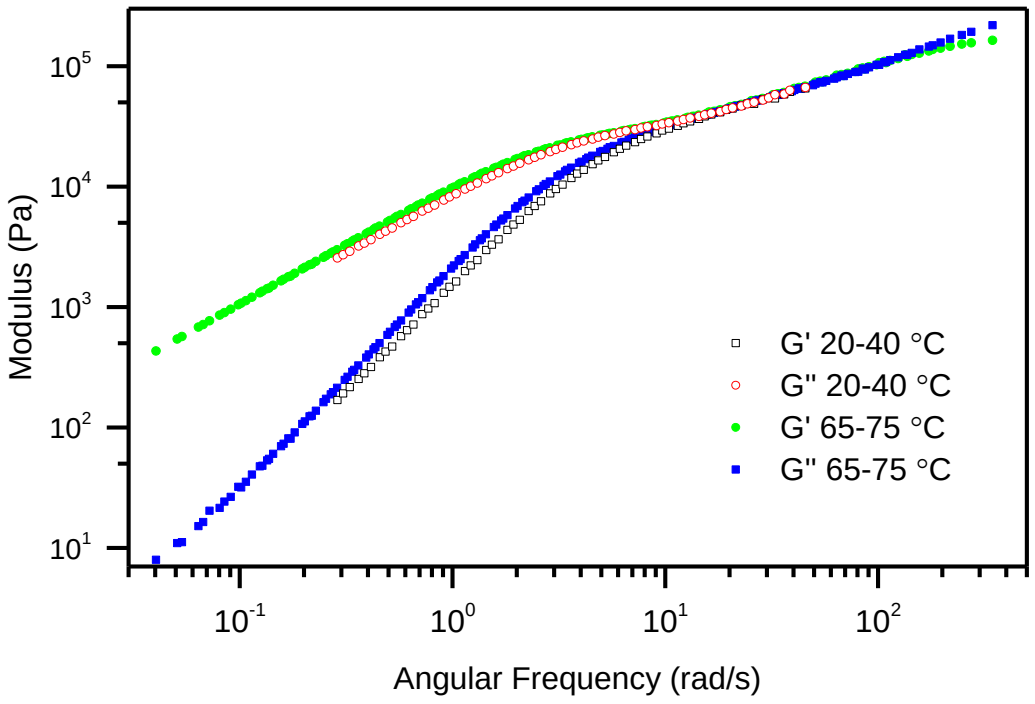

Figure 2.10: Variation of elastic modulus (G') and viscous modulus (G'') with frequency for a 1:1 blend of PBD40K and PI150K shifted to a temperature of 25 °C using WLF theory. Temperatures of 25 to 40 °C were shifted with C_1= 4.95, C_2=151 K, C_3=-1.58 and 65 to 75 °C with C_1 = 3.84 , C_2= 143 K, C_3=1.00 .

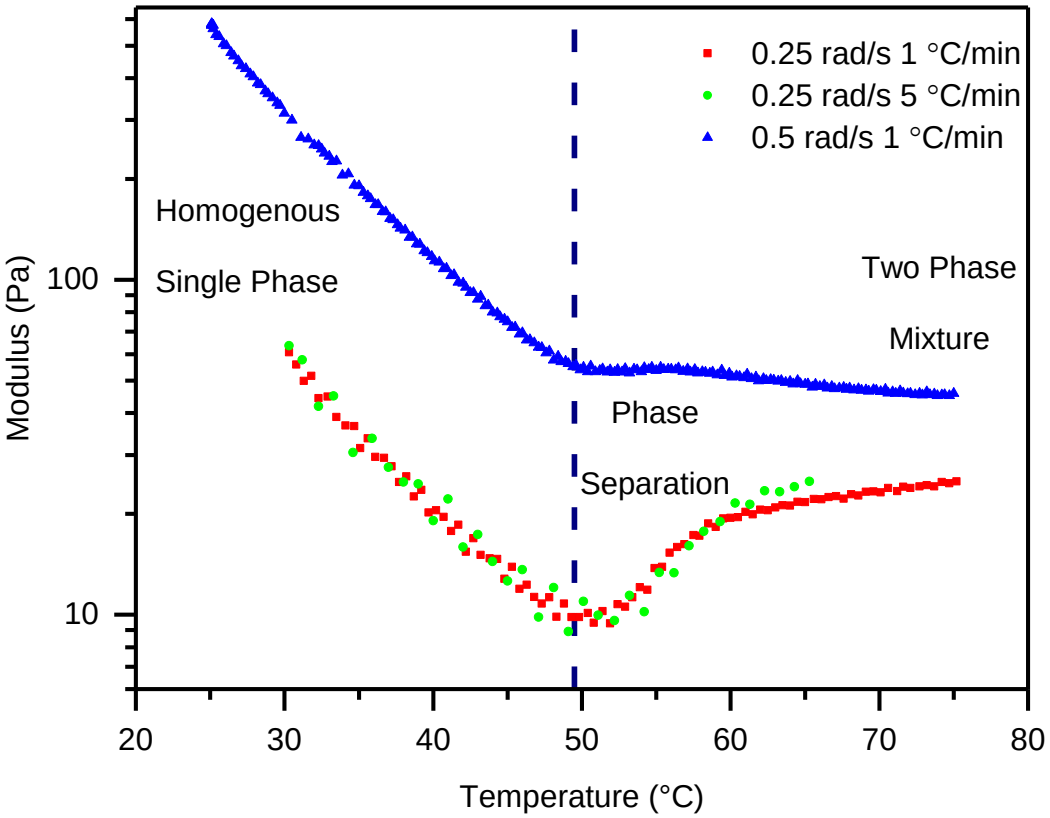

Figure 2.11: Graph showing the variation of G' with temperature at different angular frequencies and heating rates, the blue dashed line shows the extracted binodal temperature (49.5 °C)

at the phase transition that is only observed at lower frequencies (Figure 2.11).

A binodal temperature can be extracted from the point at which the data stops decreasing uniformly. The spinodal temperature of the blend was determined to be 49.5 °C. The spinodal temperature can be calculated by extrapolation of a $\left(\frac{G''^2}{G'T}\right)^{2/3}$ vs $\frac{1}{T}$ graph, as shown in Figure 2.12 and reported previously.[80] The spinodal temperature extracted in this way was 63.5 °C.

2.6.4 Discussion: SAOS across the phase boundary

The difference in the frequency sweeps before and after the phase transition is small, however it is significant enough that a single set of TTS parameters fails to fit all temperatures. Despite the small changes, this is likely an indicator of the phase transition that has taken place in between the temperatures of 40 and 65 °C. This is a low critical solution temperature blend, so the blend has phase separated as the temperature is increased.

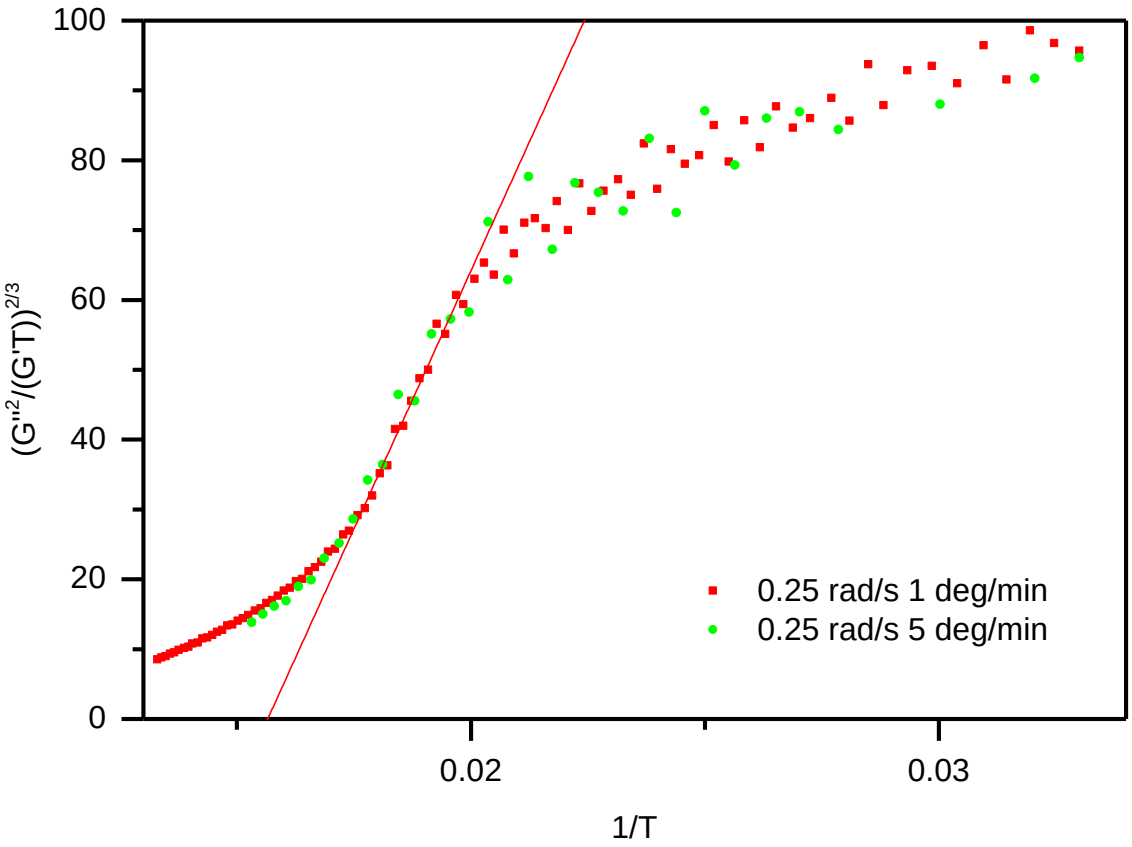

Figure 2.12: Heating ramps at 0.25 rad/s with extrapolated line in red to give the Spinodal temperature (63.5 °C)

The change in elastic modulus G' with temperature clearly shows the onset of phase separation. The three main contributions to G' arise from the bulk dynamics of chains and entanglements, concentration fluctuations caused by thermal noise, and interfacial contributions between any phase separated domains. Initially, increasing temperature causes G' to decrease, here the bulk contribution dominates; the higher temperature causes a decrease in viscosity and an increase in the mobility of the polymer chains. However increasing temperature also causes an increase in concentration fluctuations and when the phase boundary is reached, this effect combined with the creating of new interfaces dominates, causing an increase in G'. As new interfaces are no longer created, the bulk contribution begins to take over and the modulus again starts to decrease. This effect has been observed in literature and is consistent with measurements on similar systems.[79-80, 82-84]

It is seen that this feature is observed less at higher frequencies, despite both frequencies being well into the terminal region for all temperatures observed. This is likely because although the effect is still present, it is relatively small and still of the same magnitude regardless of frequency ($\Delta G'$ ~ 10 Pa). Hence, it is much harder to

identify at higher frequency where G' is larger and the relative size of the effect is smaller.

The heating rate appears to have very little effect on the results, apart from reducing the frequency of points that can be taken over the experiment. However, two relatively fast heating rates were chosen (in order to observe the effect). It would be expected that if slower rates were chosen, the increase would be smaller or not present, as this would decrease the amplitude of the concentration fluctuations, making the bulk dynamics more dominant.

2.6.5 Conclusion

A technique for identifying phase transition temperatures from rheological measurements was demonstrated, using a blend of polyisoprene and polybutadiene. Extrapolation of $\left(\frac{G''^2}{G'T}\right)^{2/3}$ vs $\frac{1}{T}$ was used to extract the spinodal temperature and the point that G' stopped decreasing uniformly was used as the binodal temperature. This gave values of 63.5 °C and 49.5 °C, for binodal and spinodal temperature respectively the blend of 40K linear PBD and 150K linear PI respectively which are in line with similar blends from literature.

2.7 Validation of the Cox-Merz rule

While the usefulness of the elastic modulus and viscous modulus has been demonstrated extensively in this chapter, the other parameter that can be calculated from oscillatory measurements is the complex viscosity. It has been discussed in the introduction that for many polymers it has been observed that the complex viscosity is equal to the steady shear viscosity when the frequency of the oscillation is equal to the shear rate of the shear flow. This is known as the Cox-Merz rule.[138] In order to demonstrate this, the viscosity of a linear polystyrene has been compared under steady shear and oscillatory flow in a rotational rheometer, as well as under steady shear in a capillary rheometer.

2.7.1 Materials

Polystyrene PS315K was purchased as pellets from Sigma-Aldrich (Product code: 441147 ALDRICH).The materials parameters were: M_w = 315 kg/mol, M_n = 111 kg/mol, PDI = 2.84, as determined by gel permeation chromatography a dn/dc value of 0.184 mL/g for polystyrene

2.7.2 Experimental

The material was characterised using a TA Instruments HR2 rheometer using an 25 mm parallel plate geometry. Samples were pressed into 1 mm thickness discs of the 25 / 8 mm diameter using a mould in a hydraulic press, under a pressure of 4 tonnes for 10 minutes at 150 °C.

Measuring gap was determined by the procedure described in 2.2.2. The ETC, supplied with nitrogen gas was used to maintain temperature. Frequency sweeps were performed at each temperature at 1 % strain between frequencies of 0.1 and 600 rad/s recording 10 points per decade. A WLF TTS was applied to give one spectrum for each material at 25 °C. The parameters were fit to give best overlap of the data and the values used for each material are given in Figure 2.13.

The steady shear measurements were performed using the same geometry in the TA HR2, at 170 °C and shear rates of 0.001 s^{-1} to 0.3 s^{-1}, since at higher shear rates the sample began to escape the gap.

Pellets of the sample were loaded into a twin bore Malvern RH2000 rheometer fitted with a capillary with diameter of 1.5 mm, 1.0 mm or 0.5 mm each with a length/diameter ratio of 16 and a matching diameter orifice die. Measurements were performed at 170 °C at speeds of 0.1 – 10 mm/s. The Bagley correction[13] was

applied for the exit and entry effects and the Rabinowitsch correction[28, 111] made to the shear rates to account for shear thinning.

2.7.3 Results: Comparison of complex and steady shear viscosity for a polymer melt

The frequency sweep results are shown in Figure 2.13, the full range of behaviour from the terminal region to the chain stretching region was observed. The rheology is typical of a linear polymer, but is clearly polydisperse, as the crossover is fairly broad and G' does not show double the gradient of G' in the terminal region.

The complex viscosity for this same experiment is shown in Figure 2.14, alongside the steady shear viscosities extracted from flow measurements in the rotational rheometer and capillary rheometer. The capillary results match the complex viscosity well, however the shear results in the rheometer are significantly different.

2.7.4 Discussion: Comparison of complex and steady shear viscosity for a polymer melt

The deviation seen for the steady shear measurements on the rotational rheometer is likely because of wall slip and other effects such as sample escaping the gap or edge fracture. Any of these effects would cause a drop in viscosity as is observed. The open sided geometry is not ideal for measuring steady shear data for rubbery polymers as these effects are prevalent. It is for this reason that the Cox-Merz rule is important for these materials, as steady shear measurements are not necessary, as

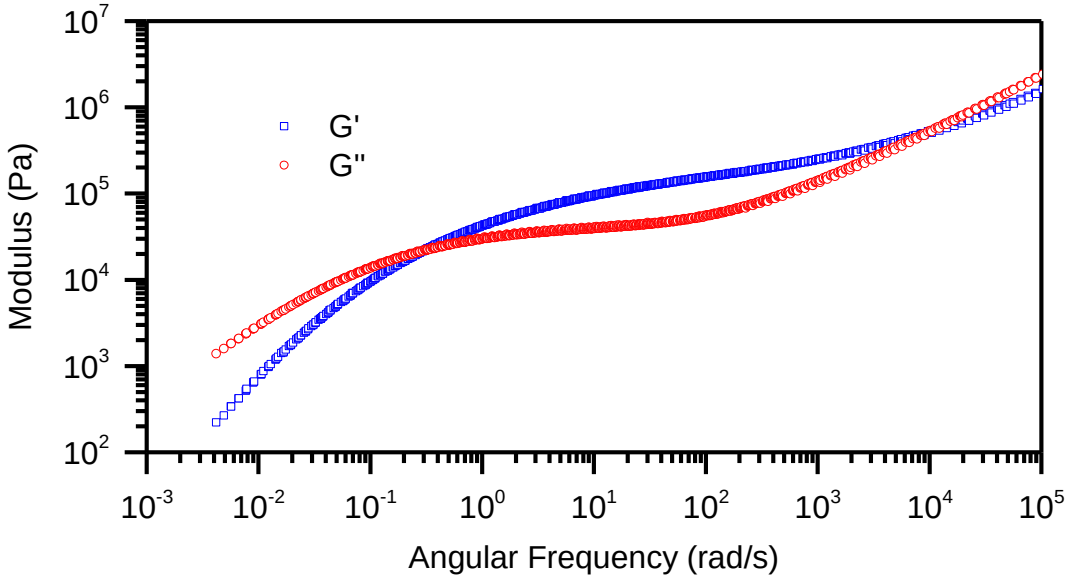

Figure 2.13: Rheological spectrum of PS, a combination of measurements made between 130 and 210 °C and shifted to 170 °C using a WLF time-temperature superposition with the parameters C_1=5.15, C_2=-60.3, ρ_0=0.950 C_3=-5.14

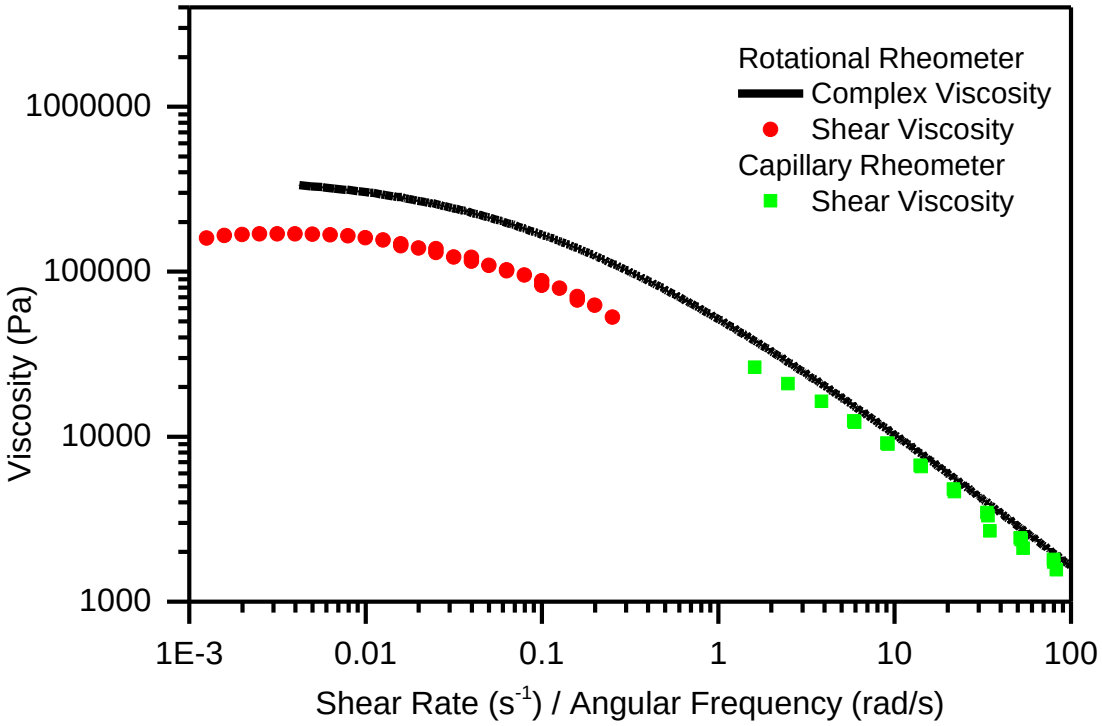

Figure 2.14: Comparison of the complex viscosity extracted from oscillatory shear measurements with steady shear measurements made in a rotational and capillary rheometer

complex viscosities from SAOS can be used.

Despite this, the fact that the complex viscosity matches well with the measurements from the capillary rheometer shows that the Cox-Merz rule holds for the material. This is expected as it has been observed in literature previously for many polymers. The relationship is an empirical one, and while it has been shown to work for many systems experimentally[138-139] and in constitutive models[8], it also fails for systems including biopolymers and foods.[7, 140-141]

The consequence of the Cox-Merz rule holding for the majority of polymer melts, is that the oscillatory measurements, such as those detailed in this chapter, can be applied to steady shear systems such as industrial mixing and extrusion problems.

2.7.5 Conclusion

By comparing capillary rheometry to complex viscosity from oscillatory measurements, the Cox-Merz rule was validation for a linear polystyrene. Shear measurements from the rotational rheometer however were shifted from the values of the capillary rheometer and complex viscosity, which is believed to be due to slip and sample escaping the gap during the measurement.

Although polystyrene was chosen for ease of the capillary rheometry measurements, this relationship has been previously shown to hold for polyisoprene[142] and polybutadiene[142-143], and hence is applicable to the majority of melts studied in this work, however it does fail for more complex systems such as when filler is introduced to the polymer.[144]

2.8 Concluding remarks

In this chapter, small amplitude oscillatory shear has been used to characterise polymer melts and their blends. SAOS has been shown to be sensitive to molecular weight in linear polymers, as well as the structure in more complex materials (e.g. introducing a branch point increases relaxation time significantly). Through fitting of molecular models, materials parameters can be extracted and predictions of polymer structure can be made. Branch-on-branch theory was shown to be a powerful tool for structure prediction and even for identifying the amount of different components in a blend. However, complexity can increase rapidly in polymeric systems, as polydispersity is introduced as well as blends of different components. Since rheological response is not unique, as this complexity increases, the amount of systems that can give the same response also increases rapidly, and so the predictive ability of SAOS still fails for many systems. It is for this reason that rheology must be combined with other techniques in order to fully characterise a material. Alternatively, more novel rheological techniques can be used, as will be explored in the following chapters.

It is possible to study phase separation events using linear rheology, but when the polymers chemistry is similar, the signal characteristic of phase separation is small compared with features that could arise due to structure. Hence they could easily be missed and experimental setup much be specifically tailored to the system in order to study the phase separation.

The Cox-Merz rule has been shown to be useful in extending the applicability of oscillatory measurements, but it should ideally be validated in each case since exceptions are known.[7, 140-141]

3 Extensional rheology

Extension is an alternative method of measuring rheological properties, where the sample is deformed in a way which leads to a velocity gradient in the same direction as the applied force, i.e. the material is stretched (see Section 1.1). Many industrial flows include both shear and extensional components, and hence it is important to understand the behaviour under both types of deformation, which can be very different.

However, methods for measuring extensional rheology are generally less well developed and used than those to quantify the shear response. In this chapter, multiple methods are used to gain insight into the extensional rheology of various materials. Firstly, Sentmanat extensional rheometry (SER) is used to characterise the behaviour of some of the polyisoprenes and polybutadienes from Chapter 2, examining the effect of molecular weight in linear polymers and the effect of branching.

Alternative methods of studying extensional rheometry are also introduced, capillary breakup extensional rheometry (CaBER) is used to study those materials with viscosities too low for the SER. In this way a linear and branched material are compared. Finally, a falling weights experiment is conducted with similar low viscosity samples, in order to quantify the force on the sample, and hence the stress in the material, and so extract information about the extensional viscosity.

3.1 Sentmanat extensional rheometry

Sentmanat Extensional Rheometry[22], is one of the most commonly used techniques for measuring extensional rheometry, as it is commercially available as an attachment for existing shear rheometers, as shown in Figure 3.1. It is capable of measuring the force on the sample during extension, and hence the extensional viscosity. Since it is compatible with existing temperature systems (ovens which can also be supplied with liquid nitrogen) it can measure a wide range of materials under different conditions. However sample breakup is an issue which can prevent a steady state being reached.

Here a range of linear polyisoprenes are studied as well as polybutadienes of different architecture in order to examine difference in behaviour between shear and extension, and study the effect of structure on extensional behaviour. Extensional rheology for linear polyisoprenes[145-147] and polybutadienes[148-149] has been previously reported, although surprisingly, there does not exist a systematic study across molecular weights. This is possibly due to the fact that temperature above room temperature are usually used, which limits the range of molecular weights of PI/PBD that can be studied. The low temperatures here reported allow lower molecular weights to be measured than in previous studies. The linear materials are fitted with rolie-poly theory which can capture extensional behaviour and allows stretch times to be extracted. The randomly branched PBD is studied by SER for the first time, again possibly due to random structures having high polydispersity and relatively low viscosity leading to difficulties in measurement. Material with long chain random branching has been studied by SER[150], which has a long backbone, and hence is higher viscosity and easier to handle.

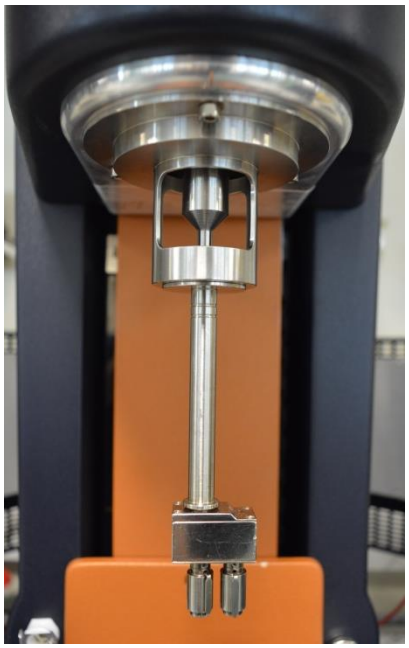

Figure 3.1: SER attachment applied to the rotational rheometer

3.1.1 Experimental

Polyisoprenes PI100K, PI300K, PI390K, PI500K, PI1380K and polybutadienes 3ARM and RB480K, as characterised in Chapter 2, were studied in extension. PBD28K is also used, which is a 28K molecular weight linear polybutadiene supplied by the synthetic labs at Michelin. The linear rheology of this is reported in Appendix 1.

A TA instruments HR-2 rheometer was used,

equipped with the SER2 attachment. The sample is fixed between cylindrical drums which rotate to stretch the sample up to Hencky strains of 3.8 (as defined in Section 1.2.3).

The samples were pressed into a template 10 mm long and 0.5 mm thick using a hydraulic press under a pressure of 4 tonnes for ~10 minutes at room temperature. For the low viscosity samples, in order to ensure samples kept their shape, the material in the mould was dipped into liquid nitrogen before it was applied to the drums.

The temperature was maintained using the ETC, closed around the SER and cooled with liquid nitrogen where necessary. A 100 s pre stretch at a rate of 0.001 s^{-1} was applied to prevent any sagging and ensure the sample was taut. The experimental stretches were then applied, at a range of rates between 0.01 and 100 s^{-1}, up to a maximum Hencky Strain of 3.8 (although data was trimmed when the sample broke up before this point). Each experiment was repeated three times to ensure reproducibility and the result which reached the longest time chosen to reduce the effect of imperfections in the pressed sample causing early breakup.

Four Maxwell modes[2] were fit to the shear rheology (as given in Chapter 2) between the low frequency crossover and the plateau in G'' (i.e. in the rubbery region). The values extracted are given in Table 3.1. These parameters were then fed into the rolie-poly equation.[56, 151] This is a theory for non-linear rheology incorporating convective constraint release due to flow of neighbouring polymers. It accepts as input the values of relaxation times and plateau moduli from the modes fit to the linear viscoelasticity (see Section 1.3.1 for full equation). In these fits, a single

Table 3.1: Parameters from Maxwell mode and rolie-poly fits to SER data

	Material					
	PI100K	**PI300K**	**PI390K**	**PI500K**	**PI1380K**	**PBD28K**
G1 (Pa)	1.71E+05	1.82E+05	1.83E+05	1.70E+05	2.67E+05	3.65E+05
G2 (Pa)	1.18E+05	9.10E+04	8.82E+04	8.73E+04	1.27E+05	3.45E+05
G3 (Pa)	8.39E+04	6.48E+04	5.91E+04	4.79E+04	6.21E+04	1.16E+05
G4 (Pa)	1.09E+05	6.42E+04	5.47E+04	5.64E+04	4.92E+04	1.61E+05
Tau1 (s)	1.51E-01	4.84E+00	1.42E+01	3.62E+01	1.08E+03	4.13E-03
Tau2 (s)	2.09E-02	8.23E-01	2.22E+00	7.33E+00	1.19E+02	5.83E-04
Tau3 (s)	2.91E-03	1.40E-01	3.49E-01	1.49E+00	1.30E+01	8.16E-05
Tau4 (s)	4.04E-04	2.37E-02	5.48E-02	3.02E-01	1.43E+00	1.14E-05
Adjust G	1.00E+00	1.20E+00	1.24E+00	1.30E+00	1.00E+00	1.75E+00
Stretch Time (s)	5.01E-03	2.58E-02	6.79E-02	4.46E-02	7.06E-01	5.01E-04

stretching mode was used, the timescale of which was fit to the data. The adjustG parameter was also fit to the data, which adjusts the magnitude of the extensional viscosity to account for any differences between the predictions based on the shear data, and was always close to one. AdjustG and the chain stretch time were therefore the only adjustable parameters.

3.1.2 Results: Extensional response of linear polymers over a large range of molecular weight

Figure 3.2 shows the extension viscosities extracted from the SER experiments for

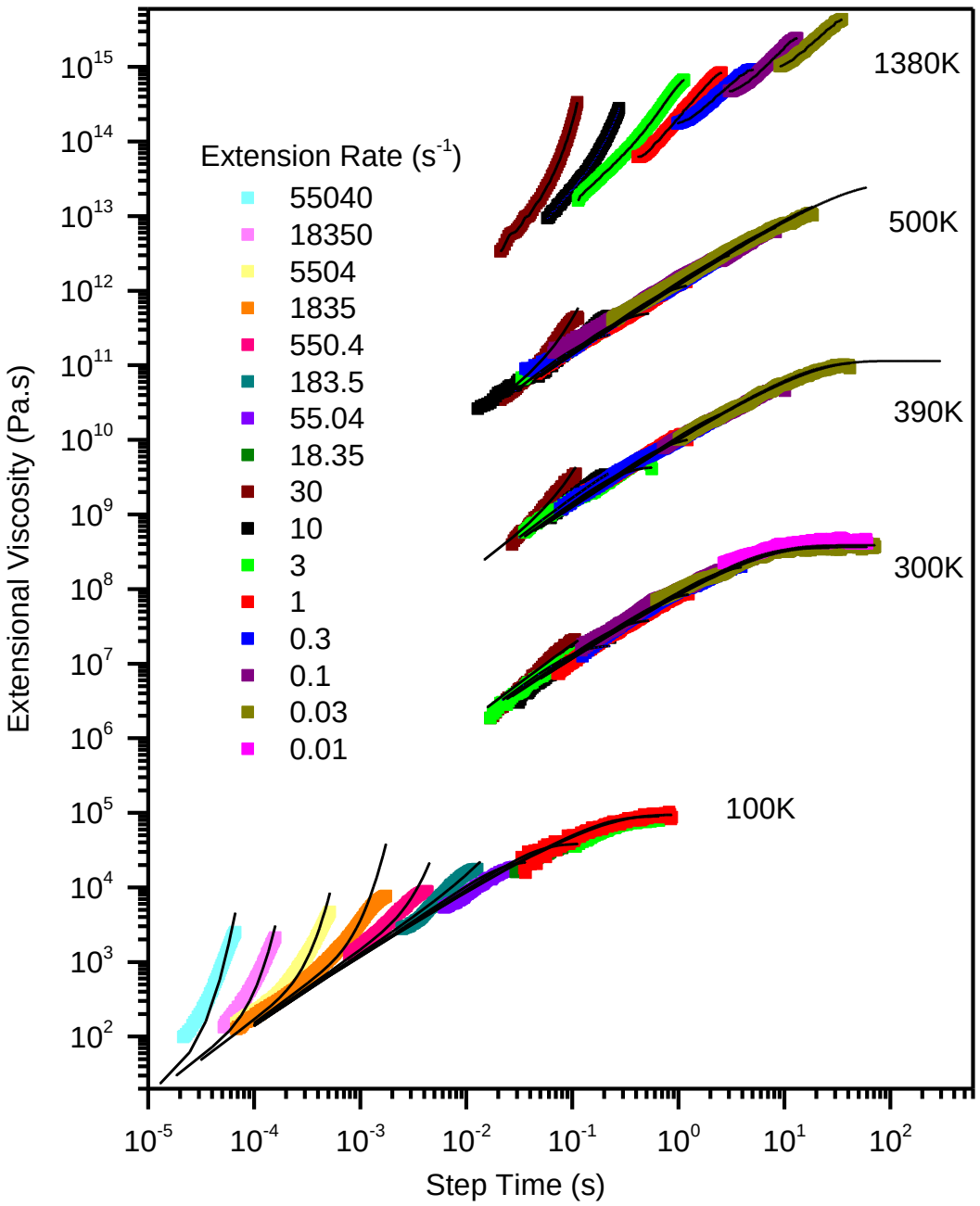

Figure 3.2: Extensional rheology measured on the SER for a range of linear polyisoprenes, shifted to 25 °C. Black lines are a rolie-poly fit with parameters given in Table 3.1. Each dataset is offset by a factor of 100.

the linear polyisoprenes. The majority of experiments at room temperature showed no extensional strain hardening. Strain hardening can be seen when the viscosities curve upwards away from the linear behaviour (i.e. when extensional viscosity = 3* shear viscosity).

Within the accessible extension rates of the SER measurement, the amount of strain hardening increases with the molecular weight, with PI1380K showing the most at room temperature. PI100K shows significant strain hardening, since measurements were conducted at a temperature of -40 °C, and this is demonstrated by the higher rates and shorter times of the experiments when the results are shifted to 25 °C, the measurement temperature of the other linear polyisoprenes.

The rolie-poly model fits the experimental data well, with only a single stretch time and the extracted stretch times appear to follow a log-log relationship with molecular weight, as shown in Figure 3.3.

For the polybutadienes, shown in Figure 3.4, a fit was only performed on the linear PBD28K (measured at -40 °C), and it again matches well with the data. There is no strain hardening observed for the 3 arm star at room temperature, however the randomly branched polymer shows a large amount of strain hardening in the tests (performed at -20 °C, necessitated by the low viscosity of the sample). In fact in the times that overlap between the linear and randomly branched polymer, the extensional viscosities before strain hardening are very similar for both materials (note that in Figure 3.4 the two materials are offset by a factor of 100), however the amount of strain hardening for the randomly branched material is much greater.

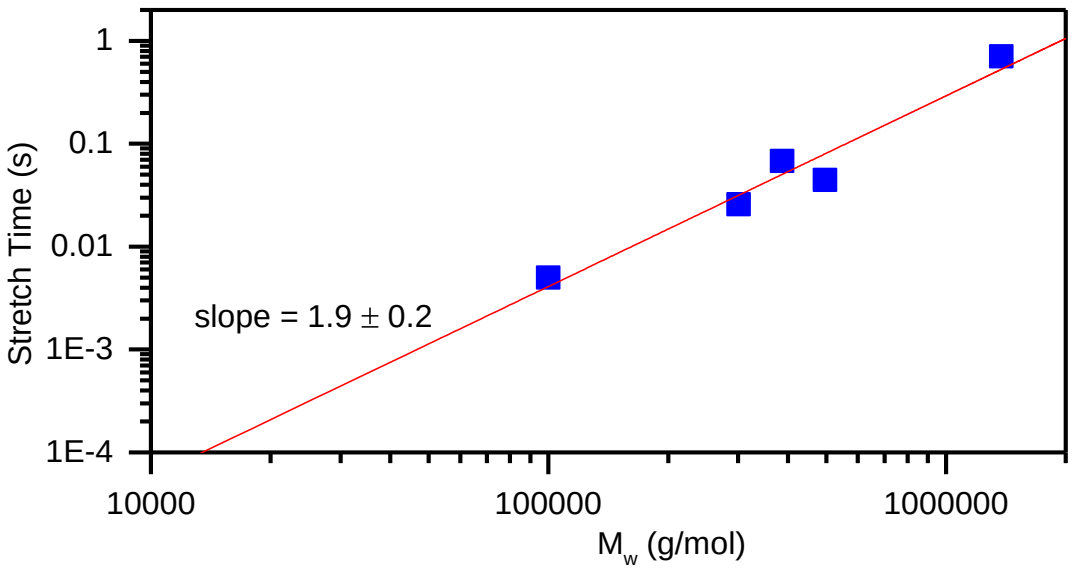

Figure 3.3: Stretch times at 25 °C measured from the one stretching mode rolie-poly fit to the experimental SER data for linear polyisoprenes.

3.1.3 Discussion: Extensional response of linear polymers over a large range of molecular weight

Where strain hardening is seen for the linear polymers, the strain rate is exceeding the inverse Rouse time of the polymer, i.e. the deformation is fast enough to cause stretching of individual chains, causing alignment which opposes further extension and leads to a steep increase in viscosity. Hence, the observed dependence of this time on the molecular weight seen in Figure 3.3, as the speed required to stretch the chains will drop with chain length. According to Likhtman-McLeish Linear theory[52], the Rouse time is given by:

$$\tau_R = \tau_e Z^2 = \tau_e \left(\frac{M_w}{M_e}\right)^2 \tag{3.1}$$

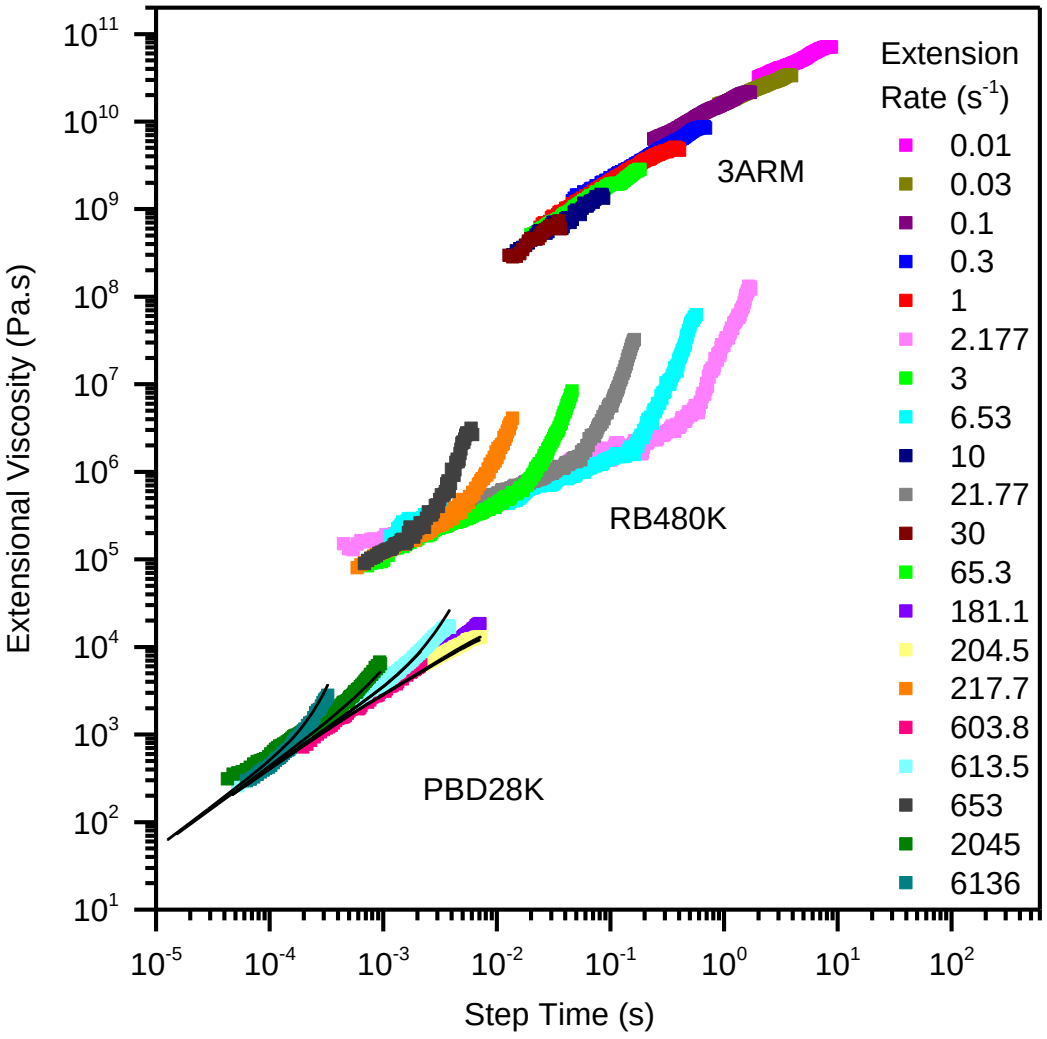

Figure 3.4: Extensional rheology measured on the SER for a range of polybutadienes, shifted to 25 °C. Black lines are a rolie-poly fit with parameters given in Table 3.1. Each dataset is offset by a factor of 100.

where τ_e is the entanglement time, Z is the number of entanglements, M_e is the entanglement molecular weight and M_w is the molecular weight of the polymer. As M_e and τ_e are constant for a single material, we would expect a dependence of the stretch time on molecular weight squared. This is within the error of the observed slope in Figure 3.3.

No strain hardening is seen for the branched 3 arm star, as molecules have a single branch point, which has no effect on the extensional behaviour, and so it will only strain harden when the linear sections begin to stretch. However, in molecules with multiple branch points, the extensional viscosity is much increased, as the sections between branch points (with no free ends), cannot retract and can be stretched much more easily under an extensional flow than if it was a lone linear chain (due to the bulky chains on each end).[152-153] This leads to significant strain hardening with a rapid onset, as it seen for RB480K, which is a highly branched material.

Few of the tests, particularly those that demonstrate strain hardening, reach a steady state (i.e. a plateau in extensional viscosity with time). This is a problem with Sentmanat extensional rheometry, as steady state extensional viscosities can be difficult to obtain without break-up of the sample. However, there is a large amount of information that can be obtained from the transient extensional viscosities, and it is clear that SER is sensitive to molecular weight and the level of branching in a material, and can be used to identify material with multiple branch points.

3.1.4 Conclusion

The extensional rheology has been quantified for series of linear polyisoprenes over a large range of molecular weight. Extensional strain hardening was observed which cannot be predicted using linear rheology alone. Rolie-poly theory was shown to give good fits to the data using only a single stretching mode. The chain stretch times extracted in this way followed the expected dependence on molecular weight. Polybutadienes with linear, star and randomly branched structures were also examined, using low temperature SER measurements to allow measurement of low viscosity samples. The randomly branched material showed significant strain hardening, despite having a relatively low initial shear and extensional viscosity, due to its highly branched structure. In this way, the amount of strain hardening in extensional rheology has been shown to be sensitive to multiple branch points in a sample.

3.2 Capillary breakup extensional rheometry

Capillary breakup extensional rheometry is an alternative commercially available rheometer for measuring extensional properties. Although generally the CaBER is most suited to low viscosity materials such as polymer solutions, it can also be used to give information about the extensional properties of polymer melts, when they are too low in viscosity to be studied with the SER. Here two polymer melts are used as examples, PI20K and RB150K, which could not be studied in the SER, even with liquid nitrogen and careful setup. By choosing these samples, a linear and a branched material, the difference in extensional properties could be captured using this technique.

3.2.1 Experimental

Materials were PI20K and RB150K, as characterised in Chapter 2. The CaBER, equipped with 6 mm diameter plates, was setup to perform a step strain in 20 ms, moving from a starting separation of 3 mm to end separation of 12 mm. The experiments were performed at room temperature, measured at ~25 °C throughout all the tests. The diameter of the filament was observed using a laser micrometer placed at the midpoint of the filament (i.e. halfway between the final positions of the plates). A camera was also used to observe the thinning as it took place and identify any irregularities.

3.2.2 Results: Relaxation after a step strain for a linear and branched material

Images on an experiment on PI20K can be seen in Figure 3.5, showing the initial strike and subsequent relaxation of the filament over time. The evolution of the filament diameter as read by the laser micrometer is shown in Figure 3.6 for the two materials. It is clear from the timescale of the two decays that the RB150K has a

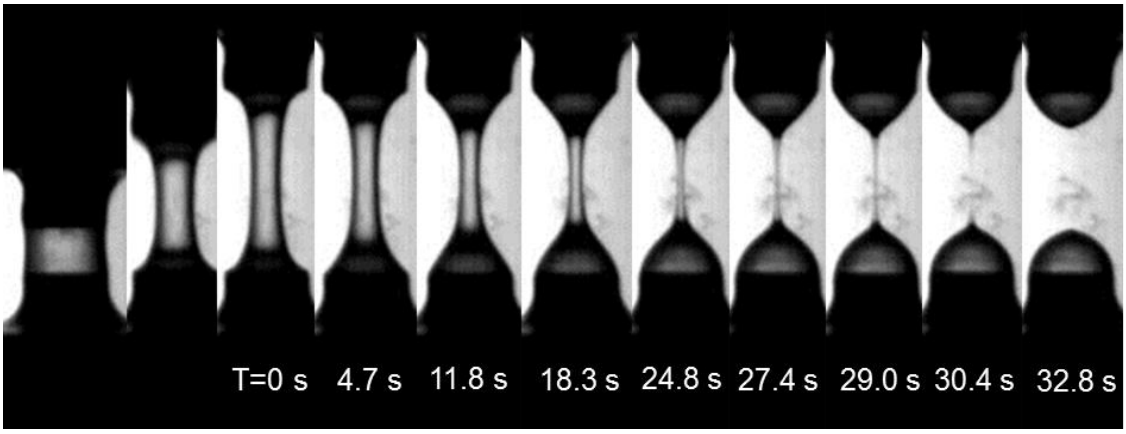

Figure 3.5: Images of a CaBER experiment of PI20K, at approximately 25 °C, with a 6 mm plate and a 9 mm, 20 ms strike and the subsequent thinning of the capillary. Time starts at the end of the strike.

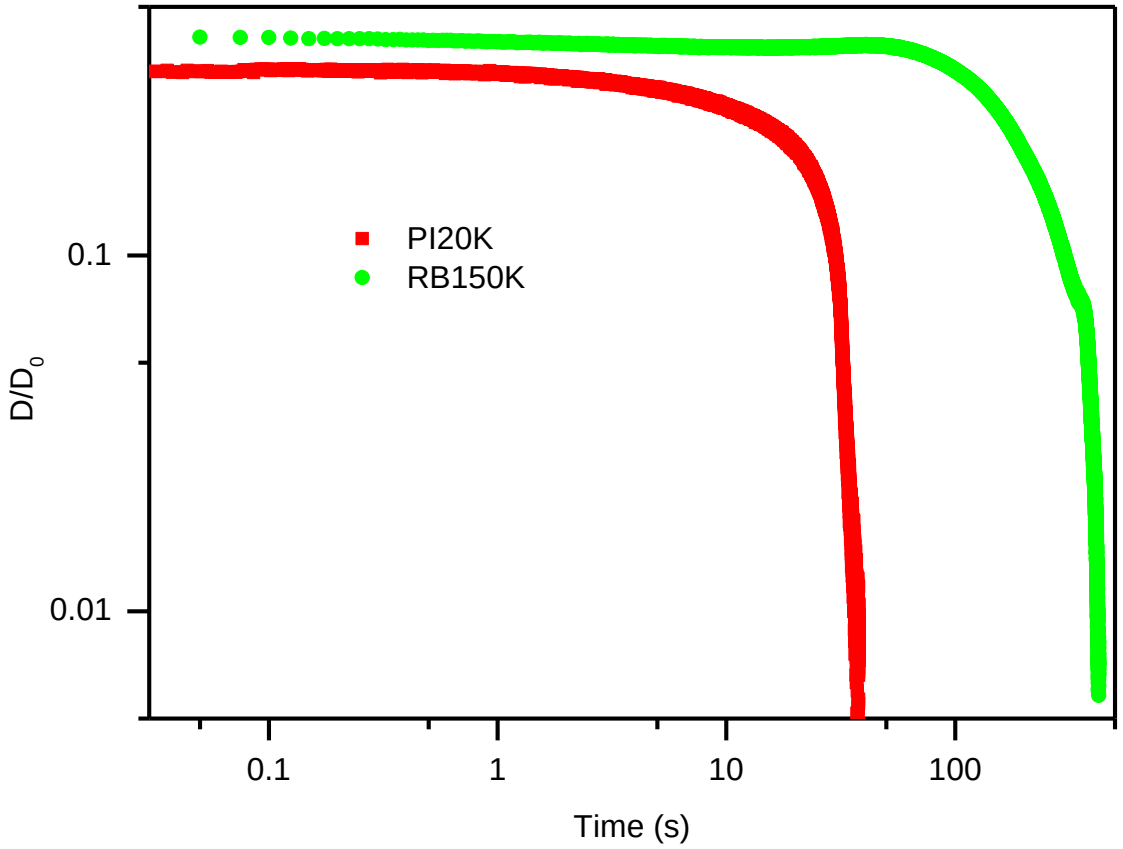

Figure 3.6: Thinning of filaments of PBD28K and RB150K after a 9 mm 20 ms step strain. Filament diameter is normalised by initial plate diameter.

much longer relaxation time than PI20K. CaBER results can be fit with various models[24], for a Newtonian fluid the diameter should decay linearly with time and this fits the results of the PI20K well, as shown in Figure 3.7. The diameters drop off more quickly than expected for a Newtonian fluid at long times due to onset of capillary breakup. However, the results of the RB150K do not behave in this way, but rather the logarithm of the diameter appears to decay linearly with time, as shown in Figure 3.8, which indicates a weakly elastic fluid. For RB150K, as well as a drop off at long times there is also an initial plateau which does not follow weakly elastic behaviour.

3.2.3 Discussion: Relaxation after a step strain for a linear and branched material

The fact that PI20K behaves as a Newtonian fluid suggests that we are not stretching the material fast enough to stretch the individual chains. The extension rate of the initial step strain can be calculated using:

$$\dot{\varepsilon} = \frac{1}{L_0}\frac{dL}{dt} \tag{3.2}$$

where L is the separation and L_0 the initial separation. Hence the extension rate for the 20 ms strike from a separation of 3 to 12 mm is 150 s^{-1}. This is slightly higher than the range of extension rates accessible in the SER at room temperature (where most materials showed Newtonian behaviour), but this material is much lower molecular weight than those studied in the SER. Extrapolation of Figure 3.3 gives a value of ~0.0002 s for 20K linear polyisoprene at 25 °C, which would give a Weissenberg number of 0.03, hence we would expect a Newtonian response during the step strain. The subsequent relaxation will have a different extension rate, depending on the relaxation time of the fluid, but it will be much lower than this value, particularly because the extension rate will be highest for materials that thin and break up quickly (on the scale of milliseconds), but the high viscosity of these samples mean the experiments are much longer. Therefore it is no surprise that Newtonian behaviour is observed. This behaviour is seen up until long times, when the filament begins to neck and breaks up, this is commonly reported in CaBER measurements.[24]

The results of the RB150K are more interesting, as they show a non-Newtonian response. According to the definitions proposed by McKinley[24], the material would fall into the category of weakly elastic fluid. The non-Newtonian behaviour indicates that there are multiple branch points in the material, since a similar molecular weight linear polybutadiene would not show strain hardening at room temperature. The material must therefore contain components with multiple branch points, where the chains in between branch points are unable to retract and relax extensional stress. This information is difficult to obtain from SAOS (as given in Section 2.3), since a similar linear response could have been obtained for a combination of linear polymers, or stars, rather than highly branched material. It is also interesting that the short time data does not show the same dependence, and there appears an initial plateau. This is more characteristic of a Bingham plastic or power law fluid[24] and could possibly be a signal of a change between regimes. In the initial strike, the strain rate (150 s^{-1}) would be expected to give a significant amount of strain hardening in a highly branched material. This opposition to stretch may give the material more plastic behaviour. However, it does not reach the point of breakup, and the subsequent relaxation is at a much lower strain rate, so it is plausible that the material returns to weakly elastic behaviour.

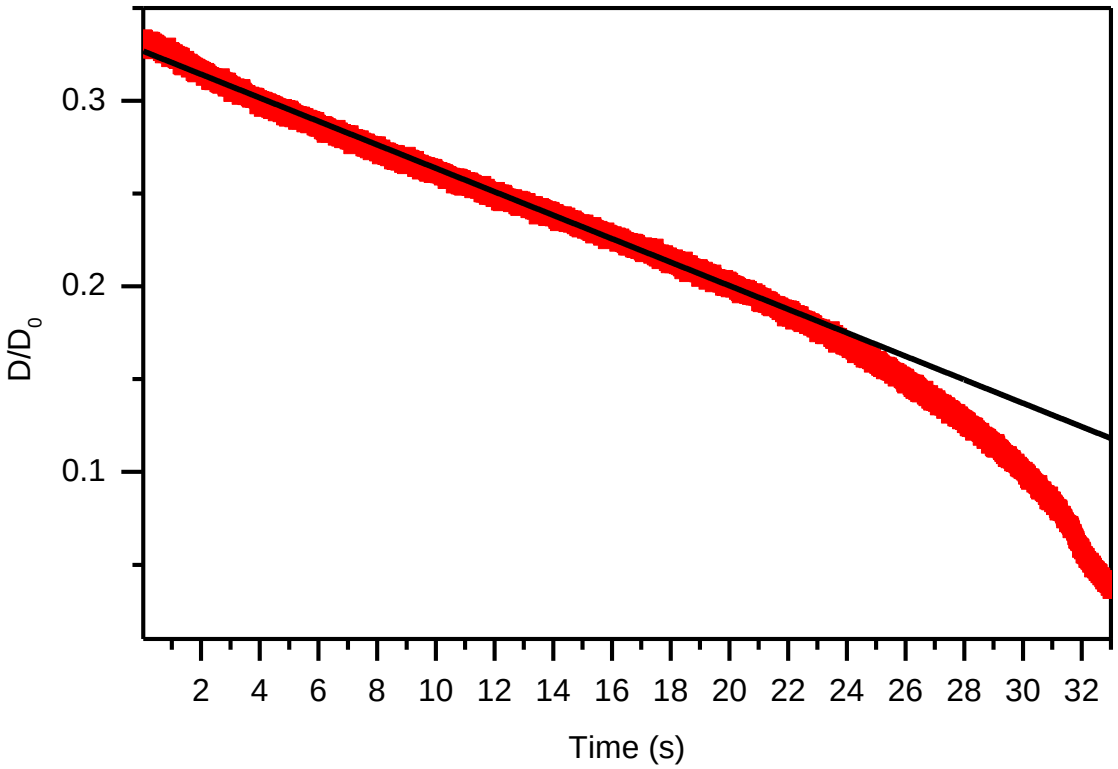

Figure 3.7: Thinning of a filament of PI20K after a 9 mm 20 ms step strain. Filament diameter is normalised by initial plate diameter and is shown with a linear fit.

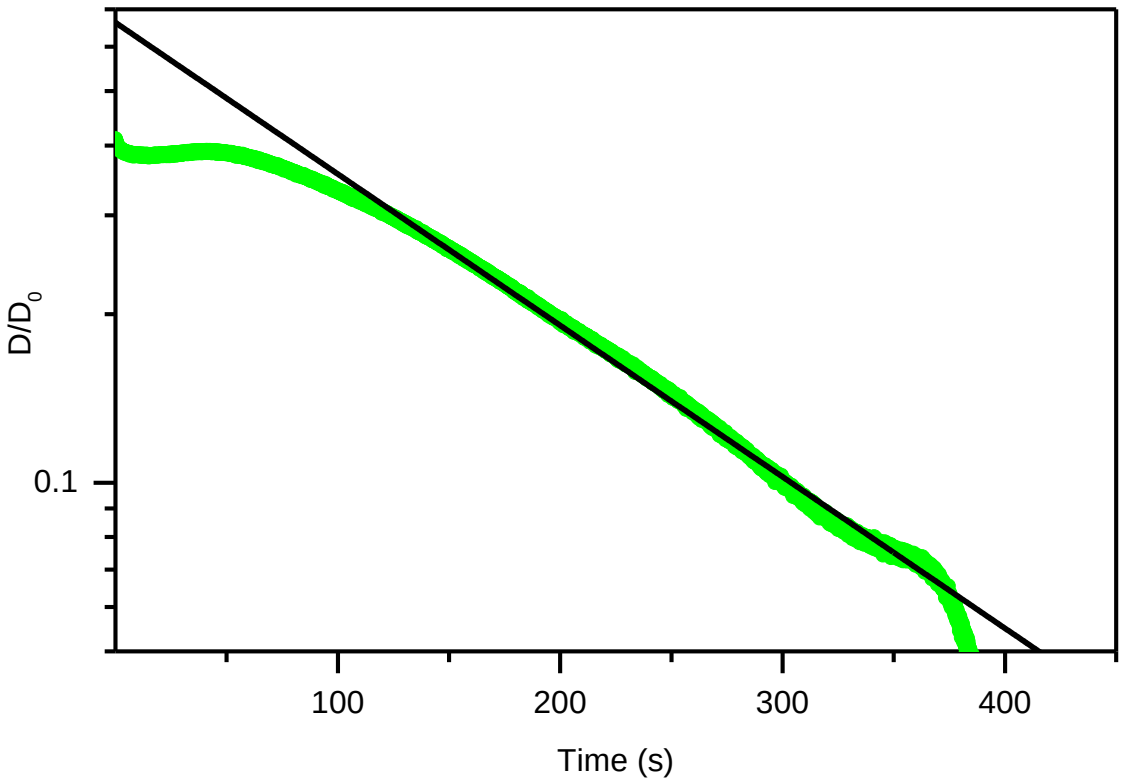

Figure 3.8: Thinning of a filament of RB150K after a 9 mm 20 ms step strain. Filament diameter is normalised by initial plate diameter and is shown with an exponential fit.

Although this technique gives a less quantitative description of the extensional behaviour of a material, it is useful for characterising extensional properties in materials too low viscosity to be analysed in the SER. At these viscosities (and consequently molecular weights), it would be highly unlikely that linear or star polymer melts would show any non-Newtonian behaviour, as the extension rates possible in the CaBER would be far below those required to stretch the short chains involved. Hence the presence of non-Newtonian behaviour can be used as a signature of multiple branch points.

The only issue preventing this technique being applicable to a wider range of materials is the viscosity requirement. With polymer melts, the viscosity quickly becomes too high to perform CaBER measurements as molecular weight is increased. This is since, even when the material will stick sufficiently to the plates, it can be very difficult, or impossible to find a set of conditions (strike time, plate size, strike distance) where the material does not break up under the strike, and the distance the plates move apart is sufficient to observe some thinning. It is for this reason that RB480K and PBD28K were not measured in the CaBER. However, for low molecular weight polymer melts, the signature of multiple branch points is easy to obtain and could be a powerful tool.

3.2.4 Conclusion

A linear and randomly branched material have been analysed by capillary breakup extensional rheometry in standard mode of operation. The technique was applicable to samples that were too low viscosity for the SER, but only gives a qualitative indication of the extensional properties of the material, since the force on the material is not measured. Nevertheless, for the polymer melts measureable in the CaBER, a clear difference can be seen in results for those with multiple branch points, and it is a simple tool for identifying interesting extensional behaviour.

3.3 Constant force extension: falling weights

One of the main pieces of information that is missing from the CaBER results is the stress on the filament. This cannot be determined without fitting the data because although the speed of the deformation is known, the resulting force on the sample is not measured. There are other rheometers that overcome this by adding force transducers (e.g. filament stretching extensional rheometers[25, 154]), however one simple way of performing an extension with known force is by using a weight.[155-156] Allowing the material to be extended under the influence of a known weight, the force on the filament can be simply calculated. This produces a different mode of extension to the CaBER and SER, as the extension rate is not fixed. This technique has been previously reported for polymer solutions but not applied to polymer melts.[155] Here, this is demonstrated for linear and branched polybutadienes in order to examine the information on the branching structure that can be extracted.

3.3.1 Experimental

Materials examined were PBD28K, RB150K and RB480K as characterised in Chapter 2. Materials were filmed falling under the mass of weights of 1 g, 2 g, 5 g and 10 g, using a camera at 38 fps. An example set of images is shown in Figure 3.9.

Using the multi-pass rheometer, the top piston was fitted with a plate matching the size of the weight required (6 mm for 1, 2 and 5 g and 8 mm for 10 g).The weight was rested on the bottom piston with a 1 mm gap between the top plate and the top of the weight, which was filled with the material.

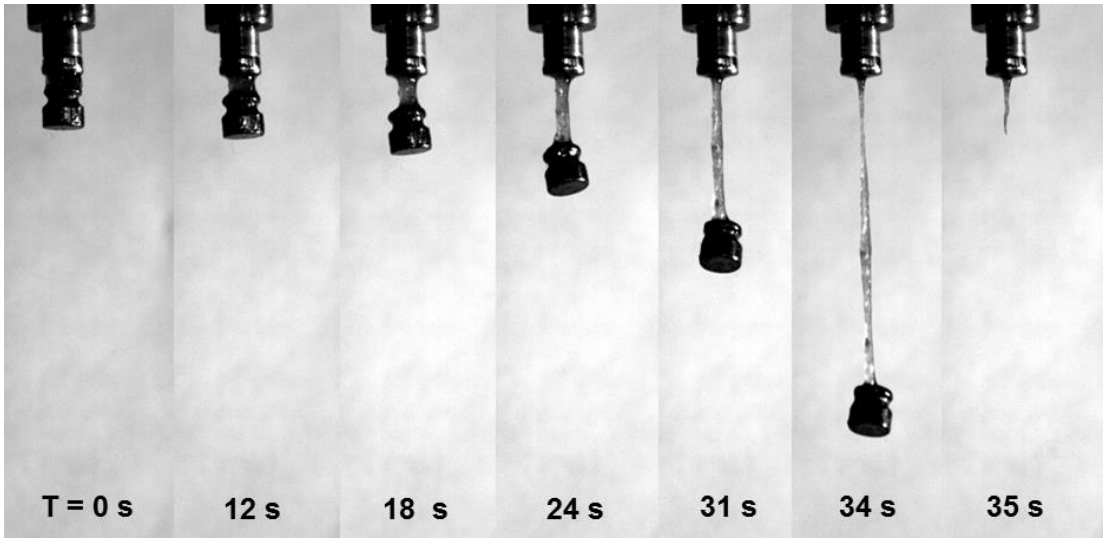

Figure 3.9: Images of PB28K falling under a 1 g weight

The top and bottom pistons were set to move apart at a speed of 100 mm/s for a distance of 40 mm, giving a total separation of 80 mm. After this quick initial step, the weight was allowed to fall under gravity. MATLAB code was written (given in Appendix 3) to analyse the images and extract the filament diameter (at the midpoint of the top plate and top of weight) over time. $T = 0$ was taken as the point when the movement of the pistons ended.

Each experiment was repeated 3 times to ensure reproducibility and a single dataset chosen for analysis (in cases where the filament broke, the dataset which reached the largest separation before breakup was chosen, similar to the SER procedure).

Balancing the forces at the centre of the filament, the gravitational force on the centre of the filament can be approximated as 9.81 kgm/s^2 times the mass of the weight. This must act counter to the forces caused by surface tension and the viscoelastic force in the capillary, so the extensional stress can be calculated as:

$$\sigma = \frac{9.81 * m}{\pi \left(\frac{d}{2}\right)^2} - \frac{\gamma}{\left(\frac{d}{2}\right)} \tag{3.3}$$

where m is the mass of the weight, d is the filament midpoint diameter, and γ is the surface tension, taken as 32 mN/m for polybutadiene.[157] The strain rate was then calculated from the position of the weight (x) over time, which was differentiated to give the speed. This was then fit with an exponential, with the equation

$$v = \frac{dx}{dt} = v_0 + Ae^{\left(\frac{t}{\tau}\right)} \tag{3.4}$$

where A, τ and v_0 were fit to the data. This exponential was used to give the extensional strain rate using Equation 3.2.

The original separation of the plates was measured from the images rather than assuming it was constant between experiments. The ratio of stress to strain rate then gave an extensional viscosity, which is transient because the strain rate is constantly changing.

3.3.2 Results: Constant force extension of linear and branched material

The parameters obtained from the fitting are shown in Table 3.3 and an example of the fit compared to the experimental data is shown in Figure 3.10. A single

exponential fit was found to fit the data well and effectively provide a ‘smoothed’ strain rate.

The extracted diameters, normalised by the initial diameter is shown in Figures 3.11 and 3.12. The experiments with different masses appear to give similar results apart from increased mass decreasing the timescale of the experiment. RB480K has timescales much larger than PB28K and RB150K, which both took similar times to fall. However there is a clear difference in the shape of the linear polybutadiene, which, although taking a while for thinning to begin, begins abruptly and thins very quickly, whereas for the randomly branched material the decrease is much more gradual. The extensional viscosity of PB28K and RB150K behave similarly, although the viscosity values are higher for the linear polymer and possibly a little strain hardening is seen at the end of the randomly branched experiments (although this is close to the point of breakup).

3.3.3 Discussion: Constant force extension of linear and branched material

The fact that the experiments on RB480K were much longer suggests a much higher extensional viscosity, however it also has a much higher shear viscosity (its zero shear viscosity is approximately 10 times larger than PB28K), so even if the material was Newtonian, some increase in timescale would be expected. Comparing the experiments at 1 g mass for PB28K and RB480K, the randomly branched material has extensional viscosity approximately 10 times larger than the linear, as would follow from shear viscosities. However, strictly these cannot be compared as the strain rates will be different. It is difficult to distinguish between the other two materials using diameters alone, although the abrupt decrease seen in the PB28K

Table 3.3: Parameters from Equation 3.4 fit to the extracted speeds of the dropped weights

Mass	Parameter	PB28K	RB150K	RB480K
1 g	v_0	0.050	0.30	0
	A	0.00054	0.0025	0.0021
	τ	2.5	0.44	66
2 g	v_0	0.050	0.30	0
	A	0.0024	0.0026	0.015
	τ	1.4	0.37	35
5 g	v_0	0.050	0.15	0
	A	0.0018	0.0037	0.035
	τ	1.0	0.28	32
10 g	v_0	0.10	0.35	0
	A	0.0063	0.051	0.053
	τ	0.67	0.22	25

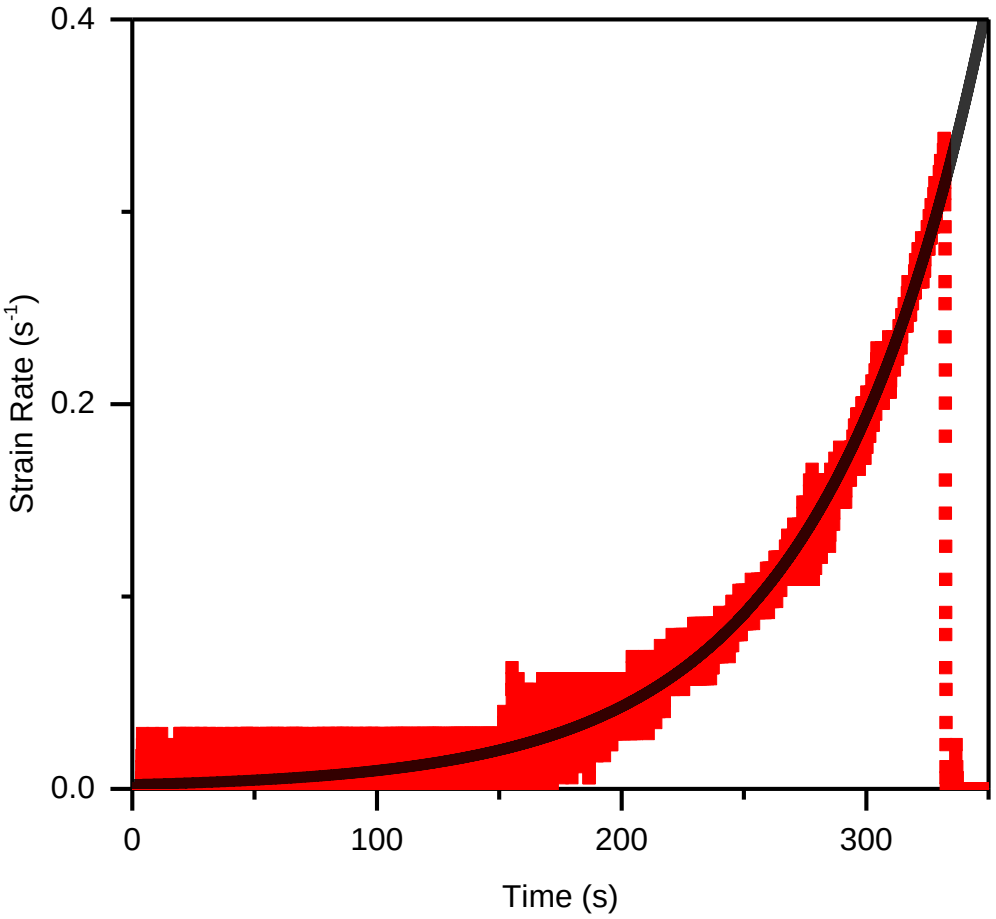

Figure 3.10: Strain rates for the 1 g mass falling with RB480K. Points show the values calculated by dividing difference in the plate position between the given time and the previous point, by the time step. The line shows the fit values according to parameters in Table 3.3.

suggests a more monodisperse material, (with a narrow range of extensional viscosity and defined by a single relaxation time) and perhaps points to a linear structure as larger components beginning to strain harden could contribute to the gradual decrease in the randomly branched materials.

However, when extensional viscosity is calculated, the difference is clearer. It should be noted that these are transient extensional viscosities, because the speed is constantly changing and the material cannot reach a steady state. A constant speed experiment with measurable force would be required to obtain steady state values (although as with the SER, this would be limited by the point at which the material breaks up). It is also important to remember that the strain rate is changing for each of these materials during an experiment, and in a different way (evidenced by the different parameters in Table 3.3). Hence it is not possible to directly compare the results with time. For example the RB480K has a much narrower range of strain

rates because the experiment was slower and did not reach as high a speed as the other materials.

Nevertheless, these transient extensional viscosities allow us to observe the extensional behaviour of these materials and make some distinctions between them. The decays for PB28K (Figure 3.11 a) have a certain 'yield time' after which the decays are exponential. There is a change in gradient towards the end of the decays, but this is likely due to the onset of breakup, as the decays drop off in a similar way to the CaBER experiments in Section 3.2. Similarly, the extension viscosities (Figure 3.12 a) show an initial plateau followed by a smooth and sharp decay, which is mainly due to the increase in strain rate with speed rather than due to an increase in stress in the material. For RB150K the decays (Figure 3.11 b) begin to look less exponential and curve from the initial plateaus, although show exponential behaviour at longer times. In the extensional viscosities (Figure 3.12 b), for the largest masses, 5 g and 10 g, some extensional strain hardening can be seen towards the end of the decays. For RB480K this effect is more pronounced, in the diameter decays (Figure 3.11 c) this curve from the initial plateau can be seen clearly for the 1 g results, where the entire decay is a curve and is non-exponential. This continues in the higher masses where there appears to be no initial plateau and the whole decay is characterised by the viscoelastic thinning. There is a kink seen towards the end of the higher mass results, which could indicate the onset of strain hardening, as the decay is slowed at this point. In the extensional viscosity results (Figure 3.12 c), significant strain hardening can be seen at the end of the extensional viscosity decays due to the inclusion of multiple branch points in the material. The shape of the RB480K decays are similar to those observed for polymer solutions (e.g. 0.025 % 2,840,000 g/mol PS in styrene oligomer[155]). The solutions reported in literature fall faster (giving higher extension rates) and include high molecular weight linear polymers, so significant strain hardening will be observed, as is seen for our randomly branched material. However, counter to our measurements, increases and decreases in acceleration are observed (deemed a 'bungee jump'). This is due to the cyclic nature of the increased acceleration causing a higher response from the polymer which in turn slows the acceleration and so on. The speeds in our experiments did not show this and the speeds showed an exponential increase, although it is possible that a subtle effect was not observable within the error of observing the weight position. However this could also be an effect only observed in solution, where the properties of the fluid and polymer compete.

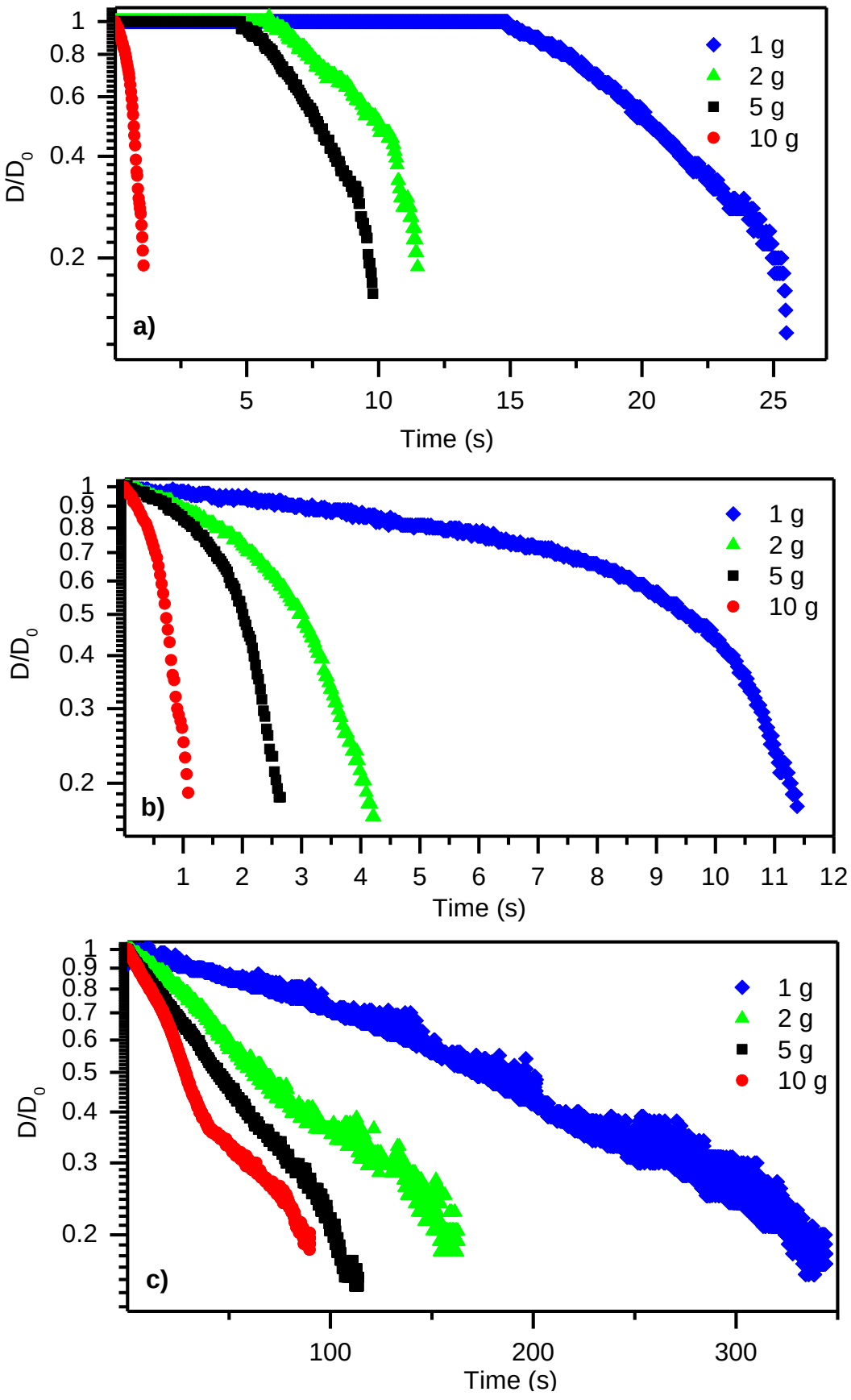

Figure 3.11: Evolution of the filament diameter (normalised by initial diameter) during a falling weight experiment for a) PBD28K, b) RB150K and c) RB480K

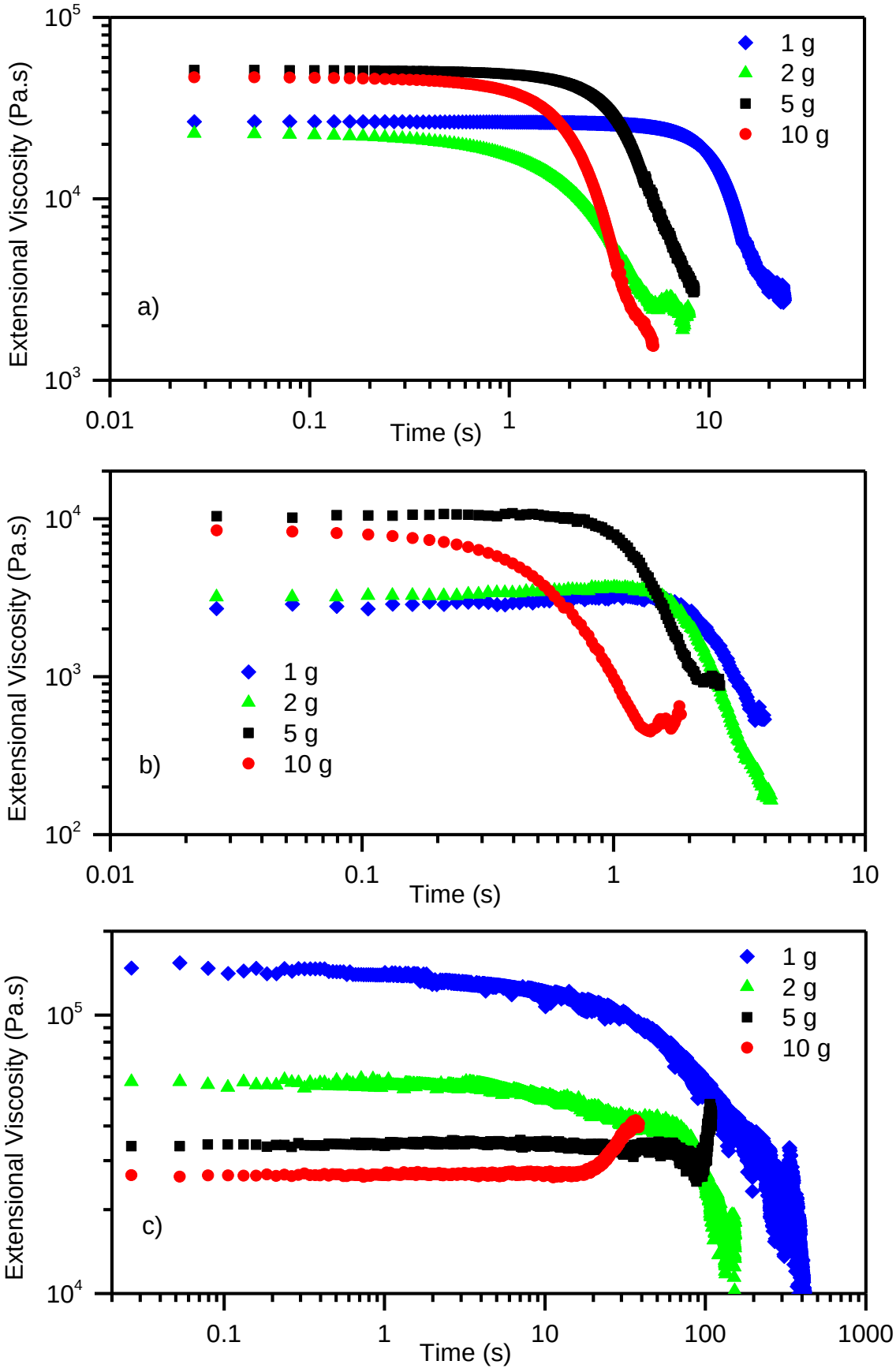

Figure 3.12: Evolution of the transient extensional viscosity during a falling weight experiment for a) PBD28K, b) RB150K and c) RB480K

Since the values of extensional viscosity are difficult to directly compare without knowing the strain rate, a comparison of the viscosities measured against the strain rate of the measurement is shown in Figure 3.13. As expected, the viscosities are highest for RB480K and the results span the lowest range of strain rates. PBD28K has intermediate values of extensional viscosity, since it has a higher complex viscosity than RB150K, which has the lowest extensional viscosities, despite the inclusion of some branch points.

v_0 was necessary to fit the strain rate data for the less viscous materials, but was less important for RB480K. This suggests there were some inertial effects, likely from the initial step to move the plates apart. This could be reduced by only moving away the bottom plate but this would reduce the plate separation and hence the distance the weight could fall. The effect only affected short timescales (< 0.1 s which were not significant on the scale of the experiment but if lower viscosity materials such as polymer solutions were used, this effect would become more prominent.

3.3.4 Conclusion

Falling weights experiments have been used to quantify the extensional properties of a linear and two randomly branched polybutadienes. Overall using dropped

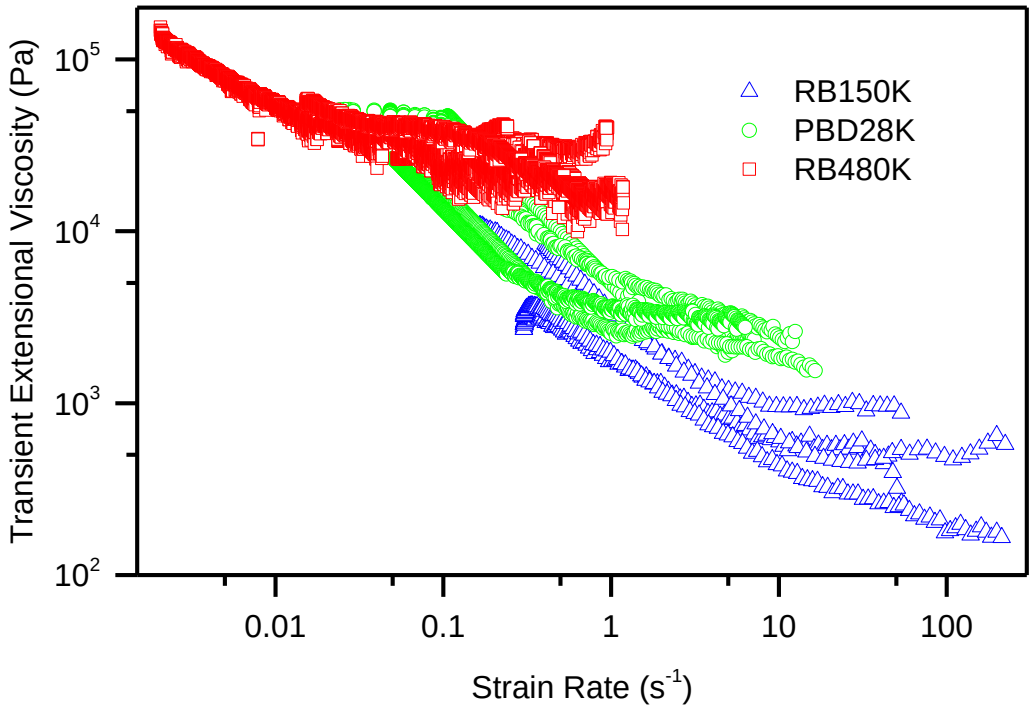

Figure 3.13: Transient extensional viscosities extracted from dropped weight experiments (all masses combined) plotted against the strain rate of the experiment.

weights has been shown to give a large amount of information about the extensional properties of a material, which is remarkable for a test that is very simple to execute. It gives similar information to CaBER experiments but knowledge of the forces involved allows calculation of the transient extensional viscosity. It is also works particularly well for higher viscosity materials (such as PB480K), for which it is difficult to perform CaBER measurements. A possible improvement would be adding some temperature control, (e.g. performing the test in an oven), which would allow more materials and conditions to be explored.

3.4 Concluding remarks

Sentmanat extensional rheology has been reported for a range of linear polyisoprenes and polybutadienes of varying structure, demonstrating the use of low temperatures to measure low viscosity samples. For samples too low viscosity even for this procedure, capillary breakup extensional rheology and falling weights rheology has been tested. CaBER measurements were shown to give a good indication of extensional properties (and can detect multiple branch points) but the force on the sample is required to quantitatively evaluate extensional viscosity at steady state. Counter to this, falling weights have a well-defined force during the measurement, but are accelerating, causing a constantly changing strain rate, hence the viscosity measured is transient and steady state cannot be reached. Despite this, the technique again gave a good indication of extensional properties and was equally as effective at identifying multiple branch points.

Extensional rheology has been shown to be a powerful tool for the identification of polymer structure, in particular for the detection of multiple branch points which cause strain hardening in extension. This branching is difficult to detect in linear rheology. Although increases in relaxation time are seen in SAOS with the introduction of a single branch point (as demonstrated for stars in Section 2.2), adding more branch points has a smaller effect on the relaxation process. It can also be difficult to determine whether increases in relaxation time originate from branching or other factors such as molecular weight. Since the strain hardening in extension (when combined with knowledge of the molecular weight) can usually uniquely be assigned to the presence of multiple branch points. However, since such a large effect is seen, it can be difficult to determine precisely the branching structure of the material, especially in polydisperse samples, where various combinations of arm lengths and branches would give similar results.

4 Complex flow: multi-pass rheometer studies

Most flow in industrial processes such as extrusion and mixing of materials is much more complex than simple shear or extension. In this chapter, flows which contain both components are studied, making use of the multi-pass rheometer (MPR) apparatus, as introduced in Section 1.2.5.

Firstly, a simple geometry is chosen, a contraction-expansion geometry, or narrow slit. Polystyrene is studied in flow through this geometry in order to study the change in relaxation times of the material with respect to flow rate, pressure and temperature. These results are divided into three subsets of results, Section 4.2, in which measurements are performed to design a procedure for exploring the influence of pressure, speed and temperature on this relaxation. Section 4.3 details a systematic study of the effect of shear rate, necessary to explore the relationship between the imposed deformation and the relaxation times of the polymer. Finally, in Section 4.4 pressure was studied in more detail, by making some adaptations to allow better pressure control, and through determination of Barus constants for the viscosity and relaxation times. The final set of results are also analysed by a comprehensive fitting procedure in order to extract relaxation times from both the pressure drop and stress fringes, and this work is published in Reynolds *et al*.[158]

Following the stress decays, extensional behaviour in the MPR is studied using a cross-slot geometry, which creates flow in perpendicular directions and generates extensional flow at the centre point. In this way the extensional behaviour of materials at steady state could be studied; data that could not be extracted from SER measurements. Selected results from these experiments are then compared to Flowsolve simulations based on the shear and extensional rheology from the SER.

Finally an experiment is performed to examine the structural changes in polymers arising from degradation, which has applications to processing situations, such as recycling polymers, where repeated heating and complex flow is required to reform and reuse the material.

4.1 The multi-pass rheometer

In order to generate the complex flow required for the experiments in this chapter, the multi-pass rheometer (MPR) was employed. The principle of the MPR is detailed in Section 1.2.5 of the introduction, but the apparatus details will be given here in

order to make the experimental set-up clear and to avoid repetition throughout the chapter.

The MPR apparatus is shown in Figure 4.1 and consists of two cylindrical reservoirs of polymer either side of a test section. Pistons in the top and bottom sections can drive the polymer into the test section at a set speed. This can be repeated multiple times at different speeds, pressures or temperatures, in this way, many experiments can be performed on the same sample. Pressure sensors in the top and bottom sections allow the pressure before and after passing through the test section to be measured, and hence the pressure drop caused by the test section can be calculated. The test section can be fitted with various geometries including slits, capillaries, cross-slots and more complex flow geometries. Windows on the sides of the test section allow the polymer flowing through to be observed, and if circularly polarised light is passed through, birefringence can be seen proportional to the stress experienced by the material. The MPR is heated with silicone oil, which flows from a circulator into jackets around each section. This allows the sample to reach temperatures of over 200 °C (this can be extended using oil that is stable at higher temperatures).

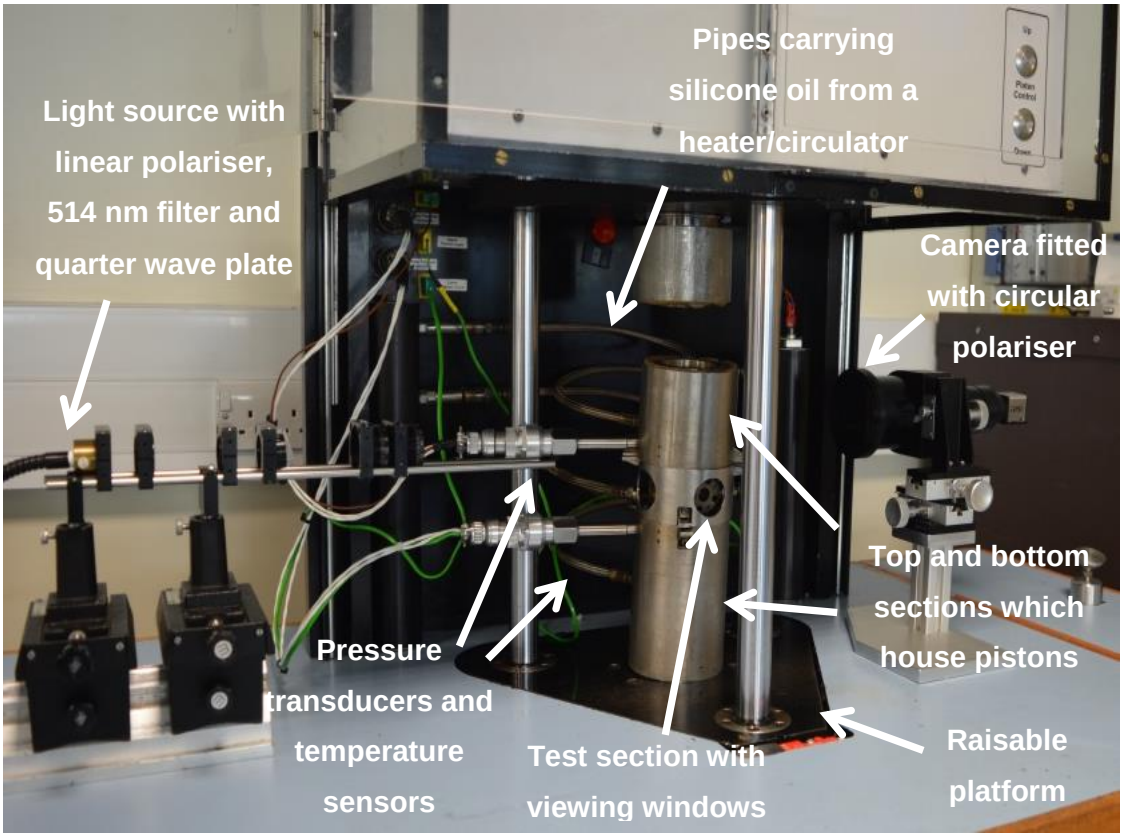

Figure 4.1: Multi-pass rheometer setup

4.2 Contraction-expansion flow: initial tests

In these experiments, the MPR was used to observe the decay of both stress and pressure in polystyrene, by observing flow through a contraction-expansion geometry with a well-defined shear rate. The pressure drop across the geometry was observed as well as the fringe pattern throughout the flow. By using the single shot mode of the MPR, these could be observed during a deformation until a steady state was reached, and then after the movement was stopped, the decay could be observed. Initial experiments were planned to span a range of shear rates, temperatures and pressures in order to explore the effect of these factors on the decays.

4.2.1 Materials

Polystyrene (PS315K) was obtained from Sigma Aldrich (SKU: 441147). The molecular weight distribution, M_w = 315 kg/mol, M_n = 111 kg/mol, was determined by gel permeation chromatography using a Viscotek TDA 302 with triple detection (light scattering, viscosity and refractive index) with tetrahydrofuran as solvent at 35 °C and a flow rate of 1 ml/min.

4.2.2 Experimental

4.2.2.1 Shear rheometry

A heated press was used to with a mould to create a disc of sample, 1 mm thick with a diameter of 25 mm. The sample was pressed at 150 °C under 5 tonnes pressure for 5 minutes. Rheological characterisation of this material was performed on a TA AR-2000 rheometer using a 25 mm parallel plate and an environmental test chamber supplied with nitrogen gas. Oscillatory frequency sweeps were performed at temperatures from 130 to 210 °C, using a strain of 1 % and frequency spanning from 0.1 rad/s to 600 rad/s. The results were overlaid in a single spectrum at at reference temperature of 170 °C by applying a Williams-Landel-Ferry (WLF) time-temperature superposition using REPTATE software [10].

4.2.2.2 Multi-pass rheometry

Initial MPR data in Section 4.1 was collected by Stephen Boothroyd and Naomi Withey at Durham University, with all processing and analysis being performed by the author.

The MPR4, was fitted with a contraction-expansion geometry, with dimensions as given in Figure 4.2. Approximately 10 g of polystyrene pellets were loaded into the top and bottom reservoirs and heated to 170 °C with an oil bath connected to

jackets around each of the sections, and monitored with three temperature sensors, one in each section. A light source was passed through a 514 nm filter, a linear polariser and a quarter wave plate. The resulting light was used to illuminate the sample through the quartz windows. Video of the sample was recorded during the measurement at 18 fps using a camera fitted with a circular polariser (a combined linear polariser and quarter wave plate) from the quartz window on the opposite side.

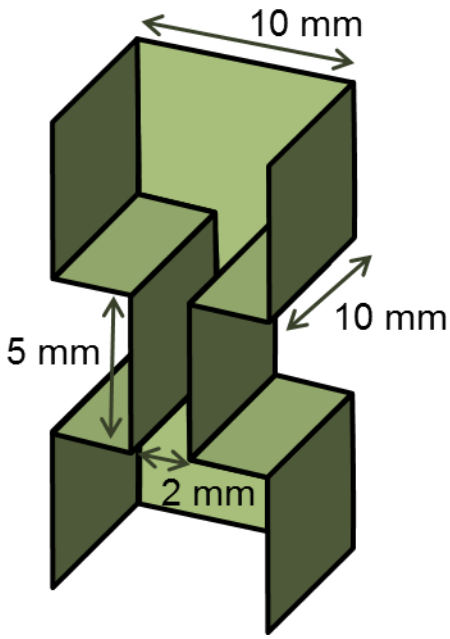

Figure 4.2: Dimensions of the contraction-expansion geometry.

The single shot mode of the multi-pass rheometer was used in order to reach a steady state flow and then stopped to observe the resulting decay. The pistons were driven towards the geometry to give an initial pressure, before moving both together, one towards and one away from the test section, keeping the spacing constant, in order to create flow through the test section. Pressure transducers in the top and bottom reservoir walls were used to monitor the pressure drop across the geometry. Pressure was recorded at 200 Hz. After allowing sufficient time for a steady state in pressure drop to be reached and the stress fringes to become stable, the flow was stopped. The pressure and stress were continually monitored to observe the decay.

The pistons were driven at various speeds between 0.004 mm/s and 1.25 mm/s. Initial pressure was applied before beginning the experiment; this was varied between 1 and 100 bar.

The number of fringes was counted as shown in Figure 4.3. Using the number of fringes and pressure at the steady state, the stress optic coefficient was calculated, as discussed in the following section. This was then used to calculate the stress from the number of fringes and follow the stress as it decayed after the piston was stopped.

Wall shear rates were calculated using:

$$\dot{\gamma} = \left(\frac{6Q}{w^2 d}\right)\left(\frac{2+n}{3}\right) \tag{4.1}$$

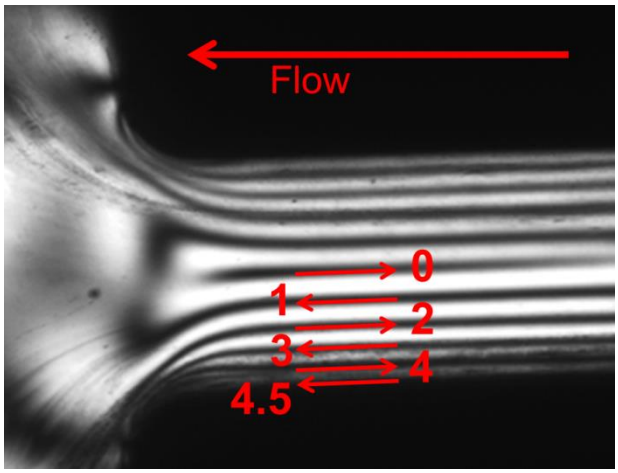

Figure 4.3: PS flowing through a narrow slit at 0.125 mm/s, 200 °C, 1 bar, showing how fringes are counted outwards from a central zero fringe, including half a fringe counted for the dark area at the wall

where w is the slit width (mm), d the slit depth (mm) and Q is the fixed flow rate (mm^3/s), equal to the piston speed (mm/s) multiplied by the cross-sectional area of the reservoir ($\pi * \left(reservoir\ radius\ (mm)\right)^2$). n is the Rabinowitsch correction factor, which can be determined from the steady state shear stress values[28, 159].

4.2.3 Results

4.2.3.1 Shear rheometry

The shear rheology results are shown in Figure 4.4, along with a fit performed using

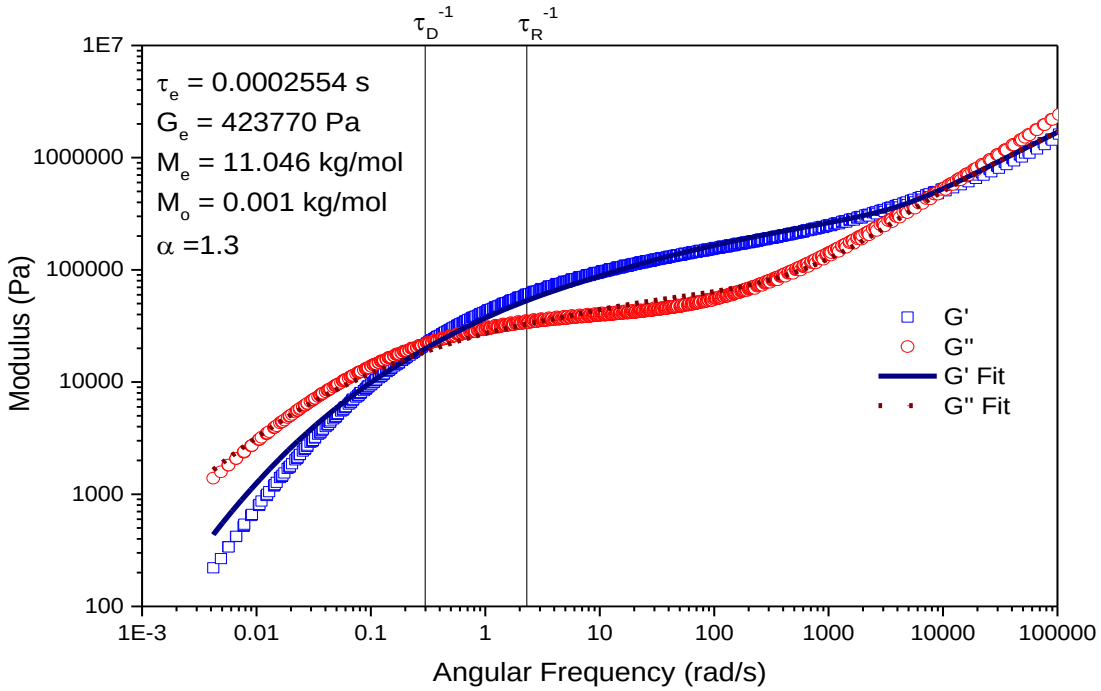

Figure 4.4: Rheological spectrum of PS315K, measured from 130- 210 °C and shifted to 170 °C using a WLF TTS with the parameters C_1=5.15, C_2=-60.3 K, ρ_0=0.950 C_3=-5.14. Also shown is a fit to the data using double reptation theory from the REPTATE software package along with the parameters used.

double reptation theory [52, 160-161] using REPTATE [10] software. In order to obtain this fit, the molecular weight distribution as determined by GPC was discretised to 20 values per decade and input to the theory. Materials parameters were fit to the data and are given in Figure 4.4, where τ_e is the Rouse time of one entanglement segment, G_e is the entanglement modulus and M_e is the entanglement molecular weight. A value of 0.001 kg/mol was used for M_0 (the molecular weight of a Rouse monomer) as recommended[135] and α (the dilution exponent for treating constraint release), was set to 1.3, in accordance with the recommendation of van Ruymbeke *et al.*[162] The extracted τ_e G_e and M_e were consistent with established literature values for polystyrene. A weight averaged Rouse time can then be calculated by incorporating the GPC results into the relation from Likhtman-McLeish theory[52] (Equation 3.1), giving:

$$\tau_R = \sum^{a} \tau_e \left(\frac{M_{w_a}}{M_e}\right)^2 w_a \tag{4.2}$$

where M_{w_a} is the molecular weight and w_a is the weight fraction of that molecular weight. Using the range of molecular weights in the GPC, a value of 0.434 s was obtained. The inverse of the low frequency crossover in G' and G'' was used as the reptation time, giving a value of 3.34 s.

The linear rheological characterisation was also repeated on a sample after the MPR experiments were performed, in order to observe any degradation that had taken place. These results showed no change, as expected for polystyrene which is relatively stable with respect to oxidation at 170 °C.

4.2.3.2 Rabinowitsch correction

The factor for the Rabinowitsch correction[28] was found by plotting a ln(stress) vs ln(shear rate) graph for both the pressure drop and stress fringe results, as shown in Figure 4.5. The results at different pressures were combined. As the gradients from the fringes and pressure drop were similar, they were averaged and a value of n of 1.59 was used for shear rate calculation (Equation 4.1).

4.2.3.3 Calculation of the stress optic coefficient

The stress optic coefficient (SOC) is the ratio of the birefringence to the principal stress difference, which is dependent on the chemistry of the sample not on physical factors such as molecular weight, hence is constant for a given material. A value for the SOC is necessary to calculate the stress from observed birefringence. Values of

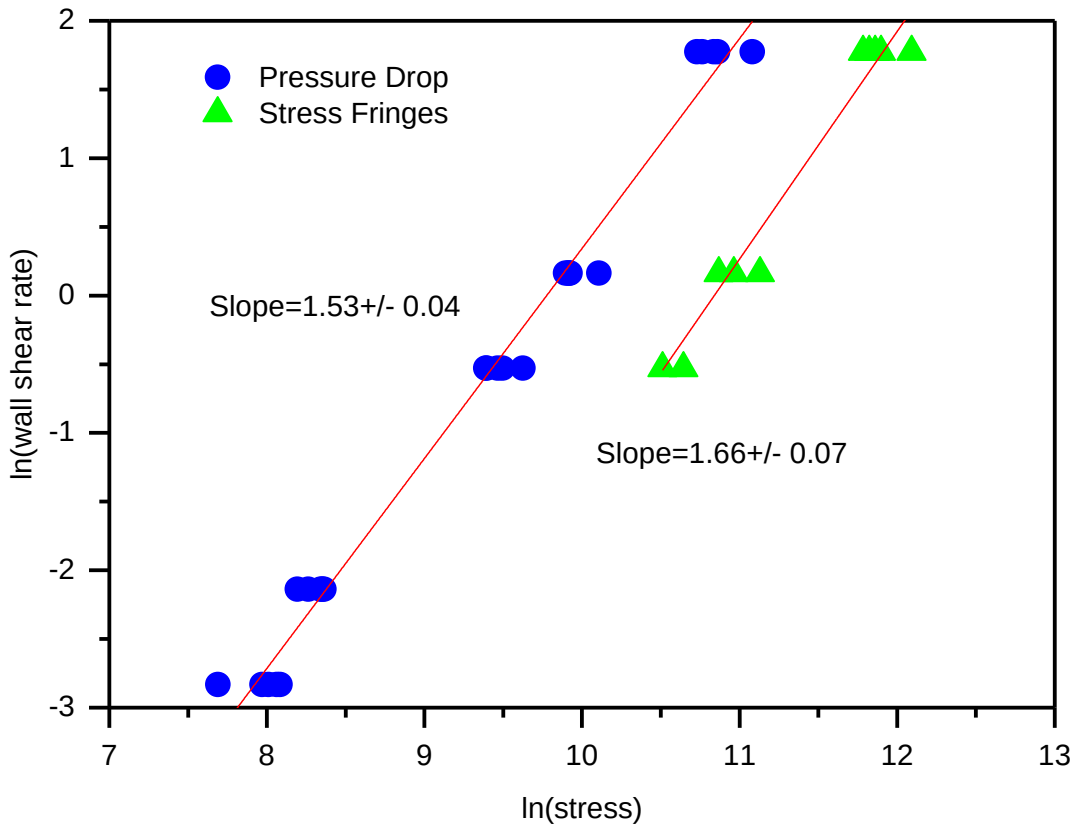

Figure 4.5: Flow curves of PS315K used to calculate the Rabinowich correction factor

the SOC are available from a variety of sources[74, 163] but can also be calculated from the contraction-expansion measurements reported here.

Using a long, narrow slit geometry, the main resistance to flow can be assumed to be from the slit walls and the effects on the pressure drop due to entry and exit can be assumed to be negligible. Hence, the total pressure drop over the geometry is proportional to the wall shear, according to:

$$\sigma_w = \frac{Pressure\ drop\ (Pa) * Flow\ area\ (m^2)}{Wall\ surface\ area\ (m^2)} \tag{4.3}$$

where the flow area is the cross sectional area acted on by the pressure i.e. the cell length multiplied by the slit width (for a 2 mm slit in a 1 cm cell this is 0.00002 m^2) and the wall surface area can be calculated as twice (for the two walls) the length of the slit multiplied by the cell length (for a 5 mm long slit in a 1 cm cell this is 0.0001 m^2).

As described by Coventry[39-40], the stress optic coefficient is given by:

$$SOC = \frac{F\lambda_{\text{light}}\sin(2\theta)}{2l\sigma_w} \tag{4.4}$$

where F is the number of fringes, l is the path length in m, and θ is the angle of rotation of the principle stress with respect to the flow direction. At low shear θ tends to 45°, which means, as the wall shear tends to zero, the SOC tends to,

$$SOC = \frac{F\lambda_{\text{light}}}{2l\sigma_w} \tag{4.5}$$

which can be calculated. By plotting this against wall shear at various piston speeds and pressures, the graph can be extrapolated back to zero wall shear to give a value for the stress optic coefficient. This plot is shown in Figure 4.6, and the resulting value of the SOC for polystyrene is 4.9 ± 0.2 Pa^{-1}.

The initial pressure may be expected to have an effect. However, extrapolating separately data at 1 bar and 100 bar gives values of the SOC of 4.91 and 4.96 Pa^{-1} respectively, which are both within the range of error. This suggests pressure has a negligible effect and so the data was combined.

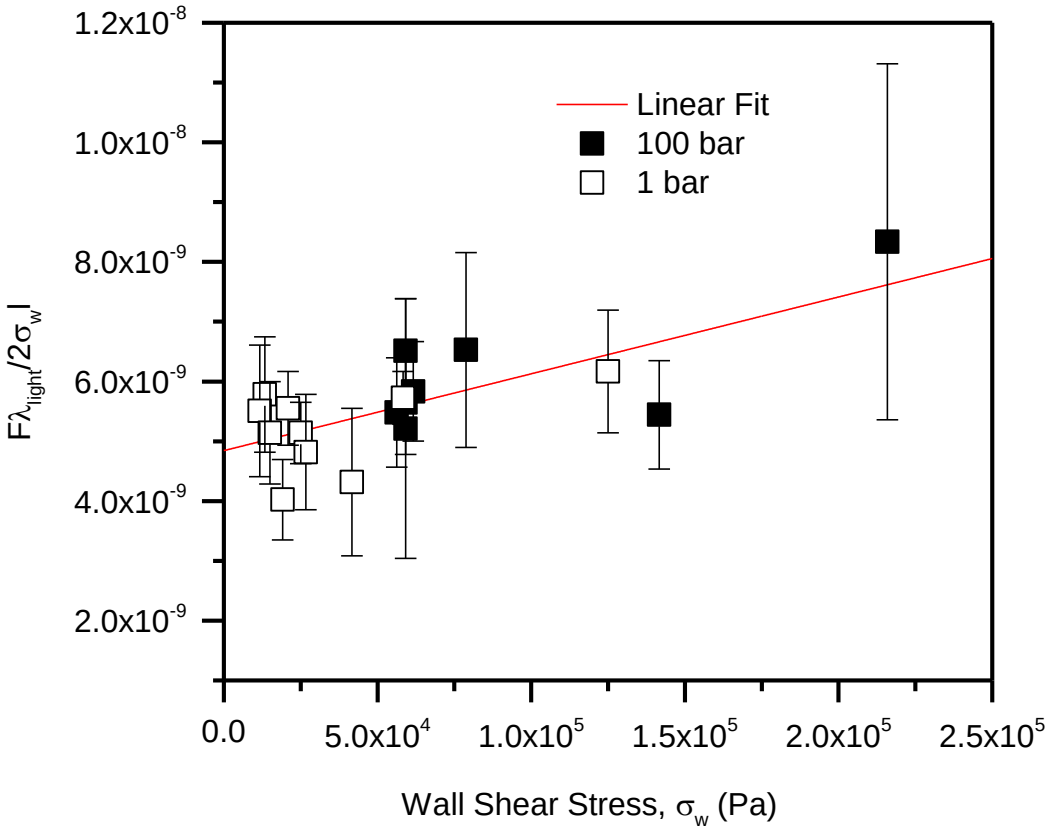

Figure 4.6: Graph of $F\lambda_{light}/2\sigma_w l$ against wall shear, showing data at 1 and 100 bar and a linear fit of the combined data. This fit is extrapolated back to zero for determination of the stress optical coefficient

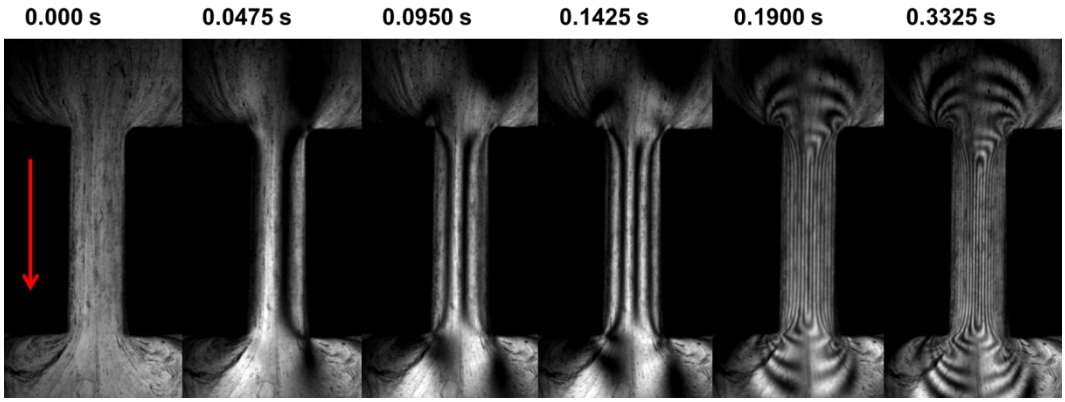

Figure 4.7: Build-up of stress fringes to a steady state as PS315K is driven through a narrow slit at a piston speed of 0.5 mm/s under 30 bar of initial pressure at 170 °C. Arrow shows flow direction

4.2.3.4 Pressure drop and stress decays

In each experiment, the number of observed fringes was seen to increase as the flow was established until a constant state was reached. Typical results for the build-up of fringes as flow is established are shown in Figure 4.7. Once the steady state is established (after 0.19 s in the series shown), it is possible to select an individual frame and measure the stress within the geometry by counting the fringes as is shown in Figure 4.3.

The difference between the pressure at the top and bottom transducers was calculated in order to measure the 'pressure drop' across the geometry. The time dependence of pressure drop reveals the steady state condition, where the pistons are moving at constant velocity and the pressure drop is constant (Figure 4.8). After this point the pistons are stopped and the decay in pressure drop can be observed as well as the stress fringes.

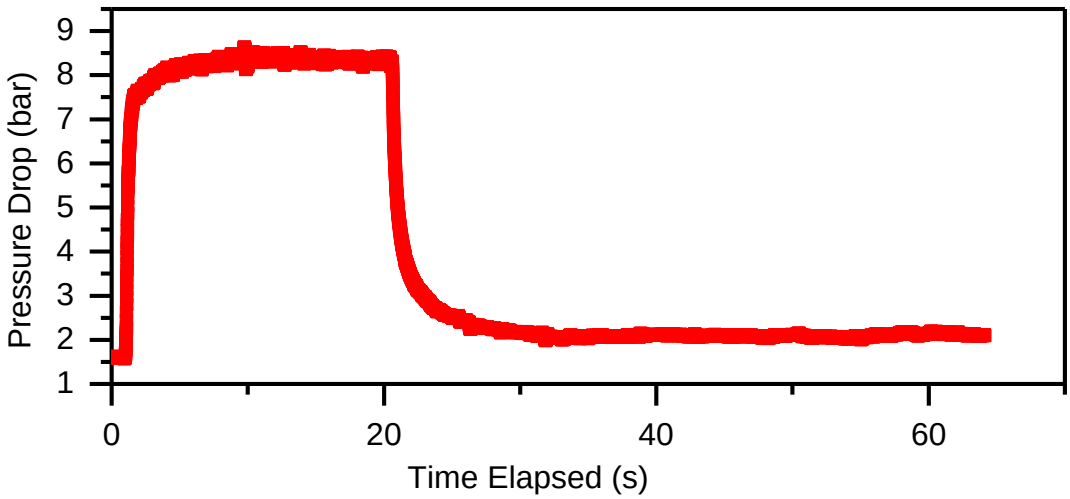

Figure 4.8: Pressure drop over the contraction-expansion geometry for PS at 0.5 mm/s and 170 °C, with 30 bar of initial pressure, showing the initial build up to a steady state and then decay.

The dimensionless Weissenberg numbers were calculated by multiplying the rate of shear (calculated from the piston speed and dimensions of the capillary and slit) by the Rouse and reptation times as determined from shear rheometry and GPC.

The Weissenberg numbers (see Table 4.1) indicate that the polymer moves through three regimes as the piston speed is varied. The first region is where both Rouse and reptation Weissenberg numbers are below 1 (at speeds less than 0.022 mm/s) Here, the rate of deformation is slower than both the relaxation by Rouse motion and reptation, so there is expected to be little deformation to the material.

Secondly, when the reptation Weissenberg number is greater than 1, but the Rouse Weissenberg number is not (speeds between 0.022 and 0.16 mm/s). Here the rate of deformation is faster than the polymer can relax by reptation but not via Rouse motion. Hence the polymer chains would be expected to become oriented with respect to each other, but there would be no stretching of individual chains.

Finally where both Weissenberg numbers exceed 1, (speeds over 0.16 mm/s) the rate of deformation is faster than both relaxation times. Here stress would be expected to build up significantly due to stretching of individual chains. These regimes will be observable in the birefringence which is sensitive to the relaxation at the length of the entanglement tube. There can be anisotropy and relaxation, on larger scales, which can affect the properties of solidified polymer products, but this does not affect the stress in the material and requires techniques such as neutron scattering to investigate.[164]

Higher piston speed was seen to increase the number of fringes, and hence stress at the steady state as well as the pressure drop across the geometry. Although the

Table 4.1: Rouse and reptation Weissenberg number calculated for different piston speeds in the MPR for PS350K at 170 °C.

Speed (mms^{-1})	Flow Rate (mm^3s^{-1})	Rabinowitsch Corrected Shear Rate (s^{-1})	Weissenberg number	
			Rouse	Reptation
0.004	0.314	0.0564	0.024	0.19
0.013	0.982	0.176	0.076	0.59
0.042	3.30	0.592	0.26	2.0
0.125	9.82	1.76	0.76	5.9
0.420	33.0	5.92	2.6	20
1.250	98.2	17.6	7.6	59

speed increased the initial pressure drop and stress, the rate of decay was similar between the results, for both stress (Figure 4.9) and pressure drop (Figure 4.10). However, there was a change as the speed exceeds the reptation (speeds over 0.021 mm/s) and Rouse times (speeds over 0.16 mm/s). When the inverse reptation time was exceeded, the decays had a longer decay overall and showed a more noticeable decay (rather than a plateau) at times shorter than the reptation time. Similarly, when the Rouse time was exceeded, decay could be seen at times shorter than the Rouse time.

The pressure initially applied to the sample had a large effect on the rate of decay of the stress and pressure drop. Comparing results at 1 bar to 100 bar for the same shear rate, the higher pressure increases the initial stress but also appears to

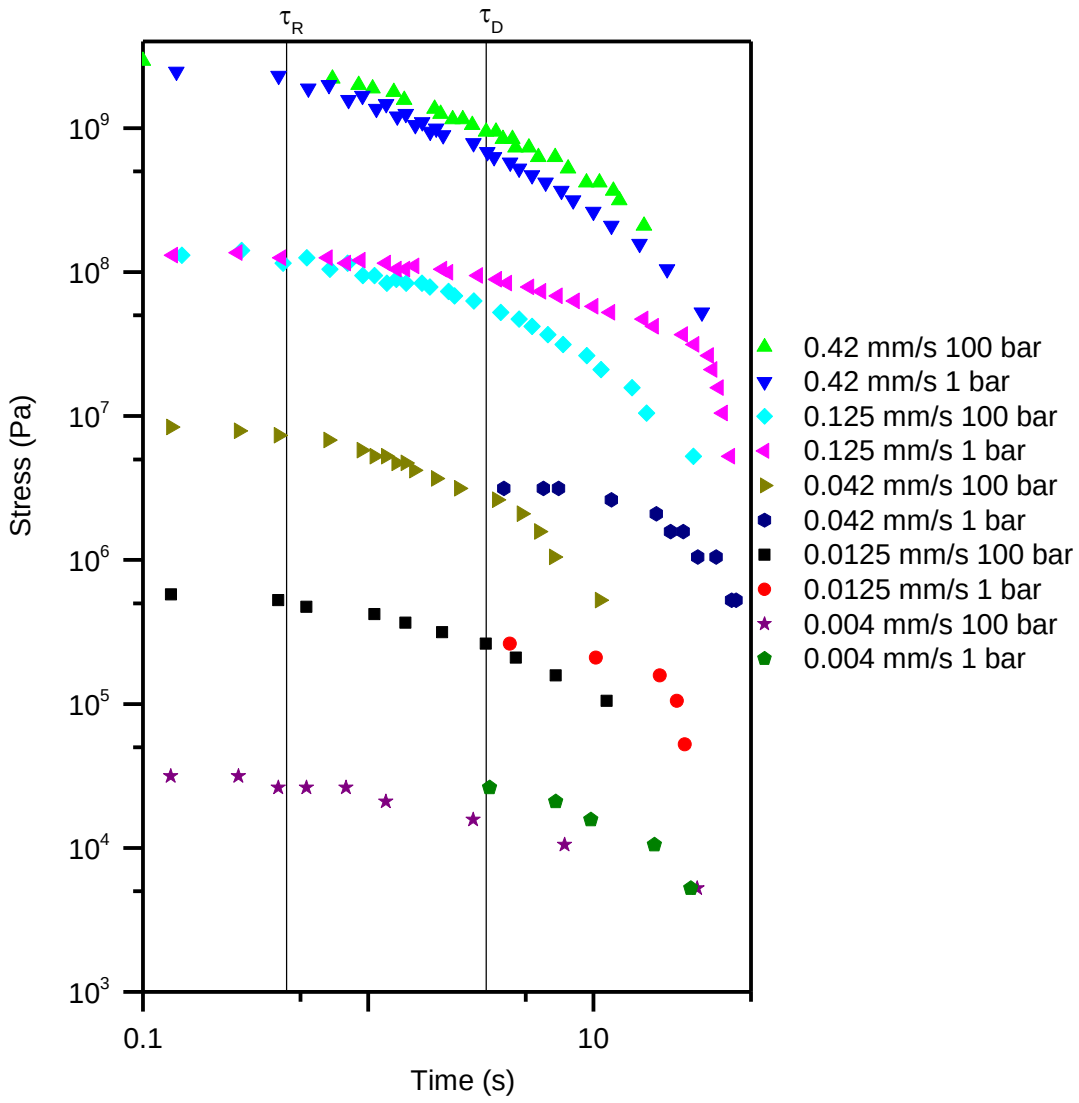

Figure 4.9: Stress decays (from fringe counting) after pistons are stopped after experiments under a variety of speeds and initial pressures. Each speed is offset from the last by a factor of 10.

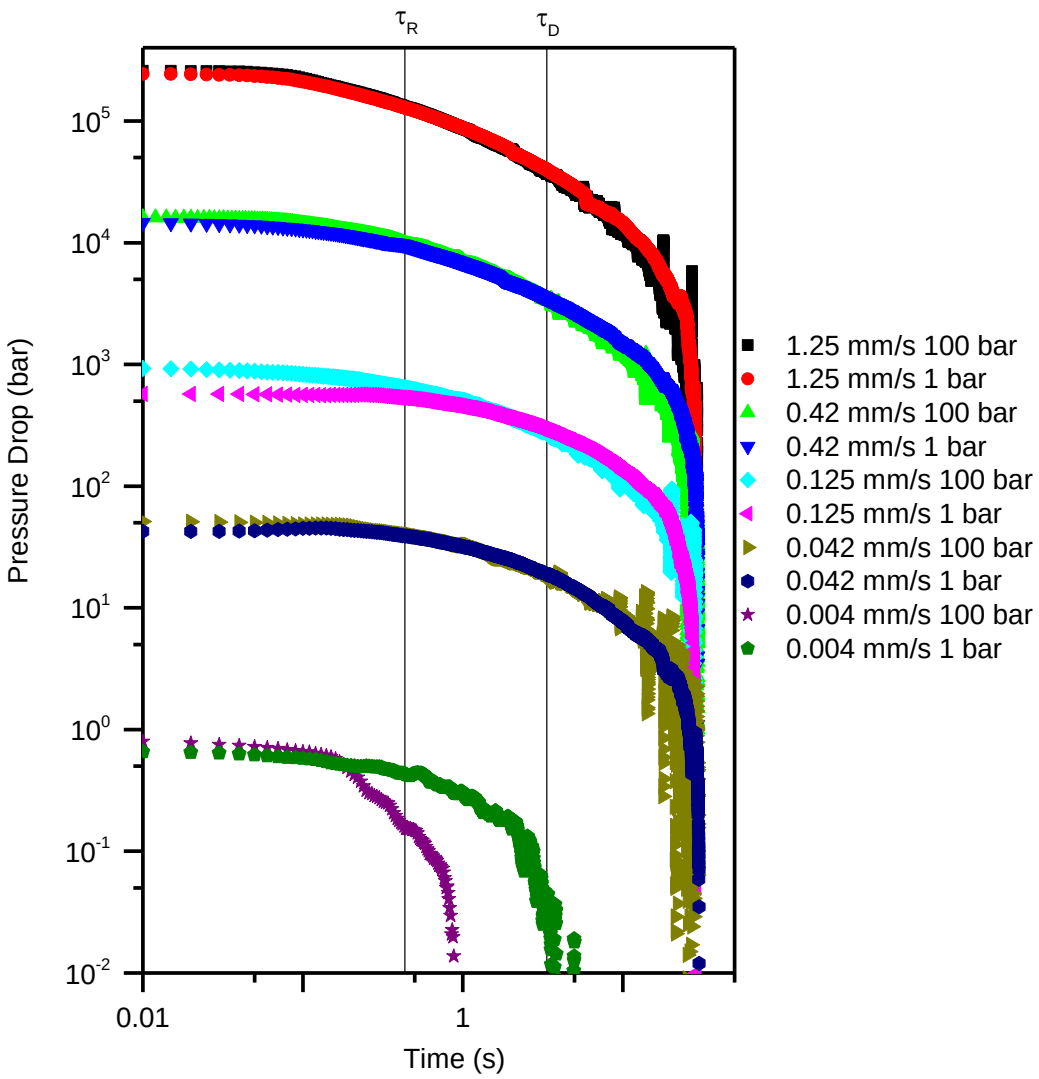

Figure 4.10: Pressure drop decays after pistons are stopped after experiments under a variety of speeds and initial pressures. Each speed is offset from the last by a factor of 10.

increase the rate at which it decays. However this difference gets less pronounced at high speeds, where stress is higher overall.

The pressure drop decays behave similarly, increasing the initial pressure increases the pressure drop at the steady state (from which the decay begins), but it also appears to increase the rate of pressure decay (see Figure 4.10). This effect is most noticeable at the slowest speed, which has a reptation Weissenberg number of 0.19.

As shown in Figure 4.11, the stress is greatly reduced by increasing temperature from 170 °C to 200 °C. The decay rate is also much faster; the timescale of the decay is approximately 4 times as fast for the higher temperature. Pressure drop shows a similar trend (Figure 4.12), increasing temperature causes a large drop in steady state pressure and increases the rate of decay. Both systems were in the

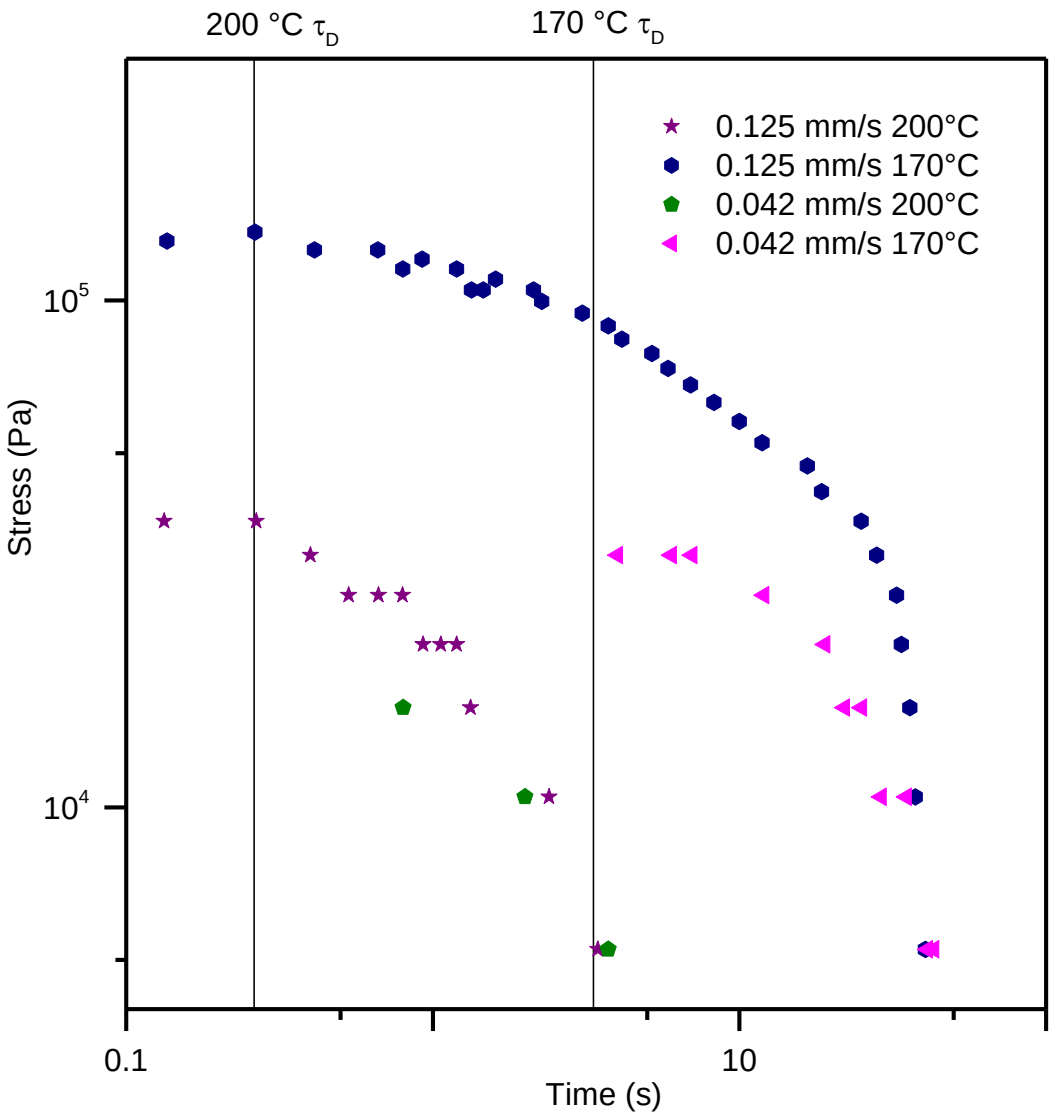

Figure 4.11: Comparison of stress decays at 1 bar showing two temperatures and speeds. No offset is applied

same regime having a Weissenberg number for reptation of over one and for Rouse motion of less than one.

4.2.4 Discussion

4.2.4.1 Shear rheology

The fit to the data in Figure 4.4 captures the terminal crossover and rubbery region well, although slightly overestimates the complex moduli in the terminal region. This could be due to some very short chains which were not detected in the GPC. The presence of additional short chains could have contributed to the difference in the terminal region, although these also would be expected to have an effect on the plateau modulus. Nevertheless, the key aspects of the data required to determine relaxation times are well captured by this model.

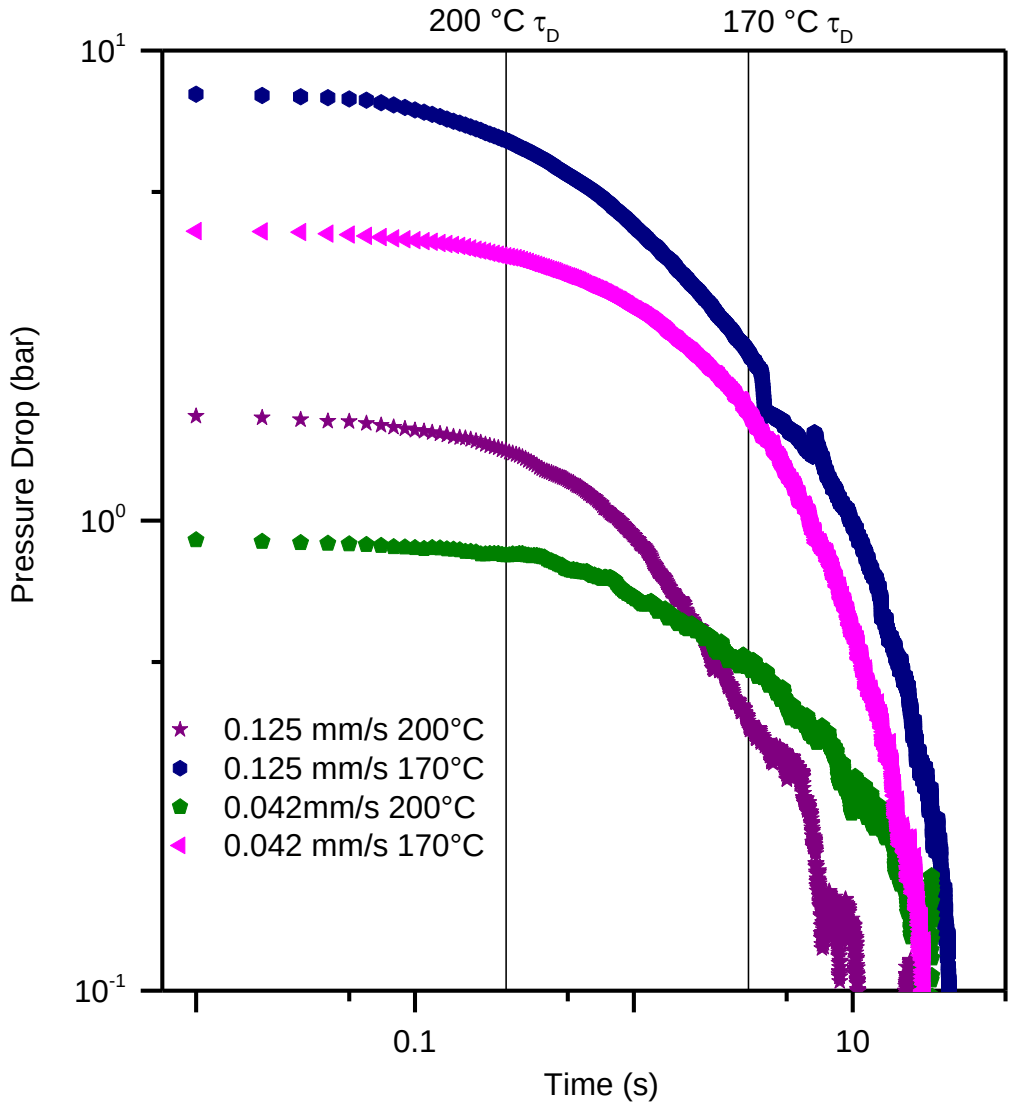

Figure 4.12: Comparison of pressure drop decays at 1 bar showing two temperatures and speeds. No offset is applied

The reptation time from the REPTATE[10] materials database is 9.24 s for 315k monodisperse linear PS at 170 °C. The inverse of the crossover of G' and G'' in the linear rheology differs significantly from this, giving a value of 3.34 s. The polydispersity of the sample, particularly the inclusion of shorter chains, causes this shift to a faster reptation time. The Rouse time is less dependent on the polydispersity and the value extracted from the fit to data (0.434 s) is similar to the expected value for monodisperse 315K polystyrene (0.379 s from the REPTATE[10] materials database).

4.2.4.2 Rabinowitsch correction

The resulting flow curve is linear and fits well to a power law, although the exact value of the correction factor is dependent on the rheometer setup, die size and temperature of the measurement, the value obtained of 1.59 and gives a shift of

approximately ~20 % to the shear rate. The same magnitude of shift has previously been observed in literature.[3, 165] Larger shifts have also been observed for polystyrene (e.g. 45-50 %[166]) but the value is specific to each experimental setup, as it is dependent on the geometry and instrument and not specific to the material.

4.2.4.3 Calculation of the stress optic coefficient

The value of the SOC is consistent with literature values[40] which range between 4 and 6 × 10^{-9} Pa^{-1}. Venerus *et al.*[163] reported a value of 4.8 × 10^{-9} Pa^{-1}, which is within the range of error of the determined value. To reduce the error in the measured value, a longer or narrower slit could be used to reduce entry and exit effects, or simply more experiments could be undertaken over a wider range of conditions. However, the conditions used here are sufficient for accurate determination of the stress.

4.2.4.4 Pressure drop and stress decays

The relationship with pressure in the pressure drop results (Figure 4.10) is interesting, as pressure would be expected to slow molecular motion and slow down the rate of decay, however the opposite was observed. This result is also counter to literature reports, which observe the expected relationship.[18, 27, 112, 115-117, 119-120, 167-176] It was therefore suspected that this was an apparatus effect rather than a molecular effect. In the MPR setup, there is a release valve which is designed allow air to escape. Since sample is loaded into the top and bottom sections and pushed together, there will be air trapped between the two parts of the sample, which this valve is designed to remove. However, some polymer was found to have escaped from this valve during these experiments. Normally, since the valve protrudes significantly from the test section, the material would cool and block the valve, allowing pressure to be maintained. However it is possible that the high pressures could force sample out of the valve and cause faster than expected relaxation. It would follow that the pressure would have less effect at higher piston speeds, as they could also generate enough pressure on entry to the test section to force sample out of this valve.

The stress fringe results (Figure 4.9) show a similar trend, only at the shear rate above the inverse Rouse time is pressure seen to slow the decay, as expected. At the slower speeds the decays at 1 bar are longer than at 100 bar, even at speeds below the inverse reptation time (and in the pressure drop, the pressure drop is greatest at the slowest speed). At these speeds, the origin of the relaxation is unclear, as significant amounts of stress should not be able to build up in the

sample. It is possible the polydispersity could mean there are chains still above their inverse reptation time, however the trend with pressure suggests that the relaxation could be due to an apparatus effect, e.g. the air release valve. Further tests are required to remove the effect of this valve and evaluate the true pressure response.

The shear rate dependence of the results shows the onset of additional regimes of relaxation with higher shear rate, but not a shear rate dependence of the relaxation. This is due to the relaxation of the polymer changing from the reptation to Rouse regimes and appears to match well with the calculated Weissenberg numbers, however more speeds would be required to evaluate exactly how well the transitions align with the change in Weissenberg number.

The temperature dependence is as expected, increasing temperature from 170 to 200 °C reduces the amount of stress fringes (Figure 4.11) and pressure drop (Figure 4.12) significantly and speeds up the relaxation, since the higher temperature will speed up molecular motion and allow faster relaxation by both reptation and Rouse motion. The results of the stress fringes align well with the reptation times at 170 °C and 200 °C (shifted using WLF theory). The stress fringes begin to relax at a time similar to the reptation relaxation time in each case, and are at a plateau until this time. The pressure drop results do not align as well with these times, as there is significant relaxation at shorter and longer times as well as the contribution from the stress fringes. This is likely due to the contribution of entry and exit effects, as well as the possibility of sample escape during the experiment affecting short times. Nevertheless the relationship with temperature is the same, speeding up the relaxation and reducing the magnitude of the pressure drop.

4.2.5 Initial conclusions

A procedure has been detailed for examining stress and pressure drop decays in the multi-pass rheometer, allowing temperature, shear rate and pressure to be controlled and the effect of each to be examined. In this way polystyrene was studied varying all three conditions. Changing shear rate appeared to have little effect on the relaxation time, but could change the regime of the relaxation from the reptation to Rouse regimes, and this aligned well with the calculated Weissenberg numbers, however more shear rates are necessary to properly study the behaviour at the transition between these regimes, and this process is detailed in Section 4.3. Temperature, as expected was seen to reduce the stress in the polymer and speed up the relaxation, and the change agreed well with the shift in relaxation time predicted by WLF theory. The results of pressure were not clear, as it was believed

sample had escaped from the air release valve at high pressures. This meant the pressure was not maintained throughout the experiment and so effect of pressure could not be elucidated. Adaptations to the apparatus are required to properly study pressure dependence, which were performed and are detailed in Section 4.4.

4.3 Contraction-expansion flow: detailed study of shear rate

The effect of Weissenberg number was noticeable in the results in Section 4.1. However, it was difficult to evaluate the exact dependence without more data at speeds closer to the transition from Weissenberg numbers below to above one. Hence this section gives a detailed study using many piston speeds spanning a large range in order to better observe the effect of the different molecular relaxation processes.

4.3.1 Experimental

Sigma Aldrich polystyrene pellets (ALDRICH 441147, M_w ≈ 350,000 g/mol, M_n ≈ 170,000 g/mol) were loaded into the MPR fitted with a narrow slit geometry, 2 mm wide, 5 mm long and 10 mm in depth. The pistons were moved at speeds between 0.002 mm/s and 1.00 mm/s. The Weissenberg numbers corresponding to flow rates at these piston speeds were calculated using a reptation time of 3.34 s and a Rouse time of 0.434 s and are shown in Figure 4.13. The temperature was maintained at 170 °C and a 1 bar of initial pressure. The pressure drop over the slit was recorded over time using the pressure transducers as well as the stress (from counting of the imaged fringes).

4.3.2 Results: Piston speed dependence of stress and pressure drop decays

The stress decays are shown in Figure 4.14 and the pressure drop decays in Figure 4.15. It is noticeable in both the pressure drop and stress decays that at speeds below the inverse reptation time, the decay is almost flat at times below the reptation

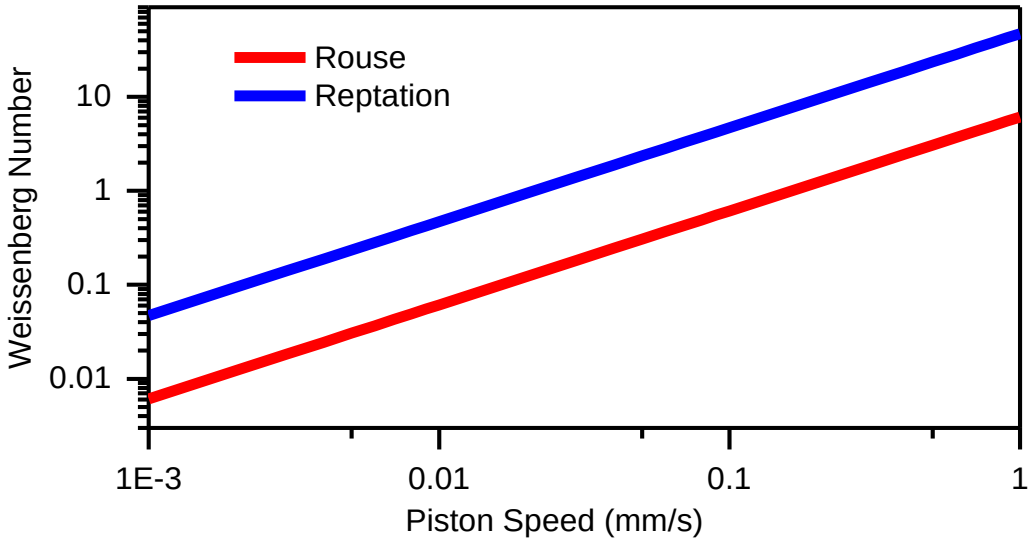

Figure 4.13: Change in the reptation and Rouse Weissenberg numbers with piston speed. The Weissenberg number for reptation exceeds 1 at 0.022 mm/s and for Rouse motion at 0.164 mm/s

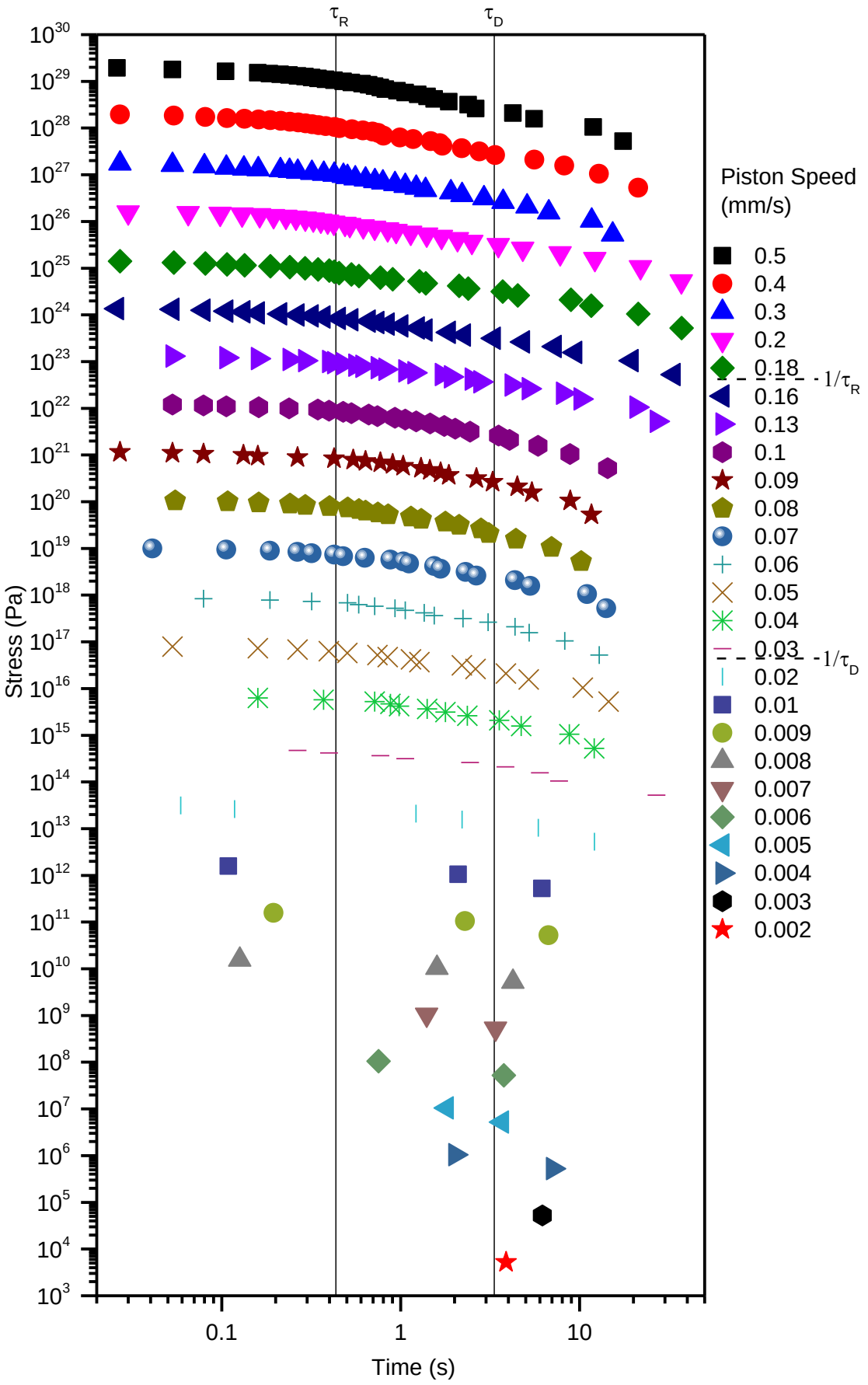

Figure 4.14: Stress decays at 170 °C, 1 bar, stress data for each speed is offset by a factor of 10.

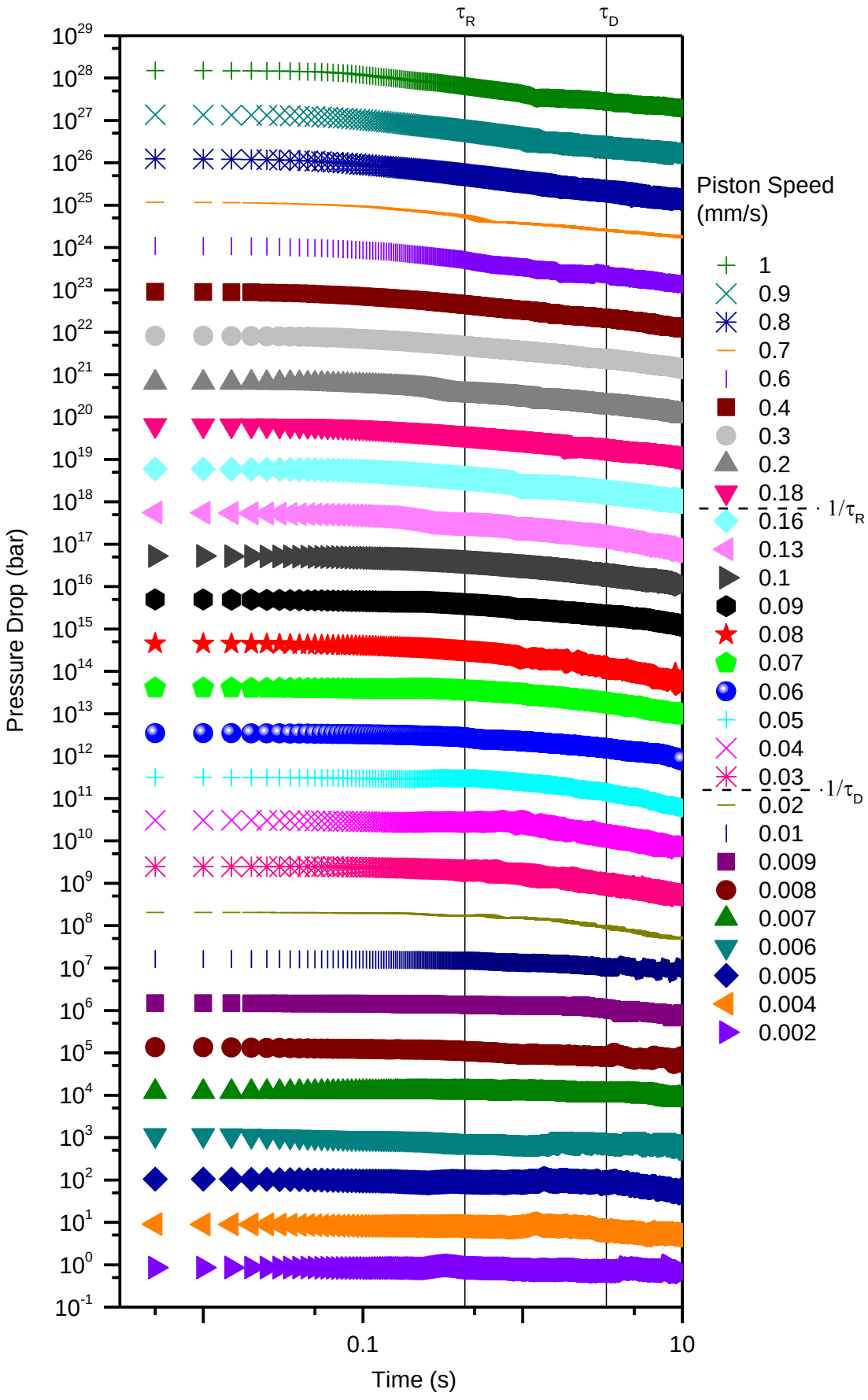

Figure 4.15: Pressure drop decays at 170 °C, 1 bar, stress data for each speed is offset by a factor of 10.

time. There is some decay but it is generally at longer times than τ_D. However, once the shear rate exceeds the inverse reptation time, there is a more noticeable decrease at times below τ_D. A similar effect is seen with Rouse time, once τ_R is exceeded, the decays are decreasing rather than flat at short times below τ_R.

4.3.3 Discussion: Piston speed dependence of stress and pressure drop decays

The Maxwell model (simply modelling viscoelastic fluids as a combination of a spring and a dashpot) predicts that stress will decay exponentially over time.[177] Hence, for a simple viscoelastic material, by plotting the logarithm of the stress against time, a linear graph would be expected, and assuming that the pressure decays proportionally to the stress in the sample this can also be applied to the pressure drop results.

Doing so (as shown in Figure 4.16) reveals multiple regions in the decay. At the highest speeds, this consisted of a fast decay at very short times (which is often difficult to see in the fringe counting results due to the limited time resolution; this could be improved with a faster camera).

For an entangled polymer, there are expected to be two regions due to relaxation via reptation and Rouse motion, however the reason for the fast decay at short times (shorter than τ_R) is not obvious. One possibility is the influence of

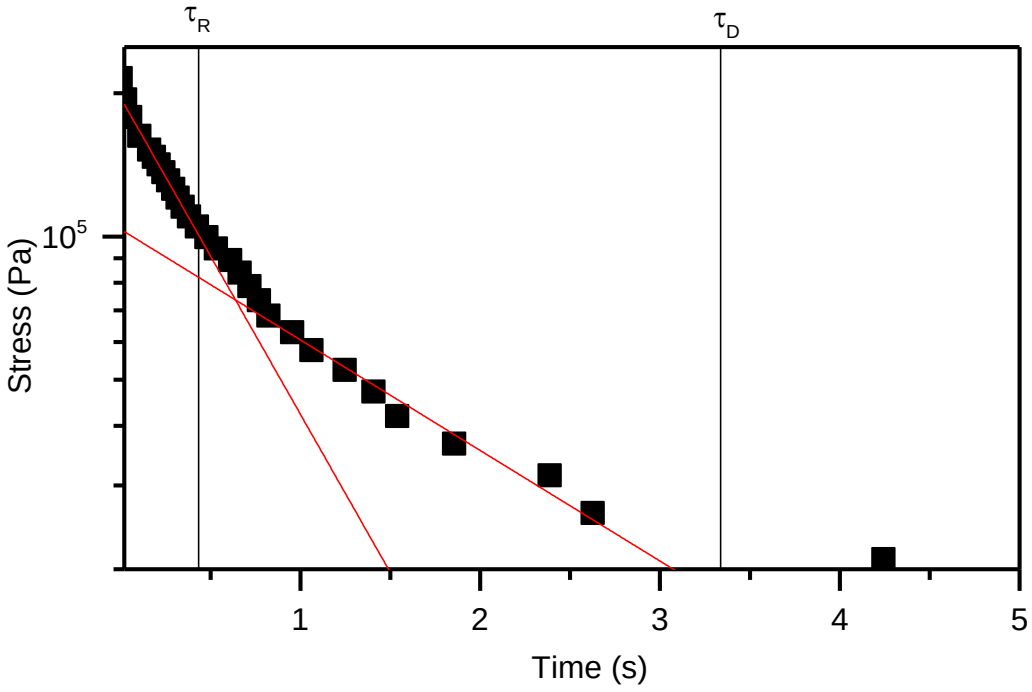

Figure 4.16: Stress decay at 170 °C, 1 bar after a deformation at a piston speed of 0.5 mm/s, red lines are shown to guide the eye to the regions dominated by Rouse motion and reptation

compressibility effects, rather than viscoelastic relaxation of the polymer.

Ranganathan *et al*.[30] observed multiple regimes in the flow curve for HDPE in an MPR. As piston speed was increased, they observed a discontinuity in the pressure drop suggesting unstable flow. When the same flow curves were plotted from our measurements on polystyrene, no discontinuity was observed, suggesting all our measurements were in the region of stable flow (Figure 4.17), and that flow instability cannot account for the different relaxation rates that are apparent in the stress and pressure drop decays. Ranganathan modelled pressure drop decay in this region using an adapted version of the Molenaar-Koopmans model for pressure changes during capillary flow, and showed that compressibility played an important part in the stress decay. Valette *et al.*[178] expanded on this by using rolie-poly[56] (based on viscoelasticity) and Carreau-Yasuda[179] (based on compressibility) models to calculate pressure drop decays for LLDPE, and showed that the decays were more dominated by compressibility effects early on and viscoelastic effects later in the decay, and the decay could be well represented using a rolie-poly model incorporating compressibility. We would expect our decays to be particularly dictated by the viscoelasticity of the polymer because of the broad plateau region measured in the linear rheology (and hence broad viscoelastic relaxation spectrum of the polymer). Hatzikiriakos and Dealy[180] note that short rise times to steady state (as seen in our experiments, on the scale of a few seconds) usually produce

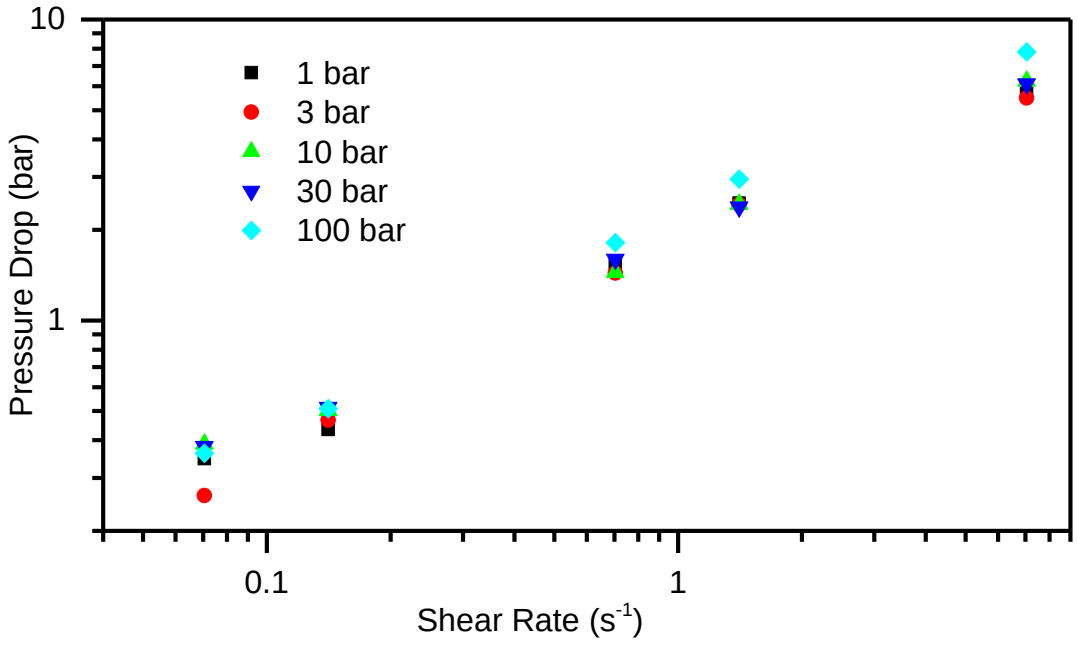

Figure 4.17: Flow curve of polystyrene at all pressures at 170 °C. The points show a power law relationship and show no discontinuity

viscoelastically driven flows, and purely compressibility driven flows are usually characterised by rise times to steady state of several hours.

It is therefore valid to assume that the decays seen are mostly dominated by viscoelasticity. However, since, even in viscoelastically driven flows, compressibility effects have been observed at very short times it seems unlikely that the fast decay seen in our results is part of the polymer relaxation, and therefore can be separated out from the viscoelastic relaxation times.

It was initially postulated that the fast decay could be due to the polymer continuing to flow after the pistons have stopped. In order to test this, the flow stop time can be calculated. The wall shear rate in a narrow slit is given by,

$$\dot{\gamma} = \left(\frac{6Q}{w^2 d}\right)\left(\frac{2+n}{3}\right) \tag{4.6}$$

where w is the slit width (mm), d the slit depth (mm) and Q is the fixed flow rate (mm^3/s), equal to the piston speed (mm/s) multiplied by the cross-sectional area of the reservoir ($\pi * \left(reservoir\ radius\ (mm)\right)^2$). n is the Rabinowitsch correction factor, determined as 1.59 in Section 4.2. The timescale of the flow stop is then given by:

$$\tau_{flow} = \frac{\Delta V}{Q} \tag{4.7}$$

where Q is the flow rate and ΔV is the change in volume due to pressure, which can be calculated:

$$\Delta V = V\frac{\Delta P}{G_B} \tag{4.8}$$

where V is the volume of the slit, ΔP is the pressure difference above and below created by the motion, and G_B is the bulk modulus of the material.

Using the definition of viscosity $\eta = \sigma/\dot{\gamma}$, Equation 4.6 for the shear rate, and Equation 4.3 for the wall shear, the flow rate for the slit can be calculated as:

$$Q = \frac{\Delta P d w^3}{4\eta L(2+n)} \tag{4.9}$$

where d, w and L are the slit depth, width and length respectively, and η is the viscosity of the material.

Combining Equations 4.7-9 and substituting in the volume of the slit (Lwd) gives

$$\tau_{flow} = \frac{4L^2\eta(2+n)}{Bw^2} \tag{4.10}$$

Using the value of the bulk modulus of 1.988 GPa at 167 °C given by Mott *et al.* [181] and a value of the zero shear viscosity obtained from linear rheology of 1.96×10^5 Pa.s, for a slit length 5 mm, width 2 mm and depth 10 mm, and using an n of 1.59 as determined in Figure 4.5, the resulting flow time is 8.8×10^{-3} s. This is much smaller than the smallest time step recordable by the camera (0.056 s at 18 frames per second). Hence it should not be visible in our results.

It is also unlikely that the polymer leaking into some gap or part of the system that was not fully sealed, could contribute to the fast relaxation observed. Great care was taken to fully seal the cavity, and any such loss would cause the pressure and stress to decrease during the deformation, resulting in a decrease rather than a constant steady state.

However, a very small overshoot is noted in the retreating lower piston (see Figure 4.18). This overshoot is not present for the advancing top piston, and so would cause a small relaxation in pressure and stress. Despite the small magnitude of this effect with respect to the stroke amplitude, it may have caused the initial fast decay

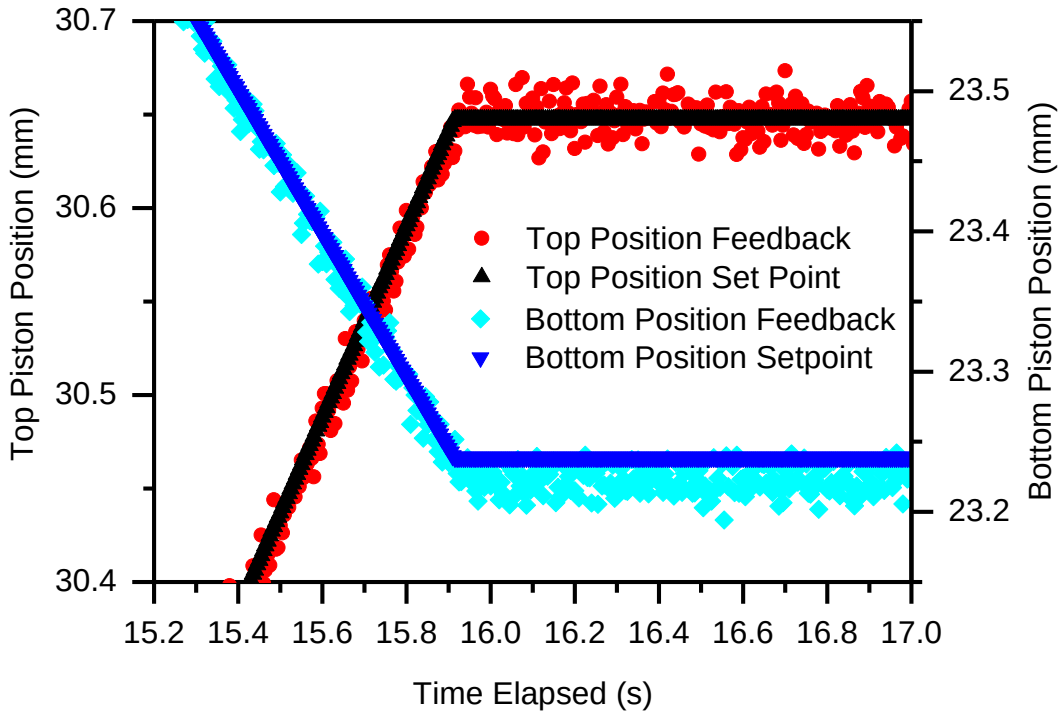

Figure 4.18: Feedback (actual) positions of the pistons during a 15 mm downward stroke at 0.5 mm/s and 100 bar initial pressure, showing overshoot of the bottom receding piston.

of stress observed. Careful observation of particles present in the recorded videos supports this. Observing a single particle in the flow, a stop in motion is noted on stopping the pistons, after which a little forward flow continues (Figure 4.19). This suggests that there is an initial abrupt stop in movement, followed by the small overshoot in movement of the retreating piston causing the residual forwards flow (within 0.1 s of the stop in movement). This effect is likely the origin of the abnormally fast decays, which occur on a similar timescale (~0.1 s). This could be tested by using a slower relaxing polymer, which would be expected to have the same fast relaxation independent of its molecular relaxation time.

After this fast decay, two further regimes are observed which are attributed to the Rouse and reptation relaxation of the polymer. The three regions can be identified in the decays at piston speeds of 0.20 mm/s and above, which corresponds to the point at which the inverse Rouse time is exceeded. Similarly, two regions can be seen at slower speeds, until speeds of 0.02 mm/s and below, after which only a single region is seen. This corresponds to the point where the inverse reptation time is exceeded. This indicates that there is a clear effect of the Rouse and reptation times and the agreement between these results and the times extracted from linear rheology and GPC results is remarkable. There is little change in the rate of the decays with speed apart from the transitions with changing Weissenberg number. This strengthens the conclusion that we are observing molecular relaxation pathways, as the shear rate would only be expected to affect which pathway was accessed (i.e. Rouse motion or reptation). These tests could be used to determine Rouse and reptation times in several ways, firstly as demonstrated in this chapter, a series of speeds could be examined and changes in the decays examined in order to determine the point at which additional components of the decay appear. Alternatively, fits could be performed to extract decay times which would give an indication of the rates of the molecular processes.

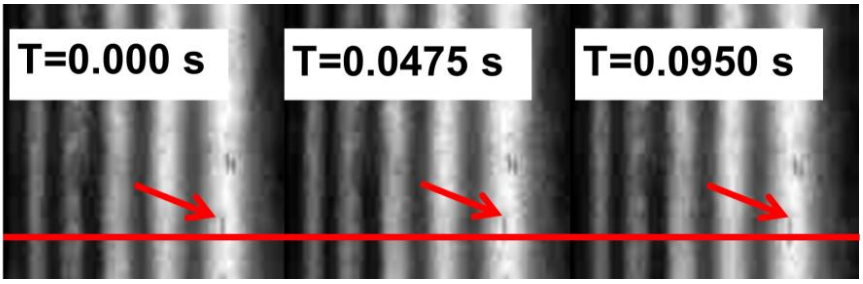

Figure 4.19: First three frames of video after piston stopped (noted from fringe decay) after a deformation at 0.1 mm/s and 170 °C with 10 bar initial pressure. A particle can be seen to stop between the first two frames before continuing to move a little, indicating residual flow due to overshoot of the lower piston.

4.3.4 Conclusions

A systematic study of the effect of piston speed was performed on the stress and pressure drop decays of polystyrene. In this way it was confirmed that the decays are highly sensitive to the Weissenberg number of the measurement, and showed different regimes attributed to both the reptation and Rouse relaxations. A third regime was identified at fast times (shorter than the Rouse time) which was found to be caused by overshoot of the retreating piston.

4.4 Contraction expansion flow: well controlled pressure study

Since the initial studies found a relationship with pressure that was not expected (as discussed in Section 4.1) further study was planned to observe if this was an apparatus effect. The air release valve was replaced with a solid piece (after air had been excluded) so that the pressure was maintained. This final set of results was fit with multiple exponentials in order to extract relaxation times from the decays and evaluate the pressure dependence of these times.

4.4.1 Experimental: Multi-pass rheometry

Pellets of PS315K were loaded into the MPR at a temperature of 170 °C, fitted with a narrow slit geometry, 2 mm wide, 5 mm long and 10 mm in depth. The pressure drop over the slit was recorded over time using the pressure transducers as well as the stress, from counting of the imaged fringes.

Experiments were performed at piston speeds between 0.005 mm/s and 0.5 mm/s. The speeds were chosen to span from shear rates that are below both the inverse Rouse and reptation times, to those where both were exceeded (see Table 4.2). For each piston speed, experiments were performed at initial pressures of 1, 3, 10, 30 and 100 bar.

4.4.2 Results

As has been seen in Section 4.2 and 4.3, the polydispersity of the polymer is an important consideration in these measurements, and was seen to change the reptation and Rouse times from the monodisperse case. In order to evaluate the

Table 4.2: Piston speeds used in these experiments, and the corresponding flow rates in the reservoir, shear rate at the wall and the Rouse and reptation Weissenberg numbers, calculated using τ_D = 3.34 s, and τ_R = 0.434 s

Speed (mms^{-1})	Flow rate (mm^3s^{-1})	Apparent wall shear rate (s^{-1})	Rabinowitsch corrected shear rate (s^{-1})	Weissenberg number	
				Rouse	Reptation
0.005	0.39	0.059	0.071	0.031	0.24
0.01	0.79	0.12	0.14	0.061	0.47
0.05	3.9	0.59	0.71	0.31	2.4
0.1	7.9	1.2	1.4	0.61	4.7
0.5	39	5.9	7.1	3.1	24

dependence of relaxation times on this polydispersity, the proportion of chains with Rouse and reptation Weissenberg numbers above 1 was calculated for each shear rate and is given in Table 4.3. The REPTATE[10] materials database was used to identify values for the molecular weights of polystyrene at 170 °C required to give a reptation Weissenberg number, W_D of 1 at each speed, and the GPC results were used to calculate the weight fraction of chains exceeding this molecular weight. For the Rouse times, Equation 4.2 with the materials parameters from the fit to linear rheology (as given in Figure 4.4) was used to calculate the molecular weight corresponding to a Rouse Weissenberg number, W_R of one.

4.4.2.1 Multi-pass rheometry

In order to confirm there was no significant pressure loss over an experiment, the average pressure across the two transducers was monitored throughout each experiment. No significant change in the average value was noted on starting the movement of the pistons, although the individual transducers' values changed due to the pressure drop across the geometry, as shown in Figure 4.20 and observed previously for pre-pressurised MPR experiments by Valette *et al.*[178]

Observing the pressure on long times after the cessation of movement, some decrease in mean pressure was noted (~10 % over ~40 minutes at 100 bar). However, the experimental deformations were short (< 1 min) and the stress relaxation analysed was within the first 20 s of stopping the pistons, when change in mean pressure from the initial value was negligible. Hence it is valid to assume that the initial pressure applied to the sample was maintained throughout the experiment

Table 4.3: Calculated weight fractions of chains above their Rouse and reptation times for each piston speed used, calculated from the GPC results and using the REPTATE materials database.

Speed /mms^{-1}	**Rabinowitsch corrected wall shear rate /s^{-1}**	***M*** **(W_D=1) /gmol^{-1}**	**Polymer chain fraction above M (W_D=1)**	***M*** **(W_R=1) /gmol^{-1}**	**Polymer chain fraction above M (W_R=1)**
0.005	0.071	358000	0.308	2950000	0.000891
0.01	0.14	293000	0.381	2080000	0.00360
0.05	0.71	186000	0.541	933000	0.0503
0.1	1.4	154000	0.607	660000	0.118
0.5	7.1	99600	0.730	295000	0.379

and the results can be studied without the concerns present in Section 4.1, that polymer was escaping during the experiment.

4.4.2.2 Steady state stresses and pressure drops

The wall shear stress was obtained both by counting the fringes and using the pressure drop across the geometry (using Equation 4.3). The apparent shear viscosity was then calculated as the ratio of the steady state to the wall shear rate. Both these methods are compared to the complex viscosity (measured in an oscillatory test in 4.1) and steady shear viscosity measured using a capillary rheometer (Section 2.6) in Figure 4.21. Values for the pressure dependence of viscosity, β were obtained using the Barus equation[112] (Equation 1.24).

The values extracted are shown in Figure 4.22. β values were not extracted from the stress fringes for the two slowest speeds, because the change in the number of fringes with pressure was not above the measureable error (0.5 fringes). However these speeds could be analysed by the pressure drop.

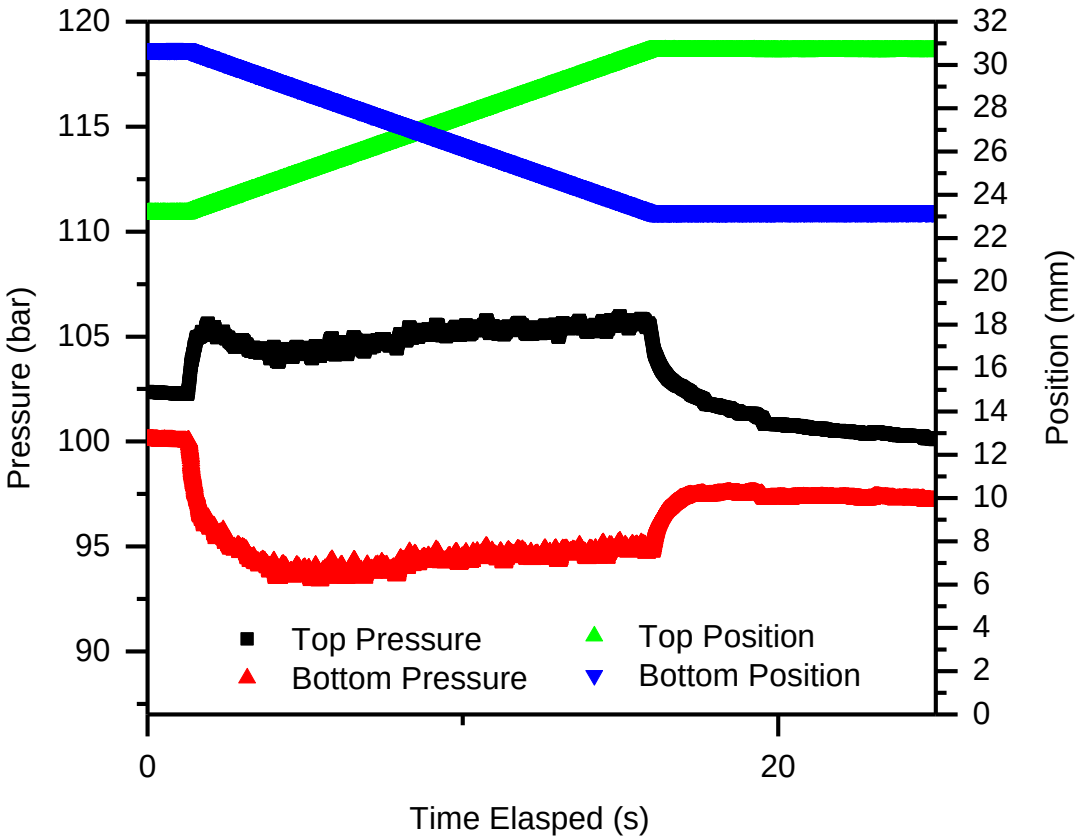

Figure 4.20: Values of the pressure and position of individual transducers during an experiment at 170 °C, 100 bar initial pressure and a speed of 0.5 mm/s.

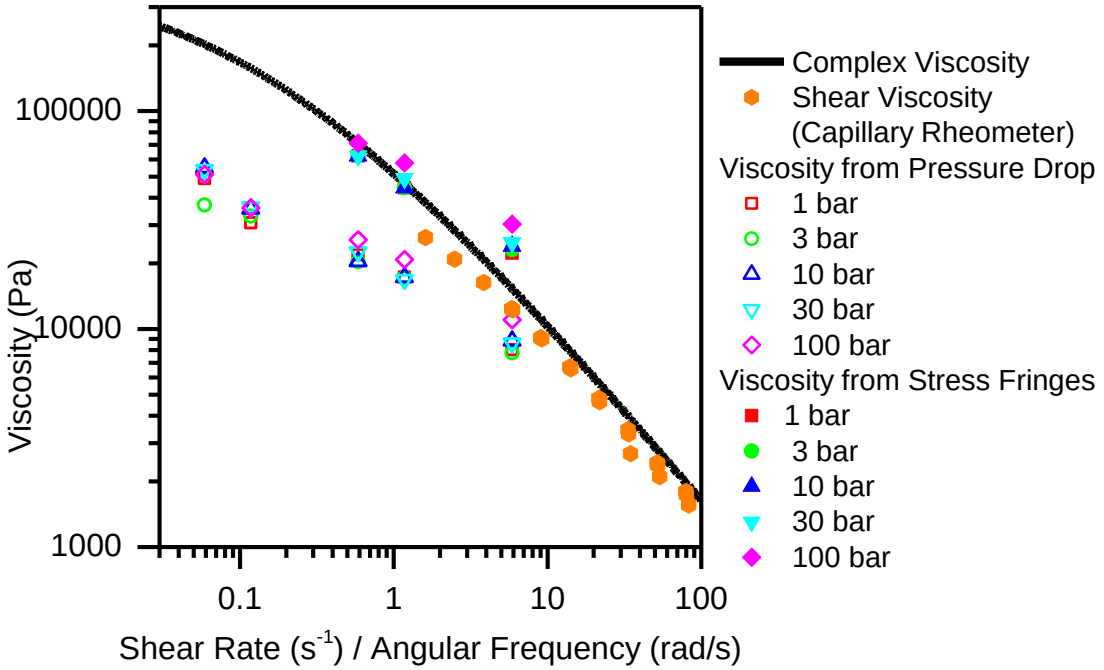

Figure 4.21: Comparison of the viscosity at 170 °C measured from the fringe count and pressure drop at the steady state with the complex viscosity extracted from oscillatory rheology and steady state viscosity from capillary rheometry.

4.4.2.3 Pressure drop decays

Figure 4.23 shows an example of the decay in pressure drop over the geometry, after a deformation. The zero time (when the pistons stopped) was calculated from the starting time of the experiment and the duration of the deformation. Notably, the pressure drop did not return to zero over the window of observation. Because all the stress fringes had decayed at this time, it is valid to assume that this was not due to ongoing relaxation in the slit.

It was not possible to represent the majority of the pressure drop decays with a single exponential decay. However, a combination of exponentials with different relaxation times gave good fits. In the decays at the highest shear rates, as many as three regions were observed, as there was seen an initial fast decay, at short times (usually < 0.1 s) in addition to two slower relaxation timescales. Hence the pressure drop decays could be fit with a three term exponential decay, including an offset term, given by:

$$\frac{\Delta P}{\Delta P_0} = \mathrm{y}_0 + A_p e^{\left(-\frac{t}{\tau_1}\right)} + B_p e^{\left(-\frac{t}{\tau_2}\right)} + \left(1 - A_p - B_p\right) e^{\left(-\frac{t}{\tau_f}\right)} \qquad (4.12)$$

where ΔP is the pressure drop, ΔP_0 the initial pressure drop established under steady flow, t the time after pistons are stopped, y_0 the fit offset, τ_1, τ_2 and τ_f are

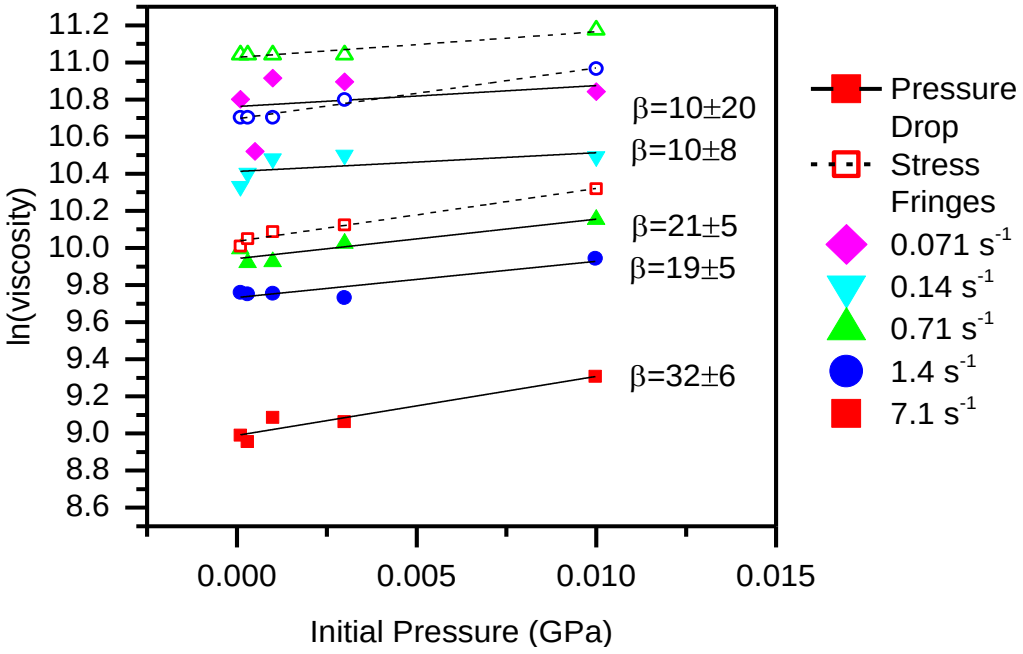

Figure 4.22: Steady state viscosities at 170 °C measured from pressure drop and stress fringes, labelled with gradients in GPa^{-1}, equal to β in Equation 1.24. Pressure drop data are represented by solid symbols and solid lines. Stress birefringence data are shown as open symbols and dotted lines. The two slowest shear rates did not create enough stress fringes to capture a change with pressure above the error (0.5 fringes) and hence the viscosities from stress fringes are not included.

the fit timescales and A and B are fit magnitudes of the decays. τ_1 is an early relaxation time which appears to correspond to Rouse behaviour, τ_2 is a late relaxation time which is consistent with the timescale of reptation and τ_f is included to represent the initial fast decay. The coefficients *A* and *B* therefore represent the relative contributions of the early and late relaxation processes respectively. Although the initial fast decay may not be exponential, it is so brief that it can be approximated by including a single exponential term alongside the early and late relaxations, giving Equation 4.12.

As most decays were at shear rates slower than the calculated inverse Rouse time, the τ_1 term was not always necessary. τ_1 was noted at the three highest shear rates, where the late relaxation time was observed at all shear rates. Also τ_f was only observed at the highest shear rates. For the lower shear rates, the effect of the initial fast decay was not significant enough to be observed, so the τ_f term could also be excluded. The decays were fit using the minimum possible number of terms that yielded significantly different relaxation times. The magnitudes of the fast and

early relaxation times were similar in all experiments but the fast relaxation time was always below 0.21 s and could be distinguished from the early relaxation time. The parameters of the fits and their uncertainties are given in Appendix 4.

4.4.2.4 Stress decays

As the video recording was started independently from the piston movement, the zero point for the decays was instead taken as the point at which the fringes begin to decay. The stress analysis has been focussed on the three highest shear rates because they show sufficient fringes to allow accurate characterisation of the stress decay within the error of counting the fringes. Examples of these decays can be seen in Figure 4.24.

Multiple exponential decays were again necessary in order to fit the stress relaxation process; the stress decays were fit to an exponential decay according to:

$$\frac{\sigma}{\sigma_0} = \mathrm{y}_0 + A_\sigma e^{\left(-\frac{t}{\tau_1}\right)} + B_\sigma e^{\left(-\frac{t}{\tau_2}\right)} + (1 - A_\sigma - B_\sigma) e^{\left(-\frac{t}{\tau_f}\right)} \tag{4.13}$$

where σ is the stress, σ_0 the initial stress established under steady flow, t the time after pistons are stopped, y_0 the fit offset, τ_1, τ_2 and τ_f are the fit timescales and A and B are fit magnitudes of the decays. Because the stress decayed to zero in every case, the offset term, was constrained to +/- half a fringe (~5000 Pa) to account for any error in fringe counting. This approach gave good fits to the observed stress

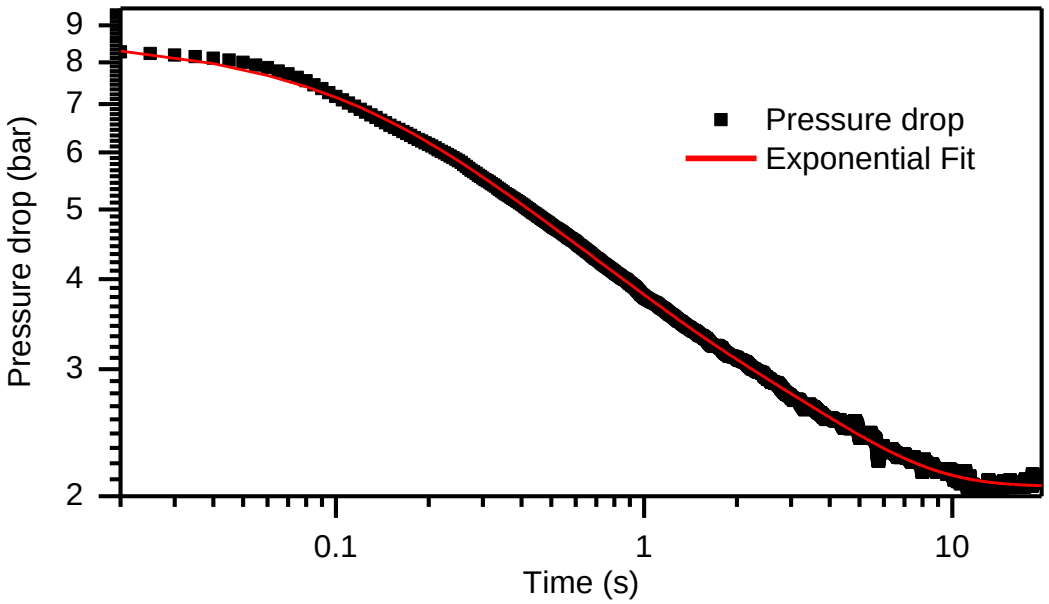

Figure 4.23: Pressure drop decay of polystyrene after a deformation at 7.1 s^{-1} and 170 °C with 30 bar initial pressure applied. The red curve is the result of a multi-exponential fit using Equation 4.12.

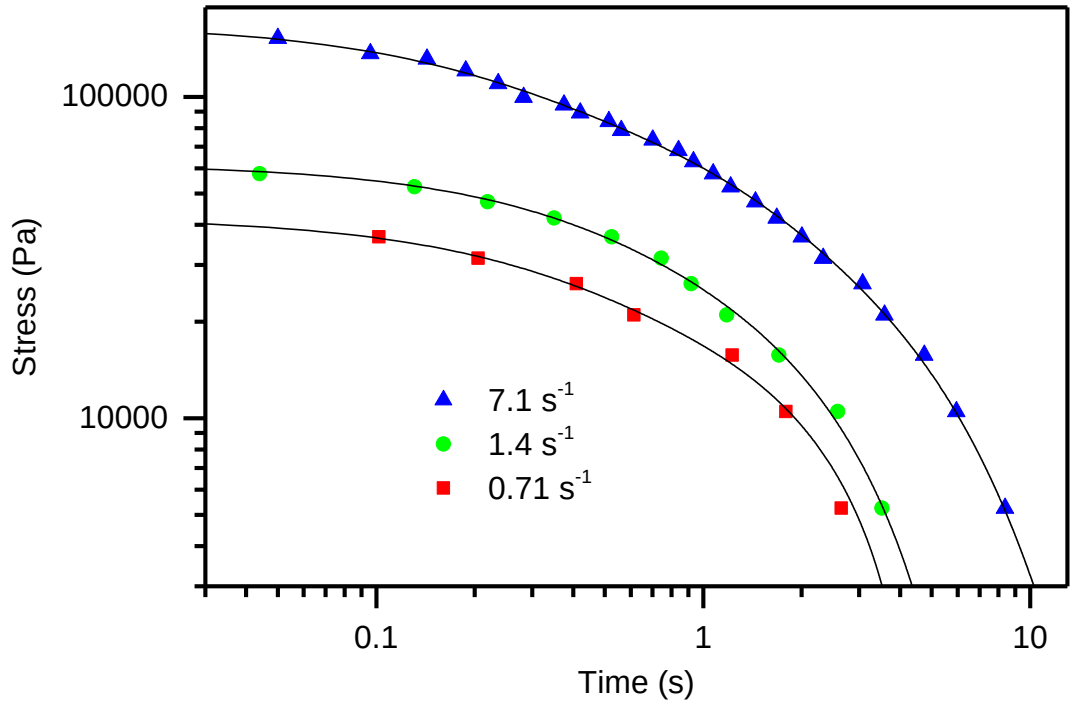

Figure 4.24: Stress decays at 100 bar of initial pressure at 170 °C, shown with the exponential fits using Equation 4.13 (black lines).

decays for all of the data (see Figure 4.24). The early relaxation time, τ_1, was typically of the order of 1 s or less, and was consistently observed at the highest speed, and in some of the decays at lower speeds. The late relaxation, τ_2, was observed at all speeds, and was generally found to be in the range 1-4 s. The initial fast decay, τ_f, was seen to be most significant at the highest speeds and pressures.

4.4.2.5 Relaxation times

The early and late relaxation times were found to correlate well with the Rouse and reptation times respectively, determined from the linear rheology and scaling. Both early and late relaxation times were seen to increase with applied pressure (Figure 4.25), in contrast to the results of Section 4.2. The relaxation times from both the pressure drop and stress fringes were compared and were seen to give similar values but the pressure drop results produced significantly more variation. No clear dependence of the relaxation time with shear rate was noted (Figure 4.26). Hence an average of the late relaxation time could be calculated across the different shear rates, which reduced the variation and still showed a positive relationship with pressure (Figure 4.27). To quantify this relationship, they were fit with beta values according to the equations,

$$\beta_{\mathrm{E}} = \frac{d\ln(\tau_1)}{d\,p} \tag{4.14}$$

$$\beta_{\mathrm{L}} = \frac{d\ln(\tau_2)}{d\,p} \tag{4.15}$$

where β_E represents the pressure dependence of the early relaxation time τ_1 and β_L represents the pressure dependence of the late relaxation time τ_2. These fits are shown in Figure 4.28, all values showed a positive value above the error except the pressure drop early relaxation times for which the value is of the same magnitude as the error.

4.4.3 Discussion

4.4.3.1 Multi-pass rheometry

The observation of the pressure confirms that there were not significant losses over the experiment, which means that sample was not escaping from the test section as was observed in Section 4.1. Hence the true pressure dependence can be evaluated in these experiments.

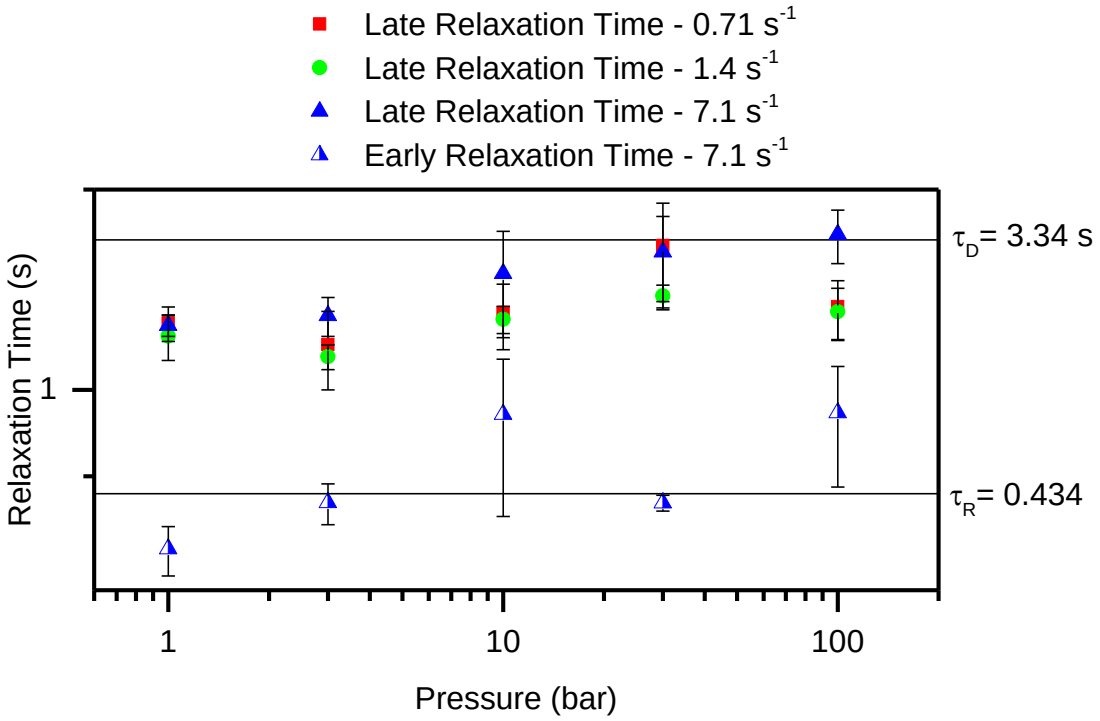

Figure 4.25: Early (τ_1) and late (τ_2) relaxation times at 170 °C extracted from exponential fits of the stress decays at different pressures using Equation 4.13. The Rouse and reptation times obtained from oscillatory rheology at 1 bar are annotated as horizontal lines for comparison.

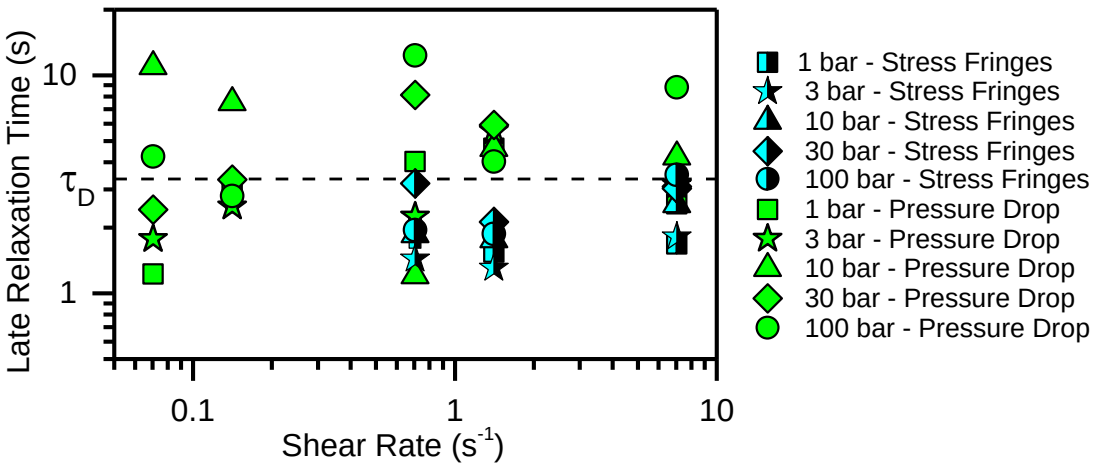

Figure 4.26: Late (reptation) relaxation times at 170 °C shown at different shear rates (proportional to piston speed, see Table 4.2). Both those obtained from exponential fits of the stress and pressure drop decays are shown, the pressure referred to is the initial pressure applied before the shear. The reptation time obtained from oscillatory rheology at 1 bar (3.34 s) is annotated as a horizontal line for comparison.

4.4.3.2 Steady state stresses and pressures

The two lowest shear rates showed relatively little build-up of stress (1-1.5 fringes). At these piston speeds, the wall shear rates are below the inverse reptation time and so the polymers can fully relax on a shorter timescale than it takes to build up a deformation of order 1. On this basis, it might be considered surprising that any stress fringes at all are observed, since W_D is much less than one. However the calculated data in Table 4.3 shows there is a significant proportion of chains that are above their inverse reptation times at all piston speeds, and a small fraction may even fall into the W_R > 1 regime. The faster speeds showed significantly higher stress birefringence as an increasing proportion of the molecular weight distribution is unable to relax.

The extracted viscosities and β values are included here as a method of comparing results with existing literature and ensure consistency before discussing the more novel stress decays. Steady shear data from a capillary rheometer is provided alongside the complex viscosity extracted from the oscillatory measurements, the two show good agreement and demonstrate that the Cox-Merz rule[138] holds for this material.

The viscosities extracted from the fringe counting were significantly higher than for the pressure drop results at the same speed, and the values from fringe counts showed better agreement with the complex viscosity from oscillatory shear (Section 4.1). This is due to the contribution of the entry and exit effects to the pressure drop

which are minimised when counting fringes by only examining those in the gap. These additional contributions to the strain could have reduced the viscosity of the material (since it is a shear thinning polymer). The stress calculated from the pressure drop is therefore lower than that from fringe counting, which gives rise to the lower apparent viscosity.

It has been observed that β values vary when determined from different techniques (involving different methods of calculation).[170] Comparing the β values obtained by stress fringes to those from pressure drop analysis in our experiments, however, there is some deviation between the two methods, but it is not systematic and differences are close to the range of error (Figure 4.22). The value of the SOC used could be a contributing factor as it is an average over many experiments and is seen to vary with shear rate. The uncertainty in the SOC of 0.2×10^{-9} Pa^{-1} is achieved by fitting to many measurements, whereas it is of the order 1×10^{-9} Pa^{-1}, (+/- 20 %) in individual measurements. There is a much greater error in the values extracted from the pressure drop and the values fluctuate more significantly. This is likely due to

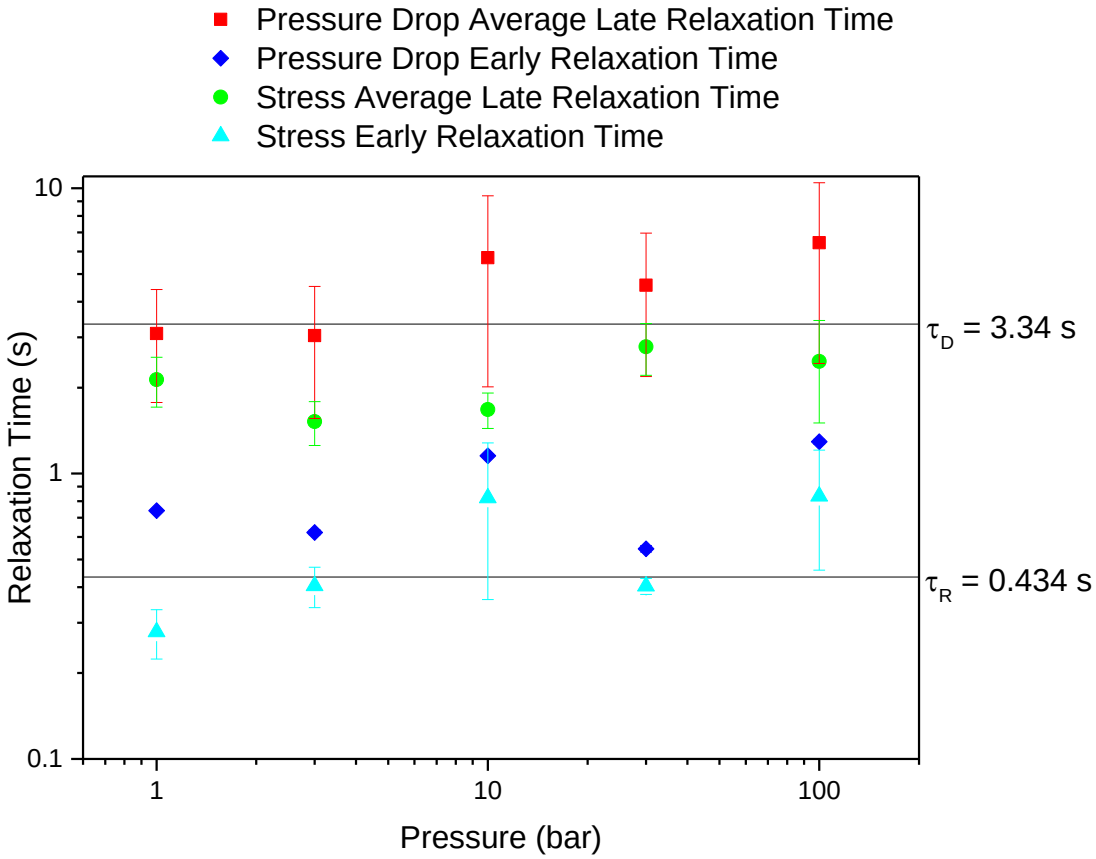

Figure 4.27: Early and late relaxation times at 170 °C calculated from fits to both pressure drop and stress decays. The late relaxation times are averaged over all shear rates, whereas the early relaxation time is only seen at the highest shear rate. The Rouse and reptation times obtained from oscillatory rheology at 1 bar are annotated as horizontal lines for comparison.

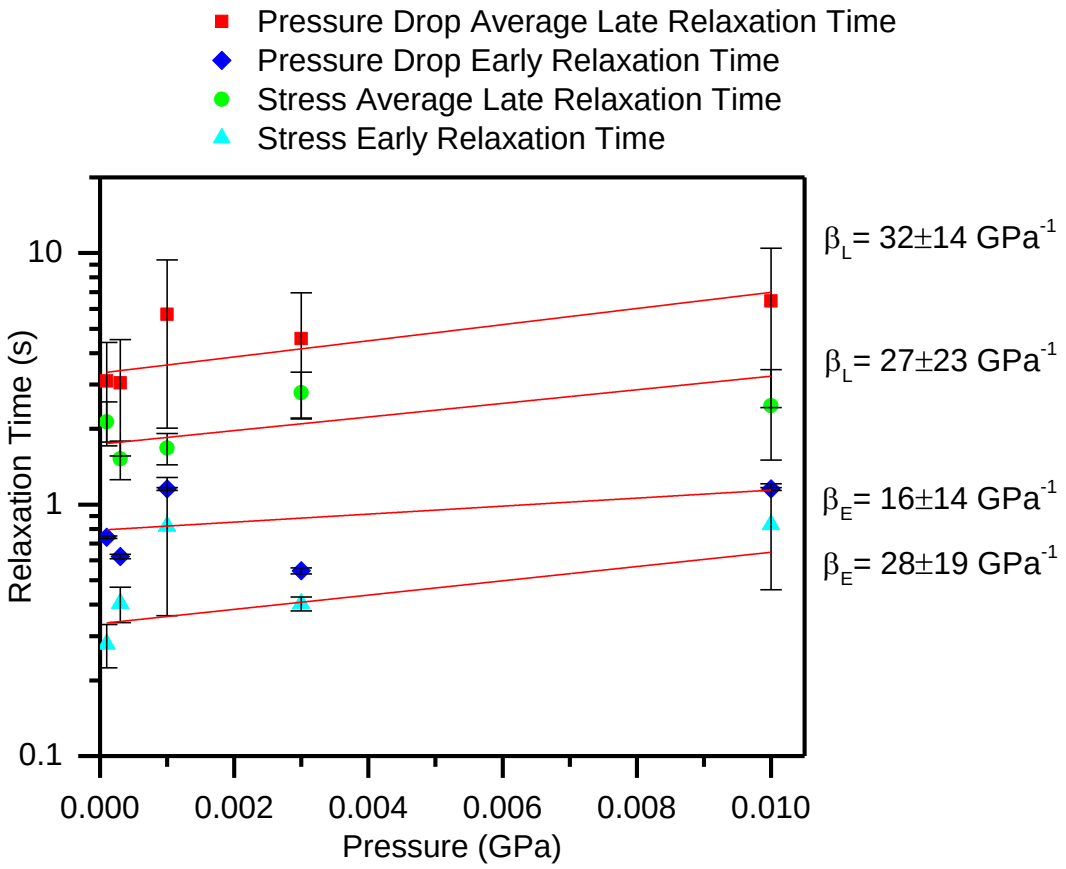

Figure 4.28: Early and late relaxation times at 170 °C calculated from fits to both pressure drop and stress decays, with fits to show the trend with pressure.

effects outside the slit that cause fluctuations in viscosity, and could be reduced by recording more points at different pressures should a more accurate β be required from pressure drop alone. At the two lowest shear rates, a change in the number of fringes with pressure could not be separated from the error (0.5 fringes). However pressure drop was observed, which suggests the pressure drop was not measuring shear stress in the slit, and could have been dominated by exit and entry. This could explain the anomalous results at these shear rates.

As the experiments were designed to span a logarithmic range of pressures (in order to study the stress relaxations) there is significant error introduced by fitting the limited range of points on a linear pressure scale. Despite this, it appears that values of β obtained with the MPR are in line with those obtained by other techniques. Notably, Kamal and Nyun[116] obtained a value of 20.7 GPa^{-1} for PS at 2500 s^{-1} and Sedlacek *et al.*[115] obtained a shear independent (zero-shear) value of 43.45 ± 12.1 GPa^{-1}. Volpe *et al.*[176] reported values in the range 5-40 GPa^{-1}, for PS at temperatures in range 220-260 °C and showed the value decreased with shear rate. As discussed in the introduction, it can be difficult to obtain reliable values of the

pressure coefficient as strictly it is defined only at a specific shear rate and temperature. For the values extracted from both the stress fringes and pressure drop, β is seen to increase with shear rate. This appears to contradict some reports in literature which show an increase [118-119], or that suggest β is independent of shear rate Goubert *et al.* [168]. The β values are plotted against shear rate in Figure 4.29.

4.4.3.3 Pressure drop decays

The pressure drop decays following cessation of flow were seen to follow a complex decay. This could however be modelled using several exponential decays (as in a simple Maxwell model of viscoelasticity[177]) with different timescales expected to be present in a polymer melt. There is expected to be relaxation due to both Rouse motion and reptation, which explains the presences of two different regimes, however there was also noted a third regime, very fast decay at very short times (much shorter than the Rouse time) due to the overshoot of the retreating piston. This was seen at all pressures, although the magnitude of the decay occurring in

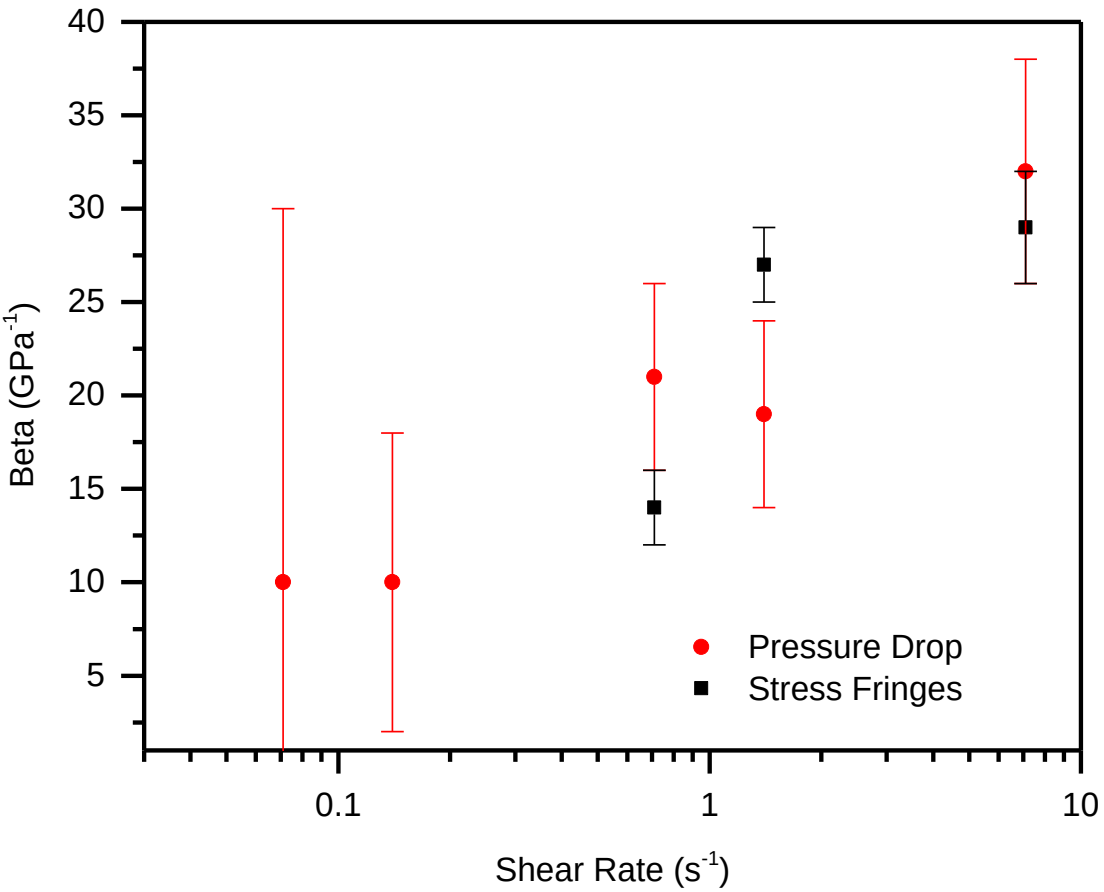

Figure 4.29: Beta values extracted from the steady state viscosities at 170 °C with different initial pressures, calculated from both pressure drop and fringe counting.

this region increased with pressure and shear rate, making it most noticeable at the highest shear rates and pressures.

Predictions from linear rheology suggest the mean Rouse time should only contribute at the highest shear rate, however it is was possible to observe the early relaxation time from experiments at 1.4 s^{-1} and 0.69 s^{-1}. This is consistent with our calculations from the GPC which suggest 5 – 10 % chains are still above their inverse Rouse times at these rates.

At shear rates exceeding the inverse reptation time, the magnitude of the pressure drop is seen to increase with shear rate, and a significant increase is seen in the number of stress fringes. Nevertheless, a significant pressure drop is observed following flow cessation after the shear rates below the inverse reptation time, as well as stress fringes (1-1.5). The GPC analysis suggests this is due to the presence of higher molecular weight chains, as at all speeds there are significant amounts of chains (> 25 %) above their inverse reptation time, and the longest relaxation times are predicted to dominate viscoelastic effects.

4.4.3.4 Stress decays

Since the pressure drop across the geometry is proportional to the wall shear stress, the stress should also be expected to decay exponentially. This is seen in our results and as with the pressure drop decays, three regimes are observed. The three term exponential fits therefore gave very good agreement with the experiment data.

As for the pressure drop, all three of these regions are only observable at the highest shear rate. The initial fast term again is most apparent at the highest shear rates and pressures. However, it was not captured in many of the stress decays, likely because of the reduced frequency of points. The camera frame rate of 18 fps gives a frame every 0.056 s and as the fast decay occurs on a timescale of around 0.1 s, there may not have been enough data to isolate it for some decays.

4.4.3.5 Relaxation times

The β values for calculated for the relaxation times with pressure each show a small positive value, with the exception of the pressure drop early relaxation times, which has a β value close to the level of error (as shown in Figure 4.22). The pressure drop early relaxation times are expected to be the most effected by error since the pressure drop fluctuates more than the stress fringes and the early relaxation time has a lower value than the late (so is more effected by short timescale fluctuations).

Both the early and late stress relaxation times show a similar increase with pressure, which implies that both the local stretching and long range orientational relaxation are retarded by increasing pressure. The increased pressure causes a slowing in molecular movement, resulting in an increase in viscosity (as observed in literature[27]). This effect reduces the speed of both Rouse and reptation processes.

Overall no significant effect on relaxation time with shear rate is noted, as shown in Figure 4.26. Although the shear rate can change relative contribution from each the regime of the relaxation behaviour, it would not be expected to influence the Rouse or reptation relaxation times directly.

There is clearly more fluctuation in the relaxation times obtained from the pressure drop decays than the stress fringes, however, the two methods are in relatively good agreement and the early and late relaxation times are distinct from one another in each case. Overall, the optical capability clearly provides a more accurate measure of the relaxation time and provides other benefits such as being able to see the distribution of stress around the geometry, allowing analysis of exit and entry effects and the identification of wall-slip effects.

It is unclear why the pressure drop gives slightly higher values for the relaxation time than the optical analysis. The offset term, necessary to facilitate the exponential fits since the pressure drop did not decay to zero, could have contributed to this difference. Despite this, the trends are consistent between methods, and using either pressure or stress data has been shown to give reliable information on the relaxation times of the polymer. This suggests relaxation times could be obtained from the pressure decays alone, e.g. for an opaque sample. Furthermore, because the nature of the MPR allows multiple experiments, multiple decays could be recorded and averaged in order to minimise fluctuations.

4.4.4 Conclusions

Using a multi-pass rheometer for study of stress decay on cessation of a contraction-expansion flow, it has been possible to elucidate the pressure dependence of the viscoelasticity of polystyrene melts as well as several aspects of the underlying molecular rheology. Results for the pressure dependence of viscosity were broadly in line with those obtained using other methods on similar materials. The decay of stress could be described by a sum of up to three characteristic relaxation processes. The fastest process, most apparent after high shear rates and high pressures, is thought to arise from apparatus compliance in the form of an overshoot of the retreating piston. The remainder of the relaxation can be described

by two characteristic time scales, which correspond well to the Rouse and reptation times of the polymer. Interestingly, the stress measured is significant even at inverse shear rates slower than the mean reptation relaxation time. We believe that this is because the dispersity in molecular weight gives rise to a small fraction of material with much longer relaxation times, and significant chain orientation and even stretch are possible at low shear rates.

This method allows study of behaviour originating from chain stretch and orientation, in a manner that is non-destructive to the sample and repeatable. Study of this range of behaviour allows the interrogation of a range of behaviour linked to molecular relaxation, and with careful recording and observation of the stress fringes, relaxation times for a polymer after steady shear can be extracted. As well as allowing the study of the response to pressure, these relaxation times can also reveal information about the molecular weight, polydispersity and structure of the polymer. Using a long narrow slit, extensional effects at the entry and exit can be negated, as they are difficult to separate from the effect of the shear. However to gain information about the steady shear extensional behaviour of a material, a cross-slot can be used to generate pure extensional flow, and this process is detailed in Section 4.5.

4.5 Cross-slot flow of polydisperse trans-polyisoprene

The multi-pass rheometer can also be used to examine extensional effects using cross-slot flow. The test section can be replaced with a cross-slot, where the pistons push the polymer in from the top and bottom and it flows out through the two sides. Slave pistons are used in the sides which can be driven back under nitrogen pressure to repeat experiments (as shown in Figure 4.30).

This geometry produces a central stagnation point at the intersection of the two directions of flow where the flow is purely extensional, which allows steady state extension to be studied at higher rates than in the SER as breakup of the samples is not an issue. This behaviour has been studied previous for high temperature melts, e.g. polystyrene[39-40], however experimental limitations mean that room temperature melts, such as polyisoprene and polybutadiene have not been studied in this way,

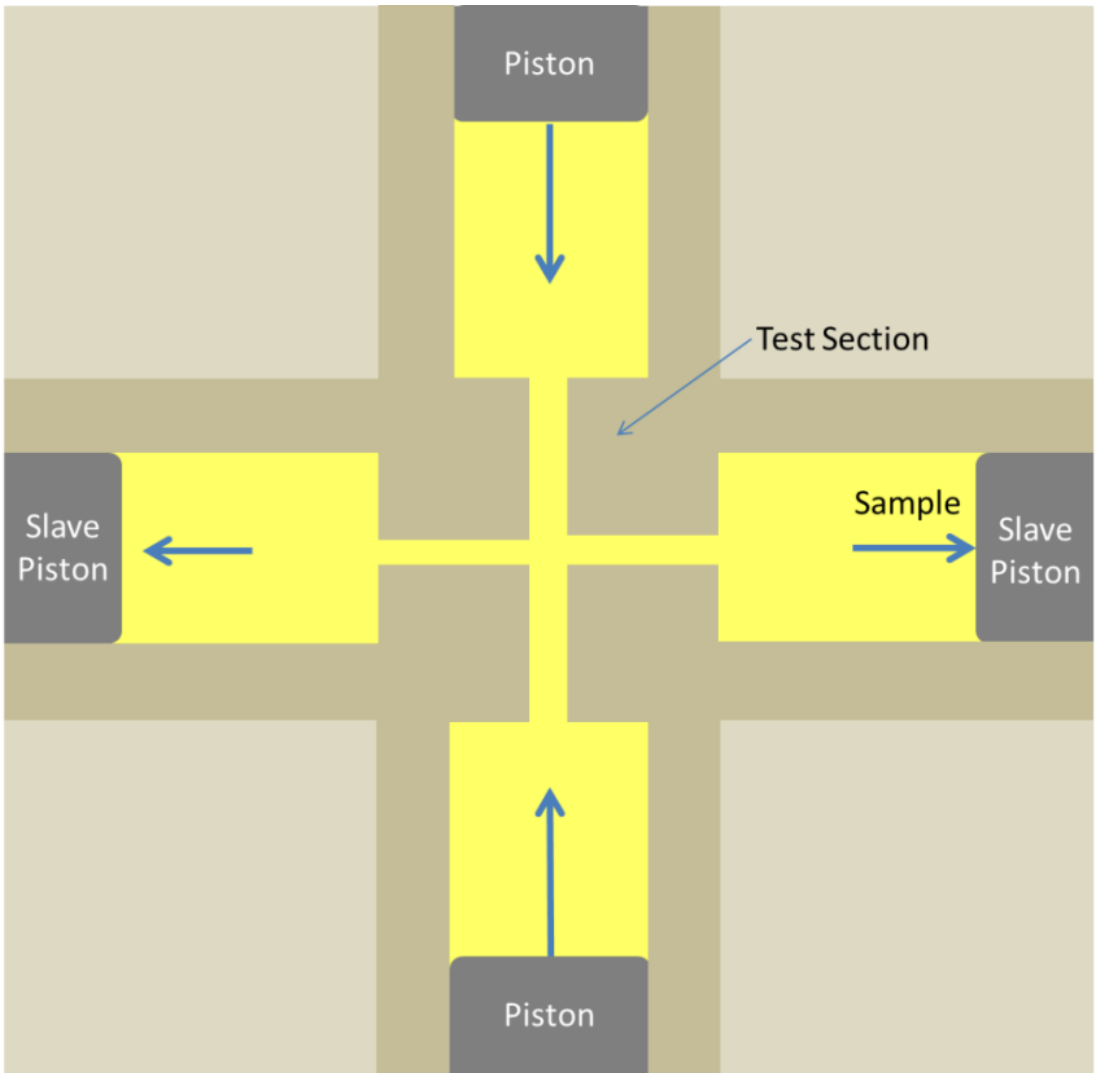

Figure 4.30: Illustration of the operation of the MPR with a cross-slot test section. The top and bottom pistons are driven inward forcing polymer out via the slave pistons at the sides.

and it is difficult to get steady state extensional viscosities at all for these materials. The main reason for this is that PI and PBD are generally more sensitive to oxidation, which means high temperatures are not possible and in fact, heat generated by the moving parts of the MPR must be excluded. This is a particular problem as monodisperse PI and PBD is not generally available in large quantities, and since ~10 g is required for the cross-slot experiment, it is desirable to reuse the same sample throughout the tests. In addition, using these low temperatures means that the polymer is highly viscous and so large pressures are required to drive the polymer through the cross-slot (higher than can be created with gas pressure on the slave pistons).

In this section, initial studies are performed with trans-polyisoprene, which is solid at room temperature, less sensitive to oxidation and in terms of experimental set up behaves similarly to polystyrene, so is a good initial test material to help formulate an approach for polymers which are a mixture of isomers.

4.5.1 Materials

Material used (TPI420K) was Sigma Aldrich trans-polyisoprene pellets (ALDRICH 182168, M_w ≈ 420,000 g/mol).

4.5.2 Experimental

4.5.2.1 Shear rheology

A heated press was used with a mould to press sample into a disc, 1 mm thick with a diameter of 25 mm. The sample was pressed at 80 °C under 5 tonnes pressure for 5 minutes. Rheological characterisation of this material was performed on a TA AR-2000 rheometer using a 25 mm parallel plate and an environmental test chamber supplied with nitrogen gas. Oscillatory frequency sweeps were performed at temperatures from 70 to 190 °C, using a strain of 1 % and frequency spanning from 0.1 rad/s to 600 rad/s. The results were overlaid in a single spectrum at a reference temperature of 170 °C by applying a Williams-Landel-Ferry (WLF) time-temperature superposition using REPTATE software.[10]

4.5.2.2 Multi-pass rheometry

TPI420K pellets were loaded into the MPR fitted with a cross-slot geometry with a channel width of 1.5 mm and a depth of 10 mm. The pistons were driven at various speeds between 0.004 mm/s and 1 mm/s, inwards, forcing polymer through the slot and out into the side reservoirs, where it could be driven back by applying nitrogen pressure. Experiments were performed at temperatures of 80 °C and 170 °C.

Using 514 nm green light, birefringence was imaged and observed over the same time. The pressure at the top and bottom pistons was measured, and the pistons driven until both pressures reached a steady value, at this point the number of fringes at the stagnation point was counted as in Figure 4.31.

A stress optical coefficient for polyisoprene of 1.9 x 10^{-9} Pa^{-1} at 22 °C[74, 182-183] was then used to calculate the stress from the number of fringes. Since the SOC is proportional to the reciprocal of the temperature[74], it could be shifted to the temperature required.

The extension rate was then calculated using the following equation, specific to the geometry used,

$$\dot{\varepsilon} = 8.75.v_{piston} \tag{4.14}$$

Extensional viscosity could then be given by the stress over the extension rate.

4.5.3 Results: Steady state extensional viscosity

The shear rheology was shifted with WLF parameters, fitted to give best overlap of the data as shown in Figure 4.32. The same parameters were then used to shift the extensional results at 80 °C to 170 °C for comparison. This gave a relatively good overlap although there is still a shift between the results at the two different temperatures. The results are compared to the complex viscosity which can be multiplied by a factor of 3 to give the extensional viscosity if the behaviour was

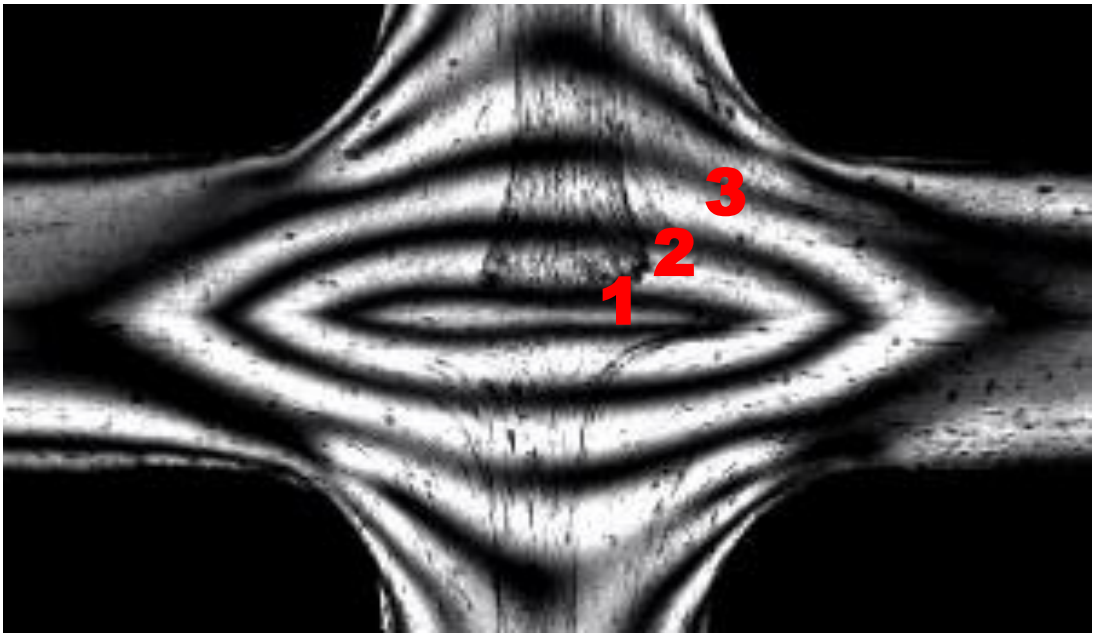

Figure 4.31: Example birefringence pattern showing how fringes are counted at the stagnation point.

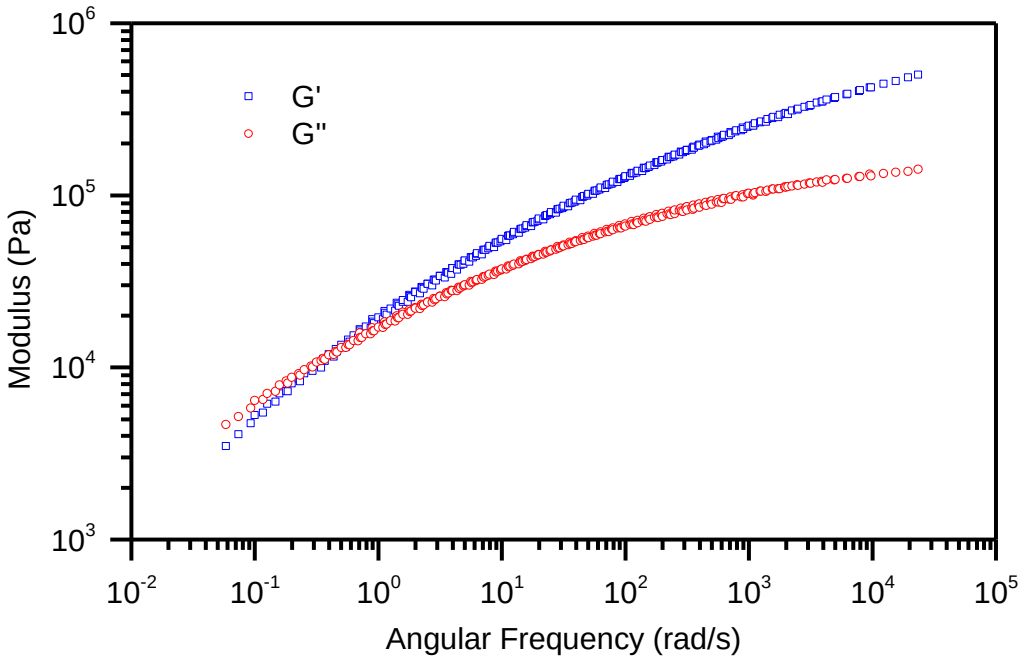

Figure 4.32: Oscillatory shear measurements of trans PI at temperatures between 70 °C and 190 °C, shifted to 170 °C with WLF parameters: C_1=5.22, C_2=258 K, C_3=-0.833.

Newtonian. The results are much higher than the Newtonian response which indicates the material strain hardens significantly in extension.

4.5.4 Discussion: Steady state extensional viscosity

It has been demonstrated that the cross-slot geometry in the MPR can be used to measure extensional viscosity in materials that are relevant to this project, in a way that has not been done previously. However some limitations remain to be addressed.

As the material is commercial, trans-polyisoprene, the materials parameters for cis-polyisoprene may not be applicable. It is for this reason that the WLF parameters were fit to the data. Due to the regularity in its structure, the material is much more crystalline than cis-PI, and the crossover in the linear rheology is seen at much lower frequency than a similar molecular weight cis-PI. The high values of the extensional viscosity are also likely due to this effect, as a similar cis-PI would not be expected to strain harden at the extension rates used.

Though the WLF parameters were fit to the data, a single set of parameters provided good overlap of all the temperatures measured and could be applied to the extensional results, however it did not provide an exactly overlap of the results at the two temperatures. The measurements at 80 °C are close to the melting point of the

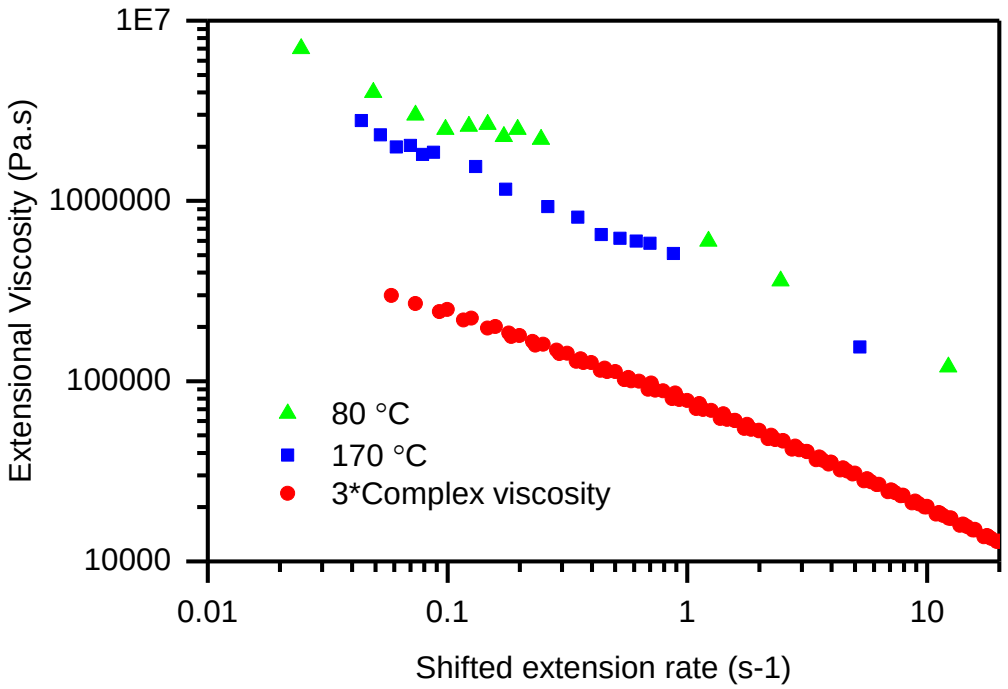

Figure 4.33: Extensional viscosity measured from fringe counting in a cross-slot for trans-polyisoprene. Also shown is the complex viscosity from linear rheology multiplied by 3 (i.e. the extensional viscosity if the material was Newtonian).

polymer (around 65 °C) and if the polymer was not fully melted then this could explain the slight failure of the TTS, however it appeared to be valid for the shear measurements at this temperature. Alternatively, the difference could be due to oxidation of the polymer. A shift in the crossover point in the linear rheology by a factor of approximately ~3 was seen after the MPR experiments, which suggests some of the long chain molecules had been broken up. Hence oxidation had occurred and these temperatures would not be suitable for the monodisperse materials.

The crystallinity of the material makes it difficult to say whether molecular models are valid (and hence calculate Weissenberg numbers for example). Hence while this material was useful for proving the utility of the MPR for these experiments, monodisperse cis-polyisoprenes at lower temperatures are required to better study the extensional behaviour of polyisoprene.

4.5.5 Conclusions

The multi-pass rheometer equipped with a cross-slot geometry was used to extract extensional viscosity of trans-polyisoprene. The technique was effective at isolating extensional properties, but the results at two different temperatures did not completely agree when time-temperature superposition was applied. The high temperatures used were seen to degrade the sample resulting in a change in the

linear rheology. It was difficult to relate the behaviour to molecular properties because the material was not well-defined, and monodisperse cis-PI would be required to better relate the extensional properties to the underlying structure.

4.6 Cross-slot flow of monodisperse polyisoprene

In order to explore the extensional behaviour under different conditions, monodisperse material is desirable, since predictions can be made about its behaviour from the linear rheology and linear models. There is also little work in the literature on the extensional properties of these rubbery materials as it is very difficult to achieve a steady state in extension with current methods.

However, to use rubbery polyisoprenes at temperatures not significantly above ambient (40 °C or less is required to prevent degradation of the samples) modifications to the MPR were required. The nitrogen pressure on the slave pistons is not sufficient to drive polyisoprene through the geometry at these temperatures; hence a simple vice was fabricated to allow repeat experiments at these temperatures (Figure 4.34). Water cooling was also added to the oil bath to maintain low temperatures as the hydraulics often heat up during use.

4.6.1 Experimental

4.6.1.1 Multi-pass rheometry

Materials used were PI300K and PI500K as characterised in Chapter 2. Material was loaded into the MPR fitted with a cross-slot geometry with a channel width of 1.5 mm and a depth of 10 mm. Experiments were also performed on PI300K using a cross-slot with a depth of 1 mm.

The pistons were driven at various speeds between 0.001 mm/s and 1.00 mm/s, inwards, forcing polymer through the slot and out into the side reservoirs, where it could be driven back using a vice. The temperature was maintained at 30 °C by

Figure 4.34: Vice attachment made to drive slave pistons

water cooling the circulating oil, this was carefully controlled as (due to large sample requirements) the same sample was used over the experiments (in total lasting a maximum of 3 days) and so an increase in temperature of 5 - 10 °C could cause the polyisoprene to degrade over these prolonged times.

Using 514 nm green light, birefringence was imaged and observed over the same time. The pressure at the top and bottom pistons was measured, and the pistons driven until both pressures reached a steady value, at this point the number of fringes at the stagnation point was counted as in Figure 4.31.

A stress optical coefficient for polyisoprene of 1.9 x 10^{-9} Pa^{-1} at 22 °C[74, 182-183] was then used to calculate the stress from the number of fringes. Since the SOC is proportional to the reciprocal of the temperature[74], it could be shifted to the temperature required.

The extension rate was calculated using Equation 4.14, and adjusted by the ratio of the cross sectional area of the slits for the 1 mm deep cross-slot. Rouse and reptation Weissenberg numbers were calculated using relaxation times for monodisperse polyisoprene from the REPTATE materials database.[10]

4.6.1.2 Flowsolve simulations

The results for the PI300K in the 10 mm deep cross-slot were modelled using Flowsolve, a Langrangian-Eulerian finite element solver[57] The software solves the material equation, here the rolie-poly[56] model, over a mesh of triangles which can be moved throughout the geometry, here the cross-slot, in order to predict the stress in the flow, and hence the pattern of stress fringes.

The materials parameters needed for the equations were fit to linear rheology and extension from the SER, and are shown in Table 4.4.

Table 4.4: Parameters used for rolie-poly model to perform Flowsolve simulations

Mode	Modulus (Pa)	Relaxation Time (s)	Chain Stretch Time (s)
1	58130	0.00193	-
2	45620	0.01328	-
3	69960	0.09122	-
4	91810	0.6267	-
5	181000	4.306	-
6	18210	29.58	0.5

4.6.2 Results

4.6.2.1 Multi-pass rheometry

It was found that there were a very large number of fringes even at slow speeds, due to the low temperatures and rubbery nature of cis-polyisoprene, which made counting them very difficult. For this reason, stress values were only obtained for a limited range of speeds. The resulting viscosities plotted against extension rate are shown in Figure 4.35. They match well with the values calculated from the complex viscosity from oscillatory shear measurements, although the cross-slot values are slightly higher. The results from the 1 mm deep cross-slot are however much lower than expected, as fewer fringes were observed.

The average pressure measured by the pressure transducers was also examined, this time allowing for a wider range of speeds to be analysed. The results are shown in Figure 4.36 and 4.37. For PI500K, there is a clear increase in pressure once the Rouse Weissenberg number exceeds one, although for the final two points it is unclear whether a steady state was reached, as due to the fast speed and limited range of movement of the pistons, there is no clear plateau in the results. Despite this, if a steady state has not been reached, the actual values of the pressure would be expected to be greater than those recorded which would produce an even greater change to those points before the Weissenberg number exceeds one.

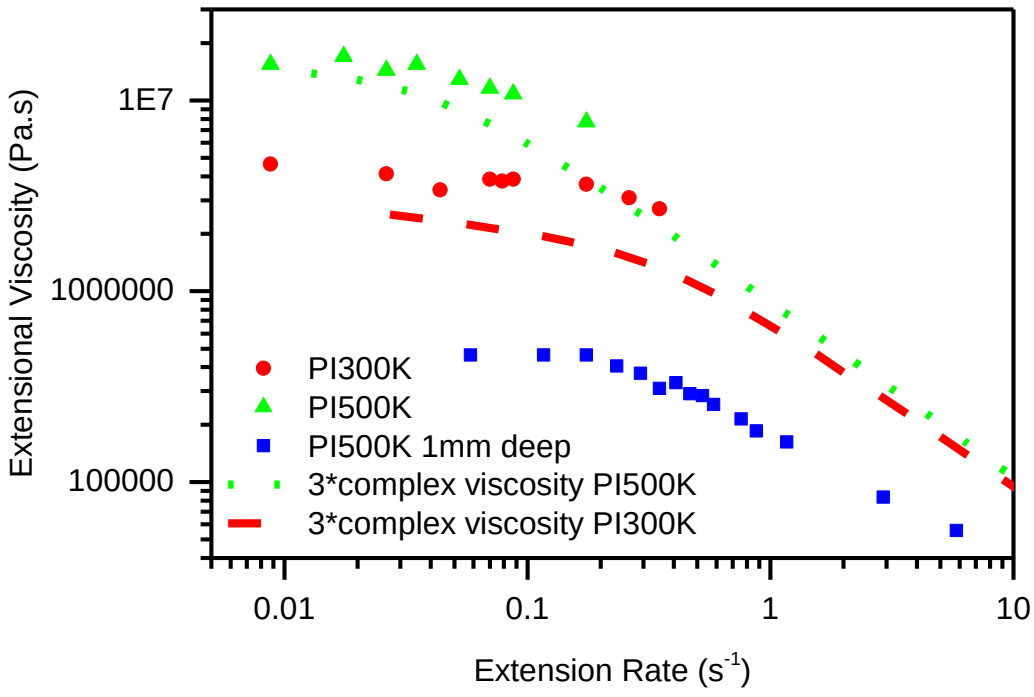

Figure 4.35: Extensional viscosity measured by fringe counting for PI300K and PI500K in the 10 mm deep cross-slot and PI300K in the 1 mm cross-slot.

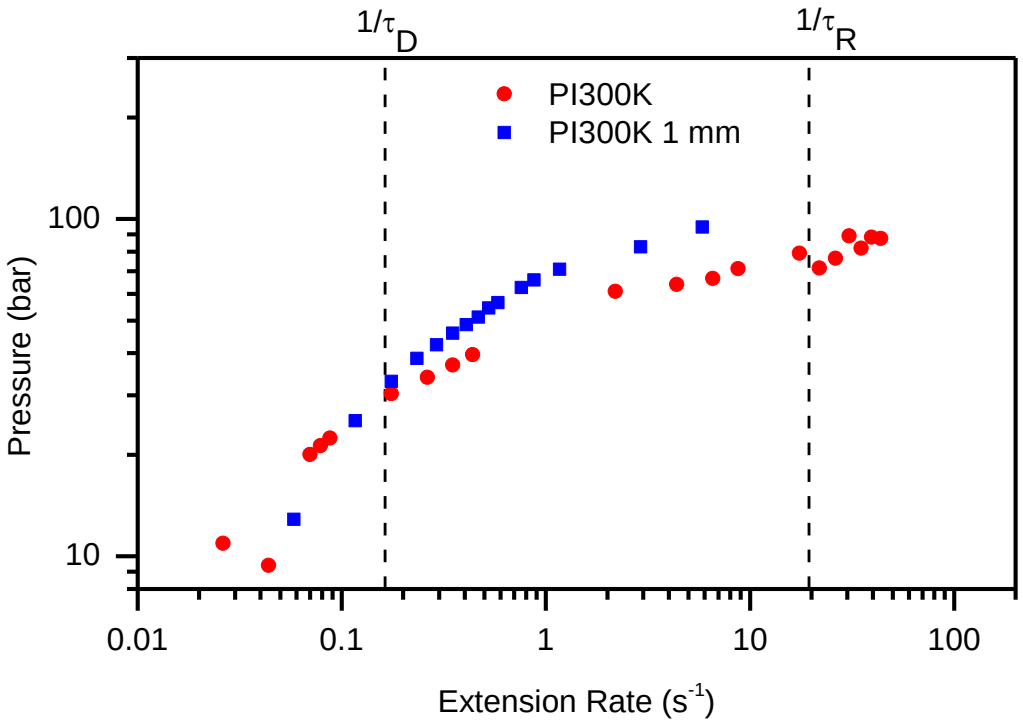

Figure 4.36: Pressure on the 1 mm and 10 mm deep cross-slots during movement at different speeds and hence extension rates, for PI300K at 30 °C. The inverse Rouse and reptation times are labelled

However, for PI300K, this increase is not seen and the results plateau around the Rouse time.

4.6.2.2 Flowsolve simulations

The Flowsolve simulation results are compared with experimental data in Figure 4.38. They capture the experimental data very well, and give fringe patterns that are remarkably similar. However the number of fringes is slightly under-predicted systematically by the Flowsolve simulations.

4.6.3 Discussion

4.6.3.1 Multi-pass rheometry

The extracted extensional viscosities are slightly higher than the Newtonian response would suggest. This could suggest there is strain hardening occurring, however it was not observed at similar extension rates in the SER, so it is likely that there is a small discrepancy between the cross-slot results and prediction from the linear rheology. This could be due to errors in the extension rate calculated due to slight differences in the gap (i.e. variations can occur due to how the geometry is set up and screwed together, but can be difficult to measure from the videos due to shadows on the image, hence the expected gap is used). Alternatively, some

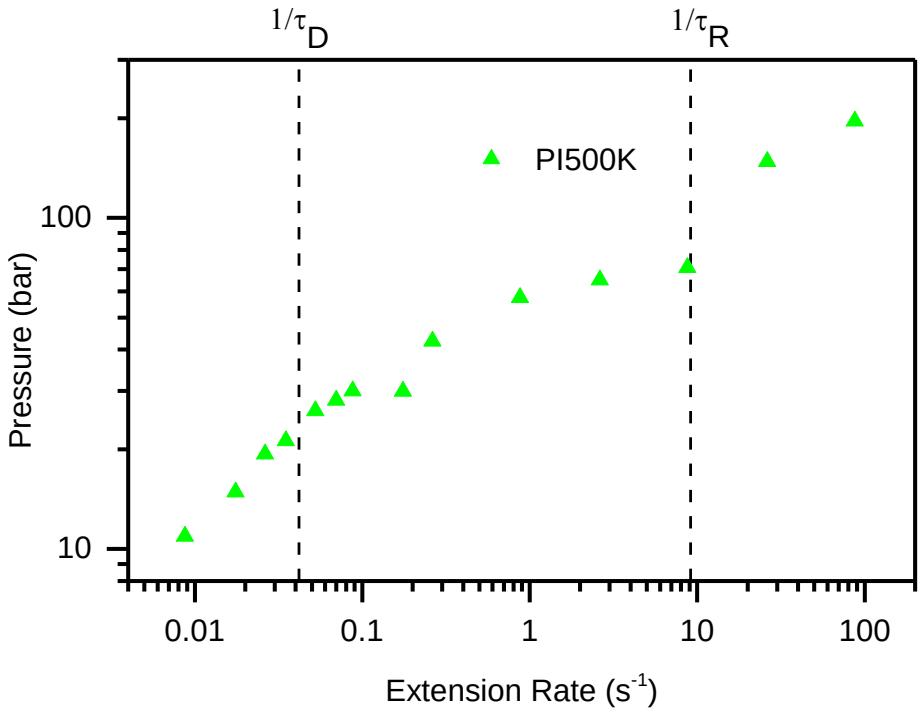

Figure 4.37: Pressure on the cross-slot during movement at different speeds and hence extension rates, for PI500K at 30 °C. The inverse Rouse and reptation times are labelled

discrepancy in temperature has been reported[27] in the MPR due to the cooling using an outer jacket, which could cause the difference.

The 1 mm deep cross-slot was seen to reduce the number of fringes significantly, which is likely due to the introduction of significant 3 dimensional effects, due to the effect of friction at the walls of the glass windows. However, the pressure measured for the 1 mm and 10 mm deep slits are similar. Since there was a similar pressure at the same extension rate, for the cross-slots of different depth, this suggests that there was a similar amount of stress generated. Since the number of fringes in the 1 mm deep cross-slot is much lower, this suggests that a different value for the SOC is needed for the shallow cross-slot, which is likely due to the assumption that flow is 2D along the depth of the geometry breaking down. Further experiments could run a variety of tests on a 1 mm deep narrow slit in order to determine the value of the SOC at this thickness, which could allow for higher extension rates to be reached in the MPR.

A significant result is the formation of “w-cusps” in these experiments which can be seen in the results for the 1 mm cross-slot in Figure 4.39. These have been observed previously in 10 mm deep cross-slots for materials with long chain branching, and were not captured in existing models.[184] Hence it is interesting that

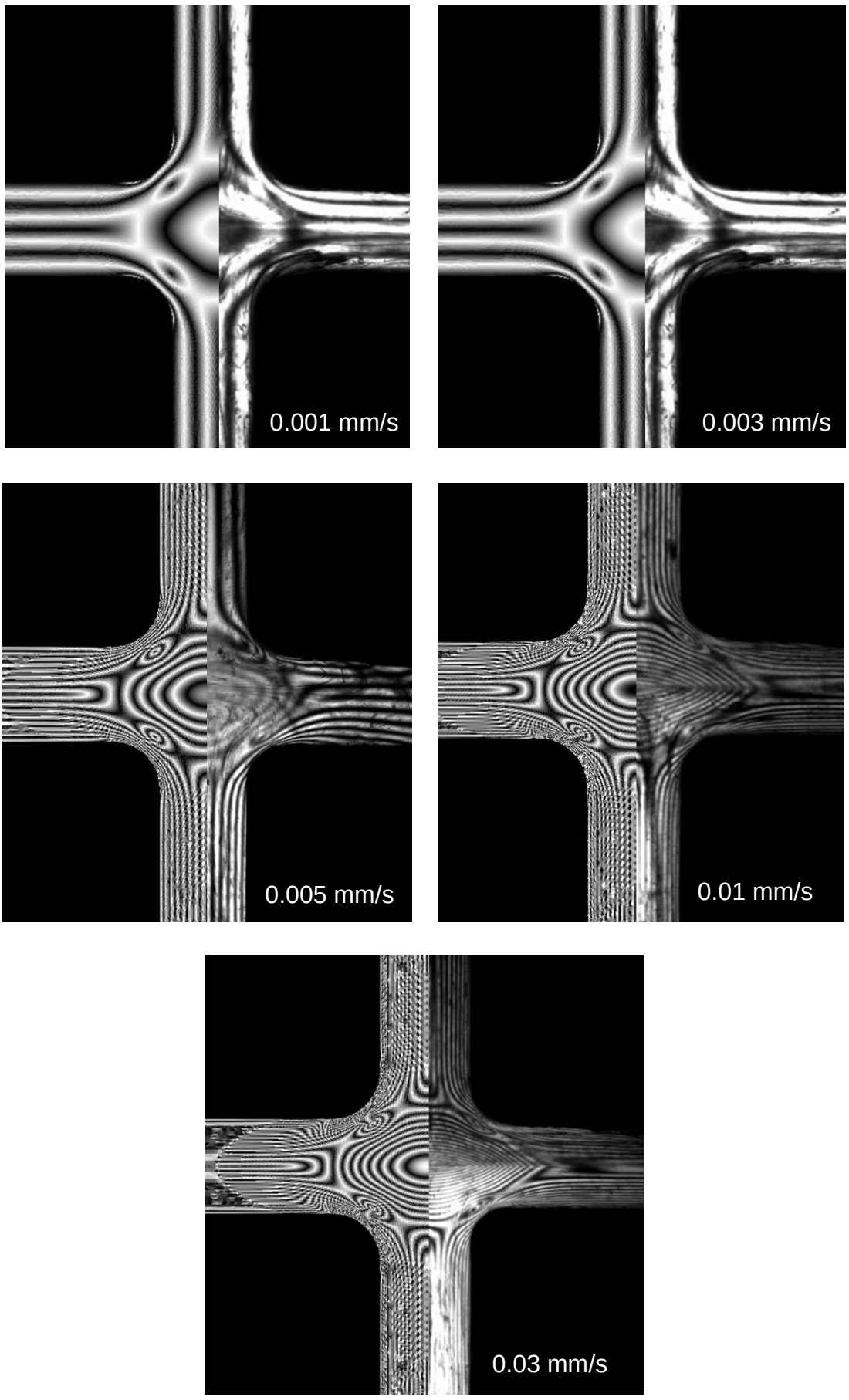

Figure 4.38: Flowsolve simulations (left) compared to experiment (right) for PI300K at 30 °C in the 10 mm deep cross-slot, at different piston speeds.

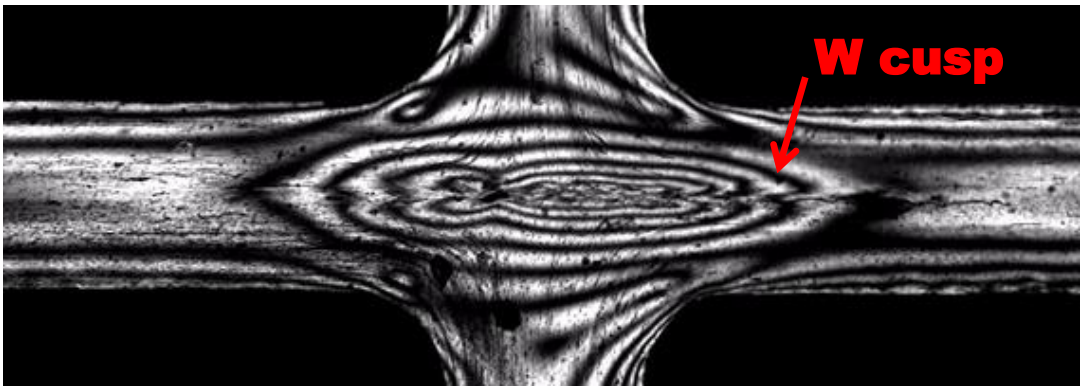

Figure 4.39: Stress birefringence image of PI300K at 30K in the 1 mm deep cross-slot at 0.008 mm/s and 30 °C

we observe this feature under flow of a linear material. The branched material is thought to increase the amount of 3D effects seen in the flow, which would explain the results here, as there will be significant 3D effects in such a shallow cross-slot. It is possible that this feature is a consequence of the 'instability' or slip of the top layer over the bottom seen at higher speeds, which would explain why it is not captured in the models. Although the cusps appear before it is obvious that there is any slip occurring, it could be a marker of the onset of this. In the results of Hassell *et al.*[184] there is no evidence of this instability for the linear or branched materials. However the images do have a similar shape to our images, with sharp points at the exit channels rather than round fringes (and the viscosity is much higher in our experiments and so the material would be expected to reach unstable regions at lower speeds).

It is not clear whether these cusps are also present in the results with the 10 mm deep cross-slot; they do not appear as significantly as in the 1 mm cross-slot but there possibly is a small 'ripple' in the fringes in the exit channel. However, if the stress relaxation is observed for speeds where there are too many fringes to count at steady state, the cusps can be seen during the decay (Figure 4.40). Since they are a 3D effect (e.g. they could be a consequence of drag at the windows rather than flow in the centre of the cross-slot), they would be expected to occur much less for a deeper cross-slot, but it is possible that the fast flow of this highly viscous material causes instabilities and 3D effects to become more prominent.

4.6.3.2 Flowsolve simulations

The Flowsolve simulations capture the behaviour in the cross-slot very well, and show the distribution of stress well. Although the number of fringes predicted is close to the number observed throughout the results, the simulations do appear to

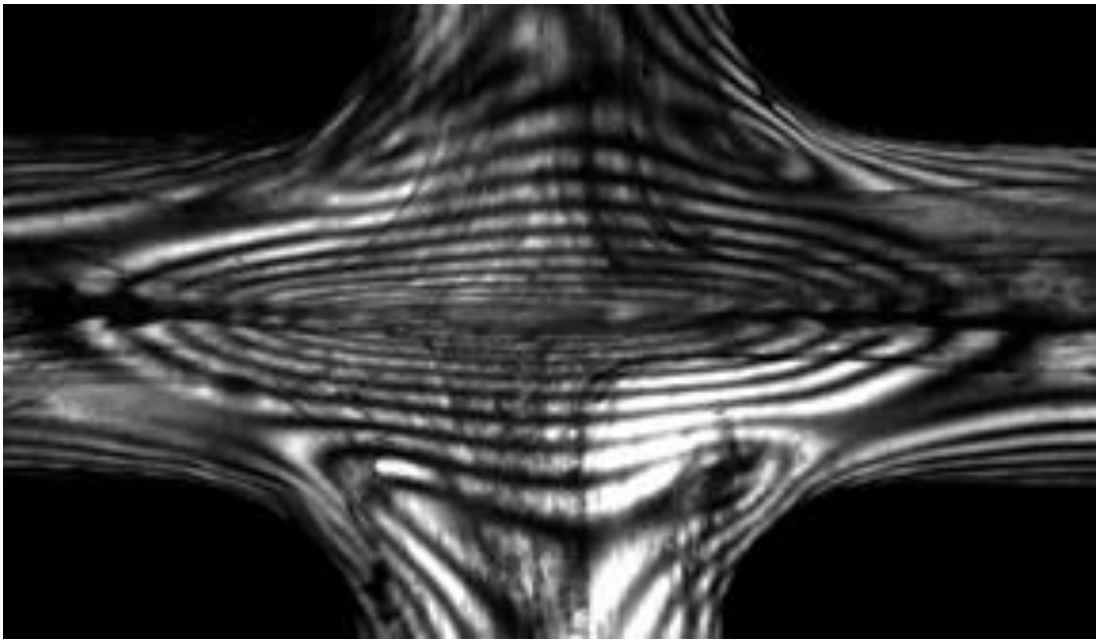

Figure 4.40: Stress birefringence image of PI300K at 30K in the 10 mm deep cross-slot at 30 °C, 10 s after a deformation at 0.05 mm/s has ended.

slightly systematically underpredict the amount of stress (and so number of fringes) There are several reasons that could have caused this, such as some degradation of the material in the MPR. However, checking the shear rheology after the tests did not reveal any significant change, so if this had an effect, it was subtle. Another option is the temperature control; the temperatures were averaged over the top bottom and middle sensors and a small difference could have caused a difference in stress. Flowsolve assumes the system is isothermal but it is possible that the polymer would be slightly cooler than the sensors located in the wall and pushed into the material, as the temperature was controlled by an outside jacket which may lead to a lower temperature in the middle of the capillary. This was suggested by Mackley *et al.*[27] although they used much higher temperatures. The difference in our case is likely to be small, but since the polymer is extremely rubbery a difference of a couple of degrees could have caused the additional stress.

There is also a difference in the highest two speeds, where the results from the simulations show rounded fringes, but the experiment shows fringes pointed towards the exit. This could be due to the Flowsolve simulations not having enough time to develop fully, although the pattern was constant for ~5 s in each case which suggests they were fully developed. Alternatively, this could be due to a flow instability not captured by the simulations. At higher speeds, an instability develops at the stagnation point, and this could be the onset of this ‘slip’ along the central exit line.

4.6.4 Conclusions

Monodisperse polyisoprene has been studied under steady state extension using the multi-pass rheometer, for the first time. Other methods of studying extension (e.g. SER) struggle to reach steady state for these materials and so this is a unique opportunity to study this behaviour. Flowsolve was used to model the results and gave good predictions using the rolie-poly model fit to the shear rheology and SER data. As the shear rate was increased, an instability developed which was not predicted by the model, which could suggest the need to improve the theory used e.g. to better capture slip at the walls. Unfortunately, at high shear rates, the number of fringes becomes too high to count and so extensional viscosity cannot be quantified. One way of reducing the number of fringes is by using a cross-slot with smaller depth, which was also demonstrated with a 1 mm geometry, however this also means that the value of the stress optic coefficient is no longer applicable to these measurements. Future work could involve studying the SOC at different depths of geometry, which may allow better determination of extensional stress at high extension rates. W-cusps were observed in the 1 mm geometry which was attributed to 3D components of the flow.

4.7 Degradation and processability study

A common issue in processing and use of polymeric materials is the ability to recycle materials. Particularly with tyre rubbers, relatively little recycled material can be used in production due to the degradation that occurs in reprocessing. The MPR provides a unique option for studying the degradation of materials and hence their recyclability, as stress in the material can be observed over time, while high temperatures, pressures and deformation (extension and shear) rates can be applied. In this section, a polybutadiene rubber is used to demonstrate this ability and study the effect of processing and subsequent properties.

4.7.1 Experimental

Approximately 10 g of PBD310K (as characterised by shear rheology and GPC in Chapter 2) was loaded into the MPR fitted with a narrow slit geometry, 1 mm wide, 5 mm long and 10 mm in depth. The MPR was operated in multi-pass mode, i.e. moving the pistons at constant speed for a given amplitude and then reversing the direction. The experiments were performed at 80 °C, with 1 bar of initial pressure, an amplitude of 25 mm and a piston speed of 0.05 mm/s. Using the crossover from linear rheology as the reptation time (0.672 s) and the Rouse time from the REPTATE materials database (0.00125 s), the corresponding reptation Weissenberg number was 1.6 and Rouse Weissenberg number was 0.003. The Rabinowitsch correction was not applied but is not expected to change the regime of the measurements. The number of fringes was observed over time using a camera at 1 fps. The motion was performed for 5 hours, and stopped each hour to take a sample for GPC analysis.

GPC was performed on a Viscotek TDA 302 with triple detection (Light scattering, viscosity and refractive index) with tetrahydrofuran as solvent at 35 °C and a flow rate of 1 ml/min.

4.7.2 Results: Following degradation over time using stress and molecular weight

The number of fringes are shown to decrease over the experiment (Figure 4.41), indicating a reduction in stress and viscosity of the material. This indicates there is a reduction in long chains in the polymer due to thermal and shear degradation. However this takes places in the first hour, and after this point, the number of fringes remains constant.

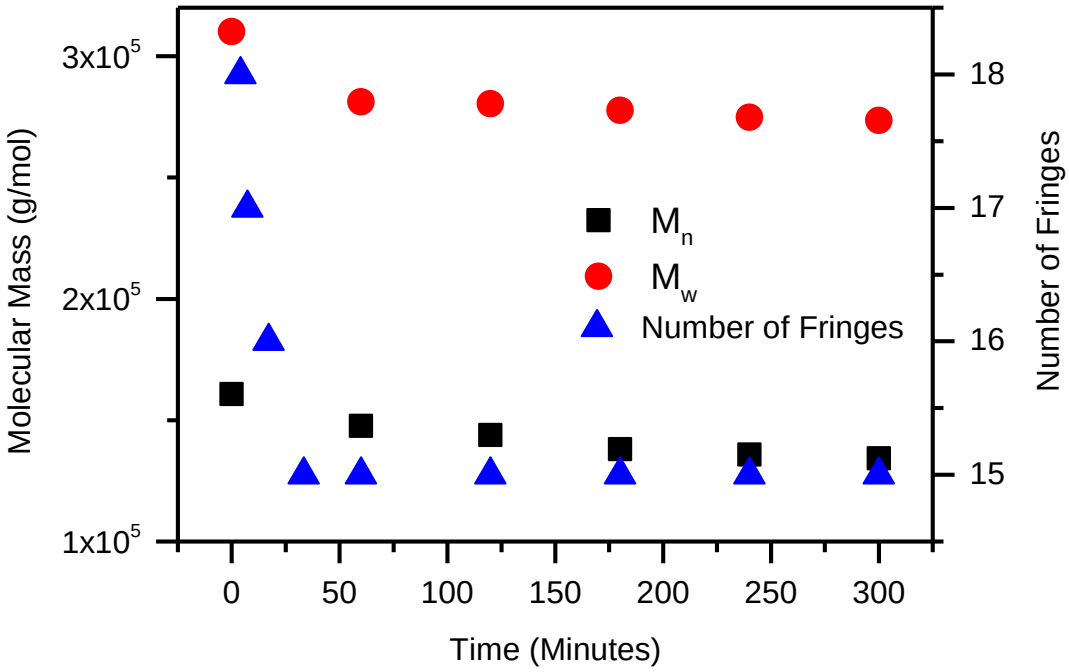

Figure 4.41: Molecular mass and fringe count of PBD310K over time undergoing a shear at 0.05 mm/s at a temperature of 80 °C.

The GPC shows a similar effect, the molecular weight of the material drops in the first hour of measurement, but after this point, the values are relatively flat. The shape of the GPC shows a shift towards lower molecular weights, as shown in Figure 4.42.

4.7.3 Discussion: Following degradation over time using stress and molecular weight

The conditions selected are representative of rubber processing conditions; the temperature is a compromise between not causing too much degradation and allowing the polymer to be processed without generating too high a pressure. The speed selected corresponds to a reptation Weissenberg number over 1 and Rouse Weissenberg number much less than one. This is typical as a very fast speed would be required to reach the Rouse stretching regime, above that reachable in processing conditions. Also due to the high viscosity of the material, such high speeds would likely block most commercial apparatus.

Hence the experiment is a good representation of the conditions that might be experienced if this rubber were to be processed and reused. The results suggest that some degradation would occur in this process, but this would occur quickly in the first 30 minutes of processing. The consequences of this are that the material would lose some of its original properties, as large chains would be broken and its

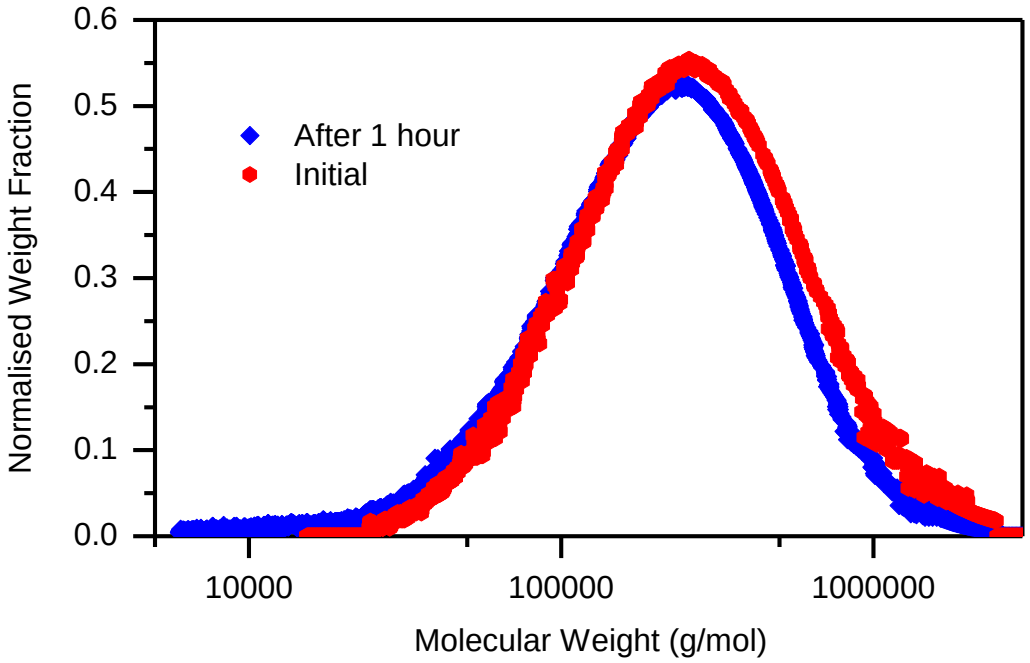

Figure 4.42: Gel permeation chromatography results of PBD310K before and after 1 hour of shear at 0.05 mm/s and 80 °C

viscosity would drop. This could be limited by processing in very short times, under 30 minutes. However if this was not possible, and the total processing time exceeds 30 minutes, it appears that the resulting properties would not be dependent on any further time under shear at high temperatures. This indicates that although the material loses some of the long chains under processing, the majority of chains are unaffected and could be reprocessed repeatedly. In terms of the material, to achieve a product similar to the original after this processing, a little high molecular weight material could be added, and it is a common practice when recycling rubbers and other polymers to only use a certain percentage of recycled material in products in order to keep the properties of the product the same.

4.7.4 Conclusions

It has been demonstrated that degradation and processability can be studied effectively in the MPR using GPC and observation of stress fringes. To better study the process of degradation for this material, taking samples at shorter times may be necessary to observe the change in molecular weight better over time. However, the results give a good indication of the stability of the material under shear rate and high temperature, and can be used to compare formulations (e.g. the effect of antioxidants). Further studies (e.g. at different temperatures and speeds) could be planned to examine how much shear or temperature each contribute to the degradation.

4.8 Concluding remarks

The multi-pass rheometer has been shown to be a versatile tool for generating complex flow. Complex flow is useful because it more directly emulates the conditions encountered in industrial processing, and allows predictions to be made about how the polymer behaves in such situations. Through well-defined geometries, it has been shown that shear and extension rates can be quantified which allow the measurement of steady shear and extensional viscosities, under the influence of different temperatures and pressures, and for materials that this otherwise may not be possible. The optical capability of the MPR4 allows the visualising of the stress in the material which is useful for separating shear and extensional components. This is key to understanding the material properties as the two components can have very different molecular origins. In addition to steady state measurements, stress decays can also be observed and it has been demonstrated that polymer relaxation times, characteristic of the underlying material, can be extracted from these measurements.

5 Large amplitude oscillatory shear rheology

SAOS has been shown to be very useful in quantifying rheological behaviour, structure and relaxation times of polymers in Chapter 2. In SAOS tests, high strains are avoided because they can introduces higher harmonics which complicate the stress signal and make it more difficult to interpret. However, with careful measurement and analysis, these harmonics can provide additional information about the material being examined. This chapter details measurements made in the large and medium oscillatory shear regime, beginning with the production and testing of code to perform Fourier transforms on raw data output by the rheometer (Section 5.1). This ensures a good understanding of the analysis performed is built up and allows the analysis to be precisely controlled to ensure accuracy.

The software is then used to analyse results of amplitude sweeps on a range of polymers with different structures (Section 5.2). In particular the high Deborah number measurements have not been previously reported for similar materials. There is also debate in the literature on the effect of measurement conditions on these measurements and the study of structures and conditions reported here is comprehensive enough to allow these effects to be quantified.

Section 5.3 details frequency sweeps in the medium amplitude oscillatory shear regime. This intermediary regime allows well-controlled experiments to be performed while studying the third harmonic. The results here are the first to report both phase and magnitude for rubbery polymers in the MAOS regime.

Finally, the applicability of the multi-pass rheometer for LAOS measurements is examined. The sealed geometry allows the elimination of troublesome effects seen in rotational rheometry (e.g. edge fracture and sample escaping the gap). The results reported show promise for advanced LAOS measurements to be performed in the MPR, with some minor modifications to the apparatus.

5.1 Development of code to perform Fourier transform analysis

5.1.1 Introduction

LAOS measurements can be analysed in a number of ways, as discussed in the Chapter 1. The method that appears to yield most structural information about the polymer is performing a Fourier transform on the signal and analysing the I_3/I_1 ratio, the gradient of which with strain is reported to vary with polymer structure.[95-96] In order to do this, there is existing software available, most notably MITLAOS, developed by Randy Ewoldt and Gareth Mckinley.[104] While existing software performs well, and provides a multitude of data for each point, the decision was taken to write a new piece of code which can perform the same transformation on multiple points, allowing a full amplitude sweep to be analysed at once. Since the Fourier analysis is all that is required in our case, this simplifies the process of extracting harmonics from LAOS data significantly. It is also beneficial to have in-house code as it is easier to make adjustments when required and ensures a thorough understanding of the analysis being performed.

5.1.2 Experimental

Several iterations of code were produced based around the fast Fourier transform functionality in MATLAB. This allows the phase and intensity of the harmonics to be extracted quickly from a large set of data points.

In order to confirm that the final version of the code produced was reliable, two types of test were performed. Firstly, an artificial stress wave was created by combining sine waves at set frequencies, using the equation:

$$\sigma = \gamma\,(\,\mathrm{I}_1\sin(\omega t + \phi_1) + \,\mathrm{I}_3\sin(3\omega t + \phi_3) + \,\mathrm{I}_5\sin(5\omega t + \phi_5) + \,\mathrm{I}_7\sin(7\omega t + \phi_7)) \quad (5.1)$$

where I_x and ϕ_x are the intensity and phase of the xth harmonic respectively, σ is the stress, γ the strain, ω the frequency and t the time. This wave was passed through the code and the results compared to values input.

Example waves at a frequency of 1 Hz and 5 % strain were generated where the phases of the harmonics were constant ($\phi_1 = 1,\ \phi_3 = 3,\ \phi_5 = 5, \phi_7 = 0.72\ \mathrm{rads}$), and the intensities of all harmonics except the first was kept at 0.1. The first harmonic was varied from 10^2 to 10^{10} to examine the effect on the higher harmonics.

Secondly data from a model produced by David Hoyle at Durham using rolie-poly theory was analysed. The code for this model was adapted to output both the

harmonics and the original stress wave. Our code could then be tested by passing the wave through and confirming the results matched the code output.

The rolie-poly code was run with 6 Maxwell modes as input fit to the linear rheology of PI100K at 25 °C. The Rouse time of the first mode was found by fitting the extensional rheology and input as well. The code was run at 30 frequencies between 0.1 and 100 rad/s each at a strain amplitude of 10 %.

5.1.3 Results

5.1.3.1 Development of code for performing Fourier transform measurements

A full annotated version of the code in MATLAB is included in the supplementary information and is available online.[185] Figure 5.1 shows a pseudocode version in order to illustrate the main principles.

	PsuedoCode	**Comments**
1	READ Strain File	Strain file will have the columns Strain, Frequency, Temperature
2	CyclesToDelete = ASK user how many cycles to delete from the start of file	Removes initial cycles to remove start-up effects
3	FOR EACH file in the directory of Stress files	Repeats for all the stress waves input
4	READ Stress File	Stress file will have the columns Time, Stress Strain
5	TimeStep = MEAN DIFFERENCE between values in time column	Measures the average time step
6	PointsPerCycle=1/(Frequency*Time Step)	Uses average time step and frequency to extract calculate the number of points in a cycle
7	PointsToDelete=ROUND(CyclesToDelete*PointsPerCycle)	Calculates number of points to delete from number of cycles requested and rounds to whole number
8	DELETE 1:PointsToDelete from each column in Stress File	Deletes request number of cycles
9	DELETE REMAINDER of SIZE(Stress File)/PointsPerCycle from each column in Stress File	Trims each column to an exact number of cycles
10	FrequencyStep=1/TimeStep	Calculates frequency step, inverse of time step

11	HalfSize = SIZE(Stress File)/2	Gets half the size of the stress file
12	FrequencyValues = FrequencyStep * (0:1/HalfSize:1-1/HalfSize)/2	Creates frequency steps from 0 to FrequencyStep*(1-1/HalfSize)/2 in increments of (FrequencyStep/Halfsize)/2 The frequency bins are the frequency step/size, but we are only using the first half because the input signal is real and so the output will be symmetrical, with the second half containing a repeat of the first
13	TransformedStress = FFT(Stress/HalfSize)	Performs FFT on stress
14	Magnitudes = MAGNITUDE(TransformedStress(1:HalfSize))	Gets magnitudes of data and discards second half
15	Phase = ANGLE(TransformedStress(1:HalfSize))	Gets phases of data and discards second half
16	Index1 = LOOKUP(Frequency, FrequencyValues)	Find the index of the first harmonic by looking up the oscillation frequency in the list of frequencies generated
17	Index3 = LOOKUP(3*Frequency, FrequencyValues)	Find the index of the third harmonic by looking up three times the oscillation frequency in the list of frequencies generated
18	TransformedStrain = FFT(Strain/HalfSize)	Performs FFT on strain
19	StrainPhase = ANGLE(TransformedStrain(1:HalfSize))	Gets phases of strain and discards second half
20	FirstHarmonicMagnitude = LOOKUP(Index1,Magnitude)	Finds Index1 in the extracted list of magnitudes
21	FirstHarmonicPhase = LOOKUP(Index1,Phase) - LOOKUP(Index1,StrainPhase)	Finds Index1 in the extracted list of phases and corrects for the initial phase of the strain
22	ThirdHarmonicMagnitude = LOOKUP(Index3,Magnitude)	Finds Index3 in the extracted list of magnitudes
23	ThirdHarmonicPhase = LOOKUP(Index3,Phase)- 3*LOOKUP(Index1,StrainPhase)	Finds Index3 in the extracted list of phases and corrects for the initial phase of the strain

24	Ge = FirstHarmonicMagnitude*cos(FirstHarmonicPhase)/(Strain);	Calculates G' from the magnitude and phase of the first harmonic
25	Gv = FirstHarmonicMagnitude*sin(FirstHarmonicPhase)/(Strain);	Calculates G'' from the magnitude and phase of the first harmonic
26	G3e = ThirdHarmonicMagnitude*cos(ThirdHarmonicPhase)/(Strain);	Calculates $G3'$ from the magnitude and phase of the third harmonic
27	G3v = ThirdHarmonicMagnitude*sin(ThirdHarmonicPhase)/(Strain);	Calculates $G3''$ from the magnitude and phase of the third harmonic
28	ADD FirstHarmonicMagnitude, FirstHarmonicPhase, ThirdHarmonicMagnitude, ThirdHarmonicPhase, Ge, Gv, G3e, G3v to Output File	Outputs calculated values
29	END FOR	Returns to repeat for next point

Figure 5.1: Psuedocode of the CDRheo Fourier Transform code for LAOS data, Pseudocommands are in red, variables in blue, comments in green

5.1.3.2 Comparison of code results to a set frequency input and to rolie-poly code

The output phases and magnitudes from the artificial waves were identical to the values input. Figure 5.2 shows the magnitude output for three different intensities of the first harmonic. In each case the magnitudes are as input and not affected by noise despite the large difference between the first and higher harmonics.

Rolie-poly and MATLAB code outputs are compared in Figure 5.3. The rolie-poly output also matches the output from the MATLAB code very well. For the linear polyisoprene shown in Figure 5.3, the match is excellent for both the parameters derived from the first (G' and G'') and third harmonics ($G3'$ and $G3''$). However the final points at the highest frequencies do deviate from the rolie-poly simulation.

5.1.4 Discussion

5.1.4.1 Development of code for performing Fourier transform measurements

The fast Fourier transform (FFT) in MATLAB converts the stress data against time into a frequency spectrum (e.g. Figure 5.2), where each point is separated by the inverse acquisition time. Some FFT code uses a ‘butterfly’ algorithm where the total number of points must be a power of two, and if this is not the case “padding”

(adding additional zero points) is used to achieve this. This can cause errors since, as shown in Equation 5.2, changing the number of points will change the frequency separation of the results and in turn make the number of cycles non-integer. This means that the oscillation frequency and the frequency of higher harmonics may no longer lie on an exact frequency bin.

$$Frequency\ separation = \frac{1}{acquisition\ time} = \frac{frequency}{number\ of\ cycles} = \frac{1}{number\ of\ points * cycle\ time} \tag{5.2}$$

The use of a butterfly algorithm can cause large errors in the resulting magnitudes and phases. However, when the number of points is not a power of two, the FFT code in MATLAB does not make use of a butterfly algorithm, and so this error is avoided.[186] It is for such reasons that it was important to write this code, as this type of error can be fully understood and avoided.

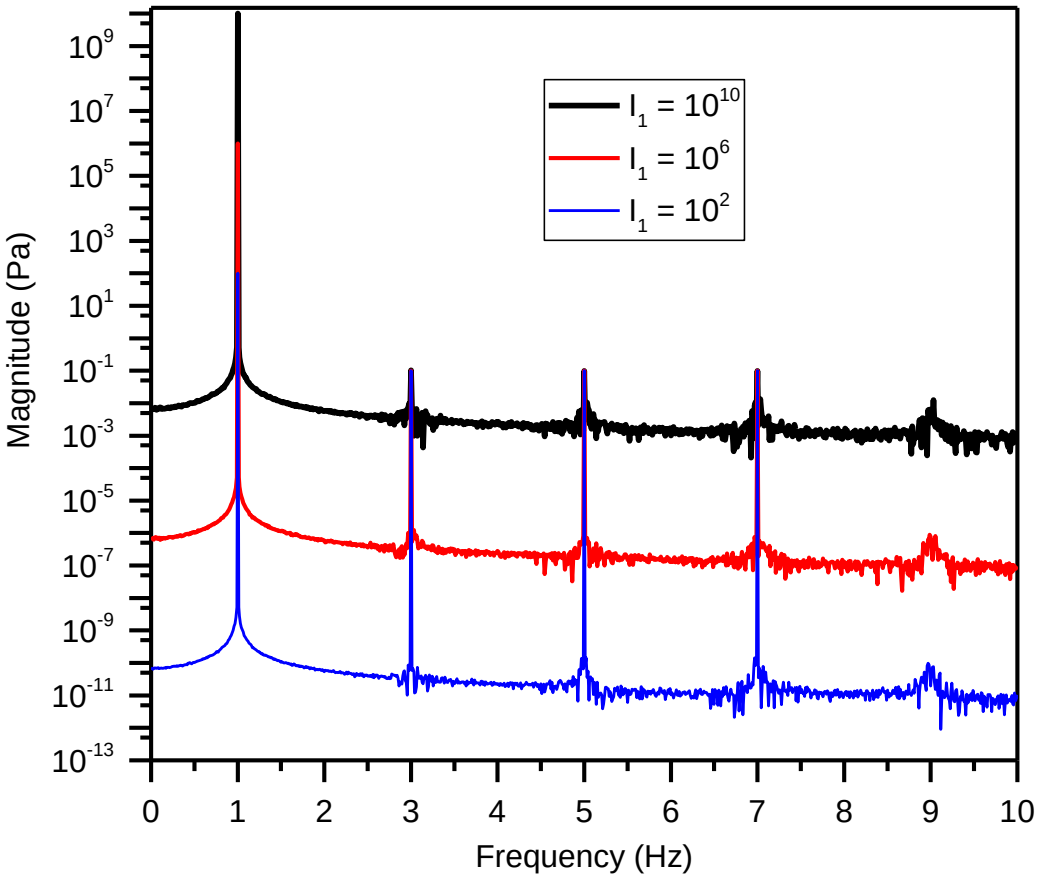

Figure 5.2: Magnitudes output by the Fourier transform for three artificial waves where the higher harmonics are kept constant at 0.1 but the first harmonic is increased from 10^2 to 10^{10}.

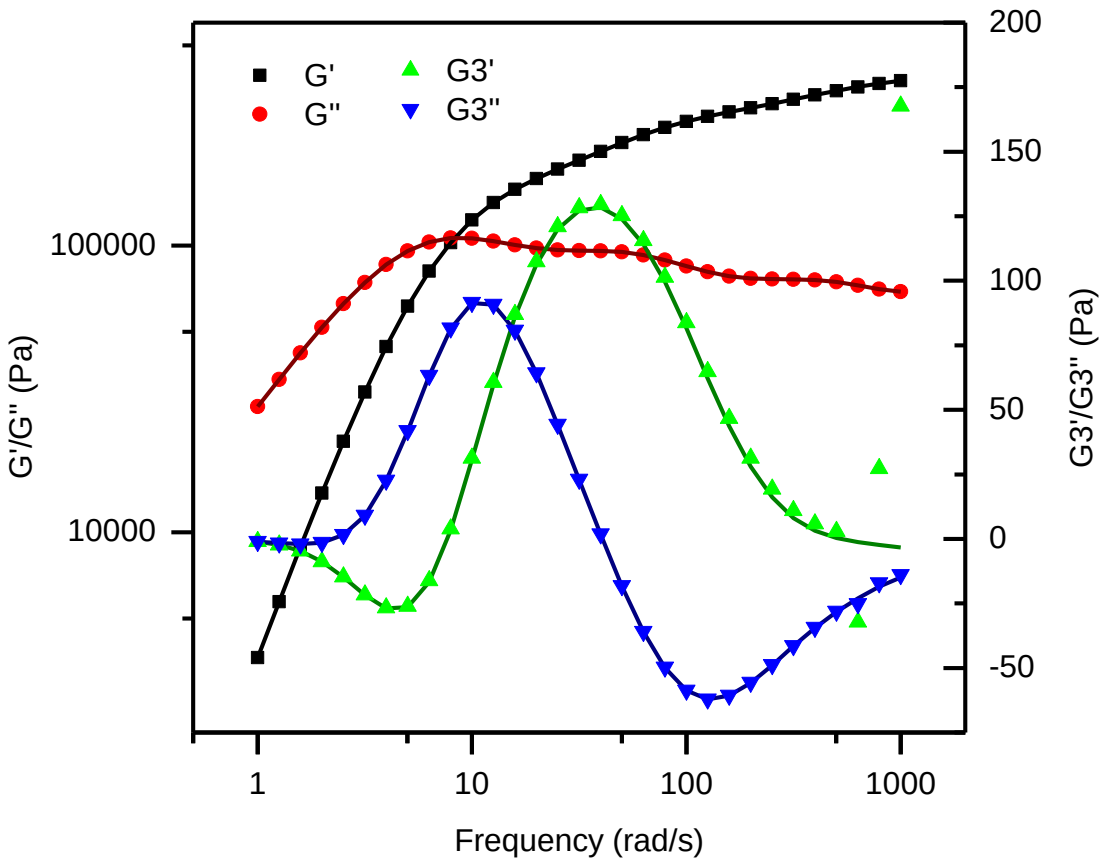

Figure 5.3: Rolie-poly prediction of PI100K (fit to experiment linear rheology and extension as given in Chapter 2 and 3). Lines show the rolie-poly prediction while points show the stress output after being passed through the Fourier transform code.

Since the built in Fourier transform in MATLAB is suitable for our application, implementation is relatively straightforward. The main difficulties arise in extracting the correct values of the phases and magnitude. To do this the correct frequency values must be calculated to go alongside the phase and magnitude data output by the FFT. The frequency step can be calculated by taking the inverse of the time step between collected data points and dividing by the size of the matrix. However, because a real input signal is being used, the FFT output will be symmetrical and the second half will be the same as the first (and can be discarded). This means that the size used will actually be half the size of the input matrix and the frequency values will span the same range but in half the number of points.

If the frequencies are determined correctly, the magnitude and phases can be read off at frequencies corresponding to the applied frequency and multiples of this to get the values of different harmonics. As the frequency of each harmonic does not always lie exactly on a frequency bin, a step was included to check the frequency closest to the required value. Alternatively, the magnitudes can be checked at

values above and below the selected frequency to ensure the peak has been found. This was done for the MPR LAOS tests where the data transfer rate is lower and hence the frequency step is larger. There is also more uncertainty in the frequency values.

The other main task required is trimming the data, which provides an exact number of cycles, as well as removing some initial cycles when start-up effects complicate the results. In the published version of the software, the user is asked how many cycles to delete from the start of the file, but this is fixed at five cycles for the majority of measurements used since this covers the range in which start-up effects are observed in all observed cases. Five cycles were added on to the desired number of cycles in order to allow this in all measurements.

To realise this practically, four cycles worth of data points are deleted initially. 5 % of a cycle is also deleted from the end, as occasionally there are several data points taken as the measurement stops, which can influence the result. Then a further number of points are deleted from the start of the data to make the total points a multiple of the number points in a cycle. The overall result is five cycles are removed, start up and end effects are taken out of the data and the data remaining corresponds to an exact whole number of cycles.

5.1.4.2 Comparison of code results to a set frequency input and to rolie-poly code

The code accepts as input a file of the frequency and amplitudes used for each point, as well as a set of input files (in the same order) each containing the time, stress and strain for that point. It outputs magnitudes and phases at exactly the values input for the artificial wave. This shows that the processing has not introduced any significant noise to the signal. Figure 5.2 compares three situations where the first harmonic varies but the higher harmonics are kept the same, the noise introduced by the first harmonic is 10^{-12} times its magnitude, so if higher harmonics drop below this value they will not be detected. This is likely an effect of the fast Fourier transform implemented. When the magnitude of the first harmonic is increased to 10^{10} (several orders of magnitude than those encountered for even the highest viscosity samples to be analysed), noise is seen on the order of 10^{-2} around the odd harmonics, even those harmonics not included in the original signal (i.e. the 9^{th} harmonic). This is an extreme case and even here, the measurement of the third and higher harmonics would not be hampered if they are greater than 0.1 Pa.

However, practically the noise generated from the experiment (i.e. precision of the rheometer, external vibrations) will be significantly larger than this noise introduced

by the processing (the minimum measurable value on the rheometer is around 10^{-4} to 10^{-3} Pa, dependant on the torque generated). Hence we can be confident that the processing executed by the code does not affecting the measurement of the harmonics, and is generates the correct phases and magnitudes of the signal input.

Figure 5.3 shows data generated from rolie-poly code. In this case linear rheology was fit to Maxwell modes and used as input for the software as well as fitting the stretching modes to extensional rheology, here PI100K was used, with the parameters given in Chapter 2 and 3 from fitting the Linear and extensional rheology. This model is discussed in greater detail and compared to experimental data in Section 5.3.5. The model calculates G', G'', $G3'$ and $G3''$ directly, but was adapted to also generate a stress wave for the modelled system that could be passed through our Fourier transform code. The values generated by the rolie-poly code and those produced from analysing the stress wave using our code are both shown in Figure 5.3. The results of the FT code are mostly exactly as predicted by the rolie-poly model, however deviation is shown at the highest frequencies in $G3''$. This is caused by the rectangular windowing implanted in the FFT, which is equivalent to assuming the data outside of the points sampled is zero. This results in the wavefunction effectively switching off outside the sample window and causes some spectral leakage, i.e. the signals are spread over a greater range of frequencies than in the original signal. This effect does not affect the peak value, so the magnitude of each harmonic is not changed; however it can cause problems if the leakage from a large signal (in our case the first harmonic) obscures the smaller ones. This is the same effect we are testing for in Figure 5.2. For the system shown (linear polyisoprene), the third harmonic is predicted to go to zero at high frequencies, while the first continues to increase. Hence, the third harmonic becomes very small compared with the first. It is therefore lost in the leakage of the first harmonic, which causes the fluctuations at high frequency. Leakage however should not affect our measurements as significantly more cycles are used (just 10 cycles are output by the rolie-poly code), and having a large window reduces the influence of the window beginning and end. Also the issue is very easy to spot in the FFT output (there is no peak above the noise for the third harmonic) so it can be easily identified in our results.

It can be concluded that the code produced in MATLAB provides a valid way of measuring the phase and magnitudes of harmonics in a stress signal, which is important going forward and applying the code to polymers and their blends.

5.1.5 Conclusions

Code has been written in MATLAB using the fast Fourier transform functionality, to analyse rheological data and extract magnitude and phases of higher harmonics, particularly relevant to LAOS data. This has been tested thoroughly and shown to produce reliable results and be suitable for application to experimental data.

5.2 Amplitude sweeps

Once the code had been optimised, a variety of LAOS testing could be performed. The most commonly encountered is an amplitude sweep, which begins in the SAOS region and increases the strain until non-linear behaviour is encountered. The ratio of the third and first harmonic and its strain dependence has previously been shown to give an indication of polymer structure and the level of branching in a polymeric material.[95-96] Hence this is a possible way to explore the underlying structure of polymers.

There are several parameters that must be optimised and effects that must be taken into account before performing these measurements, the first of which is the time dependence of the measurements. More cycles improve the signal to noise ratio of the data but longer this leads to longer measurement times which can affect the measurement. In the SAOS region, the results should be time-independent, however for LAOS measurements this is not necessarily the case. Hence, the effect of the number of cycles on the results must be examined, as when examining non-linear flow, the results may be dependent on the measurement time.

The effect of different geometries must also be explored, because it is likely that at very high strains, the results will contain effects of sample fracture, slip and escaping the gap. All these will be highly dependent on the geometry, and so testing different geometries allow us to examine how much the results are dependent on these effects and choose the best geometry for these measurements.

The limitation of amplitude sweeps is that they must be performed at a set frequency, and as can be seen in Chapter 2, there is a large dependence of rheological behaviour on frequency. This means the choice of frequency is important when comparing LAOS results. One way to normalise the effect of frequency between different polymers is to use the Deborah number, and results at constant Deborah number can be better compared for different polymers. The effect of frequency (and so Deborah number) must also be explored in order to select the best Deborah number to perform the sweeps at.

Once the effect of the measurement conditions and data processing was quantified and optimised, it was possible to compare the results and examine the effect of changing polymer structure. Filled polymers were also examined, as amplitude sweeps are a common way of examining these materials to examine behaviour such as the Payne effect, an effect which is well documented[187-189] but poorly understood

in terms of polymer structure. Hence additional insights may be gained by observing the behaviour of the third harmonic during this process.

5.2.1 Experimental

Materials were polybutadienes and polyisoprenes, as characterised in SAOS in Chapter 2, provided by Matthew Oti at Durham University. Polymer blends were produced by co-dissolving polymers in toluene followed by precipitation in methanol, and the removal of remaining filler in a vacuum oven. Filled polymers were produced by James Hart at Durham University, by swelling the polymers with toluene and mixing with the filler particles, sonicated in a minimal amount of toluene, after which the solvent was removed in a vacuum oven at room temperature, with periodic mixing. Silica used was Nanostructured and Amorphous Materials silicon oxide nanopowder, 80nm (stock number 4830HT, batch number 4830-012711). Carbon black was Sigma Aldrich mesoporous carbon nanopowder, particle size <500 nm (ALDRICH 699632, Lot MKBV0856V).

Amplitude sweeps were performed on a TA instruments HR2 rheometer equipped with one of the following geometries, as specified: 25 mm parallel plate, 8 mm parallel plate, 25 mm 4 degree cone or a 25 mm crosshatched plate. The temperature was controlled via the use of a Peltier plate for temperatures around/below room temperature. For the crosshatched geometry the Peltier was fitted with a crosshatched lower plate, otherwise the sample was applied directly to the flat Peltier surface. For higher temperatures, the environmental test chamber was closed around the sample and nitrogen flowed over the sample to minimise degradation.

Where not otherwise specified, amplitude sweeps were performed for 35 cycles per point, with the initial 5 cycles discarded to remove start-up effects. Initially, a range of 1-1000 % strain was used with 40 points per decade. However a smaller range of points is reported for the majority of materials, as points in which the data became irregular were discarded. This was clear from the decrease in G' and G'' becoming irregular, and the higher harmonics increasing rapidly. In particular the second harmonic was observed because it is not expected to be significant and is a good indicator of the presence of slip and fracture. Transient data (stress and strain over time) was output from the rheometer and passed through the CDRheo code (as described in Section 5.1) which outputs the magnitude and phases of the constituent harmonics.

The parallel plate (and crosshatched plate) I_3/I_1 results are shifted by 1.5 to account for differences in shear rate across the geometry, as reported by Song *et al*.[190]

5.2.2 Results

5.2.2.1 Time dependence of measurements

Figure 5.4 shows the results for an amplitude sweep of linear polyisoprene using 10 cycles for measurement at each amplitude point but a different amount of initial throwaway cycles before the measurement at each point. It appears that 2 initial cycles are not enough to eliminate start-up effects, as this data is noisier and differs from the results at 10 and 20 cycles. For 30 cycles, the results begin to deviate, particularly at the highest strains, and for 100 initial cycles, a clear difference can be seen, demonstrating the time dependence of the measurement.

5.2.2.2 Effect of different geometries on non-linear response

Figure 5.5 shows a comparison of results measurement with different geometries for a linear PBD and Figure 5.6 shows a similar comparison for a randomly branched PBD. The key difference between them is not just their structures, but that the randomly branched material has a much lower viscosity and is a sticky melt, whereas the linear material has a much higher viscosity and hence is rubbery.

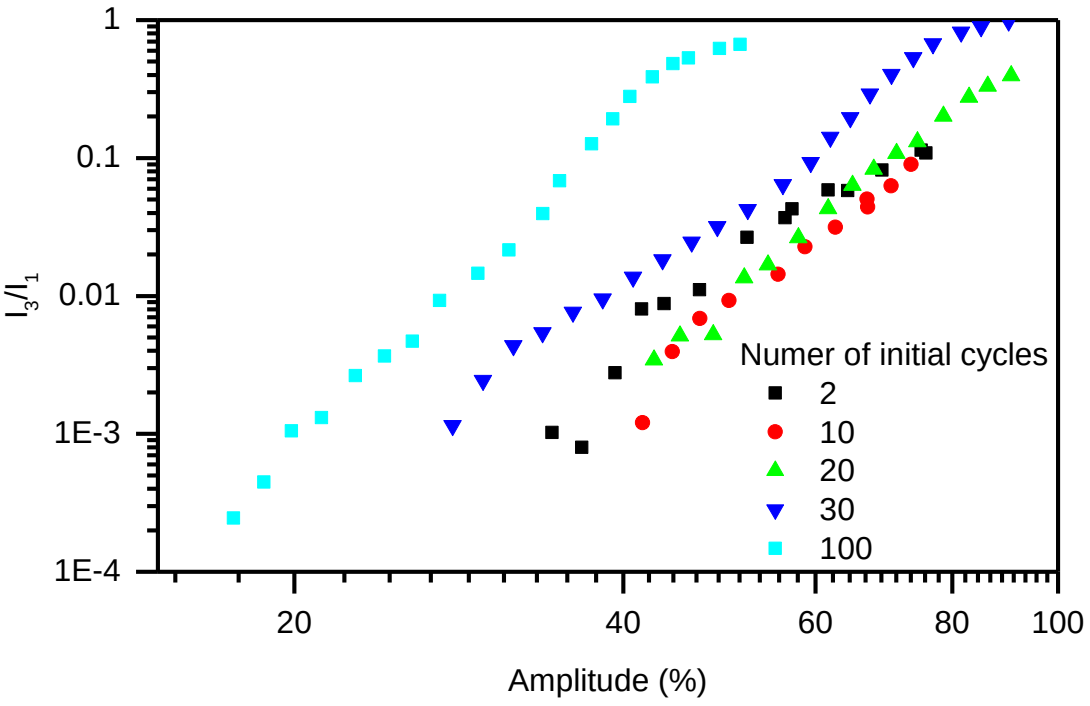

Figure 5.4: Amplitude sweeps of PI150K using a 25 mm parallel plate at 25 °C and 1 Hz. 10 cycles were used for the measurement and the number of initial cycles before taking the measurement increased from 2 to 100.

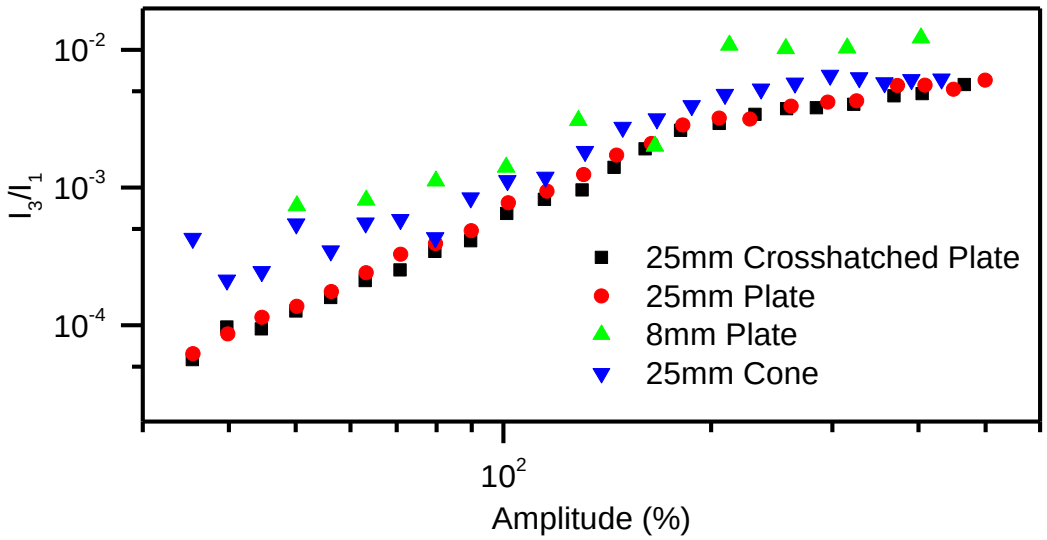

Figure 5.5: Amplitude sweeps of RB480K at 25 °C and 1 Hz using different geometries.

Hence these represent well the range of viscosities that will be examined using LAOS, and this is likely to be a determining factor for slip and fracture.

The randomly branched material shows a good match between the different geometries. The results from all but the 8 mm plate overlap and the parallel plate correction has worked well. However there is a shift and more noise seen in the 8 mm data.

For the linear material the results deviate more. The 25 mm plate and cone could not reach the high strains due to reaching the torque limit of the transducer (200 mN.m). The 8 mm plate does not reach this limit and continues to higher strain,

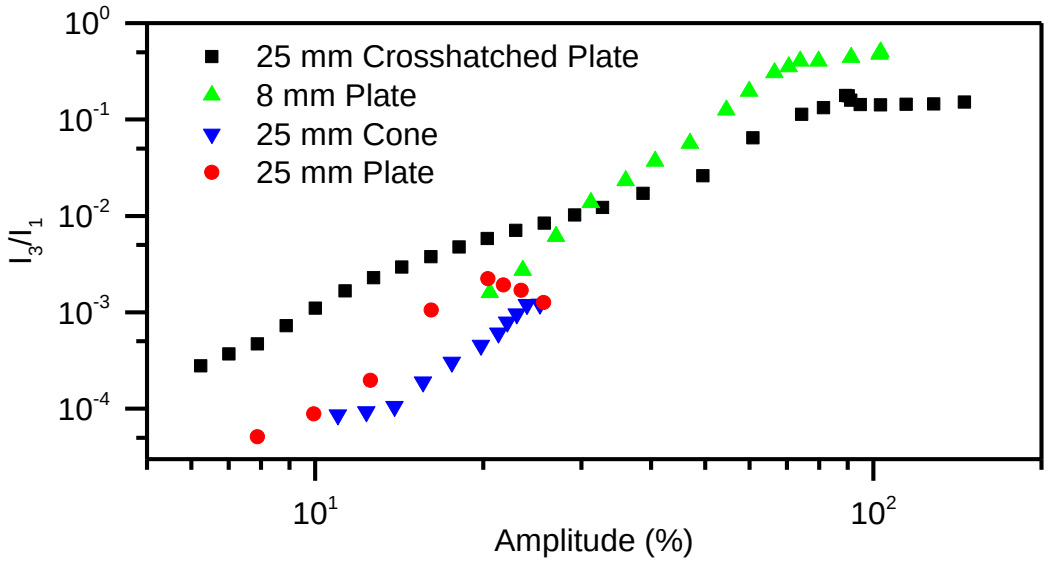

Figure 5.6: Amplitude sweeps of PBD160K at 25 °C and 1 Hz using different geometries.

showing similar behaviour to higher strains. The 25 mm rough plate also does not reach the torque limit, but appears to show different behaviour, with a much lower gradient than measured with the other geometries.

5.2.2.3 Effect of Deborah number on non-linear response

Deborah number was calculated using the crossover frequency from linear rheology (as reported in Chapter 2), and used to compare the results. In Figure 5.7 it can be seen that for a linear polyisoprene, Deborah number has a large effect on the amplitude sweeps. There is clearly a shift in I_3/I_1, with non-linearity beginning at a lower strain at higher Deborah number. There is also at significant difference in the high strain behaviour for the lowest Deborah number measurement, while the high strain behaviour of the other three tests is similar (which are close to or above a Deborah number of 1).

5.2.2.4 Comparison of polymer structure

For a Deborah number of 0.2, as shown in Figure 5.8 at low strains all the materials showed a gradient near strain amplitude squared, as expected for I_3/I_1 in the linear region.[86] However at higher strain the linear materials showed steep increases, whereas the star and randomly branched material continued with a gradient similar to strain amplitude squared. All of the star materials show near identical behaviour. Adding 5 % of randomly branched RB480K to linear PBD310K showed little

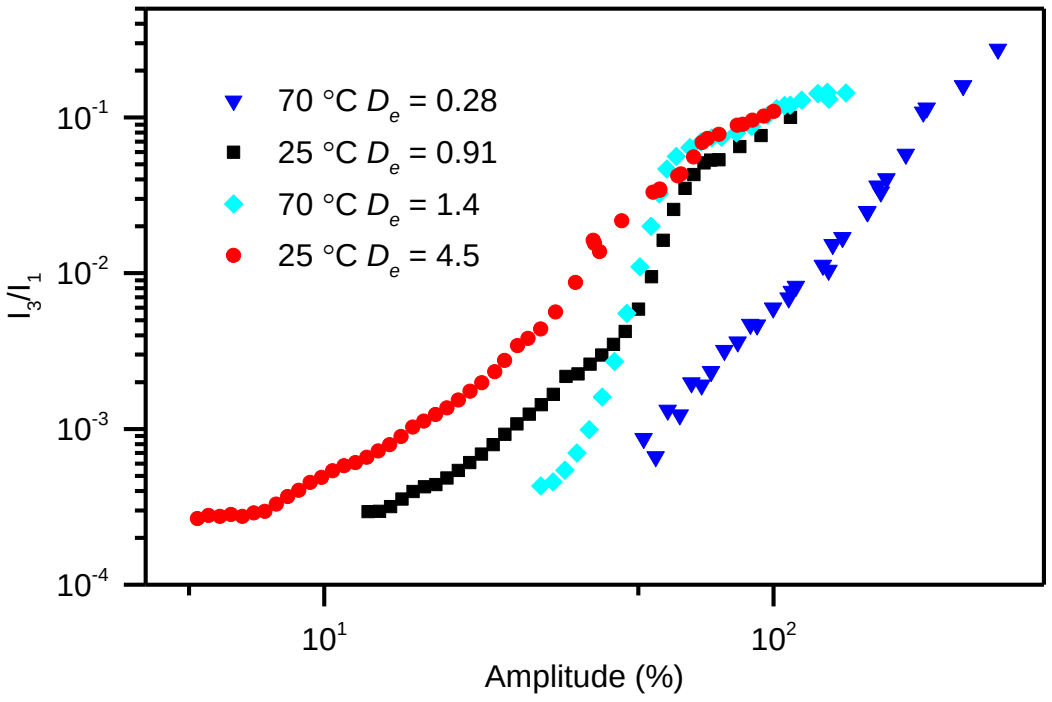

Figure 5.7: Amplitude sweeps of PI150K using 25 mm parallel plate at different Deborah numbers

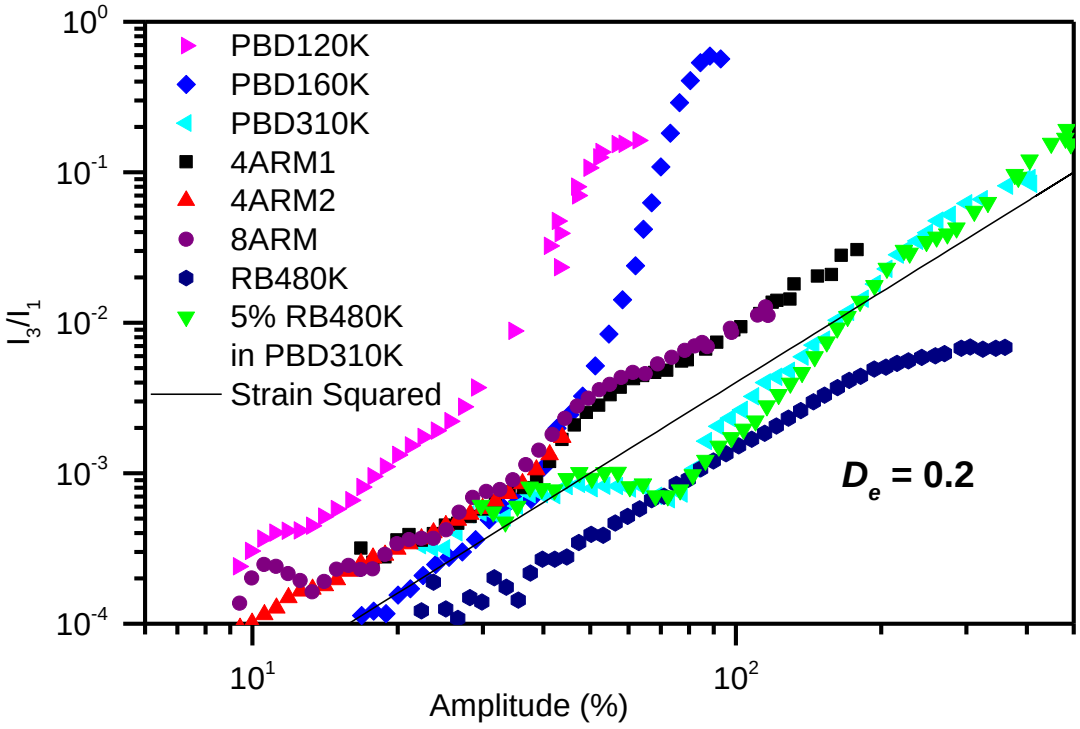

Figure 5.8: Amplitude sweeps of different PBD structures at a Deborah number of 0.2, using either a 25 mm cone or 8 mm plate where torque limits were reached.

deviation to the pure linear.

For a Deborah number of 1, as shown in Figure 5.9, again at the lowest strain the gradient of all materials is close to strain squared. However this changes rapidly with strain, and all of the materials show a rapid increase in I_3/I_1. It is difficult to identify a difference between the behaviour at this Deborah number, however it is notable that again all the star polymers' behaviour is near identical. Also the 5 % RB480K in PBD310K is slightly shifted from the pure linear towards the behaviour of the star polymers, which may be an effect of the inclusion of branching. The RB480K is the only one that does not show this steep change in gradient, although this may be due to its polydispersity in molecular weight and structure meaning it is difficult to quantify the Deborah number of the material. It is also possible that we are measuring the onset of edge fracture or slip in this rapid increase, which would be a lot less likely to occur in the lower viscosity randomly branched polymer.

A well-defined series of linear star blends were also examined, in Figure 5.10 and Figure 5.11 for Deborah numbers of 0.2 and 1 respectively. At D_e = 0.2, all the materials show a gradient close to sine squared at low strain, but the linear polymer displays higher values of I_3/I_1 than the blends and star. The star continues to show this behaviour at high strain, but the linear material and blends all show an increase in gradient.

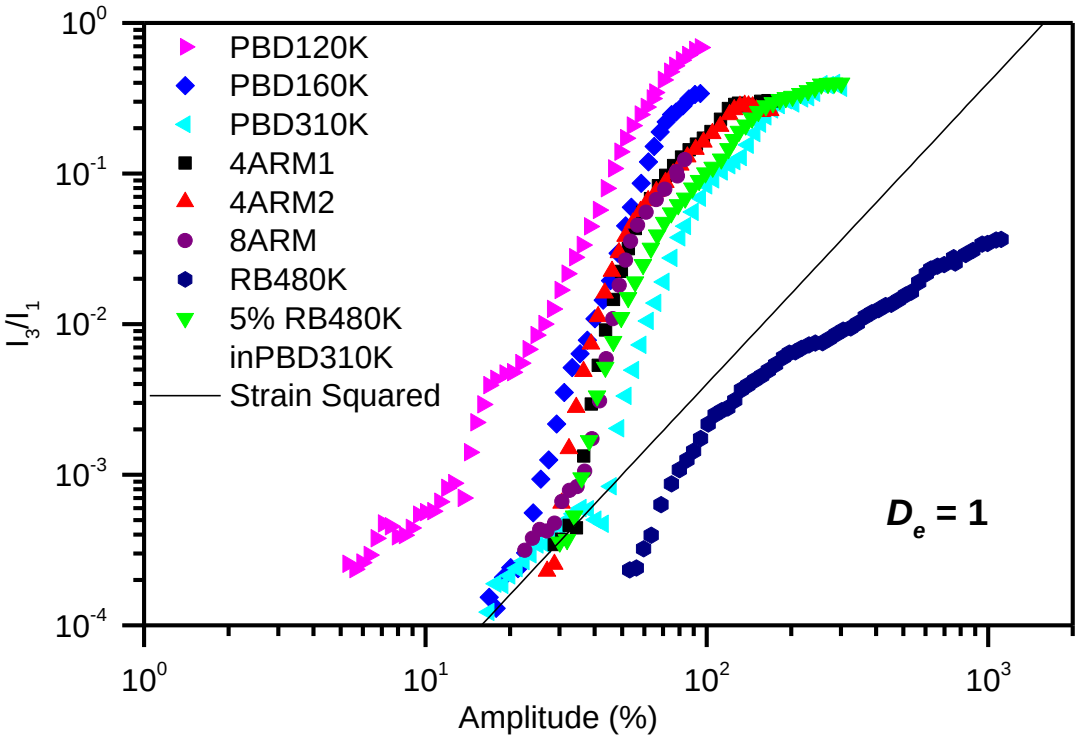

Figure 5.9: Amplitude sweeps of different PBD structures at a Deborah number of 1, using either a 25 mm cone or 8 mm plate where torque limits were reached.

At D_e = 1, again the low strain behaviour is close to strain squared, the linear again has higher values of I_3/I_1, and the increase in gradient is less pronounced only increasing slightly above strain squared. The star this time also shows an increase from the gradient of strain squared at high strain.

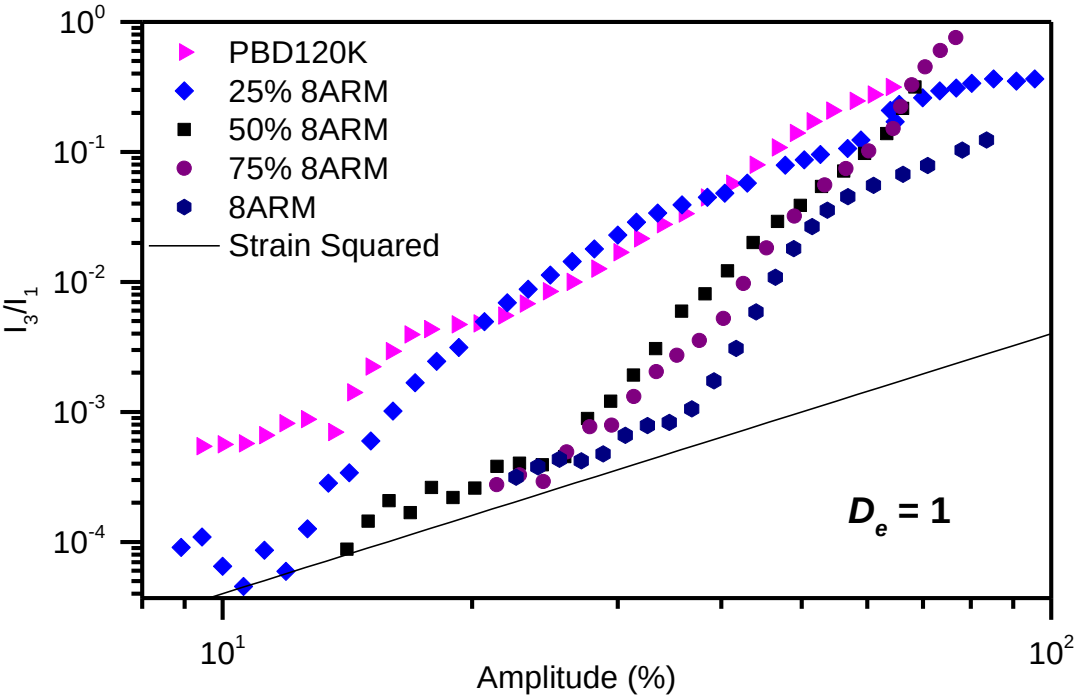

Figure 5.10: Amplitude sweeps of mixtures of PBD120K and 8ARM at D_e = 0.2 using an 8 mm geometry

The blend with the highest proportion of linear (25 % star) starts at the lower I_3/I_1 of the star at low strain but quickly increases and behaves similar to the linear polymer. The blends with a higher percentage of star polymer show this increase at higher strains, but also increase past the level of the pure star polymers to those similar to the pure linear. The onset of the increase is slightly earlier for the 50 % star than the 75 % star.

5.2.2.5 Filled polymers

The clear effect of adding filler, both silica (Figure 5.12) and carbon black (Figure 5.13) is causing the onset of non-linearity to move to lower strains. Silica particles have a greater effect on introducing non-linearity than carbon black, requiring lower loading to achieve a similar effect. Interestingly, all of the materials have the same I_3/I_1 at a point close to a strain of 100 % and show similar behaviour in this region.

5.2.3 Discussion

5.2.3.1 Time dependence of measurements

Figure 5.4 shows the results when a constant amount of cycles (10) are used for the measurement, but the number of 'throwaway' cycles before the measurement at each point was increased from 2 to 100. This was done to test the time dependence of the measurement, so the number of cycles was kept low and constant so the

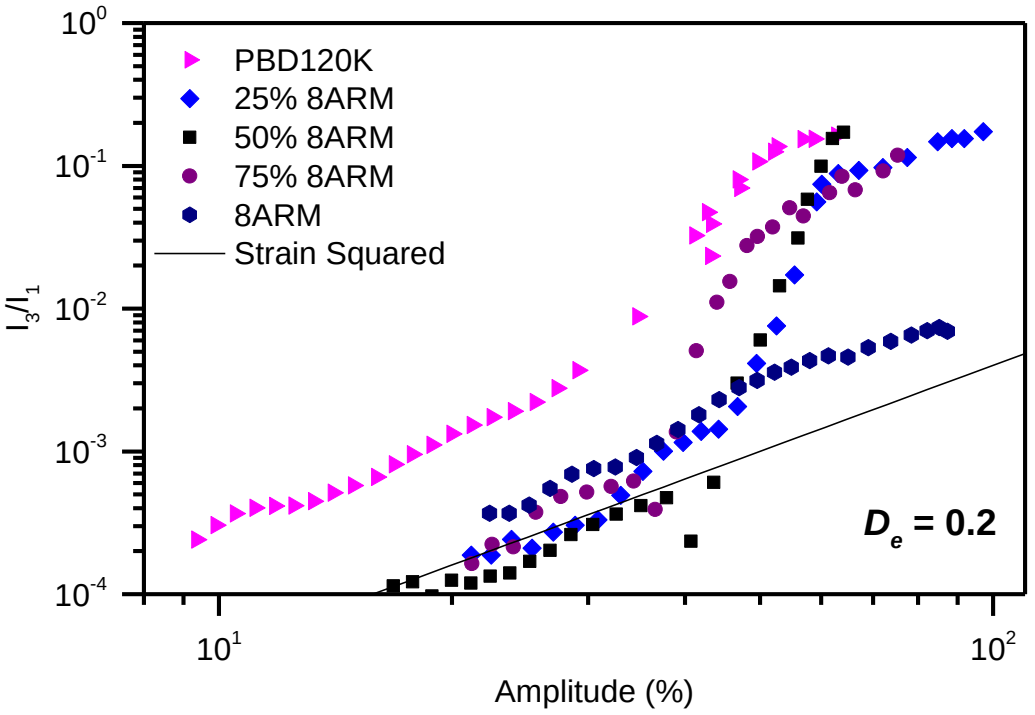

Figure 5.11: Amplitude sweeps of mixtures of PBD120K and 8ARM at D_e = 0.2 using an 8 mm geometry

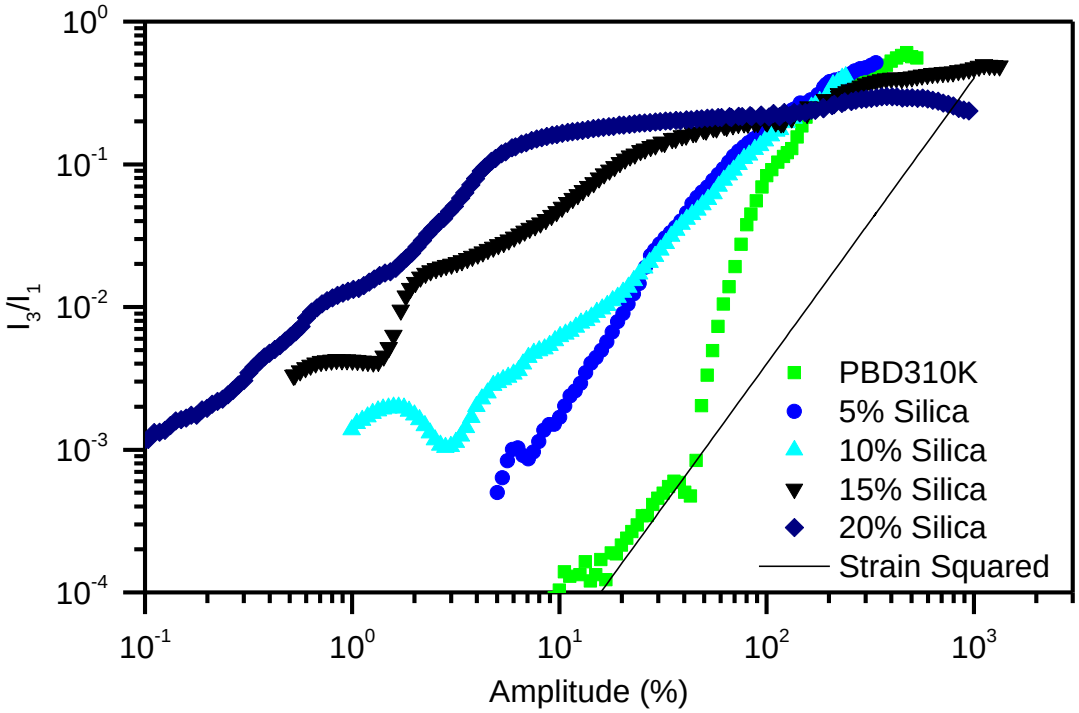

Figure 5.12: Amplitude sweeps for PBD310K mixed with different weight percentages of silica, measured at D_e = 1 for the pure polymer with the 8 mm parallel plate.

measurement was not averaged over different regions of behaviour. The results show that the onset of non-linear behaviour is affected greatly by the time, and using longer times introduces non-linearities at lower strains. This is likely due to the measurement at high strains causing edge fracture and squeezing out of the gap. This will affect the measurement more significantly for longer measurements, and it is seen that the results are similar up to 20 throwaway cycles but at 30 and 100, the deviation is significant and the I_3/I_1 ratio reaches values close to 1 at high strains. As even during LAOS behaviour, the third harmonic is expected to be significantly smaller than the first, this suggests there is significant edge fracture or sample escaping the gap at these times.

The only result that does not follow this trend is that after 2 throwaway cycles, this is due to the inclusion of start-up effects in the first few cycles which complicate the measurement. It is also seen that increasing the number of cycles to 100 increases the resolution, making lower values of I_3/I_1 measurable. The exact minimum I_3/I_1 depends on the sample and will be lower for a higher viscosity sample, where I_1 is larger and the minimum I_3 measurable above the experimental noise is similar (usually in the range 0.1-1 Pa). However it is clear that averaging over a larger number of cycles increases this resolution.

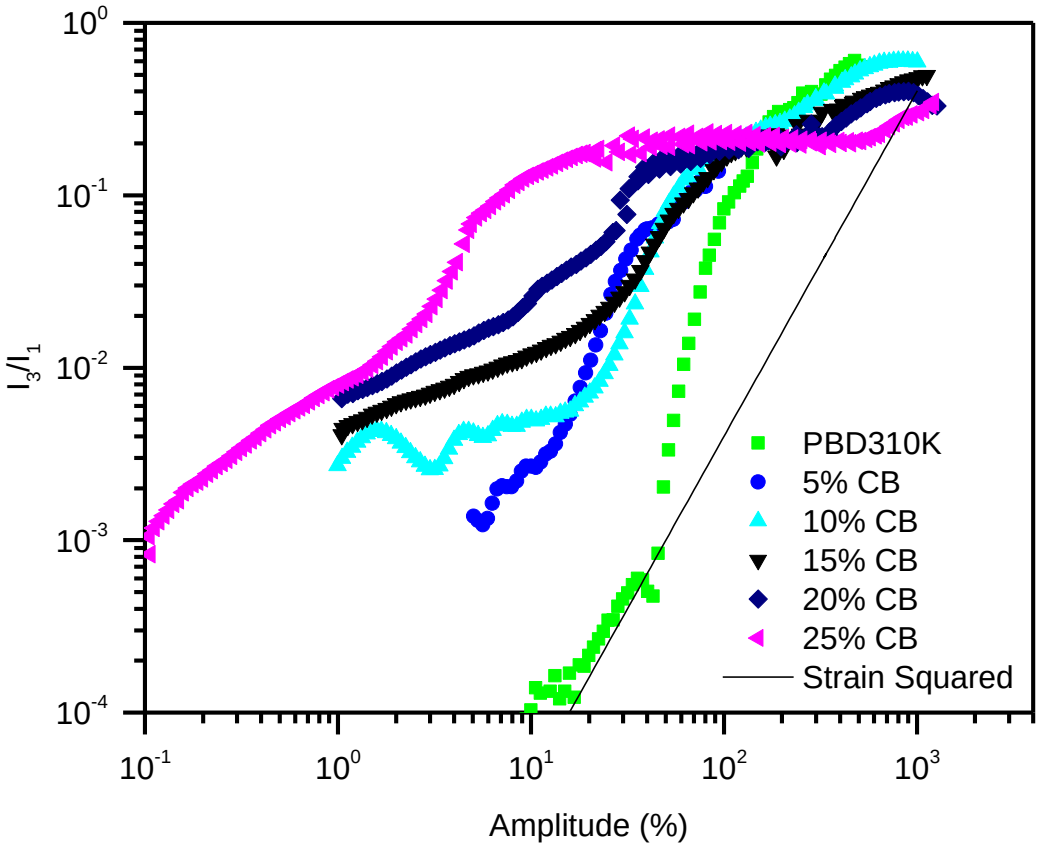

Figure 5.13: Amplitude sweeps for PBD310K miixed with different weight percentages of carbon black, measured at D_e = 1 for the pure polymer with the 8 mm parallel plate.

Although it is clear that these measurements are very dependent on the measurement conditions, they are reproducible, so if conditions are controlled, it should be possible to provide quantitative results. Based on these results, it was chosen to discard the first five cycles from further measurements, enough to remove start-up effects but not add significant time to the measurement, and use 30 cycles for measurement, which should be enough to reduce sufficiently the signal to noise ratio but not excessively affect the results.

5.2.3.2 Effect of different geometries on non-linear response

To further investigate the link between LAOS behaviour and measurement conditions, different geometries were tested, both an 8 mm and 25 mm parallel plates, to show the effect of increased torque. A difference between these may be expected due to changes in the slip/fracture/sample squeezing out, which will be affected by the sample volume and the ratio of the surface area of the edges to the remaining sample, both of which will change with diameter despite samples all being 1 mm thick. There are also cases, when using high strains on rubbery materials (linear PBDs over 100K for example), that the torque exceeded the rheometer limits,

so that the signal was clipped. An 8 mm plate may be required to reach high strains for these materials. A 25 mm cone was also used, which should give the most well defined strain across the sample. Finally a crosshatched plate (above and below the sample) was used to study the effect of slip, as the roughness should reduce the slip that occurs. However this could also introduce additional non-linearities in the LAOS results as the strain is not as well defined.

A comparison of each geometry is shown in Figure 5.5 and Figure 5.6 for RB480K and PBD160K respectively. For the randomly branched sample all the results agree remarkably well. It is reassuring that results from different geometries can be compared and suggests that we are not measuring significant fracture or sample escaping the gap, which would be greatly affected by the geometry. The correction for the strain rate in a parallel plate has worked well to account for the different strain generated by each. The cone will generate a homogenous strain across the sample but the plates will not, and so the size of the plate will affect the strain gradient across the geometry, meaning each will produce a slightly different strain in the sample. The crosshatched plate produced results almost identical to the flat plate, which suggests that there is not significant slip occurring for this sample. The 8 mm results however were noisy and did not match the other geometries. This is due to the low level of torque generated, meaning that while the third harmonic was identifiable, it was close to the level of the noise. Hence care must be taken to choose a geometry that generates significant torque to reduce the signal to noise ratio.

Linear PBD is a more rubbery sample and so may be expected to show more effects of slip. The results for the linear PBD were complicated by the fact that the torque reached its limit for the 25 mm plate and cone, after which the stress cycles were truncated and the data cannot be analysed. The 8 mm plate reduces the torque and produces results that agree well with the 25 mm plate and cone but reaches much higher strains. The results do not however overlap exactly, which is surprising since the material is a simple linear polymer and the correction for parallel plates would be expected to hold. There have been observed cases when this is not the case, but these samples are more complex (e.g. xanthan gum[190]). The values at which the two can be compared are small (and of a limited range) so it is possible that a small difference in sample loading could have caused the difference, and the difference would be less pronounced if higher strains were possible with the cone.

The rough plate interestingly does not reach the torque limit, but produces anomalous results to the other geometries. It has been previously noted that crosshatching produces a systematic error to flat plates, producing a lower stress and viscosity.[191] This was attributed to material flowing out of the grooves in the crosshatches. Although our sample is too rubbery for this to occur, it is possible that the equilibration time (~10 mins) was not long enough for the polymer to flow into all of the grooves to begin with, leaving some partially filled, which would have the effect of reducing the torque (meaning the limit is not reached) and producing lower stress and anomalous results.

For further amplitude sweeps, the cone and plate geometry was preferred, due to its constant strain and smaller sample volume, however for the samples which approach the torque limit of the rheometer or are only available in very small amounts, the 8 mm plate can be used. It has been demonstrated that with careful control the results from the different geometries can be reasonably compared.

5.2.3.3 Effect of Deborah number on non-linear response

The frequency of the measurement is expected to have a large effect on the results in an amplitude sweep.[95] Keeping frequency constant for all polymers is not necessarily a valid comparison, because changes in the polymer structure have a large impact on the behaviour at different frequencies, as evidenced by Chapter 2.

The frequency applied will change the Deborah number of the measurement, and the Deborah number can be used to standardise these measurements. Using the polymer relaxation time (here the crossover time from linear rheology) to calculate the Deborah number allows the amplitude sweeps to be performed in the same region of behaviour for all polymers. The effect of Deborah number can be seen in Figure 5.7 where amplitudes for a PI is compared at different Deborah number for two temperatures.

The temperature appears to have little effect if Deborah number is kept constant, and all of the measurements look similar, except that higher Deborah number causes instabilities to start at a lower strain. The behaviour at the two closest Deborah numbers of 0.91 and 1.4 is similar despite the difference in temperature between the two, suggesting that the Deborah number is a good way of normalising the behaviour and take into account environmental differences.

It should be expected to see a difference between polymer behaviour at Deborah numbers below and above one, since at this point, the applied deformation becomes

faster than the polymer can relax. This is seen in our results; however, the measurement at 0.91 appears to agree better with those above 1 than the measurement at low Deborah number. This could be explained by a slight polydispersity introducing some error into the calculation of the Deborah number. There is a spectrum of materials present in a polydisperse sample each with different relaxation times, so the definition of D_e as the crossover point is somewhat arbitrary.

It is clear that the behaviour well below a Deborah number of 1 deviates from the other results. It is therefore important to examine behaviour in both regions and doing so may reveal additional information about the polymer structure. For this reason, further amplitude sweeps were performed at D_e = 0.2 and D_e = 1 to quantify this different LAOS behaviour.

5.2.3.4 Comparison of polymer structure

After ensuring the effect of geometry and measurement conditions could be controlled, different polymer structures could be compared. Figure 5.8 shows a comparison of different architectures of PBD at a Deborah number of 0.2. The low strain behaviour of all the materials is as expected for SAOS measurements, with I_3 having a dependence on strain cubed and I_1 on strain, leading to an expected dependence of the ratio of I_3/I_1 on strain squared.[86, 105] This behaviour however cannot be used to distinguish the materials. However, as strain is increased, it is clear that the linear materials show a large increase in I_3/I_1 whereas the stars and randomly branched materials do not. This is useful to distinguish the two, however it does not appear to be particularly sensitive, as adding 5 % randomly branched material does not change the behaviour of the linear polydisperse material significantly. Also it is difficult to note a clear difference between the linear materials or any of the branched materials. It is interesting to note that I_3/I_1 vs strain amplitude plots for all of the star materials lie almost exactly on top of each other, despite the difference in molecular weight and number of arms. This does suggest that the behaviour observed is directly related to the architecture of the polymer, but it still may be difficult to determine exact architectures from these measurements alone.

The behaviour at D_e = 1 (Figure 5.9) is more difficult to distinguish, as all the behaviour is much more non-linear, likely due to the stress building up the in sample when the deformation becomes faster than the polymer can relax. The very low strain behaviour is still consistent with a dependence on strain squared but all

materials, except for the randomly branched material, show large increases in I_3/I_1. Despite the similar behaviour, the star materials all still show remarkably similar behaviour which suggests architecture is playing a significant role. The difference seen for the randomly branched material could be due to the calculation of the Deborah number, since the terminal region is very large of this material due to its polydispersity, and the crossover point is just an average of behaviour of a large range of different material in the mixture.

To further explore the effect of structure, star-linear blends were made and the results are shown in Figure 5.10 and Figure 5.11 for Deborah number of 0.2 and 1 respectively. At D_e = 0.2, the star shows behaviour similar to strain squared at all strains, whereas the linear shows the typical increase in gradient. The blends show a mixture of the two behaviours, starting alongside the star, but at higher strains, increasing steeply to meet the linear polymer. This again reinforces the hypothesis that this behaviour is architecture dependent. It is difficult to distinguish the blends with different amounts of star as they all show similar behaviour.

For a Deborah number of 1, the linear polymer has a higher I_3/I_1 ratio throughout and the star starts at a lower value but shows an increase at high strains. The blend with the lowest amount of star looks similar to the linear expect at the lowest strains, the blends with higher amounts of star behave similarly to the pure star, except that with greater amount of linear the increase in I_3/I_1 occurs at slightly lower strain and at high strains, they do not plateau with the star polymer. This is interesting because it appears that the behaviour can be switched between different components at different strains. There is more dependence at this Deborah number on the quantities of each component; however it would still be difficult to extract quantities values from these results.

Filled Polymers

The increase in non-linearity with filler loading seen for both silica and carbon black (Figures 5.12 and 5.13), is expected as the filler will greatly affect the rheology of the mixture, and it will no longer behave like the pure polymer. The greater effect seen for the silica over the carbon black can be attributed to the particle size of the carbon black, which is much higher than the nanofiller silica. The specific surface area of the silica is 440 m^2/g as opposed to 150-250 m^2/g for the carbon black. This means at a given filler loading by mass there will be a much greater concentration of silica particles distributed throughout the polymer, and a greater area of particles in contact with polymer. Hence the polymer-filler interactions would be expected to be

greater which could cause the non-linearity. While the filler affects the LAOS results significantly, it is notable that all of the graphs crossover at one point at a strain around 100 % and behave similarly at high strains. This is useful because if this high strain behaviour is not significantly affected by the filler loading, it could be used to obtain signatures of the underlying polymer. However further LAOS measurements on filled materials with different structures would be required to test this further.

5.2.4 Conclusions

The effect of measurement conditions and geometry has been explored for amplitude sweeps analysed by Fourier transform using the code discussed in Section 5.1. A set of conditions has been devised for measuring comparable and reproducible amplitude sweeps, and these have been performed for a range of different polybutadiene structures and filled polymers. This produced interesting results, and it has been clearly shown that the behaviour in these tests is highly dependent on architecture, but less so on the amounts of individual components in the blend. So while these tests could be used to get a signature of the components in a blend, it would be difficult to extract any quantitative information about the amount of different material in a mixture.

The results from filled polymers are particularly interesting, as these materials are very difficult to analyse by other means, and there is potential for extracting structural information using these test, even in the presence of filler, however more experiments would be required to determine the capability of this technique.

5.3 MAOS frequency sweeps

An alternative approach to amplitude sweeps is the use of frequency sweeps in the MAOS region, where the third harmonic can be detected, but the behaviour of the first harmonic is still linear. This has the advantage that the third harmonic can be studied at a range of frequencies and the results are more reproducible and less dependent of measurement conditions and geometry. However the medium strains used do not necessarily give an insight into how the polymer will behave under LAOS.

Here we perform frequency sweeps at these intermediate strains for a range of polymers, in order to observe the behaviour of the third harmonic. In these tests we use the $G3'$ and $G3''$ parameters calculated from the third harmonic. This has the benefit that both the phase and magnitude information is used, meaning that features such as the 'bounce' in the I_3 observed in literature[96, 108] can be studied in more detail and attributed to the signs of $G3'$ and $G3''$. These parameters can also be physically interpreted as described using the Chebyshev equations, as discussed in the introduction. Although some systematic studies of MAOS have been performed[192], these are the first that have been able to provide well controlled results that enable extraction of phases and magnitudes of the third harmonic for rubbery polymers.

5.3.1 Experimental

Materials were PI20K, PI100K, PI150K, PI420K, PI1380K, PBD 120K, 4ARM2 and 8ARM as characterised in SAOS in Chapter 2.

Samples were pressed into 25 mm discs using a press at room temperature. A weight of 3-5 tonnes was applied for 10-30 minutes. The low molecular weight polymers (typically under 100,000 g/mol for linear polyisoprene or 50,000 g/mol for linear polybutadiene) could be directly loaded into the rheometer.

MAOS rheology was performed in a TA HR2 rheometer, equipped with a 25 mm 4 degree cone. Frequency sweeps were performed at medium strains (5 - 20 %) and the transient data recorded. The stress and strain over time were analysed via the MATLAB code discussed in Section 5.1.

In Fourier transform rheology, commonly many cycles are averaged as discussed in Section 5.2. This can be done by extracting the magnitude data with frequency for multiple tests and averaging the various spectra. It can also be done by performing the FFT over a great number of cycles. Some care must be taken when using

polymer melts, as deformation history can affect the results. However this is most problematic for high strains where edge fracture and polymer escaping the sample gap become an issue (as discussed in Section 5.2). If the stress signals of these measurements are examined, a drop off in the stress can be observed with time. During a MAOS experiment the results are much more reproducible and no significant drop off is noted, so it is valid to perform the transform over a large number of cycles. Hence 100 cycles per point were used (plus 5 to remove start-up effects), rather than the 30 used in the amplitude sweeps.

Singh, Soulages and Ewoldt[192] have recently presented a similar technique for performing MAOS sweeps, the main difference being that they have used a systematic approach to finding the best amplitude at each point, performing multiple amplitude sweeps and changing the amplitude at each point based on these results. This allows a greater frequency range to be accessed, however we have chosen to perform fixed amplitude sweeps, because the low level noise is less limiting for polymer melts than gels (as the magnitudes of harmonics are larger), so this still allows us to explore a reasonable range of frequency. Also due to the uncertainty of using higher frequencies due to effects of the instrument frequency, using the lower range of frequencies was deemed to be sufficient. Should a wider range be required, time-temperature superposition can be used to extend the range as demonstrated. They used similar metrics to measure the quality of the third harmonic, namely the second harmonic to check the data was above the noise. In our tests, the second harmonic also provided a check that the strain was not too high, as the introduction of edge fracture, slip etc. has been seen to increase the second harmonic notably. Rather than using the fifth harmonic to determine if the data was too non-linear, we compared the first harmonic to that obtained in a SAOS test. Because our samples were mostly rubbery, this, alongside the second harmonic was a good check of strain being too high, because for these samples edge effects were encountered before the sample became 'too non-linear'.

There is a maximum frequency that can be observed in the rheometer, due to the superharmonic superposition due to an instrumental frequency, as discussed by Poulos *et al.*[102] They measured an instrument frequency of 200 rad/s found measurements above 5 rad/s were complicated by its effect. Reproducing their calculations for measurements made on the TA HR2 rheometer indicated an instrumental frequency of 1100 rad/s which should allow accurate measurements at higher frequencies, however all of our measurements were made below a frequency of 5 rad/s, so should have avoided effects of this.

The experiments were compared to a rolie-poly model, as discussed in the introduction and compiled by David Hoyle at Durham University. The single mode solution resulted in the following solution for the Rouse time (τ_R) based on the frequency of the crossover point in $G3'$ and $G3''$ (ω) :

$$\tau_R = \frac{-18\omega^5 + 39\omega^4 + 17\omega^3 + 13\omega^2 + 11\omega - 2}{36\omega^6 + 96\omega^5 - 73\omega^4 + 9\omega^3 - 35\omega^2 - 15\omega + 2} \quad (5.3)$$

5.3.2 Results: Non-linear response at medium amplitudes

An example stress signal and its Fourier transform are shown in Figure 5.14. The first, third and fifth harmonics are clearly visible. In this case the second harmonic is virtually zero although a fourth harmonic can be seen. For different measurements, the magnitude of the second harmonic varied, but was always smaller than that of the third.

The MAOS frequency sweeps are shown in Figures 5.15-19. The shape of $G3'$ and $G3''$ is reasonably consistent for all of the systems analysed. $G3'$ starts near zero and dips to negative values before increasing and becoming positive, whereas $G3''$ is always positive, and increases to a peak before falling back to zero. This leads to a crossover in $G3'$ and $G3''$, always seen at a frequency below the crossover in G' and G''.

The physical meaning of $G3'$ and $G3''$ can be described using the interpretation resulting from the Chebyshev analysis, as discussed in the introduction. For all samples shear thinning is observed at low frequencies (negative $G3''$) and linear response from the strain ($G3'$ close to zero). As frequency approaches the crossover in G' and G'' the shear response changes from thinning to thickening

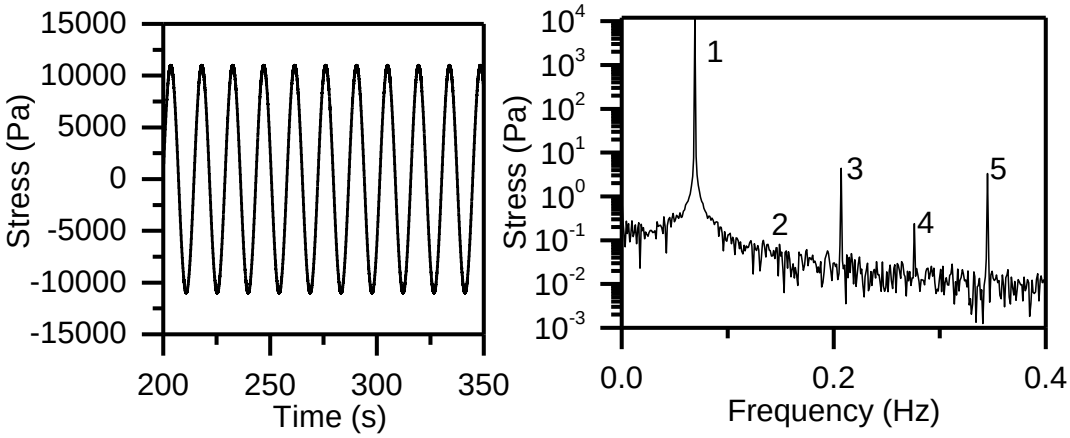

Figure 5.14: Example stress signal in the MAOS region and the resulting Fourier transform (PI150K at 23 °C, 20 % strain, 0.07 Hz)

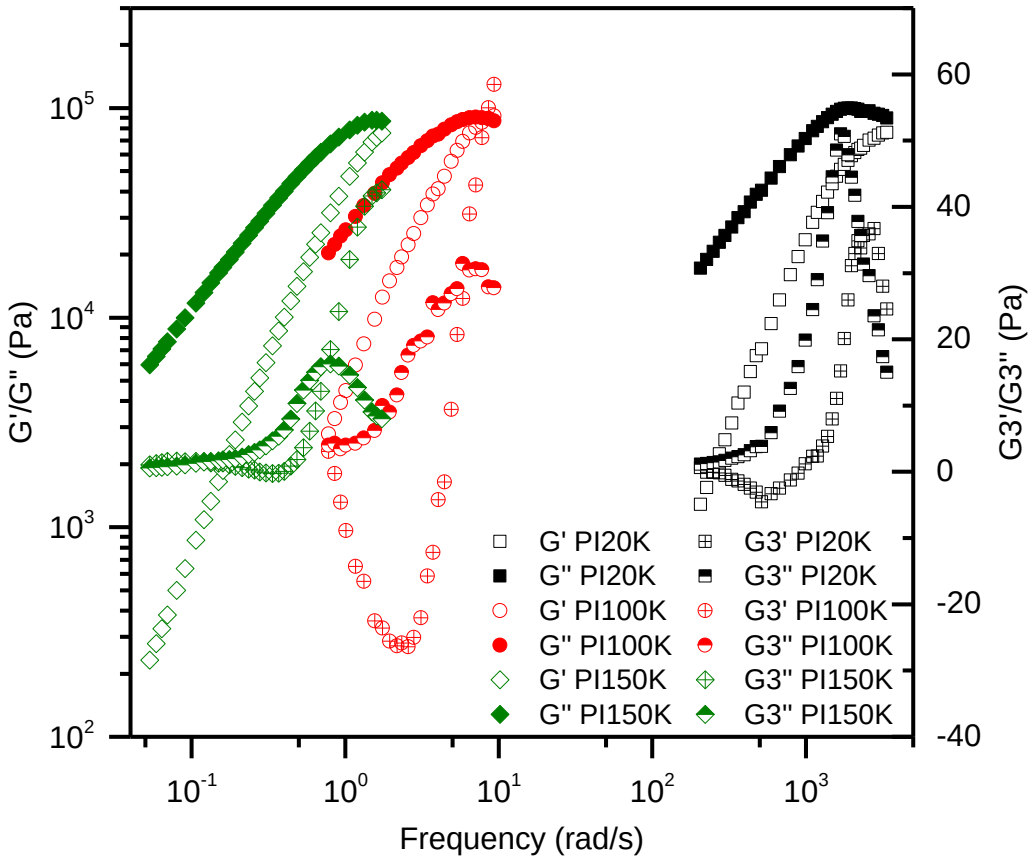

Figure 5.15: MAOS frequency sweeps of linear polyisoprenes, shifted to 25 °C, PI20K: 25%, -25 °C, PI100K: 20 % 0 °C, PI150K: 20 % 25 °C

($G3''$ increases to become positive) and strain softening begins ($G3'$ becomes positive). The crossover in $G3'$ and $G3''$ is located in the transition from this initial behaviour to the later.

5.3.3 Discussion: Non-linear response at medium amplitudes

The MAOS rheology shows consistent behaviour for all of the linear polymers studied. For PI420K (Figure 5.15), a combination of experiments performed at different temperatures is shown. Although there is some small variation between experiments, this is likely to largely arise from the sample loading. Such variations are common in rheological experiments, but in the case of the G' and G'' results usually measured, variations are hidden by the large range of magnitudes and logarithmic scales used to present them. The differences could be reduced by normalising measurements by the first harmonic, however this would also complicate the interpretation. Despite this, it is clear that the time-temperature superposition principle is still valid for both the first and third harmonics' in these measurements.

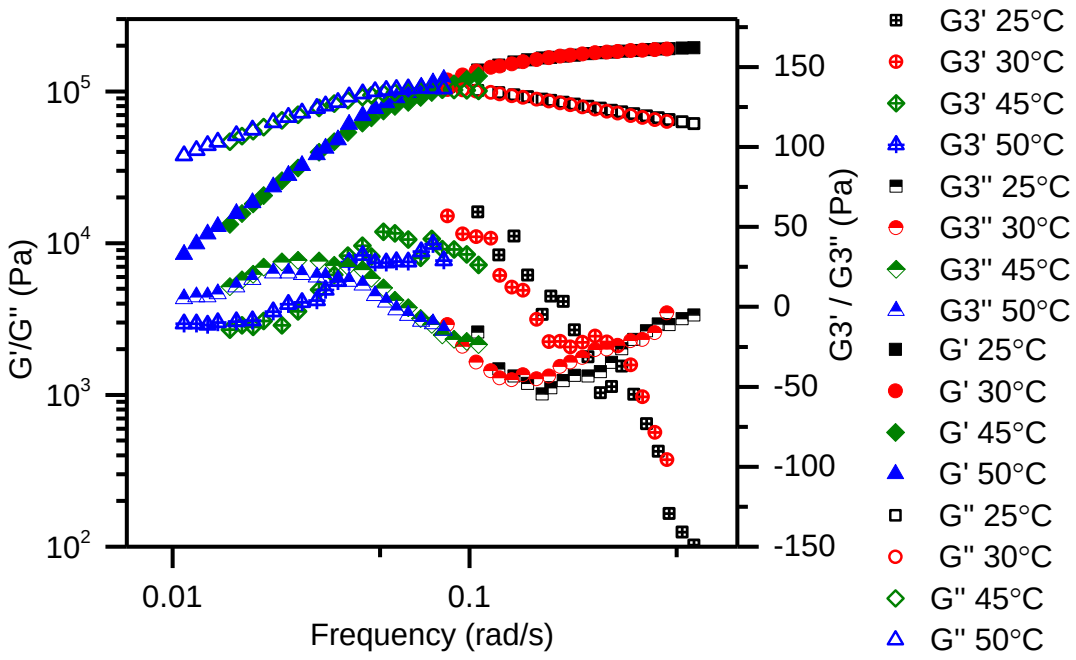

Figure 5.16: MAOS frequency sweeps of PI420K at different temperatures, overlaid at 25 °C (25 °C - 45 °C: 18 %, 50 °C: 20 %)

In order to elucidate the behaviour being probed by the $G3'$ and $G3''$ in the region observed, the rolie-poly equations were solved for Fourier transform at low strain amplitudes, which is valid for all Deborah numbers up to strains of around 100 %. This gave equations for $G3'$ and $G3''$ which are non-trivial, but are only dependent on the Rouse time of the polymer, and when solved for the crossover point give

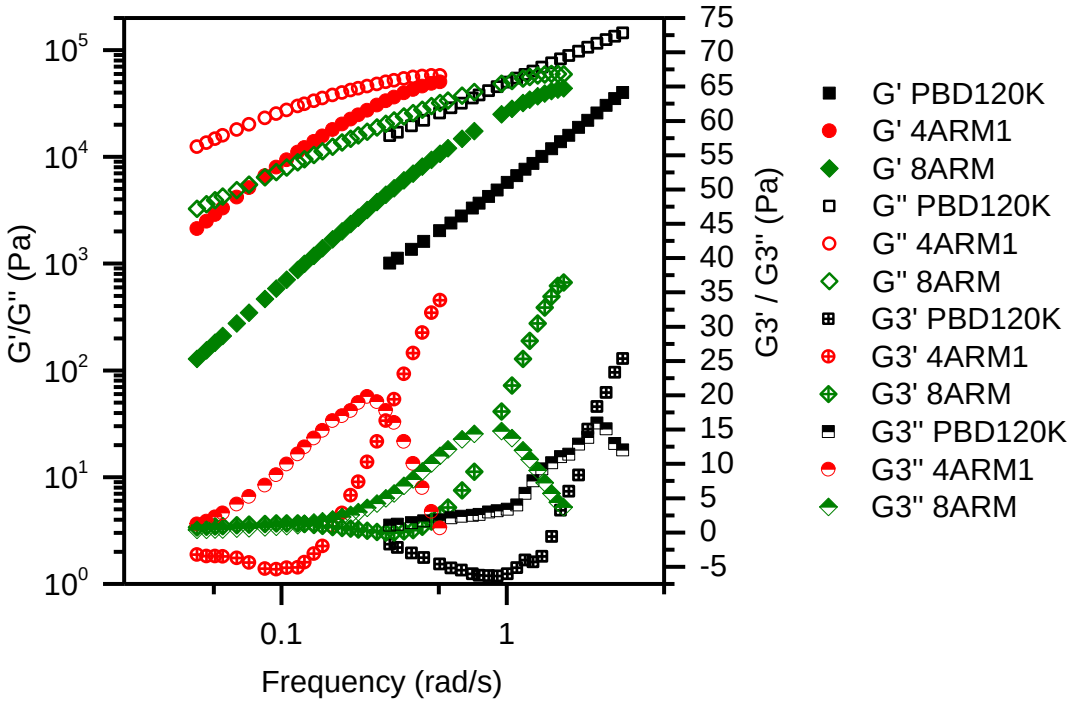

Figure 5.17: MAOS frequency sweeps of linear (20 % 10 °C) and star polybutadienes (both 20 % 30 °C), shifted to 25 °C

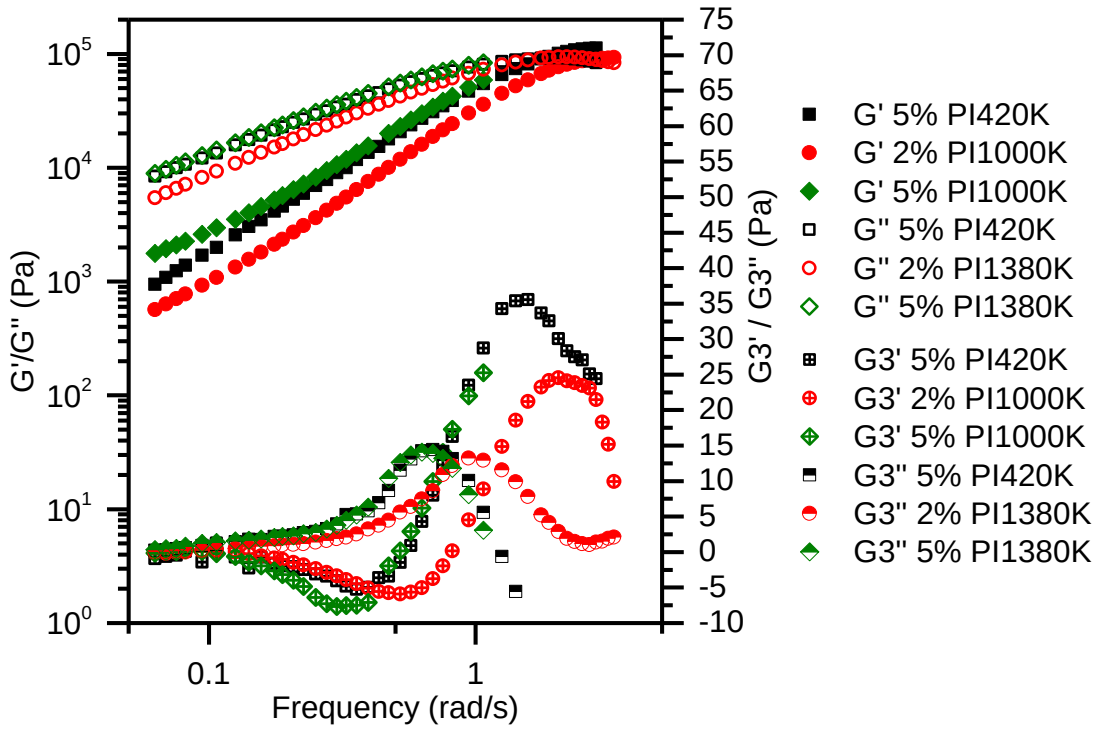

Figure 5.18: MAOS frequency sweeps of blends of PI150K with higher molecular weights, shifted to 25 °C, both at 18 % strain, 25 °C.

Equation 5.3.

Figure 5.20 shows the prediction using the rolie-poly equations (Equation 5.3) for a polymer with a Rouse time of 0.005 s (equivalent to 100K polyisoprene, predicted from the extensional rheology in Section 3.1). Although the magnitudes of the moduli have not been optimised, it shows that the key features are described very well by the rolie-poly model, even with a single mode. Since the equation for the crossover in $G3'$ and $G3''$ is solely dependent on the Rouse time of the polymer, this agreement suggests that the behaviour of $G3'$ and $G3''$ is largely governed by Rouse motion. Since the frequencies used are between two and five orders of magnitude below the inverse Rouse time, this is a very interesting result, and implies that the higher harmonics can be used as a probe to behaviour at higher frequencies, in situations when using higher frequencies is not possible or desirable.

Further evidence for the $G3'$ and $G3''$ behaviour originating from the Rouse time of the polymer can be found by comparing the MAOS data for the linear polybutadiene (Figure 5.17) to the polyisoprenes (Figure 5.15). All of the linear polyisoprenes, show a crossover in $G3'$ and $G3''$ that lies at a frequency between 0.45 and 0.68 times the frequency of their G', G'' crossover, whereas the polybutadiene crossover is significantly lower, at a frequency 0.21 times its G', G'' crossover. This could be due to the lower Rouse time of polybutadiene compared with polyisoprene, and so

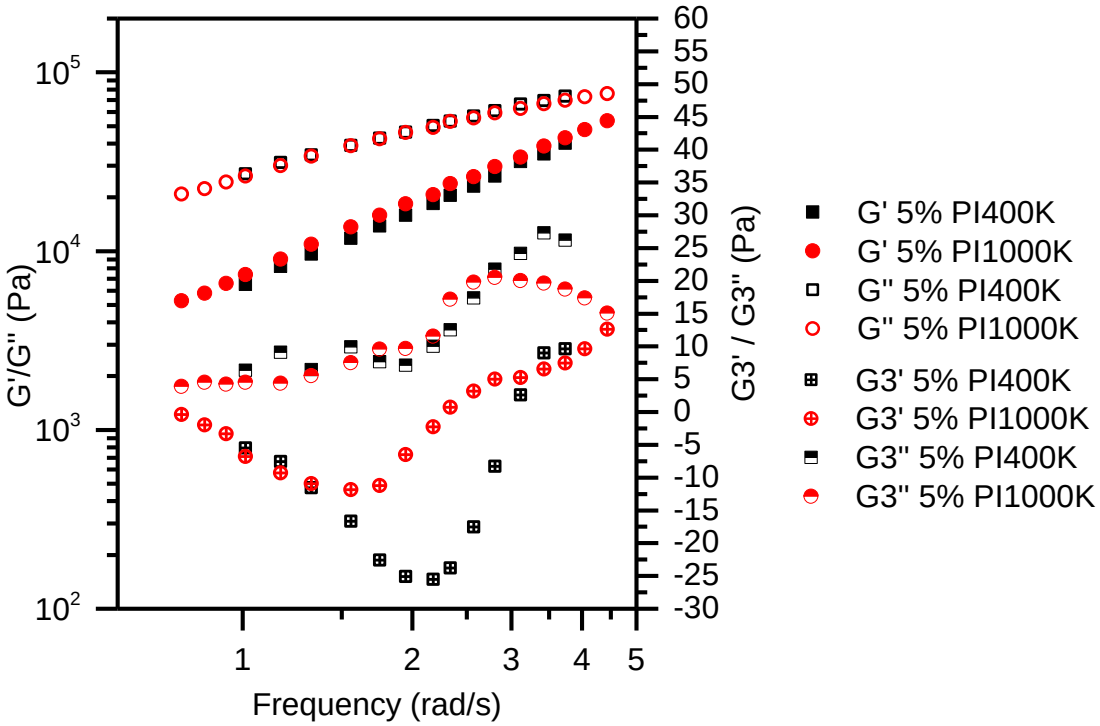

Figure 5.19: MAOS frequency sweeps of blends of PI100K with higher molecular weights, shifted to 25 °C, both at 20 % strain, 0 °C

supports the suggestion that the behaviour is driven by Rouse motion. Note that it may be expected that the lower Rouse time would shift the crossover frequency to a higher frequency, however as shown in Equation 5.3, the relationship is complex and non-linear.

For the star polymers examined, the same shape of crossover is observed (Figure 5.17). This may be expected if the behaviour is derived from Rouse motion, as the chain stretching will be driven by the arm length of the star and be unaffected by the architecture.

In the MAOS sweeps of the PI150K polyisoprene blends the negative dip is increased when higher molecular weight component is added and appears to shift to lower frequency. It is less clear for the PI100K blends, where it was more difficult to obtain a crossover, because the sample began to show effects of slip at lower frequencies with the higher molecular weight component included. However, it also appears that the crossover is shifted to higher frequency. The dip again moves more to lower frequency, but this time appears to decrease in magnitude when high molecular weight component is added.

The behaviour of the blends can also be explained using the Rouse time. When considering the blends of PI150K with PI1380K, adding 2 % of the higher molecular

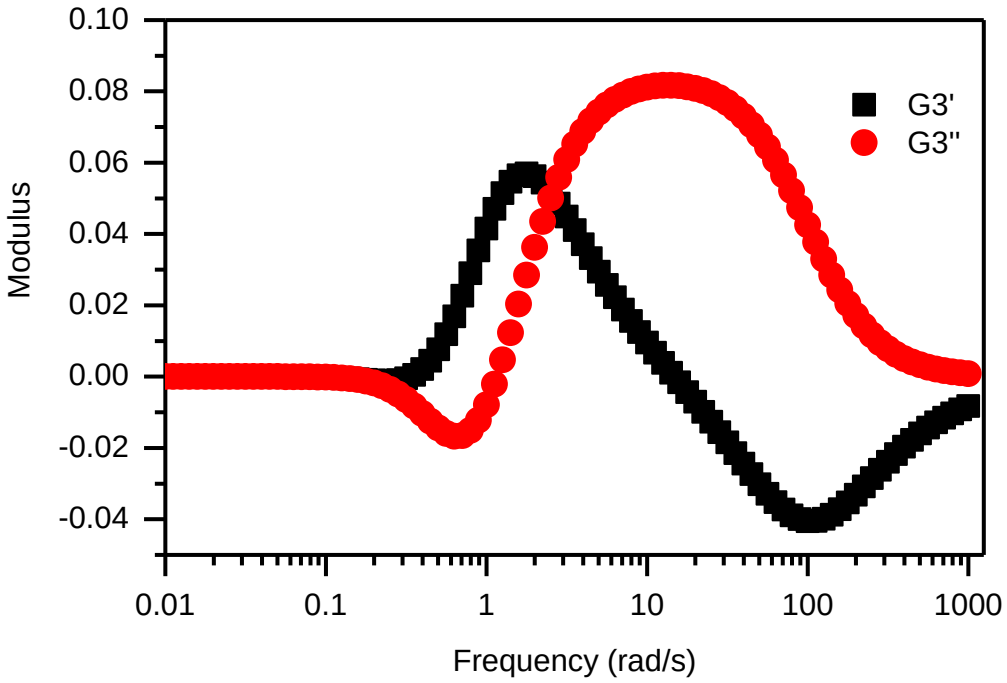

Figure 5.20: Single mode rolie-poly prediction for a polymer with a Rouse time of 0.005 s, using Equation 5.3

weight component shifts the crossover significantly towards higher frequency The dominant relaxation is now that of the high molecular weight component, which has a much longer Rouse time. Upon increasing the proportion of high molecular weight component to 5 %, the crossover shifts back towards lower frequency, indicating a shorter rouse time. This result could be due to the effect described by Auhl *et al.*[146]. They observe for a very similar system to ours (PI 400K in PI 30K) that diluting the longer chain component, increases its relaxation time (stretch time measured from extension which is essentially the Rouse time of the polymer). This would imply that the most dilute blend including the higher molecular weight component would have the highest Rouse time (provided the high molecular weight components are concentrated enough to be entangled with one another) and this would decrease with dilution, which agrees with the shift in crossover point.

Together these results suggest that, in the experimentally accessible regime, a lower frequency of the $G3'$, $G3''$ crossover indicates a longer Rouse time. As mentioned above, the relation is complex and so for some measurements this may not always be the case. The crossover frequencies predicted by the rolie-poly model for different Rouse times are shown in Figure 5.20, and the trend agrees with our experimental measurements. However, when this model is expanded to multi-mode and supplied with modes fit to the experimental linear rheology and a Rouse time

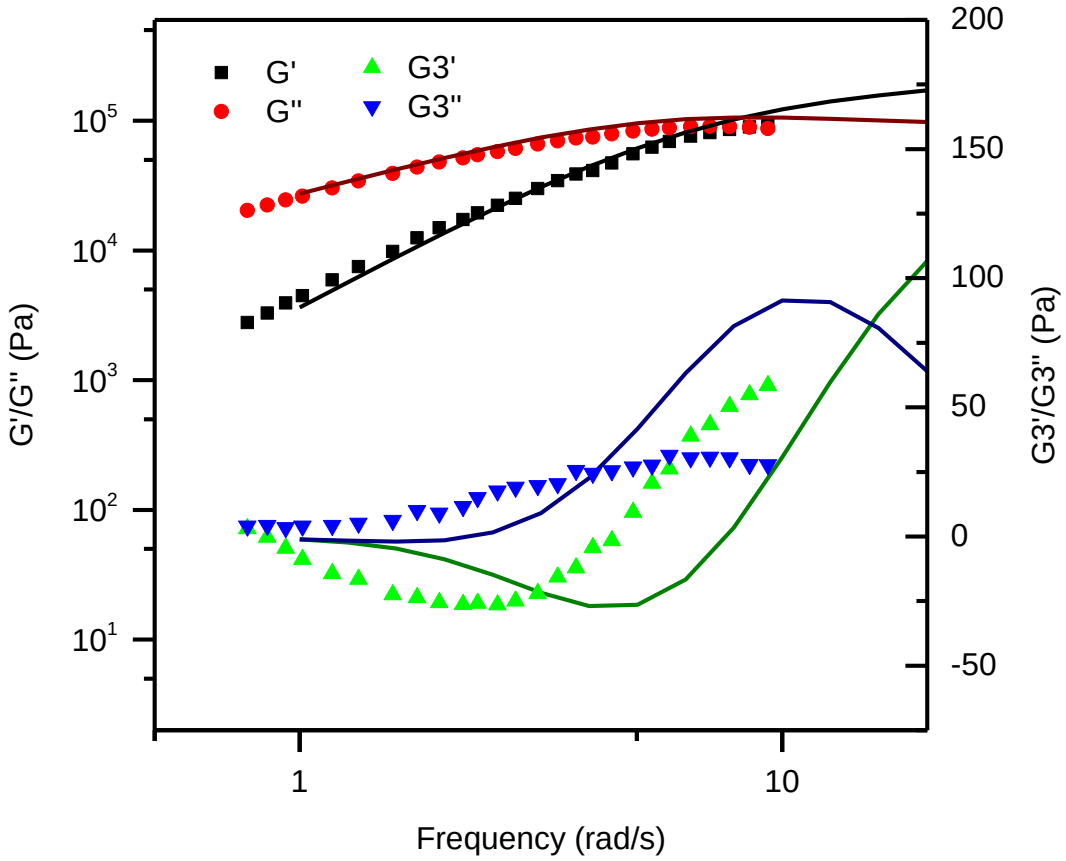

Figure 5.21: Comparison of rolie-poly data (lines) to MAOS frequency sweep of PI100K, shifted to 25 °C (points)

from the extensional data, the behaviour is captured well, but there is a clear shift in frequency between the data and the model (Figure 5.21). More detailed models may be required to capture this difference. It is possible that there is a fundamental process that the model does not take into account, which would be a surprising and exciting result, since it implies that existing constitutive models are not as quantitative as previously believed.

5.3.4 Conclusions

We have shown that frequency sweeps can be performed under medium amplitude oscillatory shear for a variety of polymeric materials. Both the phase and amplitude of the third harmonic has been recorded allowing calculation of $G3'$ and $G3''$, which display a crossover at frequencies in the viscous regime for each polymer. Using a simple model and by comparing results for different architectures and blends, this crossover has been shown to be dependent on the Rouse time of the polymer. Hence this method provides a way of gaining insight into the Rouse motion of the polymer at frequencies on the order of 10^4 times lower than linear shear measurements, which may be useful in cases where using higher frequencies is undesirable. It may also provide a method for exploring Rouse behaviour in systems

where this is difficult in linear rheology, e.g. polydisperse materials, although further experiments are required to explore this.

5.4 LAOS in the multi-pass rheometer

The MPR also has an oscillatory mode, which has potential for performing LAOS measurements, this has the potential advantage over the shear rheometer that the sample would be enclosed and so the effects of sample squeezing out of the gap and edge fracture would be reduced. It has the disadvantages that it requires a much greater mass of sample (10 g vs < 1 g) and the data transfer rate is lower, which may make it more difficult to perform MAOS measurements when the higher harmonics are small. It also does not provide a consistent strain, while a simple geometry (such as a capillary or narrow slit) can be used to make calculations of the shear rate possible, the entry and exit effects could still have a noticeable effect. However it will be a useful tool to explore the origins of the LAOS behaviour seen in the shear rheometer, to explore what are the effects of the open sides.

5.4.1 Experimental

Material used was PBD310K as characterised by SAOS in Chapter 2. Approximately 10 g was loaded into the MPR fitted with a slit, 5 mm long, 2 mm wide and 10 mm deep. The heated jackets were used to bring the temperature of the polymer to 70 °C. The MPR was operated in oscillatory mode, performing amplitude sweeps from 0.01 mm to 20 mm amplitude at a frequency of 0.164 Hz.

The results were Fourier transformed using MATLAB code written for the purpose. The code is virtually identical to that described in Section 5.1, the only difference being that the strain and frequency are extracted from the strain curves rather than using the values reported by the rheometer. This is due to the MPR sometimes giving strains significantly different to those reported, especially at the upper and lower limits of its range.

5.4.2 Results: Comparison of LAOS in the MPR and rotational rheometer

During the experiments, one issue was that the response was found to lag, i.e. the response was as shown in Figure 5.22. This effect was reduced by increasing the pressure initial applied to the sample, but was still present for the higher strain amplitudes. However comparing results where it is present to those where it is not, it does not appear to have had a significant effect on the parameters extracted from the Fourier transform.

Despite this, it is seen that the MPR produces results that are in line with those obtained from the shear rheometer (Figure 5.23). However, there is a clear difference in that the moduli drop off significantly less at high strain rates.

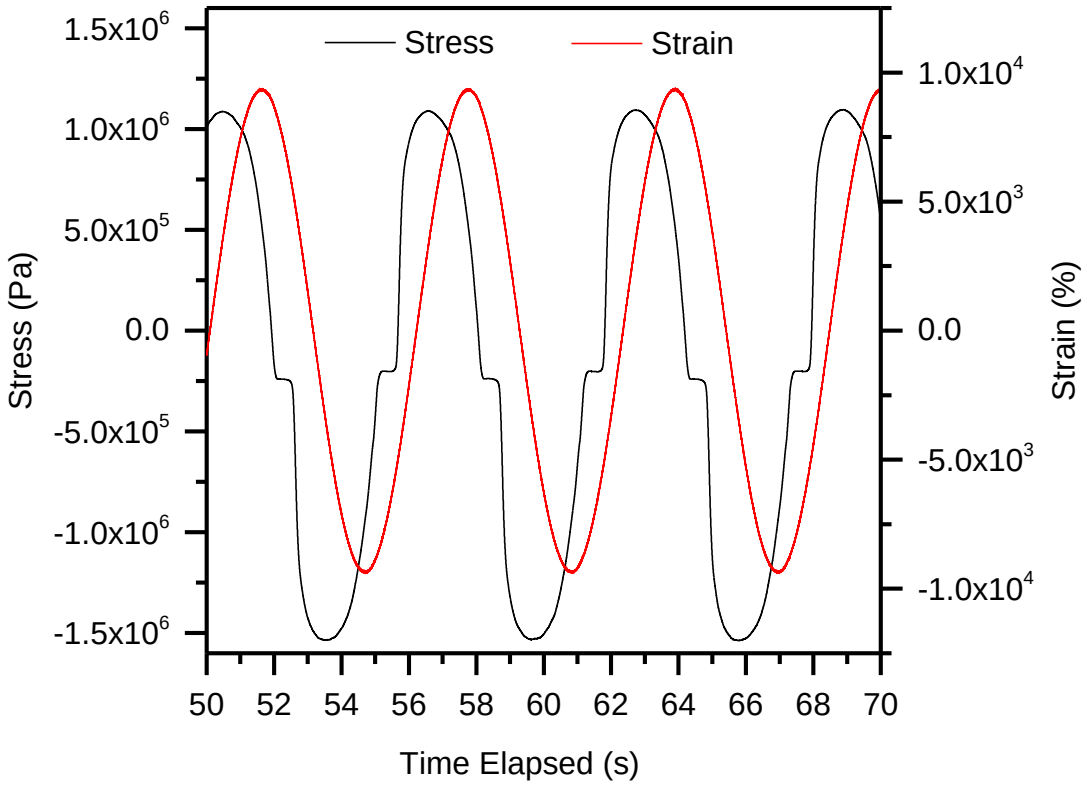

Figure 5.22: Section of an oscillation at 0.16 Hz, 70 °C and 10 mm amplitude for Aldrich polybutadiene, demonstrating the lag when the pistons change direction and one piston loses contact with the sample for a short time.

There is little overlap between the values of the third harmonic reported by the MPR and the shear rheometer, because the noise in the MPR measurements are much higher, making the low strain values much higher than the shear rheometer and at the strains when the MPR produces signal above the noise, the shear rheometer results have already become irregular (Figure 5.24).

5.4.3 Discussion: Comparison of LAOS in the MPR and rotational rheometer

The difference in the values of G' and G'' between the shear rheometer and MPR is likely caused by the wall shear rate used which ignores the entrance and exit effects. Despite the shift to lower values, the difference between MPR and shear rheometer values (20 - 40 %) is consistent with earlier work that reported that the MPR gave values 20 % different to a shear rheometer (this work used a capillary where the shear is slightly easier to define, hence the improved match).

The early drop off in G' and G'' for the shear rheometer compared with the MPR indicates demonstrates that the open sides in the shear rheometer are causing the drop of seen in our amplitude sweeps. This helps to explain why the sample rate and geometry had a large effect on the earlier LAOS results. The behaviour in the

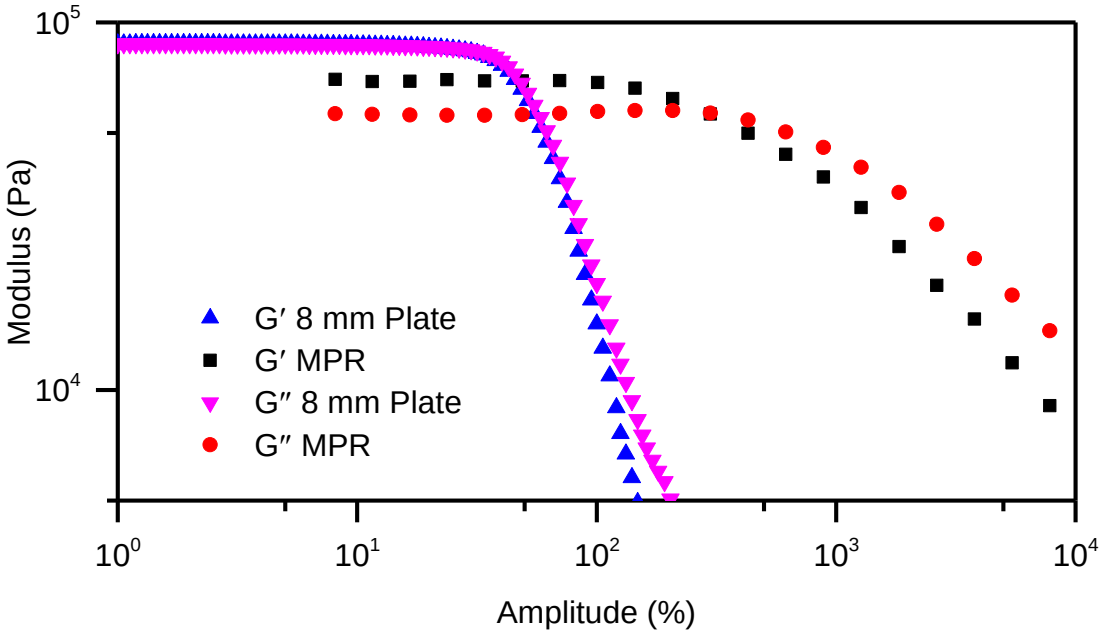

Figure 5.23: Comparison of the linear parameters G' and G'' of PBD310K measured on the MPR and using an 8 mm parallel plate on the shear rheometer.

LAOS region is caused by sample squeezing out of the gap, edge fracture and wall slip, hence it will be dependent on the experiment and difficult to model. However this does not mean that the trends seen cannot be used to distinguish architecture, if the experiment is kept consistent enough to create reproducible results.

The I_3 and I_1 results show that the MPR and shear rheometer allow a wide range of

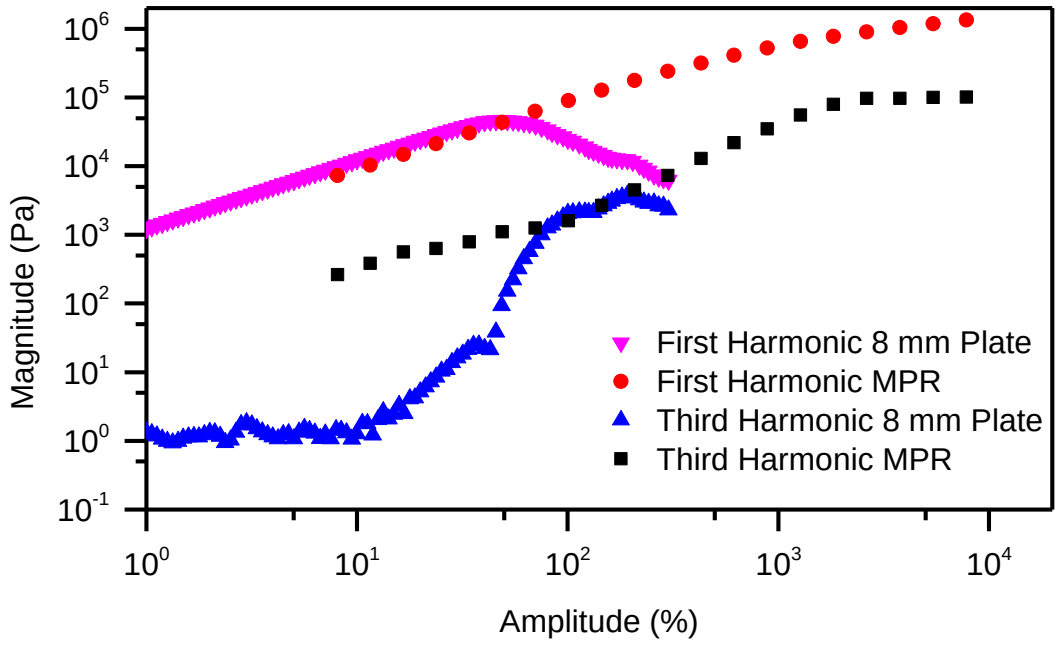

Figure 5.24: Comparison of the first and third harmonics of PBD310K measured on the MPR and using an 8 mm parallel plate on the shear rheometer.

strain rates to be covered, however more optimisation of either the MPR experiments (to reduce error) or the shear rheometry (to reduce edge effects) is required to obtain I_3 continuously over the whole strain range.

5.4.4 Conclusions

The MPR has produced reproducible LAOS data that can be used to help better explain the results from the shear rheometer. Although it does not produce pure shear, removing the effects of edge fracture and sample escaping the geometry allows much higher strains to be reached. Further adaptations could make the MPR an excellent tool for LAOS measurements. It may be preferable to use a capillary geometry, which prevents the fringes being observed (but here this is not a problem due to the number of fringes far exceeding the observable limit), however makes the strain better defined and easier to model (due to its symmetry). Also more accurate pressure transducers and a higher transfer rate would improve the signal to noise ratio and potentially allow MAOS measurements which require much better resolution. If these steps were taken the MPR could be an excellent method for high strain measurements.

5.5 Concluding remarks

This chapter details a systematic study of the behaviour in LAOS of polymer melts with varying structure, using CDRheo MATLAB code written for the purpose. There was seen a significant difference in the LAOS behaviour of linear and branched polymers, but it was unclear whether this was a due to non-linear flow or the influence of effects such as slip.

Medium amplitude oscillatory shear was also explored for a range of polyisoprenes and polybutadienes. Phase and magnitude data was extracted for the first time for these materials, and a crossover in $G3'$ and $G3''$ was observed, which was attributed to Rouse behaviour of the polymer. Rolie-poly theory predicted the behaviour well but with a systematic shift in frequency, which could provide a basis for refinement of existing constitutive models.

The multi-pass rheometer is also shown to be useful as a tool for Fourier transform rheology, and with some relatively small modifications would be a powerful tool for LAOS and MAOS measurements and allow non-linear behaviour to be studied at much higher strains than is possible in a rotational rheometer.

Both MAOS and LAOS are shown to be useful in gaining additional information form rheological measurements. MAOS shows little sensitivity to structure, but gaining information about the Rouse behaviour of the polymer could be useful in determining the chain lengths present in a material. It would be interesting in the future to study the behaviour of highly branched materials, which may show interesting chain stretching effects. LAOS however, is much more sensitive to structure. Although it is difficult to extract quantitatively the structure of polymers using LAOS, it has shown promise for the detection of components in a mixture. This is particularly interesting because it shows little dependence on molecular weight or polydispersity.

6 Conclusions and future work

In this thesis, a range of rheological techniques have been used and evaluated in terms of their ability to give information about polymer melts, particularly those relevant to tyre manufacture.

The linear rheology of a range of polyisoprenes and polybutadienes was quantified, starting from linear monodisperse material and moving to those with more complex structure. The materials were fit with various models most notably Likhtman-McLeish linear theory for monodisperse linear polymers and branch-on-branch theory for materials with more complex structure. BOB theory was shown to be very useful for making predictions from rheology and it was possible to extract fractions from a blend with knowledge of the pure components.

It was also demonstrated that via a turning point in the elastic modulus and extrapolation both the binodal and spinodal temperatures of a polymer blend can be determined by rheology, even using a blend of very similar polymers (here PBD/PI), which can be difficult to determine by other methods due to their similar refractive indexes.

The Cox-Merz rule was validated for an example polystyrene by comparison of complex viscosity from oscillatory measurements to shear viscosity measured on both rotational and capillary rheometer.

The Sentmanat extensional rheometer (SER) was used to measure extensional rheology and it was found to be useful for identifying the general behaviour of these materials with extension, however necking and early rupture prevented steady state being reached for higher strain rates. Alternative methods of extension were studied, firstly capillary breakup extensional rheometry (CaBER) which is usually used to study low viscosity solutions, was applied to polymer melts. It was shown to give a good indication of the presence of multiple branch points in a sample when the material was too low in viscosity to be loaded into the SER. Finally, a novel method of studying extensional properties was attempted, the use of falling weights, with imaging of the filament diameter over time. This gave more quantitative data than the CaBER due to knowledge of the force on the filament, but since the extension rate was constantly changing in an experiment, could only give transient extensional viscosities rather than values at steady state.

Polystyrene was studied flowing through a narrow slit in the MPR, and a stress optical coefficient of 4.9 Pa^{-1} was obtained. The decays of both stress and pressure after the pistons were stopped were examined. They were found to speed up at higher temperatures, which was expected due to the reduced viscosity allowing faster relaxation. Piston speed (and the corresponding shear rate) was found to have little effect on the rate of the decays, however could move the relaxation into different regimes (i.e. reptation, Rouse) which introduced new components into the decay. Three regimes were identified, firstly a fast decay that was found to be caused by apparatus compliance due to an overshoot in the retreating piston. There was also observed an early and a late decay which aligned well with the Rouse and reptation regimes respectively. Increasing the pressure during the measurement was seen to slow the rate of decay of both ear and late relaxations.

A cross-slot was used in the MPR to study extensional flow. It was found to enable measurement at much higher strains than the SER apparatus and allow measurement of extensional viscosity at steady state for rubbery polymers which would break up in the SER. In order to reach all regions of the Weissenberg numbers, polymers with a high number of entanglements at low temperatures are required. However, using suitable polymers, it was found that the method of measuring stress, via fringe counting, was impossible at all but very low speeds due to the number of fringes. One way of reducing the number of fringes was using a shallow cross-slot, however the approximation of 2D flow then breaks down and it is not clear how the number of stress fringes relate to the actual stress in the polymer.

One way to extend this work would be to perform measurements on a narrow slit with a shallow depth, since the pressure drop could be measured in this case, the relationship between the number of fringes are the wall shear stress (measured from the geometry dimensions) could be explored. It may then be possible to calculate a new value of the SOC which could be used with the given depth of geometry, and applied to the shallow cross-slot measurements, which would enable extensional viscosities to be extracted at higher shear rates.

Finally, novel rheological measurements were performed in the form of medium and large amplitude oscillatory shear (MAOS/LAOS). The measurements reported here are well-controlled and analysed experiments for rubbery materials that have been little reported in the literature due to the effects of edge fracture, sample escaping the gap and slip which can be present at these high strains. LAOS measurements were shown to be highly dependent on the structure, in particular linear polymers

showed a remarkably different response to branched. Although the LAOS amplitude sweeps were not necessarily free of all the effects mentioned, there were reproducible and could be used to distinguish polymer structure. The behaviour of blends was intermediate between that of the two components however the relationship was not linear, and so while the components in a blend could be identified, the proportions of each could not be quantitatively extracted.

In the MAOS results, great care was taken to ensure the results were free of slip of fracture effects. The results reported are the first to report both phase and magnitude data for rubbery polymers, and cover a range of linear polymers, star polymers and blends. The behaviour observed in the third harmonic showed little dependence on the structure, and was deemed to be dependent on the Rouse behaviour of the polymer. A single mode rolie-poly model supported this conclusion, although even with multiple modes, there was a frequency shift between the model and the experimental results. This may suggest there are improvements to be made to constitutive models to capture this difference. The results here are notable because the technique allows Rouse behaviour to be studied at low frequency and potentially for polymers (e.g. polydisperse materials) for which Rouse times are unclear from linear rheology. The next steps to take in this work are to attempt to capture the experimental data better in a model, either by incorporating additional considerations into the rolie-poly model, or by moving to an alternative constitutive model or even simulation approach. If the differences can be eliminated, then fitting the model to experimental results could provide a method for extracting Rouse times for materials where this is otherwise difficult or impossible.

Overall, rheology has been shown to be highly useful in determining polymer structure. A summary of the key results that can be obtained for linear and star polymers is shown in Figures 6.1 and 6.2, which demonstrate the applicability of different rheological techniques. SAOS is the most easy to perform and widely available technique, which when combined with molecular models, offers a great tool for structure prediction. However this relies heavily on the models, for example comparing linear and star polymers, no inherent difference in the rheology is seen according to structure that can be separated from other polymer characteristics, e.g. molecular weight. Modern models increase the complexity of systems that can be predicted, but this is reaching a limit since rheology is not unique, and the more complexity introduced, the greater the number of possible combinations of components that can give the same response. Hence novel techniques such as those detailed here, will increasingly be required.

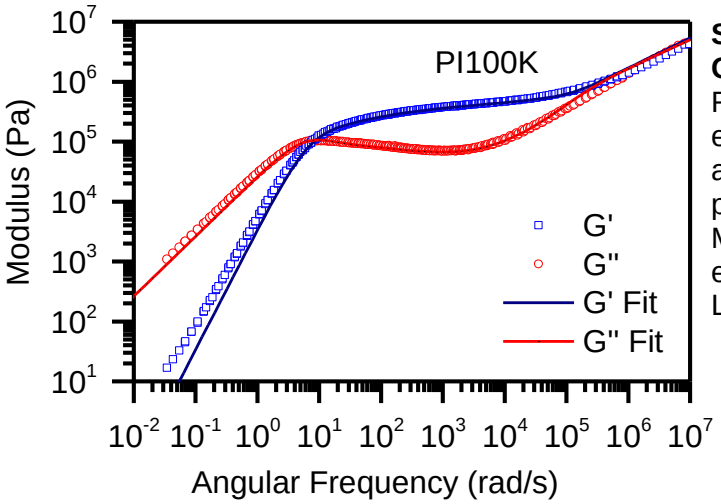

Small Amplitude Oscillatory Shear
Reptation time can be extracted from the crossover and Rouse time from the plateau in G''
Materials parameters can be extracted from fits (e.g. Linear theory)

Linear Polymers

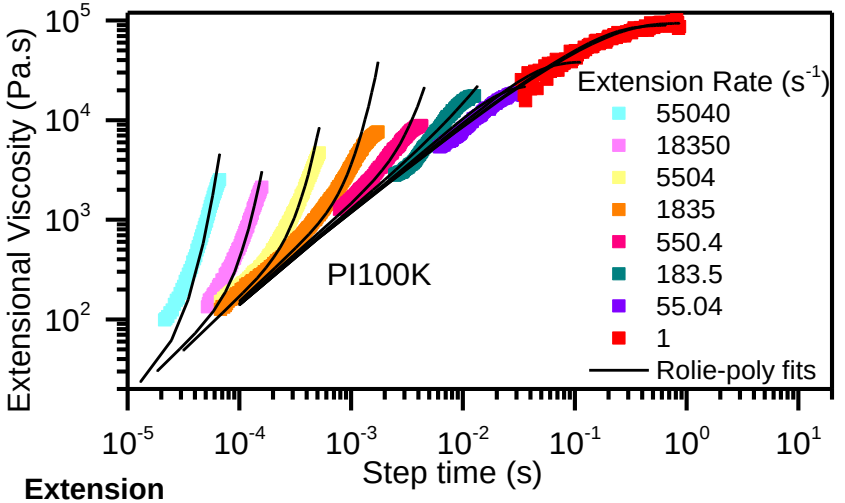

Extension
Response is linear until rate is fast enough to stretch individual chains, when strain hardening is seen.
Fitting (e.g. rolie-poly) gives chain stretch time of polymer
This is seen at lower rates the higher the molecular weight.

Medium Amplitude Oscillatory Shear
A crossover in $G3'$, $G3''$ can be observed which is related to the chain stretch time and is dependent on the chain length

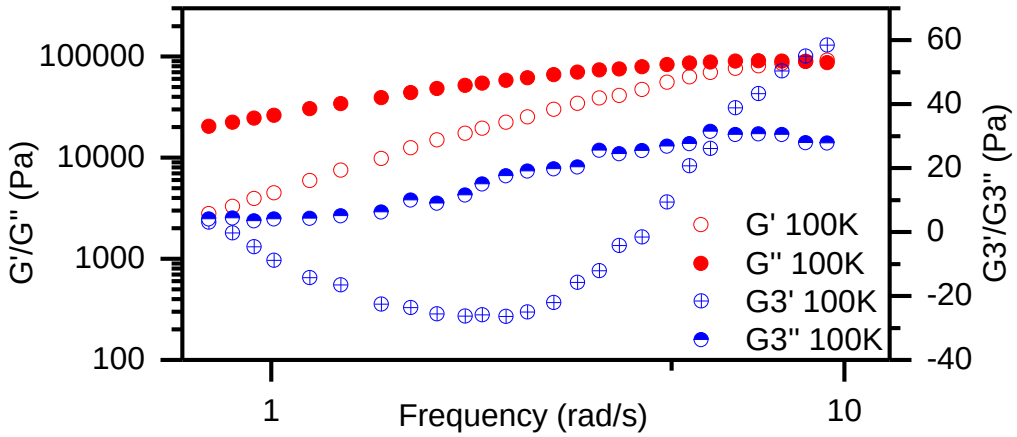

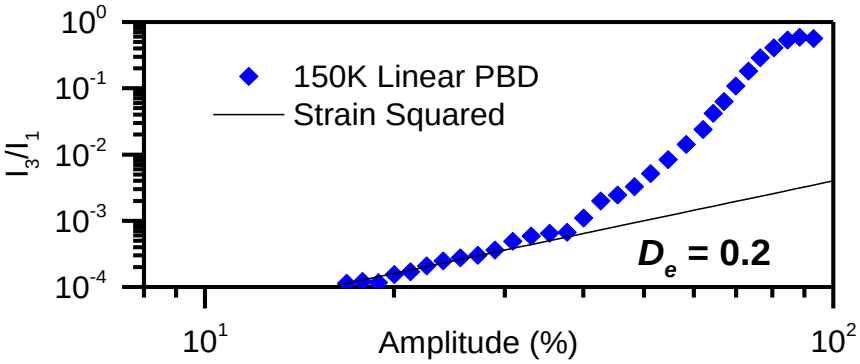

Large Amplitude Oscillatory Shear
At low strains, behaviour is linear (I_3/I_1 scales with strain squared) but large increases in non-linearity are observed at higher strains

Figure 6.1: Comparison of rheological results obtained for linear polymers

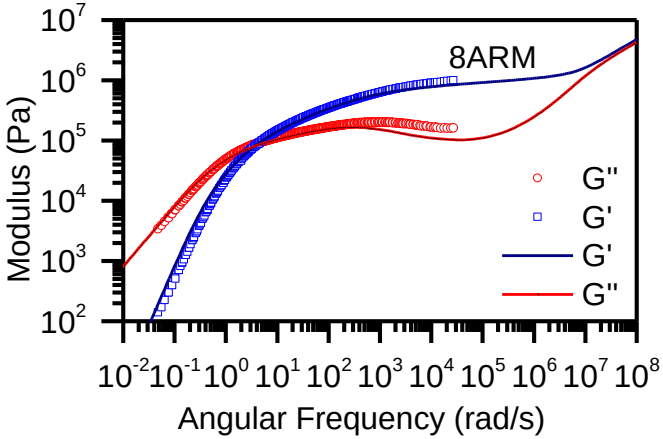

Small Amplitude Oscillatory Shear
Rheology dependant on arm length and virtually independent of number of arms
Materials parameters can be extracted from fits (e.g. BOB theory)
Compared to linear polymers of similar molecular weight:
- Higher moduli
- Longer relaxation times ($G^{'}$, G'' crossover at lower frequency)
- Rubbery plateaus over a large frequency range

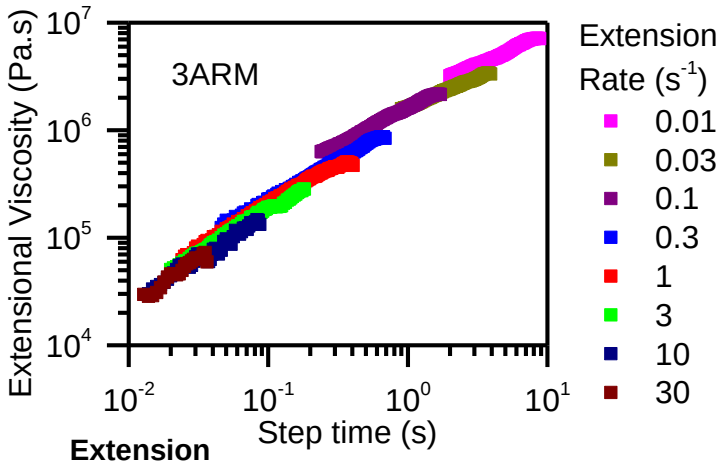

Extension
Single branch point leads to no additional strain hardening beyond that seen for stretching of the individual arms

Medium Amplitude Oscillatory Shear
Crossover in $G3'$, $G3''$ observed similar to a linear polymer. The crossover is dependent on the chain stretch time and so is only dependent on arm molecular weight

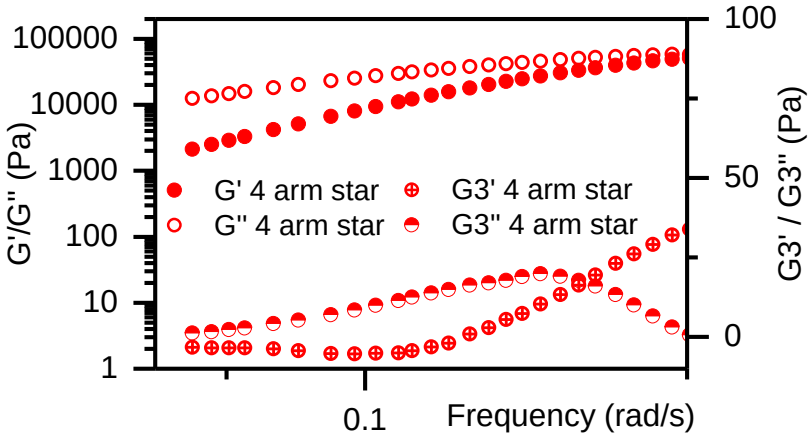

Star Polymers

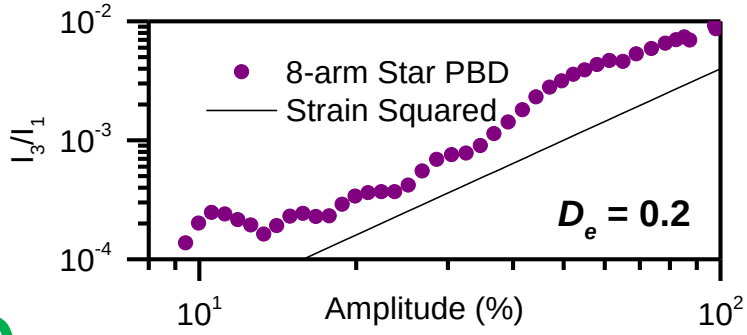

Large Amplitude Oscillatory Shear
Virtually linear behaviour at all strains (I_3/I_1 scales with strain squared). Much lower non-linearity seen than in linear materials

Figure 6.2: Comparison of rheological results obtained for star polymers

Extensional techniques are a natural progression, and using extensional results alongside linear rheology provides a more individual description of the material (but still not necessarily unique). For systems with multiple branch points, strain hardening is observed which can allow characterisation of the level of branching. However for star polymers with a single branch point, no additional strain hardening is seen above the effect of chain stretching of the individual arms. This does not mean extension provides no information for star polymers, as the reduced strain hardening compared to a linear polymer of similar total molecular weight is indicative of a star structure. Extension can be very difficult to realise experimentally, which does limit its applicability, especially when the samples have particularly high or low viscosities.

LAOS and MAOS show a great deal of promise for elucidating polymer structure. MAOS results can give insight into the Rouse behaviour of the polymer, but this is not dependent on structure and so linear and star polymers show little difference in their MAOS behaviour. LAOS is much more sensitive to structure, and clear differences are observed between linear and star structures which can be used to identify the structure present. Currently, both techniques can only provide qualitative descriptions of the material and are time-consuming to perform. However, they provide a wealth of information and with the advent of new molecular models to describe their results and experimental techniques to simplify data collection (such as an advanced MPR), they could hold the most potential for the future of rheology.

7 Bibliography

1. Malkin, A. Y.; Isayev, A. I., *Rheology: Concepts, Methods, and Applications*. ChemTec Pub., 2006.
2. Ferry, J. D., *Viscoelastic Properties of Polymers*. Wiley, 1980.
3. Mezger, T. G., *The Rheology Handbook: For Users of Rotational and Oscillatory Rheometers*. Vincentz Network, 2006.
4. Prentice, P., *Rheology and Its Role in Plastics Processing*. Rapra Technology, 1995.
5. Gauthier Jr, J., Rheology and Settling Dynamics of a Particle Filled Aqueous Polymer Gel for Hydraulic Fracturing Fluid Systems. Ohio State College of Engineering, 2015.
6. Weissenberg, K., A Continuum Theory of Rheological Phenomena. *Nature* **1947,** *159*, 310-311.
7. Morris, V. J.; Chilvers, G. R., Rheological studies on specific ion forms of ι-carrageenate gels. *Journal of the Science of Food and Agriculture* **1981,** *32* (12), 1235-1241.
8. Mead, D. W.; Monjezi, S.; Park, J., A constitutive model for entangled polydisperse linear flexible polymers with entanglement dynamics and a configuration dependent friction coefficient. Part II. Modeling "shear modification" following cessation of fast shear flows. *Journal of Rheology* **2018,** *62* (1), 135-147.
9. Wang, M.-J., Effect of Polymer-Filler and Filler-Filler Interactions on Dynamic Properties of Filled Vulcanizates. *Rubber Chemistry and Technology* **1998,** *71* (3), 520-589.
10. Ramirez, J.; Likhtman, A. E., Rheology of Entangled Polymers: Toolbox for the Analysis of Theory and Experiments (Reptate, http://reptate.com).
11. Mackley, M.; Marshall, R.; Smeulders, J., The multipass rheometer. *Journal of Rheology* **1995,** *39* (6), 1293-1309.
12. Pfitzner, J., Poiseuille and his law. *Anaesthesia* **1976,** *31* (2), 273-275.
13. Bagley, E., End corrections in the capillary flow of polyethylene. *Journal of Applied Physics* **1957,** *28* (5), 624-627.
14. Aho, J., Evaluation of different methods for determining the entrance pressure drop in capillary rheometry. *Applied Rheology* **2008,** *18* (6), 63258.
15. Wang, Z. Y.; Joshi, S. C.; Lam, Y. C.; Chen, X., End pressure corrections in capillary rheometry of concentrated suspensions. *Journal of Applied Polymer Science* **2009,** *114* (3), 1738-1745.
16. Cogswell, F. N., Converging flow of polymer melts in extrusion dies. *Polymer Engineering & Science* **1972,** *12* (1), 64-73.
17. Binding, D. M., An approximate analysis for contraction and converging flows. *Journal of Non-Newtonian Fluid Mechanics* **1988,** *27* (2), 173-189.
18. Binding, D. M.; Couch, M. A.; Walters, K., The pressure dependence of the shear and elongational properties of polymer melts. *Journal of Non-Newtonian Fluid Mechanics* **1998,** *79* (2), 137-155.
19. Musil, J.; Zatloukal, M., Entry flow vortices in polymer melt extrusion: A review. *AIP Conference Proceedings* **2017,** *1843* (1), 030004.
20. Winter, H. H., Capillary Rheometry. *Encyclopedia of Life Systems (EOLSS) UNESCO* **2008**.
21. Hatzikiriakos, S. G.; Dealy, J. M., Wall slip of molten high density polyethylenes. II. Capillary rheometer studies. *Journal of Rheology (1978-present)* **1992,** *36* (4), 703-741.
22. Sentmanat, M., Miniature universal testing platform: from extensional melt rheology to solid-state deformation behavior. *Rheologica Acta* **2004,** *43* (6), 657-669.
23. Aho, J.; Rolón-Garrido, V.; Syrjälä, S.; Wagner, M., Measurement technique and data analysis of extensional viscosity for polymer melts by Sentmanat extensional rheometer (SER). *Rheologica Acta* **2010,** *49* (4), 359-370.

24. McKinley, G. H., Visco-elastic capillary thinning and break-up of complex fluids. *Rheology Reviews* **2005**, 1-48.
25. McKinley, G. H.; Sridhar, T., Filament-Stretching Rheometry of Complex Fluids. *Annual Review of Fluid Mechanics* **2002,** *34* (1), 375-415.
26. Mackley, M. R.; Butler, S. A.; Huxley, S.; Reis, N. M.; Barbosa, A. I.; Tembely, M., The observation and evaluation of extensional filament deformation and breakup profiles for Non Newtonian fluids using a high strain rate double piston apparatus. *Journal of Non-Newtonian Fluid Mechanics* **2017,** *239* (Supplement C), 13-27.
27. Mackley, M. R.; Spitteler, P. H. J., Experimental observations on the pressure-dependent polymer melt rheology of linear low density polyethylene, using a multi-pass rheometer. *Rheologica Acta* **1996,** *35* (2), 202-209.
28. Rabinowitsch, B., Über die viskosität und elastizität von solen. *Zeitschrift für physikalische Chemie* **1929,** *145* (1), 1-26.
29. Mackley, M. R.; Hassell, D. G., The multipass rheometer a review. *Journal of Non-Newtonian Fluid Mechanics* **2011,** *166* (9–10), 421-456.
30. Ranganathan, M.; Mackley, M.; Spitteler, P., The application of the multipass rheometer to time-dependent capillary flow measurements of a polyethylene melt. *Journal of Rheology (1978-present)* **1999,** *43* (2), 443-451.
31. Durand, V.; Vergnes, B.; Agassant, J. F.; Benoit, E.; Koopmans, R. J., Experimental study and modeling of oscillating flow of high density polyethylenes. *Journal of Rheology (1978-present)* **1996,** *40* (3), 383-394.
32. Molenaar, J.; Koopmans, R. J., Modeling polymer melt-flow instabilities. *Journal of Rheology (1978-present)* **1994,** *38* (1), 99-109.
33. Scelsi, L.; Mackley, M. R., Rheo-optic flow-induced crystallisation of polypropylene and polyethylene within confined entry-exit flow geometries. *Rheologica Acta* **2008,** *47* (8), 895-908.
34. Lee, K.; Lacombe, Y.; Cheluget, E., A Novel Method of Measuring the Phase Behavior and Rheology of Polyethylene Solutions Using a Multi-Pass Rheometer. *AIP Conference Proceedings* **2008,** *1027* (1), 1174-1176.
35. Engmann, J.; Mackley, M. R., Semi-Solid Processing of Chocolate and Cocoa Butter: The Experimental Correlation of Process Rheology with Microstructure. *Food and Bioproducts Processing* **2006,** *84* (2), 95-101.
36. Lee, K.; Mackley, M. R., The application of the multi-pass rheometer for precise rheo-optic characterisation of polyethylene melts. *Chemical Engineering Science* **2001,** *56* (19), 5653-5661.
37. Taylor, G. I., *The Formation of Emulsions in Definable Fields of Flow*. 1934; Vol. 146, p 501-523.
38. Crowley, D. G.; Frank, F. C.; Mackley, M. R.; Stephenson, R. G., Localized flow birefringence of polyethylene oxide solutions in a four roll mill. *Journal of Polymer Science: Polymer Physics Edition* **1976,** *14* (6), 1111-1119.
39. Coventry, K. D.; Mackley, M. R., Cross-slot extensional flow birefringence observations of polymer melts using a multi-pass rheometer. *Journal of Rheology (1978-present)* **2008,** *52* (2), 401-415.
40. Coventry, K., Cross-slot rheology of polymers. University of Cambridge, 2006.
41. Collis, M. W.; Mackley, M. R., The melt processing of monodisperse and polydisperse polystyrene melts within a slit entry and exit flow. *Journal of Non-Newtonian Fluid Mechanics* **2005,** *128* (1), 29-41.
42. Guaily, A.; Cheluget, E.; Lee, K.; Epstein, M., A new hyperbolic model and an experimental study for the flow of polymer melts in Multi-Pass Rheometer. *Computers & Fluids* **2011,** *44* (1), 258-266.
43. Teraoka, I., *Polymer Solutions: An Introduction to Physical Properties*. Wiley, 2002.

44. Rouse, P. E., A Theory of the Linear Viscoelastic Properties of Dilute Solutions of Coiling Polymers. *The Journal of Chemical Physics* **1953,** *21* (7), 1272-1280.
45. Read, D. J., From reactor to rheology in industrial polymers. *Journal of Polymer Science Part B: Polymer Physics* **2014**.
46. Doi, M.; Edwards, S. F., Dynamics of concentrated polymer systems. Part 1.-Brownian motion in the equilibrium state. *Journal of the Chemical Society, Faraday Transactions 2: Molecular and Chemical Physics* **1978,** *74*, 1789-1801.
47. Doi, M.; Edwards, S. F., Dynamics of concentrated polymer systems. Part 2.-Molecular motion under flow. *Journal of the Chemical Society, Faraday Transactions 2: Molecular and Chemical Physics* **1978,** *74*, 1802-1817.
48. Doi, M.; Edwards, S. F., Dynamics of concentrated polymer systems. Part 3.-The constitutive equation. *Journal of the Chemical Society, Faraday Transactions 2: Molecular and Chemical Physics* **1978,** *74*, 1818-1832.
49. Doi, M.; Edwards, S. F., Dynamics of concentrated polymer systems. Part 4.-Rheological properties. *Journal of the Chemical Society, Faraday Transactions 2: Molecular and Chemical Physics* **1979,** *75*, 38-54.
50. de Gennes, P. G., Reptation of a Polymer Chain in the Presence of Fixed Obstacles. *The Journal of Chemical Physics* **1971,** *55* (2), 572-579.
51. de Gennes, P., Reptation of stars. *Journal de Physique* **1975,** *36* (12), 1199-1203.
52. Likhtman, A. E.; McLeish, T. C. B., Quantitative Theory for Linear Dynamics of Linear Entangled Polymers. *Macromolecules* **2002,** *35* (16), 6332-6343.
53. Milner, S. T.; McLeish, T. C. B., Reptation and Contour-Length Fluctuations in Melts of Linear Polymers. *Physical Review Letters* **1998,** *81* (3), 725-728.
54. Fetters, L. J.; Lohse, D. J.; Graessley, W. W., Chain dimensions and entanglement spacings in dense macromolecular systems. *Journal of Polymer Science Part B: Polymer Physics* **1999,** *37* (10), 1023-1033.
55. Graham, R. S.; Likhtman, A. E.; McLeish, T. C. B.; Milner, S. T., Microscopic theory of linear, entangled polymer chains under rapid deformation including chain stretch and convective constraint release. *Journal of Rheology* **2003,** *47* (5), 1171-1200.
56. Likhtman, A. E.; Graham, R. S., Simple constitutive equation for linear polymer melts derived from molecular theory: Rolie–Poly equation. *Journal of Non-Newtonian Fluid Mechanics* **2003,** *114* (1), 1-12.
57. Harlen, O. G.; Rallison, J. M.; Szabo, P., A split Lagrangian-Eulerian method for simulating transient viscoelastic flows. *Journal of Non-Newtonian Fluid Mechanics* **1995,** *60* (1), 81-104.
58. van Ruymbeke, E.; Keunings, R.; Stéphenne, V.; Hagenaars, A.; Bailly, C., Evaluation of Reptation Models for Predicting the Linear Viscoelastic Properties of Entangled Linear Polymers. *Macromolecules* **2002,** *35* (7), 2689-2699.
59. Cloizeaux, J. d., Double Reptation vs. Simple Reptation in Polymer Melts. *EPL (Europhysics Letters)* **1988,** *5* (5), 437.
60. Milner, S. T., Relating the shear-thinning curve to the molecular weight distribution in linear polymer melts. *Journal of Rheology (1978-present)* **1996,** *40* (2), 303-315.
61. Colley, F. R.; Collins, S. A.; Richards, R. W., Tracer diffusion of four arm polystyrene star molecules into linear and star polymer matrices from nuclear reaction analysis. *Journal of Materials Chemistry* **2003,** *13* (11), 2765-2770.
62. Clarke, N.; McLeish, T. C. B., Kinetics of concentration fluctuations and spinodal decomposition in star star and star linear polymer blends. *J. Chem. Phys.* **1993,** *99* (12), 10034-10040.
63. Pearson, D. S.; Helfand, E., Viscoelastic properties of star-shaped polymers. *Macromolecules* **1984,** *17* (4), 888-895.
64. Ball, R. C.; McLeish, T. C. B., Dynamic dilution and the viscosity of star-polymer melts. *Macromolecules* **1989,** *22* (4), 1911-13.

65. Adams, C. H.; Hutchings, L. R.; Klein, P. G.; McLeish, T. C. B.; Richards, R. W., Synthesis and Dynamic Rheological Behavior of Polybutadiene Star Polymers. *Macromolecules* **1996,** *29* (17), 5717-5722.
66. Vega, J. F.; Rastogi, S.; Peters, G. W. M.; Meijer, H. E. H., Rheology and reptation of linear polymers. Ultrahigh molecular weight chain dynamics in the melt. *Journal of Rheology* **2004,** *48* (3), 663-678.
67. Larson, R. G., Combinatorial Rheology of Branched Polymer Melts. *Macromolecules* **2001,** *34* (13), 4556-4571.
68. Park, S. J.; Shanbhag, S.; Larson, R. G., A hierarchical algorithm for predicting the linear viscoelastic properties of polymer melts with long-chain branching. *Rheologica Acta* **2005,** *44* (3), 319-330.
69. Park, S. J.; Larson, R. G., Modeling the linear viscoelastic properties of metallocene-catalyzed high density polyethylenes with long-chain branching. *Journal of Rheology* **2005,** *49* (2), 523-536.
70. Das, C.; Inkson, N. J.; Read, D. J.; Kelmanson, M. A.; McLeish, T. C. B., Computational linear rheology of general branch-on-branch polymers. *J. Rheol. (N. Y., NY, U. S.)* **2006,** *50* (2), 207-234.
71. Phan-Thien, N., *Understanding Viscoelasticity: Basics of Rheology*. Springer Berlin Heidelberg, 2013.
72. Pathak, J. A.; Kumar, S. K.; Colby, R. H., Miscible Polymer Blend Dynamics: Double Reptation Predictions of Linear Viscoelasticity in Model Blends of Polyisoprene and Poly(vinyl ethylene). *Macromolecules* **2004,** *37* (18), 6994-7000.
73. Eitouni, H. B.; Balsara, N. P., Thermodynamics of Polymer Blends. In *Physical Properties of Polymers Handbook*, Mark, J. E., Ed. Springer New York, New York, NY, 2007; pp 339-356.
74. Mark, J. E., *Physical Properties of Polymers Handbook*. Springer, 2007.
75. Flory, P. J., Thermodynamics of High Polymer Solutions. *The Journal of Chemical Physics* **1941,** *9* (8), 660-660.
76. Huggins, M. L., Solutions of Long Chain Compounds. *The Journal of Chemical Physics* **1941,** *9* (5), 440-440.
77. Scott, R. L., Thermodynamics of high polymer solutions. VI. The compatibility of copolymers. *Journal of Polymer Science* **1952,** *9* (5), 423-432.
78. Owens, J. N.; Gancarz, I. S.; Koberstein, J. T.; Russell, T. P., Investigation of the microphase separation transition in low-molecular-weight diblock copolymers. *Macromolecules* **1989,** *22* (8), 3380-3387.
79. Kapnistos, M.; Hinrichs, A.; Vlassopoulos, D.; Anastasiadis, S. H.; Stammer, A.; Wolf, B. A., Rheology of a Lower Critical Solution Temperature Binary Polymer Blend in the Homogeneous, Phase-Separated, and Transitional Regimes. *Macromolecules* **1996,** *29* (22), 7155-7163.
80. Kapnistos, M.; Vlassopoulos, D.; Anastasiadis, S. H., Determination of both the binodal and the spinodal curves in polymer blends by shear rheology. *EPL (Europhysics Letters)* **1996,** *34* (7), 513.
81. Fredrickson, G. H.; Larson, R. G., Viscoelasticity of homogeneous polymer melts near a critical point. *The Journal of Chemical Physics* **1987,** *86* (3), 1553-1560.
82. Zhang, R.; Cheng, H.; Zhang, C.; Sun, T.; Dong, X.; Han, C. C., Phase Separation Mechanism of Polybutadiene/Polyisoprene Blends under Oscillatory Shear Flow. *Macromolecules* **2008,** *41* (18), 6818-6829.
83. Zou, F.; Dong, X.; Liu, W.; Yang, J.; Lin, D.; Liang, A.; Li, W.; Han, C. C., Shear Induced Phase Boundary Shift in the Critical and Off-Critical Regions for a Polybutadiene/Polyisoprene Blend. *Macromolecules* **2012,** *45* (3), 1692-1700.

84. Liu, W.; Dong, X.; Zou, F.; Yang, J.; Wang, D.; Han, C. C., Rheological properties of polybutadiene/polyisoprene blend in the unstable and metastable regions under oscillatory shear. *Polymer* **2014,** *55* (11), 2744-2750.
85. Pearson, D. S.; Rochefort, W. E., Behavior of concentrated polystyrene solutions in large-amplitude oscillating shear fields. *Journal of Polymer Science: Polymer Physics Edition* **1982,** *20* (1), 83-98.
86. Hyun, K.; Wilhelm, M.; Klein, C. O.; Cho, K. S.; Nam, J. G.; Ahn, K. H.; Lee, S. J.; Ewoldt, R. H.; McKinley, G. H., A review of nonlinear oscillatory shear tests: Analysis and application of large amplitude oscillatory shear (LAOS). *Progress in Polymer Science* **2011,** *36* (12), 1697-1753.
87. Hemingway, E. J.; Kusumaatmaja, H.; Fielding, S. M., Edge Fracture in Complex Fluids. *Physical Review Letters* **2017,** *119* (2), 028006.
88. Léger, L.; Hervet, H.; Massey, G.; Durliat, E., Wall slip in polymer melts. *Journal of Physics: Condensed Matter* **1997,** *9* (37), 7719.
89. Sabzevari, S. M.; Cohen, I.; Wood-Adams, P. M., Wall Slip of Bidisperse Linear Polymer Melts. *Macromolecules* **2014,** *47* (9), 3154-3160.
90. Debbaut, B. t.; Burhin, H., Large amplitude oscillatory shear and Fourier-transform rheology for a high-density polyethylene: Experiments and numerical simulation. *Journal of Rheology* **2002,** *46* (5), 1155-1176.
91. Hyun, K.; Kim, S. H.; Ahn, K. H.; Lee, S. J., Large amplitude oscillatory shear as a way to classify the complex fluids. *Journal of Non-Newtonian Fluid Mechanics* **2002,** *107* (1), 51-65.
92. Ma, L. L.; Xu, J. Y.; Coulombe, P.; Wirtz, D., *Keratin Filament Suspensions Show Unique Micromechanical Properties*. 1999; Vol. 274, p 19145-51.
93. Heymann, L.; Peukert, S.; Aksel, N., Investigation of the solid–liquid transition of highly concentrated suspensions in oscillatory amplitude sweeps. *Journal of Rheology* **2002,** *46* (1), 93-112.
94. Wilhelm, M., Fourier-Transform Rheology. *Macromolecular Materials and Engineering* **2002,** *287* (2), 83-105.
95. Hoyle, D. M.; Auhl, D.; Harlen, O. G.; Barroso, V. C.; Wilhelm, M.; McLeish, T. C. B., Large amplitude oscillatory shear and Fourier transform rheology analysis of branched polymer melts. *Journal of Rheology* **2014,** *58* (4), 969-997.
96. Hyun, K.; Ahn, K. H.; Lee, S. J.; Sugimoto, M.; Koyama, K., Degree of branching of polypropylene measured from Fourier-transform rheology. *Rheologica Acta* **2006,** *46* (1), 123-129.
97. Hyun, K.; Baik, E. S.; Ahn, K. H.; Lee, S. J.; Sugimoto, M.; Koyama, K., Fourier-transform rheology under medium amplitude oscillatory shear for linear and branched polymer melts. *Journal of Rheology* **2007,** *51* (6), 1319-1342.
98. Neidhöfer, T.; Wilhelm, M.; Debbaut, B., Fourier-transform rheology experiments and finite-element simulations on linear polystyrene solutions. *Journal of Rheology* **2003,** *47* (6), 1351-1371.
99. Neidhöfer, T.; Sioula, S.; Hadjichristidis, N.; Wilhelm, M., Distinguishing Linear from Star-Branched Polystyrene Solutions with Fourier-Transform Rheology. *Macromolecular rapid communications* **2004,** *25* (22), 1921-1926.
100. Höfl, S.; Kremer, F.; Spiess, H. W.; Wilhelm, M.; Kahle, S., Effect of large amplitude oscillatory shear (LAOS) on the dielectric response of 1,4-cis-polyisoprene. *Polymer* **2006,** *47* (20), 7282-7288.
101. Giacomin, A. J.; Gilbert, P. H.; Merger, D.; Wilhelm, M., Large-amplitude oscillatory shear: comparing parallel-disk with cone-plate flow. *Rheologica Acta* **2015,** *54* (4), 263-285.
102. Poulos, A. S.; Renou, F.; Jacob, A. R.; Koumakis, N.; Petekidis, G., Large amplitude oscillatory shear (LAOS) in model colloidal suspensions and glasses: frequency dependence. *Rheologica Acta* **2015,** *54* (8), 715-724.

103. Cho, K. S.; Hyun, K.; Ahn, K. H.; Lee, S. J., A geometrical interpretation of large amplitude oscillatory shear response. *Journal of Rheology* **2005,** *49* (3), 747-758.
104. Ewoldt, R. H.; Hosoi, A. E.; McKinley, G. H., New measures for characterizing nonlinear viscoelasticity in large amplitude oscillatory shear. *Journal of Rheology* **2008,** *52* (6), 1427-1458.
105. Hyun, K.; Kim, W., A new non-linear parameter Q from FT-Rheology under nonlinear dynamic oscillatory shear for polymer melts system. *Korea-Australia Rheology Journal* **2012,** *23* (4), 227-235.
106. Kempf, M.; Ahirwal, D.; Cziep, M.; Wilhelm, M., Synthesis and Linear and Nonlinear Melt Rheology of Well-Defined Comb Architectures of PS and PpMS with a Low and Controlled Degree of Long-Chain Branching. *Macromolecules* **2013,** *46* (12), 4978-4994.
107. Wagner, M. H.; Rolón-Garrido, V. H.; Hyun, K.; Wilhelm, M., Analysis of medium amplitude oscillatory shear data of entangled linear and model comb polymers. *Journal of Rheology* **2011,** *55* (3), 495-516.
108. Song, H. Y.; Nnyigide, O. S.; Salehiyan, R.; Hyun, K., Investigation of nonlinear rheological behavior of linear and 3-arm star 1,4-cis-polyisoprene (PI) under medium amplitude oscillatory shear (MAOS) flow via FT-rheology. *Polymer* **2016,** *104* (Supplement C), 268-278.
109. Filipe, S.; Vittorias, I.; Wilhelm, M., Experimental Correlation between Mechanical Non-Linearity in LAOS Flow and Capillary Flow Instabilities for Linear and Branched Commercial Polyethylenes. *Macromolecular Materials and Engineering* **2008,** *293* (1), 57-65.
110. Cyriac, F.; Covas, J. A.; Hilliou, L. H. G.; Vittorias, I., Predicting extrusion instabilities of commercial polyethylene from non-linear rheology measurements. *Rheologica Acta* **2014,** *53* (10), 817-829.
111. Dealy, J. M.; Wang, J., *Melt rheology and its applications in the plastics industry*. Springer Science & Business Media, 2013.
112. Barus, C., Note on the Dependence of Viscosity on Pressure and Temperature. *Proceedings of the American Academy of Arts and Sciences* **1891,** *27*, 13-18.
113. Miller, A. A., Analysis of the melt viscosity and glass transition of polystyrene. *Journal of Polymer Science Part A-2: Polymer Physics* **1968,** *6* (6), 1161-1175.
114. Utracki, L. A.; Sedlacek, T., Free volume dependence of polymer viscosity. *Rheologica Acta* **2007,** *46* (4), 479-494.
115. Sedlacek, T.; Zatloukal, M.; Filip, P.; Boldizar, A.; Saha, P., On the effect of pressure on the shear and elongational viscosities of polymer melts. *Polymer Engineering & Science* **2004,** *44* (7), 1328-1337.
116. Kamal, M. R.; Nyun, H., The Effect of Pressure on the Shear Viscosity of Polymer Melts. *Transactions of The Society of Rheology* **1973,** *17* (2), 271-285.
117. Volpe, V.; Pantani, R., Effect of pressure on viscosity at high shear rates by using an injection molding machine. *AIP Conference Proceedings* **2015,** *1695*, 020060.
118. Sorrentino, A.; Pantani, R., Pressure-dependent viscosity and free volume of atactic and syndiotactic polystyrene. *Rheologica Acta* **2009,** *48* (4), 467-478.
119. Cardinaels, R.; Van Puyvelde, P.; Moldenaers, P., Evaluation and comparison of routes to obtain pressure coefficients from high-pressure capillary rheometry data. *Rheologica acta* **2007,** *46* (4), 495-505.
120. Kadijk, S. E.; Van Den Brule, B. H. A. A., On the pressure dependency of the viscosity of molten polymers. *Polymer Engineering & Science* **1994,** *34* (20), 1535-1546.
121. Akdeniz, G.; Yahsi, U.; Tav, C., Viscous behavior of PS, PP, and ABS in terms of temperature and pressure-dependent hole fraction. *Journal of Applied Polymer Science* **2010,** *117* (1), 110-113.

122. Fernández, M.; Muñoz, M. E.; Santamaría, A., A Combined Analysis of PVT and Rheological Measurements: Novel Results for Three Amorphous Polymers. *Macromolecular Chemistry and Physics* **2008,** *209* (16), 1730-1737.
123. Housiadas, K. D., Internal viscoelastic flows for fluids with exponential type pressure-dependent viscosity and relaxation time. *Journal of Rheology* **2015,** *59* (3), 769-791.
124. Tsolou, G.; Harmandaris, V. A.; Mavrantzas, V. G., Molecular dynamics simulation of temperature and pressure effects on the intermediate length scale dynamics and zero shear rate viscosity of cis-1, 4-polybutadiene: Rouse mode analysis and dynamic structure factor spectra. *Journal of Non-Newtonian Fluid Mechanics* **2008,** *152* (1), 184-194.
125. Floudas, G.; Gravalides, C.; Reisinger, T.; Wegner, G., Effect of pressure on the segmental and chain dynamics of polyisoprene. Molecular weight dependence *J. Chem. Phys.* **1999,** *111*, 9847-9852.
126. Das, C.; Inkson, N. J.; Read, D. J.; Kelmanson, M. A.; McLeish, T. C. B., Computational linear rheology of general branch-on-branch polymers. *Journal of Rheology (1978-present)* **2006,** *50* (2), 207-234.
127. Oti, M., The synthesis and characterisation of complex branched polymers by living anionic polymerisation. Durham Univeristy, Durham, 2018.
128. Hadjichristidis, N.; Iatrou, H.; Pispas, S.; Pitsikalis, M., Anionic polymerization: High vacuum techniques. *Journal of Polymer Science Part A: Polymer Chemistry* **2000,** *38* (18), 3211-3234.
129. Smith, R. F.; Boothroyd, S. C.; Thompson, R. L.; Khosravi, E., A facile route for rubber breakdown via cross metathesis reactions. *Green Chemistry* **2016,** *18* (11), 3448-3455.
130. Shapiro, Y., *Analysis of chain microstructure by 1H and 13C NMR spectroscopy*. 1985; Vol. 7, p 27-58.
131. Auhl, D.; Ramirez, J.; Likhtman, A. E.; Chambon, P.; Fernyhough, C., Linear and nonlinear shear flow behavior of monodisperse polyisoprene melts with a large range of molecular weights. *Journal of Rheology (1978-present)* **2008,** *52* (3), 801-835.
132. Tassieri, M.; Laurati, M.; Curtis, D. J.; Auhl, D. W.; Coppola, S.; Scalfati, A.; Hawkins, K.; Williams, P. R.; Cooper, J. M., i-Rheo: Measuring the materials' linear viscoelastic properties “in a step”! *Journal of Rheology* **2016,** *60* (4), 649-660.
133. Abdel-Goad, M.; Pyckhout-Hintzen, W.; Kahle, S.; Allgaier, J.; Richter, D.; Fetters, L. J., Rheological Properties of 1,4-Polyisoprene over a Large Molecular Weight Range. *Macromolecules* **2004,** *37* (21), 8135-8144.
134. Das, C.; Read, D. J., BOB rheology (https://sourceforge.net/projects/bob-rheology/).
135. Vorselaars, B., Theory Documentation: Polydisperse Double Reptation. In *‘Rheology of Entangled Polymers: Toolbox for the Analysis of Theory and Experiments (Reptate, http://www.reptate.com)*.
136. Milner, S. T.; McLeish, T. C. B., Arm-Length Dependence of Stress Relaxation in Star Polymer Melts. *Macromolecules* **1998,** *31* (21), 7479-7482.
137. Janez, S.; Aleš, M.; Carlos, M.; Siegfried, S.; Igor, S., Velocity autocorrelation spectra in molten polymers measured by NMR modulated gradient spin-echo. *EPL (Europhysics Letters)* **2014,** *106* (2), 27007.
138. Cox, W. P.; Merz, E. H., Correlation of dynamic and steady flow viscosities. *Journal of Polymer Science* **1958,** *28* (118), 619-622.
139. Al-Hadithi, T. S. R.; Barnes, H. A.; Walters, K., The relationship between the linear (oscillatory) and nonlinear (steady-state) flow properties of a series of polymer and colloidal systems. *Colloid and Polymer Science* **1992,** *270* (1), 40-46.
140. Yang, W. H.; Rao, M. A., Complex viscosity-temperature master curve of cornstarch dispersion during gelatinization. *Journal of Food Process Engineering* **1998,** *21* (3), 191-207.
141. Rao, M. A.; Cooley, H. J., Rheological behaviour of tomato pastes in steady and dynamic shear. *Journal of Texture Studies* **1992,** *23* (4), 415-425.

142. Boukany, P. E.; Tapadia, P.; Wang, S.-Q., Interfacial stick-slip transition in simple shear of entangled melts. *Journal of Rheology* **2006,** *50* (5), 641-654.
143. Park, H. E.; Lim, S. T.; Smillo, F.; Dealy, J. M.; Robertson, C. G., Wall slip and spurt flow of polybutadiene. *Journal of Rheology* **2008,** *52* (5), 1201-1239.
144. Chatterjee, T.; Krishnamoorti, R., Rheology of polymer carbon nanotubes composites. *Soft Matter* **2013,** *9* (40), 9515-9529.
145. Sun, H.; Ntetsikas, K.; Avgeropoulos, A.; Wang, S.-Q., Breakdown of Time–Temperature Equivalence in Startup Uniaxial Extension of Entangled Polymer Melts. *Macromolecules* **2013,** *46* (10), 4151-4159.
146. Auhl, D.; Chambon, P.; McLeish, T. C. B.; Read, D. J., Elongational Flow of Blends of Long and Short Polymers: Effective Stretch Relaxation Time. *Physical Review Letters* **2009,** *103* (13), 136001.
147. Nielsen, J. K.; Hassager, O.; Rasmussen, H. K.; McKinley, G. H., Observing the chain stretch transition in a highly entangled polyisoprene melt using transient extensional rheometry. *Journal of Rheology* **2009,** *53* (6), 1327-1346.
148. Bacchelli, F., A Rheotens-based setup for the constant strain rate uniaxial extension of uncured elastomers. *Rheologica Acta* **2007,** *46* (9), 1223-1233.
149. Au-Yeung, V. S.; Macosko, C. W.; Raju, V. R., Notes: Extensional Flow of Linear and Star-Branched Hydrogenated Polybutadiene with Narrow Molecular Weight Distribution. *Journal of Rheology* **1981,** *25* (4), 445-452.
150. Kasehagen, L. J.; Macosko, C. W., Nonlinear shear and extensional rheology of long-chain randomly branched polybutadiene. *Journal of Rheology* **1998,** *42* (6), 1303-1327.
151. Graham, R. S.; Likhtman, A. E.; McLeish, T. C. B.; Milner, S. T., Microscopic theory of linear, entangled polymer chains under rapid deformation including chain stretch and convective constraint release. *J. Rheol. (N. Y., NY, U. S.)* **2003,** *47* (5), 1171-1200.
152. Torres, E.; Li, S.-W.; Costeux, S.; Dealy, J. M., Branching structure and strain hardening of branched metallocene polyethylenes. *Journal of Rheology* **2015,** *59* (5), 1151-1172.
153. Kapnistos, M.; Vlassopoulos, D.; Roovers, J.; Leal, L. G., Linear Rheology of Architecturally Complex Macromolecules: Comb Polymers with Linear Backbones. *Macromolecules* **2005,** *38* (18), 7852-7862.
154. Tirtaatmadja, V.; Sridhar, T., A filament stretching device for measurement of extensional viscosity. *Journal of Rheology* **1993,** *37* (6), 1081-1102.
155. Szabo, P.; McKinley, G. H.; Clasen, C., Constant force extensional rheometry of polymer solutions. *Journal of Non-Newtonian Fluid Mechanics* **2012,** *169*, 26-41.
156. Matta, J.; Tytus, R., Liquid stretching using a falling cylinder. *Journal of Non-Newtonian Fluid Mechanics* **1990,** *35* (2), 215-229.
157. Ellis, B.; Smith, R., *Polymers: A Property Database, Second Edition*. CRC Press, 2008.
158. Reynolds, C.; Thompson, R.; McLeish, T., Pressure and shear rate dependence of the viscosity and stress relaxation of polymer melts. *Journal of Rheology* **2018,** *62* (2), 631-642.
159. Han, C. D., On Silt- and Capillary-Die Rheometry. *Transactions of the Society of Rheology* **1974,** *18* (1), 163-190.
160. Viovy, J. L.; Rubinstein, M.; Colby, R. H., Constraint release in polymer melts: tube reorganization versus tube dilation. *Macromolecules* **1991,** *24* (12), 3587-3596.
161. Des Cloizeaux, J., Relaxation of entangled polymers in melts. *Macromolecules* **1990,** *23* (17), 3992-4006.
162. Van Ruymbeke, E.; Liu, C.-Y.; Bailly, C., Quantitative tube model predictions for the linear viscoelasticity of linear polymers. **2007**.
163. Venerus, D.; Zhu, S.-H.; Öttinger, H., Stress and birefringence measurements during the uniaxial elongation of polystyrene melts. *Journal of Rheology (1978-present)* **1999,** *43* (3), 795-813.

164. Bent, J.; Hutchings, L. R.; Richards, R. W.; Gough, T.; Spares, R.; Coates, P. D.; Grillo, I.; Harlen, O. G.; Read, D. J.; Graham, R. S.; Likhtman, A. E.; Groves, D. J.; Nicholson, T. M.; McLeish, T. C. B., Neutron-Mapping Polymer Flow: Scattering, Flow Visualization, and Molecular Theory. *Science* **2003,** *301* (5640), 1691.
165. Schramm, G., *Einführung in Rheologie und Rheometrie*. Haake, 1995.
166. Hyun, K. S.; Karam, H. J., Rheological Properties of Molten Polymers. III. Shear-Dependent Melt Viscosity. *Transactions of the Society of Rheology* **1969,** *13* (3), 335-356.
167. Floudas, G.; Gravalides, C.; Reisinger, T.; Wegner, G., Effect of pressure on the segmental and chain dynamics of polyisoprene. Molecular weight dependence. *J. Chem. Phys.* **1999,** *111*, 9847-9852.
168. Goubert, A.; Vermant, J.; Moldenaers, P.; Göttfert, A.; Ernst, B., Comparison of measurement techniques for evaluating the pressure dependence of the viscosity. *Applied Rheology* **2001,** *11*, 26-37.
169. Park, H. E.; Dealy, J. M., Effects of Pressure and Supercritical Fluids on the Viscosity of Polyethylene. *Macromolecules* **2006,** *39* (16), 5438-5452.
170. Park, H. E.; Lim, S. T.; Laun, H. M.; Dealy, J. M., Measurement of pressure coefficient of melt viscosity: drag flow versus capillary flow. *Rheologica Acta* **2008,** *47* (9), 1023-1038.
171. Son, Y., Measurement of pressure dependence on the shear viscosity of polymer melts. *Journal of Polymer Research* **2009,** *16* (6), 667.
172. Aho, J.; Syrjälä, S., Measurement of the pressure dependence of viscosity of polymer melts using a back pressure-regulated capillary rheometer. *Journal of Applied Polymer Science* **2010,** *117* (2), 1076-1084.
173. Friesenbichler, W.; Duretek, I.; Rajganesh, J.; Kumar, S. R., Measuring the pressure dependent viscosity at high shear rates using a new rheological injection mould. *Polimery* **2011,** *56* (1), 58-62.
174. Guan, W.-S.; Huang, H.-X., Superimposed effects in high-shear-rate capillary rheology of polystyrene melt. *Polymer Engineering & Science* **2013,** *53* (7), 1563-1570.
175. Sorrentino, A.; Pantani, R., Determination of the effect of pressure on viscosity of an isotactic polypropylene. *Polymer Bulletin* **2013,** *70* (7), 2005-2014.
176. Volpe, V.; Pantani, R., Determination of the effect of pressure on viscosity at high shear rates by using an injection molding machine. *Journal of Applied Polymer Science* **2017**.
177. Gargallo, L.; Radic, D., *Physicochemical Behavior and Supramolecular Organization of Polymers*. Springer, 2009.
178. Valette, R.; Mackley, M. R.; del Castillo, G. H. F., Matching time dependent pressure driven flows with a Rolie Poly numerical simulation. *Journal of non-newtonian fluid mechanics* **2006,** *136* (2), 118-125.
179. Yasuda, K.; Armstrong, R. C.; Cohen, R. E., Shear flow properties of concentrated solutions of linear and star branched polystyrenes. *Rheologica Acta* **1981,** *20* (2), 163-178.
180. Hatzikiriakos, S. G.; Dealy, J. M., Start-up pressure transients in a capillary rheometer. *Polymer Engineering & Science* **1994,** *34* (6), 493-499.
181. Mott, P.; Dorgan, J.; Roland, C., The bulk modulus and Poisson's ratio of “incompressible” materials. *Journal of Sound and Vibration* **2008,** *312* (4), 572-575.
182. Vinogradov, G. V.; Isayev, A. I.; Mustafaev, D. A.; Podolsky, Y. Y., Polarization-optical investigation of polymers in fluid and high-elastic states under oscillatory deformation. *Journal of Applied Polymer Science* **1978,** *22* (3), 665-677.
183. Van Krevelen, D. W.; Te Nijenhuis, K., Chapter 10 - Optical Properties. In *Properties of Polymers (Fourth Edition)*, Elsevier, Amsterdam, 2009; pp 287-318.
184. Hassell, D. G.; Hoyle, D.; Auhl, D.; Harlen, O.; Mackley, M. R.; McLeish, T. C. B., Effect of branching in cross-slot flow: the formation of “W cusps”. *Rheologica Acta* **2009,** *48* (5), 551-561.
185. Reynolds, C., CDRheo: MATLAB tool for Fourier analysis of LAOS data (https://sourceforge.net/projects/cdrheo).

186. Frigo, M.; Johnson, S. G., *The Design and implementation of FFTW3*. 2005; Vol. 93, p 216-231.
187. Payne, A. R., The dynamic properties of carbon black-loaded natural rubber vulcanizates. Part I. *Journal of Applied Polymer Science* **1962,** *6* (19), 57-63.
188. Drozdov, A. D.; Dorfmann, A., The payne effect for particle-reinforced elastomers. *Polymer Engineering & Science* **2002,** *42* (3), 591-604.
189. Merabia, S.; Sotta, P.; Long, D. R., Unique plastic and recovery behavior of nanofilled elastomers and thermoplastic elastomers (Payne and Mullins effects). *Journal of Polymer Science Part B: Polymer Physics* **2010,** *48* (13), 1495-1508.
190. Song, H. Y.; Salehiyan, R.; Li, X.; Lee, S. H.; Hyun, K., A comparative study of the effects of cone-plate and parallel-plate geometries on rheological properties under oscillatory shear flow. *Korea-Australia Rheology Journal* **2017,** *29* (4), 281-294.
191. Carotenuto, C.; Vananroye, A.; Vermant, J.; Minale, M., Predicting the apparent wall slip when using roughened geometries: A porous medium approach. *Journal of Rheology* **2015,** *59* (5), 1131-1149.
192. Singh, P. K.; Soulages, J. M.; Ewoldt, R. H., Frequency-sweep medium-amplitude oscillatory shear (MAOS). *Journal of Rheology* **2018,** *62* (1), 277-293.

8 Appendices

8.1: Linear rheology of PBD28K used in Chapter 3

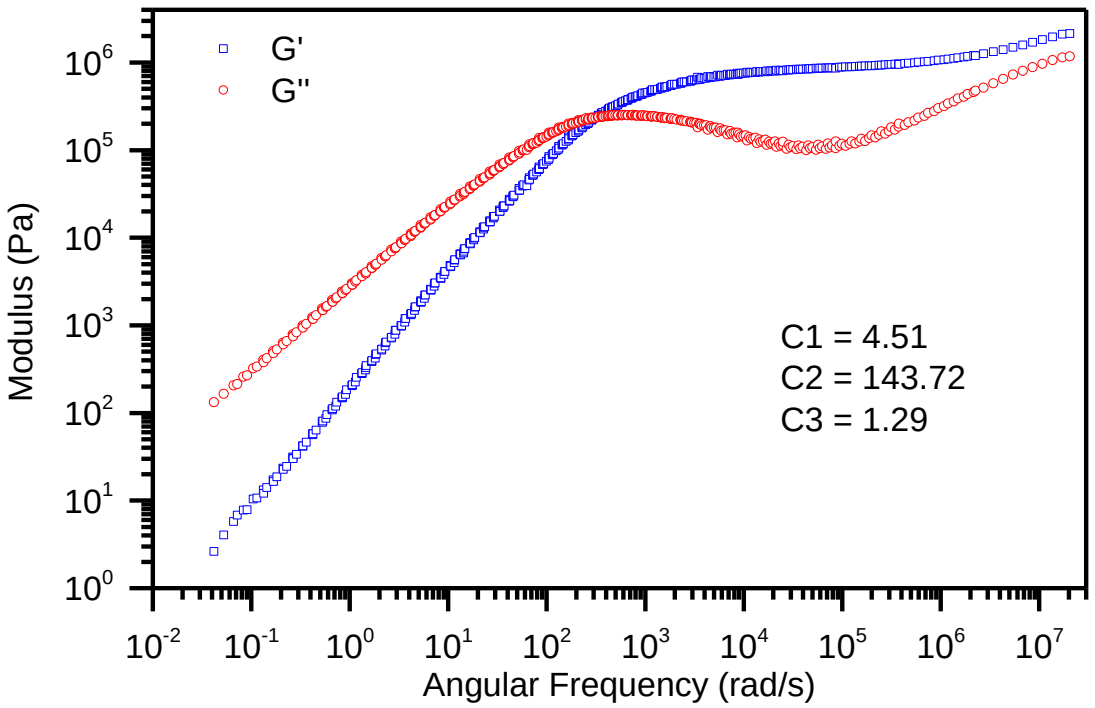

Figure 8.1: Rheological spectrum of PBD28K, measured from -60 to 40 °C and shifted to 25 °C using a WLF TTS with the parameters shown.

8.2: MATLAB code for minimising parameters in BOB theory

8.2.1: Running BOB for a range of N_e and τ_e values

```
waitfor(msgbox('select directory with inp.dat bob file')); %displays message, waits until ok clicked
    inpdata = uigetdir; %asks for folder with inp.dat file
prompt = 'Max N_e?';  %asks user for maximum N_e value
maxN_e = input(prompt);
prompt = 'Min N_e?';  %asks user for minimum N_e value
minN_e = input(prompt);
prompt = 'Max Tau_e?'; %asks user for maximum Tau e value
maxtau_e = input(prompt);
prompt = 'Min Tau_e?'; %asks user for minimum Tau e value
mintau_e = input(prompt);
File = strcat(inpdata,'\inp.dat'); % creates file name with directory
dat1 = dlmread(File); %imports file
dat = dlmread(File); %imports file to separate matrix
tau_e = logspace(log10(mintau_e),log10(maxtau_e),20); %creates log spaced vector between min and max taue
N_e = logspace(log10(minN_e),log10(maxN_e),20); %creates log spaced vector between min and max N_e
dat(dat == 0) = NaN; %replaces 0 values with NaN
dat = num2cell(dat); %converts number to cell file type
for k = 1:length(dat) %for all points in the range
    if isnan(dat{k,1}) %if value is NaN
        dat{k} = 0; %replaces with 0
    end
end
for k = 1:numel(dat) %for all points in dat
    if isnan(dat{k}) %if value is NaN
        dat{k} = ''; %make field empty
    end
end

num = floor(length(dat1)/8); %round down length of original vector over 8

for yo=1:num %checks every 8th value
   if dat1(8*yo,2) == 0 %if it is zero in original file
   dat{8,2} = 0; %sets it to zero in new file
   end
end


for tau = tau_e %for all values of tau e
   dat{5,1} = tau; %sets value in output file to tau
   for N = N_e %for all vales of me
      dat{4,2} = N; %sets value in output file to N
      n = num2str(N); %converts m to number
      t = num2str(tau); %converts tau to number
```

```
        dlmcell(strcat(inpdata,'\N_e=', n,'_tau_e=',t,'.dat'),dat, ' '); %creates file with parameters N_e and t
        str = [inpdata '\BOB -b -i ' inpdata,'\N_e=', n,'_tau_e=',t,'.dat']; %runs bob for the input file
        dos(str); %runs BOB
        output = dlmread('gtp.dat'); %reads output file
        dlmwrite(strcat(inpdata,'\N_e=', n,'_tau_e=',t,'.gtp'),output, ' '); %writes output to file
    end
end
disp('Done!');%displays done when finished
```

8.2.2: Comparing output files

```
prompt = 'How many polymers?';
nopoly = input(prompt); %prompts user to enter the number of polymers
bobdata =cell(1); %creates file for bob files
freq = cell(1); %creates file for frequency values
expmoduli = cell(1); %creates file for moduli values
names = cell (1); %creates cell variables (must be cells so can store incremental data for multiple polymers)
for x = 1:nopoly %loops for each polymer
    waitfor(msgbox('select experiment data file, .tts')); %displays message, waits until ok clicked
    [filename,pathname,filterindex] = uigetfile('*.tts'); %asks for experimental data
    expdata = (importdata(strcat(pathname,filename))); %joins filename and path and imports data
    waitfor(msgbox('select directory of bob files')); %displays message, waits until ok clicked
    bobdata{x} = uigetdir; %asks for folder with bob files
    freq{x} = expdata.data(:,1:1); %selects first column (angular frequencies)
    expmoduli{x} = expdata.data(:,1:3); %selects first 3 columns (ω, G' and G'')
    names{x} = dir(strcat(bobdata{x},'\*.gtp')); %looks up all .txt file in folder
end

count = 1; %count of number of files
out = cell(1); %creates output file as cell array

for file = names{1}' %for each BOB file in folder
    difference = 0; %sets difference (between bob theory and experimental) to 0
    for y =1:nopoly %for each polymer (files must be organised in the same order and have same names)
    File = strcat(bobdata{y},'\',file.name); %creates file name with directory
    A = importdata(File); %imports file
    bobfreq = A(:,1:1); %reads in frequencies of bob file
    for w = freq{y}' %for each frequency in exp data
      bobstorG = log(interp1(A(:,1),A(:,2), w)); %looks up BOB G', interpolates with experimental frequency
```

```
      boblossG = log(interp1(A(:,1),A(:,3), w)); %looks up G'' (uses log to stop
larger values shifting results)
      storG =  log(interp1(expmoduli{y}(:,1),expmoduli{y}(:,2), w)); %looks up
G'
      lossG = log(interp1(expmoduli{y}(:,1),expmoduli{y}(:,3), w)); %looks up
G''
      diff = abs(storG-bobstorG) + abs(lossG-boblossG); % calculates
difference
      difference = difference + diff; %adds difference to total
   end
   end
   out{count,1} = file.name; %puts file name into output file
   out{count,2} = difference; %puts difference into output file
   count = count + 1; %increments file count
end
out = sortrows(out,2); %sorts output file by difference
disp(out) %display table of results
dlmcell([inpdata '\rank.txt'] ,out, ' '); %outputs ranking of files according to
overlap
disp('Done!'); %displays Done when finished
```

8.3: Falling weights analysis MATLAB code

```
InputFolder = 'X:\XXX\XXX'; %sets input folder
FileNames = dir([InputFolder, '\*.avi']); %finds all .avi files in folder
OutputFolder = 'X:\XXX\XXX\XXX'; %Sets Output folder
WeightHeights = [20,10,5,2,1;23.77,20.66,16.96,10.45,5.62]; %creates table
of mass heights for reference
for k=1:length(FileNames) %loops over all .avi files
FileName = FileNames(k).name;  %gets file name
FileName = FileName(1:end-4); %trims .avi from file name
VidLoc = [InputFolder, '\' , FileName, '.avi']; % sets video location
mkdir([OutputFolder, '\', FileName, '_Frames']) %creates output directory for
frame images
obj = VideoReader(VidLoc); %reads in frames of video
vid = read(obj,1); %gets first frame
frames = obj.NumberOfFrames; %reads number of frames
FrameRate = obj.FrameRate; %gets frame rate
Output = [zeros(1,16)]; %creates output file with 10 columns
imwrite(vid,strcat('frame-',num2str(1),'.tif')); %saves first frame to file
Iinit= imread(strcat('frame-',num2str(1),'.tif')); %loads first frame as image
BWinit = im2bw(Iinit, 0.03); %converts frame to black and white (binary)
adjust value depending on background
BWinit = bwareaopen(BWinit,25); %removes small objects (in white) from
image
BWinit = imcomplement(BWinit); %inverts image
BWinit = bwareaopen(BWinit,25); %removes small objects (originally in
black) from image
BWinit = imcomplement(BWinit); %reverts image to original
BWxchangesinit=abs(diff(BWinit,1,2)); %finds changes along x axis
BWychangesinit=abs(diff(BWinit,1,1)); %finds changes along y axis
X1 = find(BWxchangesinit(15,:), 20, 'first'); %finds top piston
pistonwidth = X1(end)-X1(1); %measures width of piston
pistonmid = round(X1(1)+(pistonwidth/2)); %finds midpoint
delete(strcat('frame-',num2str(1),'.tif')); %deletes created frame
lastWeightPosition = 100; %sets the position of the weight to arbitrary value
stop = 0; %creates stop parameter
x=1; %creates frame count parameter x
while stop == 0 %loops until initial strike is passed
vid = obj.read(x); %reads frame
imwrite(vid,strcat('frame-',num2str(x),'.tif')); %creates tif image
I= imread(strcat('frame-',num2str(x),'.tif')); %reads image as I
BW = im2bw(I,0.03); %converts to Black and White (binary)
BW = bwareaopen(BW,25); %removes small objects (in white) from image
BW = imcomplement(BW); %inverts image
BW = bwareaopen(BW,25); %removes small objects (originally in black) from
image
BW =imcomplement(BW); %reverts image to original
BWxchanges=abs(diff(BW,1,2)); %finds changes along x axis
BWychanges=abs(diff(BW,1,1)); %finds changes along y axis
Y1 = find(BWychanges(:,pistonmid), 25, 'last'); %finds weight and bottom
plate positions on left, by looking for last two changes
```

```
if length(Y1)>0 %if both weight and bottom pistons found
WeightPosition = Y1(1); %sets weight position
FrameHeight = size(I,1); %gets frameheight
if abs(WeightPosition-lastWeightPosition)<3 &&
WeightPosition<FrameHeight-1350 %if weight position is significantly
different to the last and not still resting on the bottom piston
stop = 1; %stop point reached
startframe = x; %sets frame as the initial frame in the relaxation
else %if not continues loop
lastWeightPosition = WeightPosition; %saves weight position for comparison
end
end
delete(strcat('frame-',num2str(x),'.tif')); %deletes created frame
x = x+1; %increment frame
end
imwrite(vid,strcat('frame-',num2str(startframe),'.tif')); %saves frame as image
Iinit= imread(strcat('frame-',num2str(startframe),'.tif')); %loads first frame as
image
mass = inputdlg(strcat('Enter the mass of the weight in grams: ', FileName));
%asks user for mass weight
mass=str2num(mass{1}); %converts mass weight to number
massheight = WeightHeights(2,WeightHeights(1,:)==mass); %looks up mass
height from table of heights
Force = mass/1000*9.81; %calculates force due to gravity
msgbox('Select Crop Area');
[Iinitcrop, rect] = imcrop(Iinit); % asks user to crop frame one
close all;
imshow(Iinit); %displays cropped image
msgbox('Select two points at the top and bottom of sample');
h=ginput(2); %asks user to click two points on image to select top and
bottom of sample (order not important)
close all; %closes image
InitialSeparation=abs(h(1,2) -h(2,2)); %sets initial separation as difference
between user selected points
imshow(Iinit); %shows frame
msgbox('Select two points at the top and bottom of the weight');
w=ginput(2); %asks user to click two points on image to select top and
bottom of weight
close all; %closes image
WeightHeight=abs(w(1,2) -w(2,2)); %calculates height of weight
imshow(Iinitcrop); %displays cropped image
msgbox('Select Lower plate'); %asks user to select position of the lower plate
[centrepoint, lowerplatepos]=ginput(1);
lowerplatepos =round(lowerplatepos);  %rounds to nearest pixel position
close all; %closes image
imshow(Iinitcrop); %displays cropped image
msgbox('Select Top plate');  %asks user to select position of the lower plate
[centrepoint2, topplatepos]=ginput(1);
topplatepos =round(topplatepos); %rounds to nearest pixel position
close all; %closes image
```

```
SepLast = InitialSeparation; %sets last separation to the initial value
Pixeltomm = massheight/WeightHeight; %gets pixel conversion factor from
weight height
Pixeltom =Pixeltomm/1000; %converts mm to m
Output(1,9)= InitialSeparation*Pixeltom; %converts initial separation to m
for x = startframe : frames %for all frames
vid = read(obj,x);
imwrite(vid,strcat('frame-',num2str(x),'.tif'));
I= imread(strcat('frame-',num2str(x),'.tif')); %reads image as I
Icrop = imcrop(I, rect); %crops the same as user specified
BW = im2bw(Icrop,0.03); %converts to Black and White (binary)
BW = bwareaopen(BW,25); %removes small objects (in white) from image
BW =imcomplement(BW); %inverts image
BW = bwareaopen(BW,25); %removes small objects (originally in black) from
image
BW =imcomplement(BW); %reverts image to original
BWxchanges=abs(diff(BW,1,2)); % finds changes along x axis
BWychanges=abs(diff(BW,1,1)); % finds changes along y axis
X1 = find(BWxchanges(15,:), 20, 'first'); %finds top plate
platemid = round((X1(end)+X1(1))/2); %finds centre of plate
PlateDiam = X1(end)-X1(1); %records plate diameter
WP=0; %creates matrix
BW = im2bw(Icrop,0.25); %converts to Black and White (binary)
BW = bwareaopen(BW,25); %removes small objects (in white) from image
BW =imcomplement(BW); %inverts image
BW = bwareaopen(BW,25); %removes small objects (originally in black) from
image
BW =imcomplement(BW); %reverts image to original
BWxchanges=abs(diff(BW,1,2)); % finds changes along x axis
BWychanges=abs(diff(BW,1,1)); %finds changes along y axis
for b = 1:lowerplatepos-10 %looks between the top plate and lower plate
position
  WP(b)= any(BW(b,:)); %find changes
end
WeightPos=find(WP,1,'last'); %saves last change as weight position
BotPlatePos = WeightPos - WeightHeight; %finds bottom of the sample from
weight position
TopPlatePos = topplatepos; %gets top plate position
Separation = WeightPos - WeightHeight- TopPlatePos; %calculates
separation from weight position
BW = im2bw(Icrop,0.03); % converts to Black and White (binary)
BW = bwareaopen(BW,25); %removes small objects (in white) from image
BW =imcomplement(BW); %inverts image
BW = bwareaopen(BW,25); %removes small objects (originally in black) from
image
BW =imcomplement(BW); %reverts image to original
BWxchanges=abs(diff(BW,1,2)); %finds changes along x axis
BWychanges=abs(diff(BW,1,1)); %finds changes along y axis
MidDist = round(TopPlatePos + Separation/2); % calculates halfway point
between plates
```

```
if MidDist <= 0
   Width =0; %if no middle position is found gives 0 as the width
else
Width = find(BWxchanges(MidDist,:), 6, 'first'); %finds changes along halfway
point
end
if length(Width)>1 %if found both sides of filament
FilamentWidth = Width(end)-Width(1); %calculates filament width
Icrop(MidDist, Width(1):Width(end),1) = 255; %makes mid filament line red
Icrop(MidDist, Width(1):Width(end),2) = 0; %makes mid filament line red
Icrop(MidDist, Width(1):Width(end),3) = 0; %makes mid filament line red
else %if can't find both sides of filament
FilamentWidth = 0; % outputs zero as filament width
end
Sumdiam=0; %creates variable for sum of filament diameters
c=0; %creates counter for number of diameters measured
ThinDiam = FilamentWidth; %sets the thinnest diameter initially as the mid-
point diameter
for i = TopPlatePos:BotPlatePos %loops through the filament
   diam = find(BWxchanges(i,:), 6, 'first'); %gets changes along the filament
width
   if length(diam)>1 %if filament found
      fildiam=diam(end)-diam(1); %gets filament width
      Sumdiam = Sumdiam + fildiam; %adds width to sum to calculate
average
      c=c+1; %increments counter
      if fildiam<ThinDiam %if diameter is smallest than thinnest
      ThinDiam = fildiam; %replaces thinnest value
   end
   end
end
AverageDiam= Sumdiam/c; %calculates average diameter from sum and
number of points
Stress = Force/(pi*((FilamentWidth*Pixeltom)/2)^2); %gets stress from force
over area of midpoint filament
StressAv = Force/(pi*((AverageDiam*Pixeltom)/2)^2); %gets stress from
average filament diameter
Time = (x-startframe+1) / FrameRate; %calculates time after initial strike
Output(x-startframe+1,1)= Time; %adds time to column 1
Output (x-startframe+1, 2) = FilamentWidth*Pixeltom; %adds Filament Width
to column 2
Output (x-startframe+1,3) = Separation*Pixeltom; %adds Plate Separation to
column 3
Output (x-startframe+1,4) = x; %adds Frame Number to column 6
Output (x-startframe+1,5) =WeightPos*Pixeltom; %adds position of weight
(bottom) to column 7
Output (x-startframe+1,6) =TopPlatePos*Pixeltom; %adds position of top
plate to column 8
Output (x-startframe+1,7) =BotPlatePos*Pixeltom; %adds position of bottom
plate (top of weight) to column 9
```

```
Output (x-startframe+1,8) = PlateDiam*Pixeltom; %adds plate diameter to
output file
Output (x-startframe+1,10)=AverageDiam*Pixeltom; %adds average filament
diameter to output file
Output (x-startframe+1,11)=ThinDiam*Pixeltom; %adds thinnest diameter to
output file
Output (x-startframe+1,12)=Stress; %adds thinnest diameter to output file
Output (x-startframe+1,13)=StressAv; %adds thinnest diameter to output file

delete(strcat('frame-',num2str(x),'.tif')); %deletes created frame
imwrite(Icrop, [OutputFolder, '\', FileName, '_Frames\', num2str(x),
'.tif']);%writes frame to Frame folder
end
timesteps = Output(:,1); %writes time to new vector
platesep = Output(:,3); %writes plate separation to new vector
smoothedplateseparation= smooth(platesep); %smooths plate separation
nopoints=length(smoothedplateseparation); %gets number of points
velocity=0; %creates velocity variable
for q=11:nopoints-11 %for range of velocity (starts 10 points in)
velocity(q) = ((smoothedplateseparation(q+10) - smoothedplateseparation(q-
10)))/(((timesteps(q+10) - timesteps(q-10)))); %calculates velocity from
change in separation over 10 points
end
for q=1:11
    velocity(q) = ((smoothedplateseparation(q+10) -
smoothedplateseparation(1)))/(((timesteps(q+10) - timesteps(1)))); %for initial
points calculates velocity over 1 point
end
for q = nopoints-11:nopoints
    velocity(q) = ((smoothedplateseparation(nopoints) -
smoothedplateseparation(q-10)))/(((timesteps(nopoints) - timesteps(q-10))));
%for final points calculates velocity over 1 point
end
velocity = velocity'; %changes velocity to column vector
StrainRate = 0; %creates strain rate vector
StrainRate = 1/(InitialSeparation*Pixeltom) * velocity; %calculates strain rate
from velocity
Stressall = Output(:,12); %gets stress from output vector
ExtensionalViscosity = Stressall./StrainRate; %calculates  extensional
viscosity from strain rate and stress
Output(:,14) =velocity; %adds velocity to output
Output(:,15) =StrainRate; %adds strain rate to output
Output(:,16) =ExtensionalViscosity; %adds extensional viscosity to output
Headings = {'s', 'm', 'm', ' ', 'm', 'm', 'm', 'm', 'm', 'm', 'm','Pa','Pa', 'ms^-1','s^-
1','Pa'}; %units for output file
H = cell2table(Headings, 'VariableNames', {'Time',
'MidPoint_Filament_Diameter', 'Plate_Separation', 'Frame', 'Weight_Position',
'Top_Plate_Position', 'Bottom_Plate_Position', 'Plate_Diameter',
'Initial_Separation', 'Average_FilamentDiameter','Thinnest_Point_Diameter',
```

```
'Stress', 'Stress_From_Average_Diameter', 'Velocity', 'Strain_Rate',
'Extensional_Viscosity'}); %defines heading in output file
writetable(H, [OutputFolder, '\', FileName, '_output.txt']); %outputs headings -
change this to directory of output file
dlmwrite([OutputFolder, '\', FileName, '_output.txt'], Output,'-append'); %adds
values to output file - change to directory of output file
end
```

8.4: Fit parameters for exponential decays detailed in Section 4.3

8.4.1: Stress decay fits

Pressure (bar)	Wall Shear Rate (s^{-1})	y_0 (Pa)	Error (Pa)	σ_0 (Pa)	Error (Pa)	A	Error	t_1 (s)	Error (s)	B	Error (s)	t_2 (s)	Error (s)	t_f (s)	Error (s)
1	0.589	0	5000	37000	5000	0	0		0	0.66	0.07	1.7	0.2	0.19	0.06
1	1.178	2000	5000	50000	10000	0.31961	0.12814	0.3	0.1	0.7	0.1	1.5	0.3	0	0
1	5.89	-4000	5000	120000	10000	0.34	0.05	0.28	0.05	0.66	0.05	1.7	0.1	0	0
3	0.589	-1000	2000	38000	6000	0	0	0	0	0.77	0.07	1.4	0.4	0.1	0.07
3	1.178	1000	2000	50000	2000	0	0	0	0	1	0.04	1.3	0.1	0	0
3	5.89	0	5000	140000	20000	0.52	0.08	0.4	0.07	0.48	0.09	1.8	0.3	0	0
10	0.589	0	5000	40000	10000	0	0	0	0	0.7	0.1	1.9	0.5	0.2	0.2
10	1.178	-1000	1000	53000	5000	0	0	0	0	0.82	0.04	1.8	0.2	0.2	0.08
10	5.89	-5000	5000	150000	60000	0.3	0.2	0.8	0.5	0.3	0.2	3	1	0.14	0.02
30	0.589	-5000	5000	42000	6000	0	0	0	0	0.67	0.08	3	1	0.14	0.04
30	1.178	-5000	1000	62000	2000	0	0	0	0	0.72	0.02	2.1	0.2	0.17	0.02
30	5.89	-5000	5000	150000	10000	0.69	0.04	0.4	0.03	0.31	0.02	3	1	0	0
100	0.589	-5000	5000	45000	7000	0.27941	0.08447	0.24	0	0.72	0.07	2	0.5	0	0.09
100	1.178	-1000	2000	60000	10000	0.32412	0.10406	0.4	0.1	0.68	0.09	1.9	0.4	0	0
100	5.89	0	5000	170000	40000	0.34	0.07	0.8	0.4	0.3	0.1	3.5	0.7	0.18	0.04

8.4.1: Pressure drop decay fits

Pressure (bar)	Wall Shear Rate (s^{-1})	y_0 (Pa)	Error (Pa)	σ_0 (Pa)	Error (Pa)	A	Error	t_1 (s)	Error (s)	B	Error (s)	t_2 (s)	Error (s)	t_f (s)	Error (s)
1	0.059	1.0837	0.0005	0.383	0.003	0.000	0.00	0.00	0.00	1.000	0.009	1.23	0.02	0.00	0.00
1	0.118	1.8864	0.0006	0.41	0.03	0.000	0.00	0.00	0.08	1.000	0.00	2.12	0.03	0.00	0.00
1	0.589	2.6626	0.0009	2.95	0.01	0.54687	0.00206	0.548	0.004	0.453	0.002	4.02	0.02	0.00	0.00
1	1.178	1.6505	0.0008	2.417	0.008	0.5582	0.00192	0.507	0.004	0.442	0.001	4.63	0.02	0.00	0.00
1	5.89	1.9585	0.0006	5.83	0.07	0.539	0.003	0.742	0.009	0.286	0.005	2.57	0.02	0.120	0.004
3	0.059	1.4307	0.0004	0.235	0.002	0.000	0.00	0.00	0.00	1.000	0.009	1.78	0.03	0.00	0.00
3	0.118	1.4107	0.0009	0.58	0.04	0.21309	0.02918	0.56	0.11	0.79	0.03	2.50	0.07	0.00	0.00
3	0.589	1.8370	0.0006	1.43	0.02	0.46344	0.00716	0.40	0.01	0.537	0.007	2.25	0.03	0.00	0.00
3	1.178	1.566	0.002	2.56	0.01	0.60972	0.00296	0.60	0.01	0.390	0.002	5.55	0.06	0.00	0.00
3	5.89	2.224	0.001	5.57	0.09	0.422	0.006	0.62	0.01	0.236	0.003	3.15	0.03	0.129	0.003
10	0.059	1.4888	0.0006	0.524	0.001	0.000	0.00	0.00	0.00	1.000	0.002	10.98	0.05	0.00	0.00
10	0.118	1.720	0.001	0.43	0.01	0.41343	0.01665	0.57	0.04	0.587	0.009	7.5	0.2	0.00	0.00
10	0.589	2.3229	0.0004	1.41	0.02	0.31226	0.00696	0.00	0.00	0.688	0.005	1.208	0.008	0.124	0.005
10	1.178	1.6505	0.0008	2.417	0.008	0.5582	0.00192	0.51	0.004	0.442	0.001	4.63	0.02	0.000	0.00
10	5.89	1.745	0.001	6.47	0.06	0.353	0.003	1.15	0.02	0.165	0.004	4.23	0.06	0.191	0.002
30	0.059	2.1474	0.0009	0.68	0.01	0.000	0.00	0.00	0.00	0.379	0.007	2.42	0.06	0.202	0.008
30	0.118	1.8373	0.0006	0.692	0.005	0.000	0.00	0.00	0.00	1.000	0.007	3.33	0.03	0.00	0.00
30	0.589	2.5091	0.0003	1.69	0.01	0.59243	0.00418	0.524	0.007	0.408	0.002	8.12	0.04	0.00	0.00
30	1.178	2.498	0.002	2.33	0.01	0.68497	0.00279	0.593	0.005	0.315	0.002	5.91	0.07	0.00	0.00
30	5.89	2.066	0.001	6.6	0.2	0.382	0.01	0.55	0.01	0.280	0.003	3.09	0.02	0.162	0.005
100	0.059	2.0978	0.0008	0.379	0.002	0.000	0.00	0.00	0.00	1.000	0.004	4.25	0.04	0.00	0.00
100	0.118	2.1558	0.0006	0.553	0.003	0.000	0.00	0.00	0.00	1.000	0.005	2.79	0.02	0.00	0.00
100	0.589	2.1761	0.0007	1.969	0.007	0.5725	0.0025	0.870	0.007	0.428	0.001	12.34	0.06	0.00	0.00
100	1.178	2.6626	0.0009	2.95	0.01	0.54687	0.00206	0.548	0.004	0.453	0.002	4.02	0.02	0.00	0.00
100	5.89	2.428	0.005	8.5	0.1	0.358	0.004	1.29	0.03	0.176	0.002	8.8	0.2	0.209	0.004